THE LAW OF INTERSTELLAR EXTINCTION IN THE SOUTHERN MILKY WAY

Douglas C. B. Whittet

A Thesis Submitted for the Degree of PhD
at the
University of St Andrews

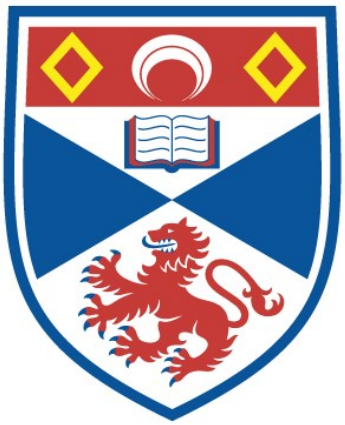

1975

THE LAW OF INTERSTELLAR EXTINCTION IN THE SOUTHERN MILKY WAY

by

Douglas C. B. Whittet

A thesis submitted for the degree of
Doctor of Philosophy to the University of St. Andrews
April, 1975.

Declaration

Except where reference is made to the work of others, the research described in this thesis and the composition of the thesis are my own work. No part of this work has been previously submitted for a higher degree to this or any other University. Under Ordinance General No. 12, I was admitted to the Faculty of Science of the University of St. Andrews as a research student on the 1st October, 1971. I was accepted as a candidate for the degree of Ph.D. on 1st October, 1972, under Resolution of the University Court, 1967, No. 1.

D. C. B. Whittet

Certificate

I certify that D. C. B. Whittet has spent nine terms in research work at the University Observatory, St. Andrews, that he has fulfilled the conditions of Ordinance General No. 12 and Senate Regulations under Resolution of the University Court, 1967, No. 1, and that he is qualified to submit the accompanying thesis in application for the degree of Ph.D.

I. G. van Breda

CONTENTS

ABSTRACT

Photoelectric scanner observations are combined with infrared photometry in the JHKL bands to give interstellar extinction curves by the colour difference method for 25 reddened stars in the Southern Milky Way. The observed stars are distributed from galactic longitude $\ell^{II} = 260^{o}$ through the Galactic Centre to $\ell^{II} = 30^{o}$. The scanner data ranges in wavelength from 3480 to 5240 A with a resolution of 40 A in the second order of diffraction, and from 5080 to 8040 A with a resolution of 80 A in the first order. The infrared photometry extends the wavelength coverage to 3.5 μ. The normalized extinction curves show appreciable variations from star to star which are not apparently related to galactic structure. In several cases stars quite close together in the sky show appreciably different curves, suggesting that fluctuations in the grain size distribution may be occurring on a fairly localized scale.

Using a graphite-iron-silicate grain model, extinction curves computed from the Mie theory are fitted to the observational data. This provides a theoretical basis for extrapolation of the curves to $\lambda^{-1} = 0$, allowing the ratio of total to selective extinction, R, to be deduced. R varies between 2.6 and 3.5 for 22 stars lying within 10^{o} of the galactic plane, and between 3.8 and 4.3 for 3 stars in Upper Scorpius.

One of the Upper Scorpius stars studied, HD 147889, lies in an HII region near the centre of the ρ Oph complex of dust and nebulosity. A variable extinction analysis applied to members of the Sco OB-2 association indicates an increase

in the value of R for stars lying towards nebulosity in the complex; for these stars alone a result of $R = 4.2 \pm 0.5$ is derived, whilst for the remainder, $R = 3.3 \pm 0.3$. The distance modulus of the association is deduced to be 6.1 ± 0.1, which is in good agreement with the kinematical value.

The scanner extinction curves contain considerable broadband structure. In particular, a depressed region between wavenumbers 1.6 and 1.9 μ^{-1} is a common feature of the curves. A similar depression was noted by Whiteoak in the extinction curves of Northern Milky Way stars. Its depth correlates well with reddening, suggesting that the feature originates in the grains. The extinction curve of HD 147889 shows a cusp-like depression at 1.97 μ^{-1} which divides the curve into two distinct sections. The ratio of the 4430 A diffuse interstellar band height to colour excess shows signs of systematic variation with longitude for stars whose reddening occurs mainly in the local spiral arm.

CHAPTER 1

INTRODUCTION

(1.1) Early Observations

It was noticed by Herschel almost two centuries ago that there are patches in the dense star fields of the Milky Way that are apparently devoid of stars. Herschel called these dark regions 'holes in the sky' as he believed he was looking through gaps in the Milky Way system. The American astronomer Barnard devoted much of his life to the study of these dark nebulae, and his results were published as a catalogue listing 182 such objects, and a photographic atlas (Barnard 1919, 1927). At this time there was a controversy among astronomers as to whether they represented genuine regions of low stellar density or whether they were caused by absorbing material in front of the stars.

The dispute was resolved by Trumpler (1930a, b) who demonstrated the existence of interstellar material causing extinction of starlight, as a result of his work on the distances of galactic clusters. Cluster distances determined by spectral classification and photographic photometry were found to disagree systematically with those deduced geometrically from the angular diameters, assuming a constant real diameter: if the photometric distances were correct it would be necessary to assume that the cluster diameters increase linearly with distance. This unlikely situation could be removed by applying a correction of about $0^{m}.8$/kpc to the photometric data, which Trumpler attributed to absorption by interstellar material.

This discovery also solved another problem which had been puzzling astronomers during the 1920's. It had been noted that the colour-temperatures of many stars close to the galactic plane are apparently much lower than the temperatures indicated by the degree of ionization in their spectra. It seemed likely that interstellar extinction would redden light in a similar way to atmospheric extinction, and Trumpler (1930c) therefore set out to investigate its dependence on wavelength. He took spectra of the brightest stars in distant clusters in the visual wavelength region, and compared them with spectra of nearby stars of similar spectral type. On the assumption that stars of similar spectral type have the same intrinsic energy distribution, the magnitude difference between the distant and nearby stars is a measure of the extinction at a given wavelength. Trumpler found this to vary roughly in proportion to λ^{-1}, thus confirming that extinction reddens starlight and explaining the anomaly of the low colour-temperature of distant early-type stars near the galactic plane. The λ^{-1} dependence also indicates that the extinction is not caused by atoms, molecules or solid particles small compared with the wavelength, as these would be expected to produce the λ^{-4} law predicted by the Rayleigh theory. Absorption and scattering by particles with sizes of the same order as the wavelength are required to produce a λ^{-1} dependence.

Once the existence of interstellar extinction was established, the main observational problems were firstly to establish its wavelength-dependence over the available spectral range, and secondly to see if this dependence varies from one region of sky to another. The wavelength-dependence is

usually represented by a plot of extinction in magnitudes against wavenumber (λ^{-1}) measured in reciprocal microns (μ^{-1}). This plot, called the extinction 'curve' or 'law', may be determined observationally by Trumpler's colour-difference method in which a reddened star is compared with a star of the same spectral type and low reddening at a number of wavelengths. OB stars are the most suitable for such investigations, in view of their relatively featureless spectra. A schematic extinction curve is shown in fig. 1.1. Early photometric wideband photometry by Stebbins, Huffer and Whitford (1939) confirmed Trumpler's result that the extinction is a roughly linear function of λ^{-1} in the visual region. The six-colour photometry of Stebbins and Whitford (1943, 1945), covering the wavelength range 3500-10300 A, suggested that slight deviations from linearity occur at the ultraviolet and infrared ends of the curves. Multicolour photometry of higher resolution (Whitford, 1958) later showed that there is a distinct change in slope in the curves at $\lambda \sim 4500$ A ($\lambda^{-1} \sim 2.2\ \mu^{-1}$), the slope for $\lambda < 4500$ being less than that for $\lambda > 4500$, as shown in fig. 1.1. This feature is generally referred to as the 'knee' of the curve.

To compare extinction curves observed in different regions of sky it is necessary to apply a process of normalization. This has the effect of standardizing the slope of the visual extinction curve, which would otherwise depend on the degree of reddening. Choosing standard wavelengths λ_1 and λ_2 (see fig. 1.1) the normalized extinction is given by

$$\Delta m'(\lambda) = \frac{\Delta m(\lambda) - \Delta m(\lambda_2)}{\Delta m(\lambda_1) - \Delta m(\lambda_2)} \qquad (1.1)$$

where $\Delta m(\lambda)$ is the magnitude difference between reddened and

unreddened stars at wavelength λ. This allows the extinction laws for stars of different reddening to be compared by direct superposition. An important parameter of the extinction curve is the ratio of total to selective extinction, given by

$$R = \frac{A_V}{E_{B-V}} \qquad (1.2)$$

in the UBV system. A_V is the total visual extinction; E_{B-V} is the colour excess, defined as the difference between the measured B-V colour index of a star and that expected for an unreddened star of the same spectral type. E_{B-V} is a directly measurable quantity but A_V is not, thus a knowledge of the value of R is important in photometric distance determinations. R may be deduced from the observational extinction curve if the way in which the curve approaches the $\Delta m'$ axis in fig. 1.1 is known. $\Delta m'$ is then replaced by an 'absolute' extinction $A(\lambda)$ (fig. 1.2) such that $A(\lambda) \to 0$ as $\lambda^{-1} \to 0$. (It is assumed that there is no neutral absorption; see Dufay, 1957, p. 177). Extrapolation of the observed mean interstellar extinction curve to $\lambda^{-1} = 0$ suggested that $R = 3.0 \pm 0.2$ (Blanco, 1956; Whitford, 1958). R may also be derived by studying the variation in extinction accross a cluster in which the distances of the stars are essentially constant. The apparent and absolute visual magnitudes and colour excesses are related to the distance d by the equation

$$V - M_V = 5 \log d - 5 + R.E_{B-V} \qquad (1.3)$$

thus a plot of $V - M_V$ against E_{B-V} should be linear with slope R. This method was used by Hiltner and Johnson (1956) for the region of h and χ Persei to give the result $R = 3.0 \pm 0.3$. The good agreement between these two independent

methods of obtaining R led to a general adoption of the value R = 3 as normal for the interstellar medium.

It was first noted by Baade and Minkowski (1937) that the extinction of stars in the region of the Orion Nebula (M42) appears to be unusual, a result later confirmed by Stebbins and Whitford (1945). This anomalous behaviour is manifested in the visual region by a greater change in slope at $\lambda \sim 4500$ A compared with the mean extinction curve for stars in other regions of the Milky Way. The extinction on the ultraviolet side of the knee appears to be almost grey for the Orion stars. Baade and Minkowski noted that the particles responsible for the extinction must be larger in the Orion Nebula than in the interstellar medium as a whole, and suggested that the radiation flux from the luminous OB stars in the nebula may cause evaporation of the smaller particles, or their selective expulsion by radiation pressure. Theoretical work by van de Hulst (1949) showed that particles required to give the Orion extinction law are $\sim$ 30% larger than those required for the mean curve. This effect implies that R must be considerably greater in this region than the normal value of 3: Sharpless (1952) derived a value of $R \sim 6$ by the variable extinction method.

From a study of the distribution of stars on the U - B/B - V diagram, Johnson and Morgan (1955) deduced that the extinction in the Cygnus Rift is unusual. The ultraviolet extinction appears to be slightly higher than the interstellar mean in this region, which is an opposite effect to that found in the Orion Nebula. The discrepancy does not apparently lead to an anomalous value of R in Cygnus (Hiltner and Johnson, 1956).

Fig. 1.1 Schematic Normalized Extinction Curve
(based on data of Whitford, 1958)

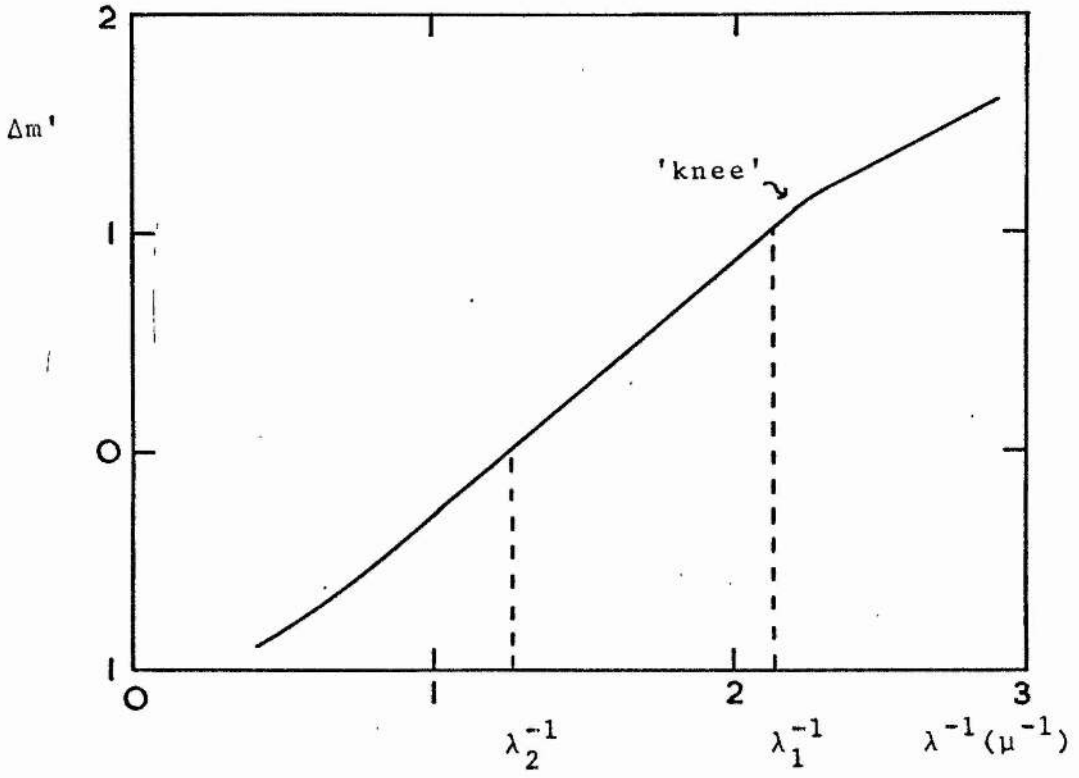

Fig. 1.2 Extinction Curve of Fig. 1.1 above adjusted to an absolute scale by extrapolation to $\lambda^{-1} = 0$

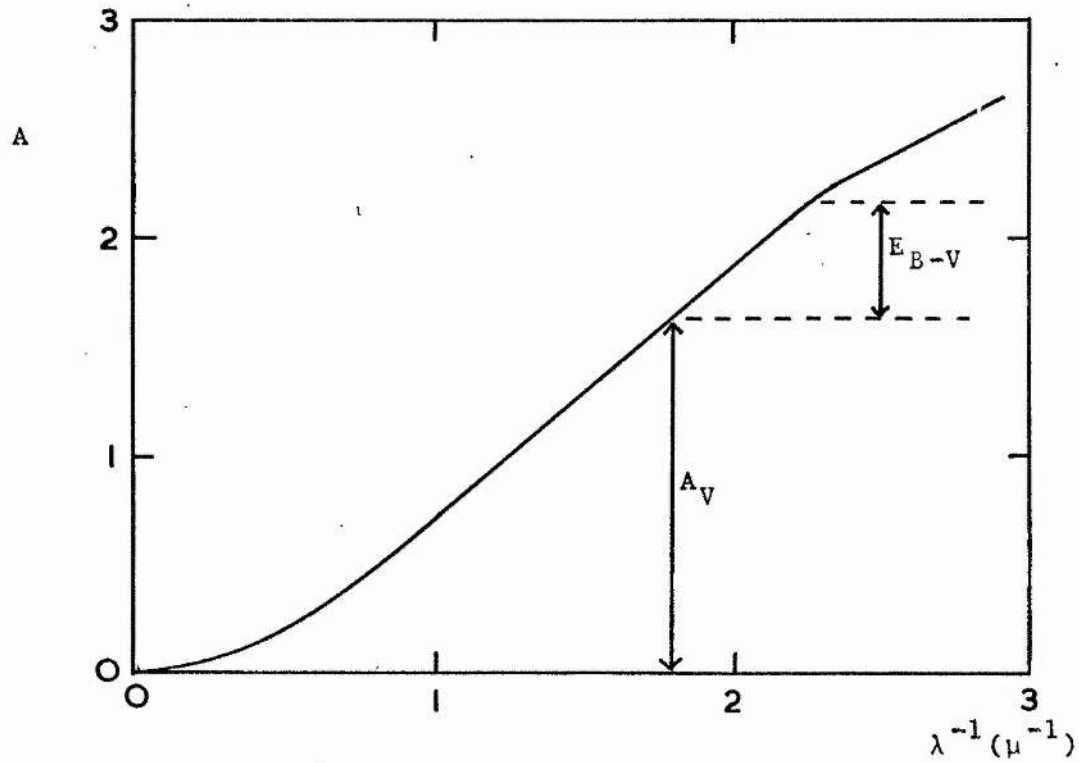

Fig. 1.3 Schematic Extinction Curves based on Satellite Data combined with Visual and Infrared Wideband Photometry (from Bless and Savage, 1972)

Curves are normalized such that $E_{B-V} = 1$

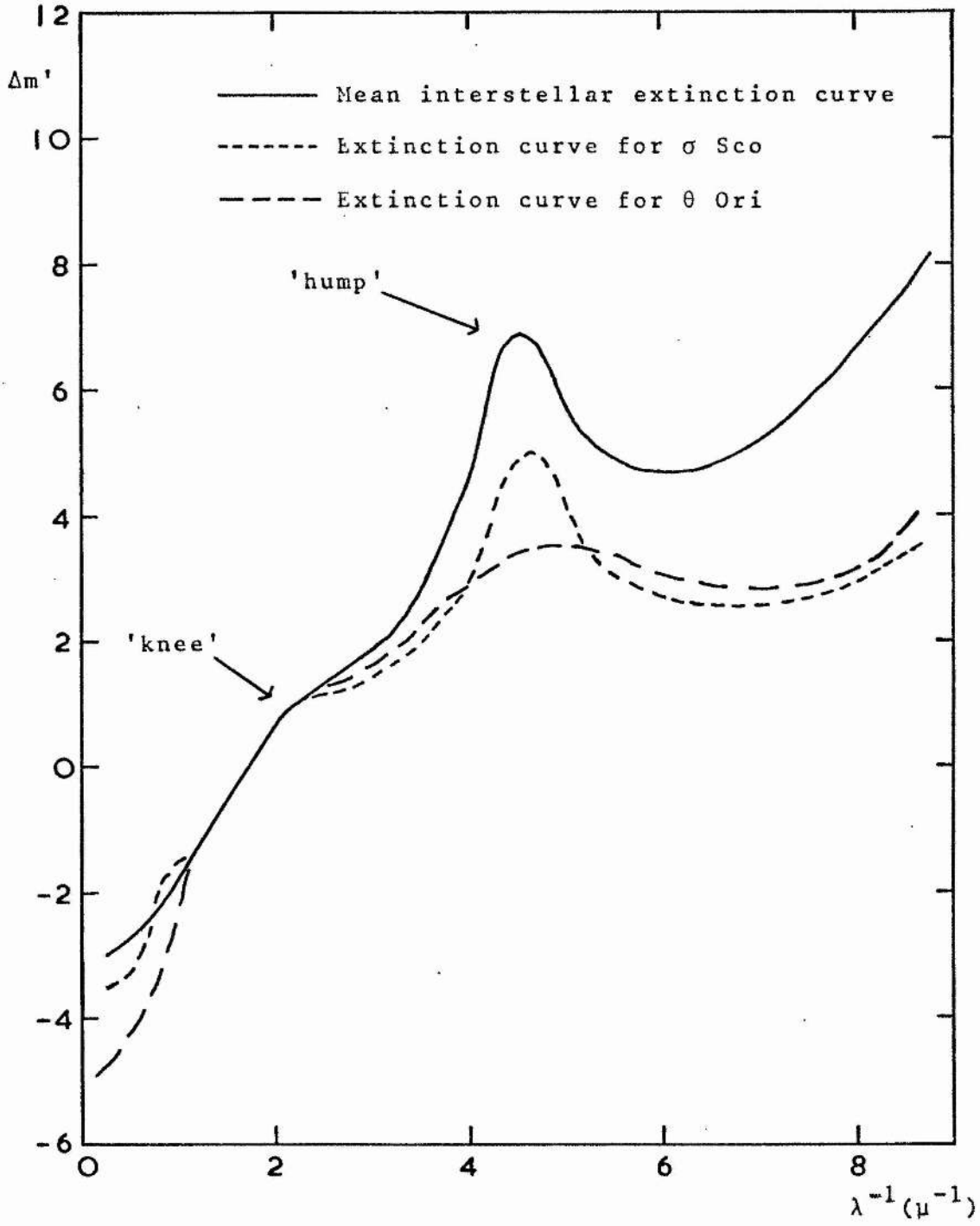

It has been recognised for several decades that certain absorption lines appearing in stellar spectra are of interstellar origin (see, for example, the review of Münch, 1968). These lines result from atomic or molecular transitions in the interstellar gas, and the processes involved in their formation are well understood. The presence of diffuse absorption bands in the spectra of reddened stars was first reported by Merrill (1936) and Merrill and Wilson (1938). These broader features are also generally believed to be interstellar in origin, but they have proved much more difficult to interpret. The principal bands occurring at wavelengths 4430, 4760, 4890 and 6180 A have half-widths of 20-40 A, and the 4430 band has 'wings' extending over about 150 A in all (Wilson, 1958). There are several narrower diffuse bands of half-widths 5-10 A. The strength of the 4430 band correlates moderately well with reddening (Duke, 1951; Binnendijk, 1952) suggesting that the band absorption is associated with the particles responsible for the extinction. The precise mechanism by which the absorption occurs is still a matter of considerable controversy.

The discovery made by Hall (1949) and Hiltner (1949), that the light from many stars is partially plane-polarized, is closely linked with the study of interstellar extinction. The degree of polarization correlates well with reddening, indicating that the polarization is produced by elongated grains which are aligned in some way (see section 2.6). The direction of polarization (i.e. the direction of the E-vector for maximum intensity) for stars lying within a few degrees of the galactic plane is predominantly parallel to the plane (Hall, 1950). There is an indication that the polarization is

parallel to the local spiral arm, as the alignment of the E-vectors is high when the line of sight is perpendicular to the arm and low when it is tangential. Wilson (1960) has suggested that the value of R may depend on the degree of polarization, in which case R may be expected to vary with galactic longitude.

(1.2) More Recent Developments

It appeared at the beginning of the 1960's that the nature of interstellar extinction was established. The extinction curve appeared to show little variation in the regions studied, with the exception of the Orion Nebula, giving a general value of R = 3 for the ratio of total to selective extinction. On the theoretical side, scattering theory applied to submicron-sized ice particles, the existence of which had been postulated by Lindblad (1935), seemed capable of explaining the observed extinction over the whole of the wavelength range then accessible (van de Hulst, 1949).

This state of affairs was short-lived. Johnson and Borgman (1963) found variations from star to star in their extinction curves derived from wideband photometry in the visual and infrared regions, and concluded that there is no unique extinction law. A variable extinction analysis carried out by Fernie and Malborough (1963) for a number of clusters and associations showed some evidence to suggest that R varies with galactic longitude, as predicted by Wilson (1960). Johnson (1968) carried out a comprehensive survey of methods for determining R, combining results from variable extinction, Trumpler's cluster diameter method, and wideband photometry

extending to 12 μ in the infrared. He reports a systematic variation in R between 3.6 and 6.0 in the longitude range $\ell^{II} = 0^{o}$-250^{o}. This effect, if real, would have important implications for the distance scale of the Galaxy. Johnson suggested that the distance to the Galactic Centre would be reduced from 10 to about 8 kpc, and that Oort's constant A would be increased from 15 to about 20 km/sec/kpc. A discrepancy noted by Kraft and Schmidt (1963) and by Stibbs (1964) between the Cepheid distance scale (which assumes R = 3) and that derived from proper motions is removed by application of Johnson's higher R values. However, Schmidt-Kaler (1967) finds that a uniform value of R = 3.2 gives a clearer picture of spiral structure in the distribution of young objects than the proposed variation of R with ℓ^{II}. He suggests that the photometry of Johnson may be affected by infrared excess radiation leading to spuriously high values of R in certain regions. Other investigations of R by various statistical methods have yielded values ranging between 3.1 and 3.6 (Lee, 1970; Bell and FitzGerald, 1971; Martin, 1971; Harris, 1973).

Variations in the extinction law in the Northern Milky Way have been studied by Nandy, using photographic spectrophotometry techniques in the wavelength range 3400-8000 A. He found that the extinction curve could be represented to a first approximation by two straight lines intersecting at 4300 A; the ratio of ultraviolet slope to blue-visual slope varies from region to region, and is greatest in Cygnus (Nandy, 1964, 1965a, 1966, 1967, 1968). Whiteoak (1966) obtained similar results by photoelectric scanner photometry, and showed that the extinction in the remainder of the Orion

region differs from that found in the Nebula. Whiteoak's data also shows some evidence to suggest that broadband structure exists in the quasi-linear sections of the curves. Investigations by Johnson (1967) and Anderson (1970) indicate that anomalies of the type found in the Orion Nebula are a general feature of the extinction curves associated with luminous OB stars imbedded in emission nebulosity.

Perhaps the most spectacular revision of our ideas on the nature of interstellar extinction during the last 12 years has resulted from the extension of spectral coverage into the middle and far ultraviolet. Rocket observations suggested a continued rise in the extinction in the 2500-2200 A region (Boggess and Borgman, 1964) which is contrary to the predictions of the ice grain model. Stecher (1965) reported the presence of a 'hump' in the curves centred at about 2200 A ($4.5\ \mu^{-1}$). Photometry obtained from the OAO satellite has been used to give detailed extinction curves extending from 3600 to 1100 A for a number of brighter reddened stars (Bless and Savage, 1972). The schematic extinction curve shown in fig. 1.3 represents satellite data combined with visual and infrared photometry. The solid line is the mean extinction curve for all the observed stars which do not show Orion-type anomalies; the other curves plotted are for the stars θ^{1+2} Ori, in M42, and σ Sco, which also lies in an H II region. The broad peak at $4.5\ \mu^{-1}$ in the mean curve is followed by a minimum at $\lambda^{-1} \sim 6\ \mu^{-1}$, and a steep rise in the far ultraviolet. In both of the other curves the extinction is virtually independent of wavelength for $\lambda^{-1} > 5.5\ \mu^{-1}$, and the 'hump' is very weak in the Orion curve. The implications of these results for the grain models used in theoretical

investigations are discussed in section 2.5.

Much of the work reviewed in this chapter, particularly that concerned with the value of R, was motivated not so much by an interest in the dust itself, but by a desire to correct photometric data for its presence. Whilst this remains a prime consideration to the optical astronomer, recent developments in other branches of astronomy have broadened interest in the subject. The radio detection of a large number of interstellar molecules has raised theoretical problems in explaining their origin. Molecule formation by a direct two-body encounter, in which the excess energy and momentum are removed by emission of a photon, is a highly improbable process. It seems much more feasible that formation occurs on the surface of grains, as the excess energy and momentum may then be absorbed by the grain lattice (see, for example, Gould and Salpeter, 1963). This is consistent with the observed correlation between regions of high grain density and strong molecular emission. It is likely that grains also play an important role in star formation. Reddish (1967) noted that the most luminous stars in young clusters tend to have the highest colour excesses, suggesting that they are surrounded by compact circumstellar dust shells from which they may have condensed. The energy balance between gravitational contraction and thermal expansion is delicate in a condensing protostar; the grains may act as a catalyst by removing excess heat by infrared radiation, thus allowing contraction to continue. The amount of dust present may well influence the eventual position of the protostar on the HR diagram (Reddish, 1973). Models involving dense dust clouds

have been invoked to explain powerful infrared sources such as that discovered by Becklin and Neugebauer (1967) in the Orion Nebula. The source is assumed to be a super-luminous star, which may be obscured by a cloud of exceptionally high optical depth. (The total visual absorption required is $A_V \sim 80^m$). Alternatively, the dust may take the form of a circumstellar shell which absorbs the ultraviolet flux from the star and reradiates in the infrared (see the discussion of Allen and Penston, 1974). A knowledge of the size, composition and space distribution of the dust grains is thus of general interest, and is of major importance to theoretical work on the early stages of stellar evolution and the chemical state of the interstellar medium as a whole.

In this and the preceding section I have tried to present a concise historical account of the main observational investigations relating to interstellar extinction, and to underline the importance of the grains in modern astronomy. Theoretical aspects of the subject are reviewed in chapter 2. Certain other areas of observation, such as the infrared spectra of cool stars, the diffuse galactic light, and the wavelength-dependence of interstellar polarization, are of relevance to theoretical models adopted for the grains and are discussed at the appropriate points in chapter 2. For further discussion of both observational and theoretical aspects the reader is referred to: Sharpless (1963); Wickramasinghe (1967); Greenberg (1968); Lynds and Wickramasinghe (1968); Wickramasinghe and Nandy (1972); Aannestad and Purcell (1973), and papers presented at the IAU Symposium No. 52 on 'Interstellar Dust and Related Topics',

held at Albany, New York in 1972 (editors: J. M. Greenberg and H. C. van de Hulst).

(1.3) General Aims

Detailed observational studies of the extinction law have so far been largely confined to the Northern Hemisphere: the Southern Milky Way, extending from $\ell^{II} = 250^{o}$ through the Galactic Centre to $\ell^{II} = 30^{o}$, is relatively unexplored. The results of Johnson (1968) and Bless and Savage (1972) for a small sample of stars in the Sco-Oph-Sgr region show variations on a similar scale to those found by Nandy (1964-1968) and Whiteoak (1966) in the North. Honeycutt and Chaldu (1970) found an extinction law similar to that in Cygnus in a limited region of Ara. The main purpose of the work described in this thesis is to derive extinction curves over a wide spectral range for early-type stars distributed along the Southern Milky Way, with a view to studying any variation in the curves and any possible longitude dependence of the associated R values. It is also intended to study interesting regions, such as the complexes associated with η Carinae and ρ Ophiuchi, to test for local anomalies.

Recent advances in instrumentation are of major importance to ground-based studies of the extinction law. In particular, the development of photoelectric spectral scanners has provided an efficient and accurate means of investigation by the colour difference method over the spectral range extending from the near infrared to the limit of atmospheric transparency in the ultraviolet. Scanners are also capable of sufficiently high resolution to permit a study of band

structure in the curves. Combination of scanner data with infrared wideband photometry gives a total spectral coverage of 0.34-3.5 μ, the long wavelength limit being set by the faintness of the blue comparison stars in the infrared. The stars selected for this investigation have visual magnitudes between 4.0 and 8.5, thus telescopes of intermediate aperture are required.

Although this investigation is primarily an observational one, the interpretation of results is closely linked with theoretical considerations. The principle objection raised to the large R values quoted by Johnson (1968) is the possibility of infrared excess radiation, probably arising from dust emission, causing distortion of the extinction curves at wavelengths greater than about 2 μ. Theoretical model fitting provides a means of overcoming this difficulty.

CHAPTER 2

THEORETICAL CONSIDERATIONS

(2.1) Light Scattering by Spherical Grains

The theory of light scattering by small particles is fundamental to a study of interstellar extinction. As noted in chapter 1, scattering by atoms, molecules or other particles small compared with the wavelength is expected to produce extinction with a λ^{-4} dependence from the Rayleigh theory. The fact that the extinction has been found observationally to follow a λ^{-1} law to a first approximation in the visual and near infrared regions suggests that scattering by particles of non-negligible size must be considered.

Energy is removed from light incident on a homogeneous spherical particle of radius a by absorption, in which radiant energy is converted into internal energy of the particle lattice, and by scattering. If I_o is the original intensity of the beam the light received by a distant observer is reduced to $I_o C_{ext}$, where C_{ext} is the cross-section for extinction given by

$$C_{ext} = C_{abs} + C_{sca}, \qquad (2.1)$$

C_{abs} and C_{sca} being the cross-sections for absorption and scattering. The efficiency factors for extinction, absorption and scattering are defined:

$$\left.\begin{aligned} Q_{ext} &= \frac{C_{ext}}{\pi a^2} \\ Q_{abs} &= \frac{C_{abs}}{\pi a^2} \\ Q_{sca} &= \frac{C_{sca}}{\pi a^2} \end{aligned}\right\} \qquad (2.2)$$

and thus from equ.(2.1)

$$Q_{ext} = Q_{abs} + Q_{sca} \tag{2.3}$$

The albedo of the particle is defined:

$$\gamma = \frac{Q_{sca}}{Q_{ext}}. \tag{2.4}$$

For a pure dielectric $Q_{abs} = 0$, thus $Q_{ext} = Q_{sca}$ and $\gamma = 1$; for absorbing spheres, $0 < \gamma < 1$.

The efficiency factors are in general functions of the wavelength of the incident light, and of the particle size and refractive index. The problem of deriving their dependence on these factors is, in principle, that of solving Maxwell's equations with appropriate boundary conditions at the grain surface. The solution was first formulated by Mie (1908) and independently by Debye (1909). Detailed accounts of their solution have more recently been given by Stratton (1941) and van de Hulst (1957), and only the basic results are given here.

It is convenient to define a dimensionless size parameter x given by

$$x = \frac{2\pi a}{\lambda} \tag{2.5}$$

and a parameter y given by

$$y = mx, \tag{2.6}$$

where

$$m = n - ik \tag{2.7}$$

is the complex refractive index of the grain, and n and k are the refractive and absorptive optical constants. The Mie solution gives the following formulae for Q_{sca} and Q_{ext}

(see, for example, Wickramasinghe, 1967):

$$Q_{sca} = \frac{2}{x^2} \sum_{n=1}^{\infty} (2n + 1)(|a_n|^2 + |b_n|^2), \qquad (2.8)$$

$$Q_{ext} = \frac{2}{x^2} \sum_{n=1}^{\infty} (2n + 1)\mathrm{Re}(a_n + b_n), \qquad (2.9)$$

where

$$a_n = \frac{x\psi_n'(y)\psi_n(x) - y\psi_n'(x)\psi_n(y)}{x\psi_n'(y)\zeta_n(x) - y\zeta_n'(x)\psi_n(y)} \qquad (2.10)$$

and

$$b_n = \frac{y\psi_n'(y)\psi_n(x) - x\psi_n'(x)\psi_n(y)}{x\psi_n'(y)\zeta_n(x) - y\zeta_n'(x)\psi_n(y)}. \qquad (2.11)$$

The functions $\psi_n(z)$ and $\zeta_n(z)$ are the Riccati-Bessel functions for a complex variable z. They are defined in terms of the Bessel functions $J_n(z)$ as follows:

$$\psi_n(z) = \left(\frac{\pi z}{2}\right)^{\frac{1}{2}} J_{n+\frac{1}{2}}(z), \qquad (2.12)$$

$$\zeta_n(z) = \left(\frac{\pi z}{2}\right)^{\frac{1}{2}} \{J_{n+\frac{1}{2}}(z) + i(-1)^n J_{-n-\frac{1}{2}}(z)\}. \qquad (2.13)$$

The third Riccati-Bessel function is

$$\chi_n(z) = (-1)^n \left(\frac{\pi z}{2}\right)^{\frac{1}{2}} J_{-n-\frac{1}{2}}(z) \qquad (2.14)$$

where

$$\zeta_n(z) = \psi_n(z) + i\chi_n(z) \qquad (2.15)$$

The procedure for evaluating Q_{ext} and Q_{sca} from equ. (2.8) and (2.9) by means of these identities is outlined in the next section.

In addition to these efficiency factors, the Mie theory allows computation of the light scattering in a given direction. The phase function $S(\theta)$ is defined such that the light intensity scattered into unit solid angle about the direction

making an angle θ with the direction of incidence is $I_o S(\theta)$. The total scattering cross-section is then given by

$$C_{sca} = \int_0^{\pi}\int_0^{2\pi} S(\theta)\sin\theta d\theta d\phi,$$

i.e.
$$C_{sca} = 2\pi\int_0^{\pi} S(\theta)\sin\theta d\theta. \qquad (2.16)$$

The mean value of $\cos\theta$ is a useful quantity as it measures the forward directivity of the scattered light. This is defined

$$\langle\cos\theta\rangle = \frac{\int_0^{\pi} S(\theta)\sin\theta\cos\theta d\theta}{\int_0^{\pi} S(\theta)\sin\theta d\theta}. \qquad (2.17)$$

The value of $\langle\cos\theta\rangle$ varies between 0 and 1, $\langle\cos\theta\rangle = 0$ implying spherical symmetry and $\langle\cos\theta\rangle = 1$ entirely forwardly directed scattering. A fraction $\langle\cos\theta\rangle$ of the scattered energy is resupplied to the transmitted beam, while the absorbed flux $I_o\pi a^2 Q_{abs}$ is lost. Thus the total energy flux removed from the forward beam is

$$I_o\pi a^2(Q_{abs} + Q_{sca} - \langle\cos\theta\rangle Q_{sca})$$
$$= I_o\pi a^2(Q_{ext} - \langle\cos\theta\rangle Q_{sca})$$

using equ. (2.3). The quantity

$$Q_{pr} = (Q_{ext} - \langle\cos\theta\rangle Q_{sca}) \qquad (2.18)$$

is called the efficiency factor for radiation pressure. The forward momentum removed from the beam is

$$p = \frac{I_o\pi a^2 Q_{pr}}{c} \qquad (2.19)$$

which is equal to the radiation pressure on the grain.

(2.2) Procedure for evaluating the Mie Formulae

In order to compute values of the efficiency factors Q_{ext} and Q_{sca} from the Mie formulae (equ. 2.8 and 2.9), a_n and b_n must be evaluated for given values of m and x.

It is helpful to define the function

$$\Omega_n(y) = \frac{\psi_n'(y)}{\psi_n(y)}. \qquad (2.20)$$

Using this definition and recurrence relations for the Bessel functions in equ. (2.12) and (2.13), it can be shown that equ. (2.10) and (2.11) reduce to

$$a_n = \frac{\left(\frac{\Omega_n(y)}{m} + \frac{n}{x}\right)\mathrm{Re}\{\zeta_n(x)\} - \mathrm{Re}\{\zeta_{n-1}(x)\}}{\left(\frac{\Omega_n(y)}{m} + \frac{n}{x}\right)\zeta_n(x) - \zeta_{n-1}(x)} \qquad (2.21)$$

and

$$b_n = \frac{\left(m\Omega_n(y) + \frac{n}{x}\right)\mathrm{Re}\{\zeta_n(x)\} - \mathrm{Re}\{\zeta_{n-1}(x)\}}{\left(m\Omega_n(y) + \frac{n}{x}\right)\zeta_n(x) - \zeta_{n-1}(x)} \qquad (2.22)$$

(See Wickramasinghe, 1967, p.11; Wickramasinghe, 1973, p.26).

The following recurrence relation holds for $\zeta_n(x)$:

$$\zeta_n(x) = \frac{(2n-1)}{x}\zeta_{n-1}(x) - \zeta_{n-2}(x) \qquad (2.23)$$

and from equ. (2.13)

$$\zeta_o(x) = \left(\frac{\pi x}{2}\right)^{\frac{1}{2}}\{J_{\frac{1}{2}}(x) + iJ_{-\frac{1}{2}}(x)\}.$$

Thus

$$\zeta_o(x) = \sin x + i\cos x \qquad (2.24)$$

since

$$J_{\frac{1}{2}}(x) = \left(\frac{\pi x}{2}\right)^{-\frac{1}{2}} \sin x$$

and

$$J_{-\frac{1}{2}}(x) = \left(\frac{\pi x}{2}\right)^{-\frac{1}{2}} \cos x.$$

Similarly, we have

$$\zeta_{-1}(x) = \cos x - i \sin x. \qquad (2.25)$$

For $\Omega_n(y)$ the recurrence relation is

$$\Omega_n(y) = \frac{-n}{y} + \left(\frac{n}{y} - \Omega_{n-1}(y)\right)^{-1} \qquad (2.26)$$

and from equ. (2.20) and (2.12)

$$\Omega_o(y) = \frac{\cos y}{\sin y} \qquad (2.27)$$

Equations (2.23) to (2.27) enable the functions $\zeta_n(x)$ and $\Omega_n(y)$ to be generated for n = 1,2,3,... and substitution in equ. (2.21) and (2.22) gives a_n and b_n. The series to be summed in equ. (2.8) and (2.9) generally converge fairly rapidly; the number of terms required to reach a given order of accuracy increases with x, but for most practical purposes no more than about 20 terms are needed.

(2.3) The Equation of Transfer and the Extinction Curve

Suppose that spherical grains of constant radius are distributed evenly with number density N_g per unit volume along the line of sight to a star. The reduction in intensity of the starlight due to extinction may be derived by considering the energy transfer through a cylindrical element of length $d\ell$ and cross-sectional area dS with its axis aligned along the line of sight (fig. 2.1). If the intensity of radiation entering the cylinder in the frequency interval ν to $\nu + d\nu$ is I_ν, then the energy flowing into the cylinder in unit time is

$$I_\nu d\nu dS$$

and the energy flowing out per unit time is

$$(I_\nu + dI_\nu)d\nu dS.$$

Fig. 2.1 Cylindrical Element considered in Section 2.3

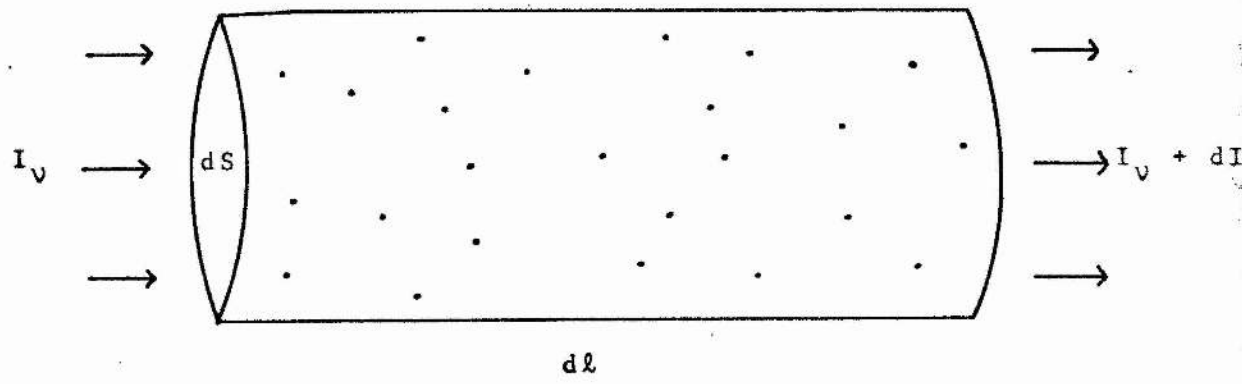

The energy absorbed and scattered by each grain is

$$I_\nu d\nu \pi a^2 Q_{ext}$$

and the number of grains in the element is

$$N_g dS d\ell .$$

Thus by conservation of energy

$$I_\nu d\nu dS = (I_\nu + dI_\nu) d\nu dS + I_\nu d\nu \pi a^2 Q_{ext} N_g dS d\ell$$

which reduces to

$$\frac{dI_\nu}{I_\nu} = -N_g \pi a^2 Q_{ext} d\ell . \qquad (2.28)$$

Integration of equ. (2.28) gives

$$\ln I_\nu = -N_g \pi a^2 Q_{ext} \ell + \text{const.}$$

If $I_\nu = I_\nu^o$ when $\ell = 0$, the constant term is $\ln I_\nu^o$ and thus

$$\frac{I_\nu}{I_\nu^o} = \exp(-N_g \pi a^2 Q_{ext} \ell) . \qquad (2.29)$$

Substituting $N = N_g \ell$ for the total number of grains along the line of sight,

$$\frac{I_\nu}{I_\nu^o} = \exp(-N \pi a^2 Q_{ext}) . \qquad (2.30)$$

Thus the intensity is reduced by a factor $\exp(-\tau)$ where

$$\tau = N \pi a^2 Q_{ext} \qquad (2.31)$$

is the optical depth. Expressing this intensity change in magnitudes,

$$\Delta m = -2.5 \log \frac{I_\nu}{I_\nu^o}$$

and from equ. (2.30)

$$\Delta m = 1.086 N \pi a^2 Q_{ext} \qquad (2.32)$$

or

$$\Delta m = 1.086 \tau .$$

The total extinction in magnitudes produced by N identical grains along the line of sight is therefore directly proportional to Q_{ext}. The expected extinction curve for given values of the grain size and complex refractive index may thus be computed from equ. (2.9) using the procedure outlined in the previous section. The constant of proportionality may be removed by normalization: choosing standard wavelengths λ_1 and λ_2, the theoretical extinction curve is given by

$$\left.\begin{aligned} \Delta m'(\lambda)_{theor} &= \frac{\Delta m(\lambda) - \Delta m(\lambda_2)}{\Delta m(\lambda_1) - \Delta m(\lambda_2)} \\ &= \frac{Q_{ext}(\lambda) - Q_{ext}(\lambda_2)}{Q_{ext}(\lambda_1) - Q_{ext}(\lambda_2)} \end{aligned}\right\} \quad (2.33)$$

If a series of monochromatic magnitudes $m(\lambda_i)$ are measured observationally for a pair of stars of high and low reddening, then

$$\left.\begin{aligned} m_1(\lambda_i) - M_1(\lambda_i) &= 5\log d_1 - 5 + A_1(\lambda_i) \\ \text{and} \\ m_2(\lambda_i) - M_2(\lambda_i) &= 5\log d_2 - 5 + A_2(\lambda_i) \end{aligned}\right\} \quad (2.34)$$

where $M(\lambda_i)$ and $A(\lambda_i)$ are the absolute magnitudes and extinctions at wavelengths λ_i and d is the distance in parsecs, the subscripts 1 and 2 referring to the reddened and comparison stars respectively. In the ideal case where the two stars have identical intrinsic energy distributions and the comparison star is completely unreddened, we have $M_1(\lambda_i) = M_2(\lambda_i)$ and $A_2(\lambda_i) = 0$. Thus the difference in apparent magnitude is

$$\left.\begin{aligned} \Delta m(\lambda_i) &= m_1(\lambda_i) - m_2(\lambda_i) \\ &= 5\log\left(\frac{d_1}{d_2}\right) + A_1(\lambda_i). \end{aligned}\right\} \quad (2.35)$$

Again the constant term $5\log(d_1/d_2)$ may be eliminated by normalization, and the observational extinction curve is given by

$$\left.\begin{aligned}\Delta m'(\lambda_i)_{obs} &= \frac{\Delta m(\lambda_i) - \Delta m(\lambda_2)}{\Delta m(\lambda_1) - \Delta m(\lambda_2)} \\ &= \frac{A_1(\lambda) - A_1(\lambda_2)}{A_1(\lambda_1) - A_1(\lambda_2)}\end{aligned}\right\} \qquad (2.36)$$

The theoretical problem is to find a grain model which produces a theoretical extinction curve $\Delta m'(\lambda)_{theor}$ which is in agreement with the observational extinction curve $\Delta m(\lambda)_{obs}$. Some grain models which have been considered are discussed in section (2.5).

(2.4) The Distribution Function for Grain Sizes

The equation (2.32) relating extinction to Q_{ext} was derived in the previous section for spherical grains of constant radius. In parctice it is preferable to consider a distribution of grain sizes when computing theoretical extinction curves for comparison with observational data. Resonance peaks tend to occur at certain size-dependent wavelengths for single grain sizes, which may be smoothed out by integration over a size distribution. Let us therefore consider a distribution function n(a) such that the number of grains with radii in the range a to a + da is n(a)da. Equ. (2.32) then becomes

$$\Delta m = 1.086\pi \int_0^\infty a^2 Q_{ext} n(a)da. \qquad (2.37)$$

Following the work of Lindblad (1935) on the condensation of grains from the interstellar gas, Oort and van de Hulst (1946) derived a distribution function by

assuming a state of equilibrium between rates of formation and collisional destruction of ice grains. (See also Oort, 1946). The mathematical form of the function is complicated, but Wickramasinghe (1967, chapter 7) has introduced an approximation to the Oort-van de Hulst formula for the destruction probability which reduces the distribution function to the form

$$n(a) = n(0)\exp\left\{-\left(\frac{a}{a_o}\right)^4\right\} \qquad (2.38)$$

where a_o is a constant. The destruction probability used depends on the particle size. Wickramasinghe et al (1966) have shown that for a size-independent destruction probability the distribution function becomes

$$n(a) = n(0)\exp\left(-\frac{a}{a_o}\right) \qquad (2.39)$$

which gives a rather better fit to observational data in the ultraviolet (see next section).

More recent investigators have favoured either a Gaussian size distribution or one of the general form

$$n(a) = Aa^{\alpha}\exp\{-Ba^{\beta}\} \qquad (2.40)$$

where A, B, α and β are constants (Wickramasinghe and Nandy 1970, 1971; Nandy and Wickramasinghe, 1971). This type of function has the property that $n(a) \to 0$ as $a \to 0$ for $\alpha \neq 0$, and has a maximum at some finite non-zero radius a_m called the characteristic size. (The Oort-van de Hulst distribution tends to a maximum as $a \to 0$). Particle distributions of the form of equ. (2.40) have been used by Diermendjian (1969) to describe the properties of terrestrial clouds. There is, of course, no direct evidence to support any one particular

distribution function for interstellar particles; however, Wickramasinghe and Nandy (1971) pointed out that quite different functions lead to similar theoretical extinction curves for a given value of the characteristic size, and so the problem is not critical. The characteristic size of the distribution and the optical constants of the grains are the major parameters in determining the shape of the curve. The former is related to the constant B in equ. (2.40) as follows. Differentiation of equ. (2.40) with respect to a gives

$$n'(a) = A(\alpha a^{\alpha-1} - a^{\alpha} B\beta a^{\beta-1}) \exp\{-Ba^{\beta}\}$$

and putting $a = a_m$ when $n'(a) = 0$ gives

$$B = \frac{\alpha}{\beta a_m^{\beta}}.$$

Substituting into equ. (2.40), we have

$$n(a) = Aa^{\alpha} \exp\left\{\frac{-\alpha}{\beta}\left(\frac{a}{a_m}\right)^{\beta}\right\} \qquad (2.41)$$

Wickramasinghe and Nandy used a function of this form with $\alpha = 3/2$ and $\beta = 3$.

(2.5) Theoretical Extinction Curves for different Grain Models

Early investigators assumed, following the Lindblad theory of grain formation, that the interstellar dust consists of solid H_2O, NH_3 or CH_4 particles (loosely referred to as 'ice'). Extinction curves for such particles with a constant real refractive index of m = 1.33 and sizes following the Oort-van de Hulst distribution were computed by van de Hulst (1949). These gave excellent fits to the observed extinction curves in the visual and near infrared, and for a number of years it

was believed that the nature of interstellar grains had been established. More recent observations in the ultraviolet and infrared have led to the downfall of the ice theory. Fig. 2.2 shows a van de Hulst curve (solid line) compared with observational points of Johnson and Borgman (1963) and Boggess and Borgman (1964). Also shown is the curve for the modified distribution of Wickramasinghe et al (1966) discussed in the previous section (broken line), using $a_o = 0.075\ \mu$ in equ. (2.39). Both theoretical curves agree quite well with the observational points for $\lambda^{-1} < 2.7\ \mu^{-1}$ but fail in the ultraviolet. This implies that ice grains alone cannot explain the observed extinction curve, but does not rule out the possibility of a model involving ice mixed with another substance. However, attempts to detect the 3.1 μ vibrational absorption band expected for solid H_2O in the infrared spectra of highly reddened stars have been unsuccessful (Danielson et al, 1965; Knacke et al, 1969a); thus, as there is no reason to suppose that NH_3 and CH_4 are more likely to condense in the interstellar medium than H_2O, ice must be ruled out as a major constituent of the grains. Recently Gillett and Forrest (1973) have detected a 3.1 μ feature in the spectrum of the Becklin-Neugebauer infrared source in the Orion Nebula, the strength of which indicates that no more than $\sim$ 7% of the total extinction may be due to H_2O grains.

It was suggested by Hoyle and Wickramasinghe (1962) that graphite particles may condense in the atmospheres of carbon-rich N stars, and may then be ejected into space by radiation pressure. The discovery of the ultraviolet hump at $\lambda \sim 2200$ A

in the observational extinction curve strongly suggests that graphite grains are indeed present in the interstellar medium. The optical constants of bulk graphite measured by Taft and Philipp (1965) show a feature close to this wavelength arising from a transition of π electrons to the conduction band. This produces a peak in the theoretical extinction curve for particles of size $\sim$ 0.05 μ which resembles the observed hump quite closely (Stecher and Donn, 1965; Wickramasinghe and Guillaume, 1965). However, observations in the far ultraviolet show that the extinction continues to rise beyond the hump (Bless et al, 1968; Bless and Savage, 1972) whereas the theoretical curves for graphite fall off for $\lambda^{-1} > 5\ \mu^{-1}$. This is illustrated in fig. 2.3 (from Wickramasinghe and Nandy, 1972). Graphite particles cannot therefore be solely responsible for the extinction. Models involving graphite grains coated with ice mantles give a better fit to the data (Wickramasinghe and Krishna Swamy, 1967; Krishna Swamy and O'Dell, 1967), but these are subject to the objection noted in the previous paragraph regarding the non-detection of the 3.1 μ H_2O ice band.

Theoretical investigations into the possibility that grains may condense in the atmospheres of oxygen-rich M-type giant stars have been carried out by Kamijo (1963), Hoyle and Wickramasinghe (1968) and Gilman (1969). Likely candidates for formation in this medium are iron, magnesium oxide, quartz (SiO_2) and various types of silicate grains such as olivine ($MgSiO_3$) or enstatite ($MgFeSiO_4$). Silicates possess characteristic spectral features at 10 μ and 20 μ in the infrared, which arise from 'stretching' and 'bending'

vibrations of the Si-O bond. A band has been detected in emission in the spectra of several red giants, and tentatively identified as being due to silicates (Woolf and Ney, 1969; Knacke et al, 1969b; Ney and Allen, 1969; Stein and Gillett, 1969). An emission band at 20 μ has been observed by Low and Krishna Swamy (1970) in the spectrum of α Orionis. The 10 μ band has also been observed in absorption towards the Galactic Centre infrared source (Hackwell et al, 1970) and the Becklin-Neugebauer object (Gillett and Forrest, 1973), but attempts to detect it in the spectra of reddened B stars have so far been unsuccessful (Hackwell et al, 1970; Stein and Gillett, 1971).

There is thus strong circumstantial evidence to suggest the presence of both graphite and silicate grains in the interstellar medium. Hoyle and Wickramasinghe (1969) computed extinction for a mixture of these grains, and showed that a reasonably good fit to the observations is possible over all of the accessible wavelength range. The ultraviolet albedo of the grains predicted by this model is $\gamma \simeq 0.7$. This is in disagreement with the results of Lillie and Witt (1969) who deduced from observations of the diffuse galactic light that $\gamma = 0.2 \pm 0.2$ in the 2100-2800 A region. Witt and Lillie (1973) have determined the wavelength-dependence of the albedo, and find that it shows a minimum at $\lambda \sim 2200$ A probably related to the feature at this wavelength in the extinction, and a sharp rise in the far ultraviolet.

Wickramasinghe and Nandy (1970, 1971, hereafter referred to as WN) showed that more satisfactory agreement with the albedo data is given by a graphite, iron and silicate grain

model. They computed curves for various proportions of these materials, and found that best results were produced using the characteristic sizes

$$a_m(gr) \simeq 0.05\ \mu$$
$$a_m(iron) \simeq 0.02\ \mu$$
$$a_m(sil) \simeq 0.15\ \mu$$

in the distribution function (equ. 2.41). The relative contributions of the components are illustrated in fig. 2.4 for the case where the extinction at 4500 A is in the proportion 3 : 0.611 : 1 for graphite, iron and silicate grains. Graphite contributes to the visual and infrared extinction as well as producing the 4.5 μ^{-1} peak; the choice of size for the graphite grains is largely responsible for the change in slope in the total curve at $\lambda^{-1} \sim 2.2\ \mu^{-1}$, corresponding to the knee in the observed extinction curves. The extinction of the iron component has little effect at longer wavelengths, but increases rapidly towards the far ultraviolet, producing the required rise. The silicates contribute largely in the visual region. The albedo for this model is consistent with the observations of Lillie and Witt. The slope of the curve in the far ultraviolet and the height of the 4.5 μ^{-1} hump may be varied by adjusting the proportion of extinction arising from the different grain species, in order to match the data for individual stars. given by Bless and Savage (1972). Nandy and Wickramasinghe (1971) showed that a good fit to the extinction curve for stars in the Orion Nebula may be obtained by reducing the relative contributions from the graphite and iron grains and by increasing the characteristic size of the silicates.

Fig. 2.2 Theoretical Extinction Curves for Ice Grains compared with Observational Data

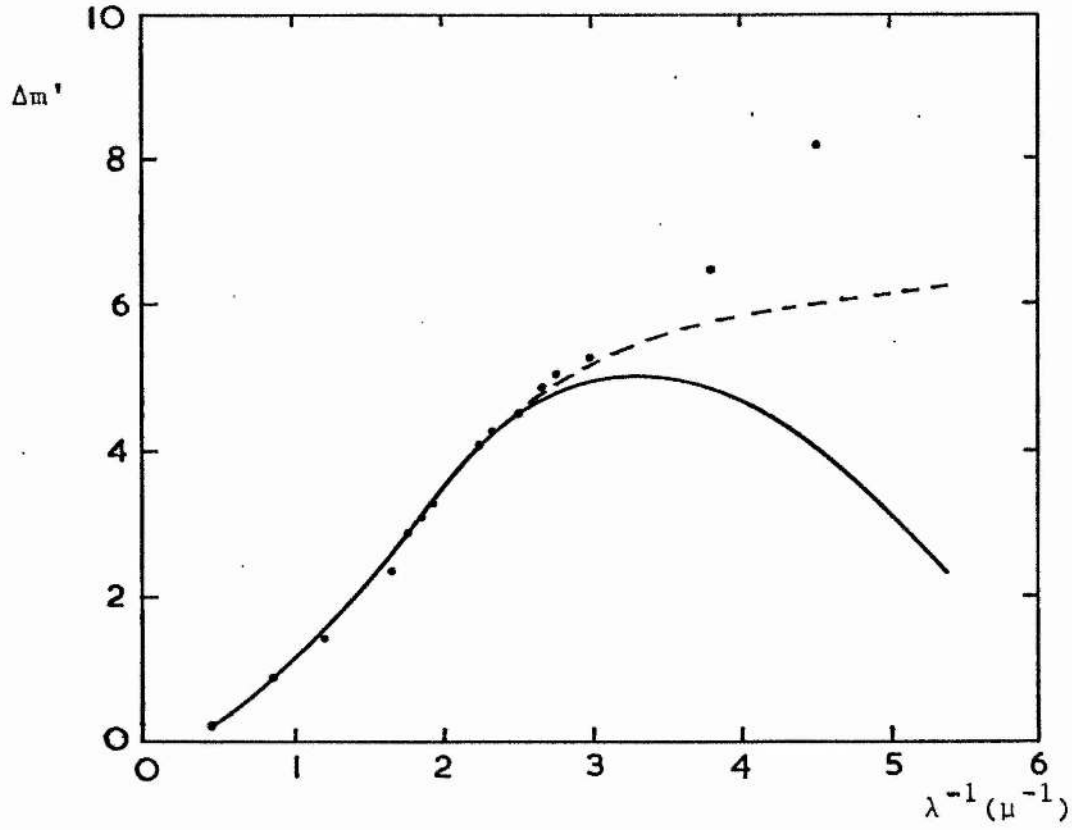

Fig. 2.3 Theoretical extinction curves for graphite grains compared with observational data

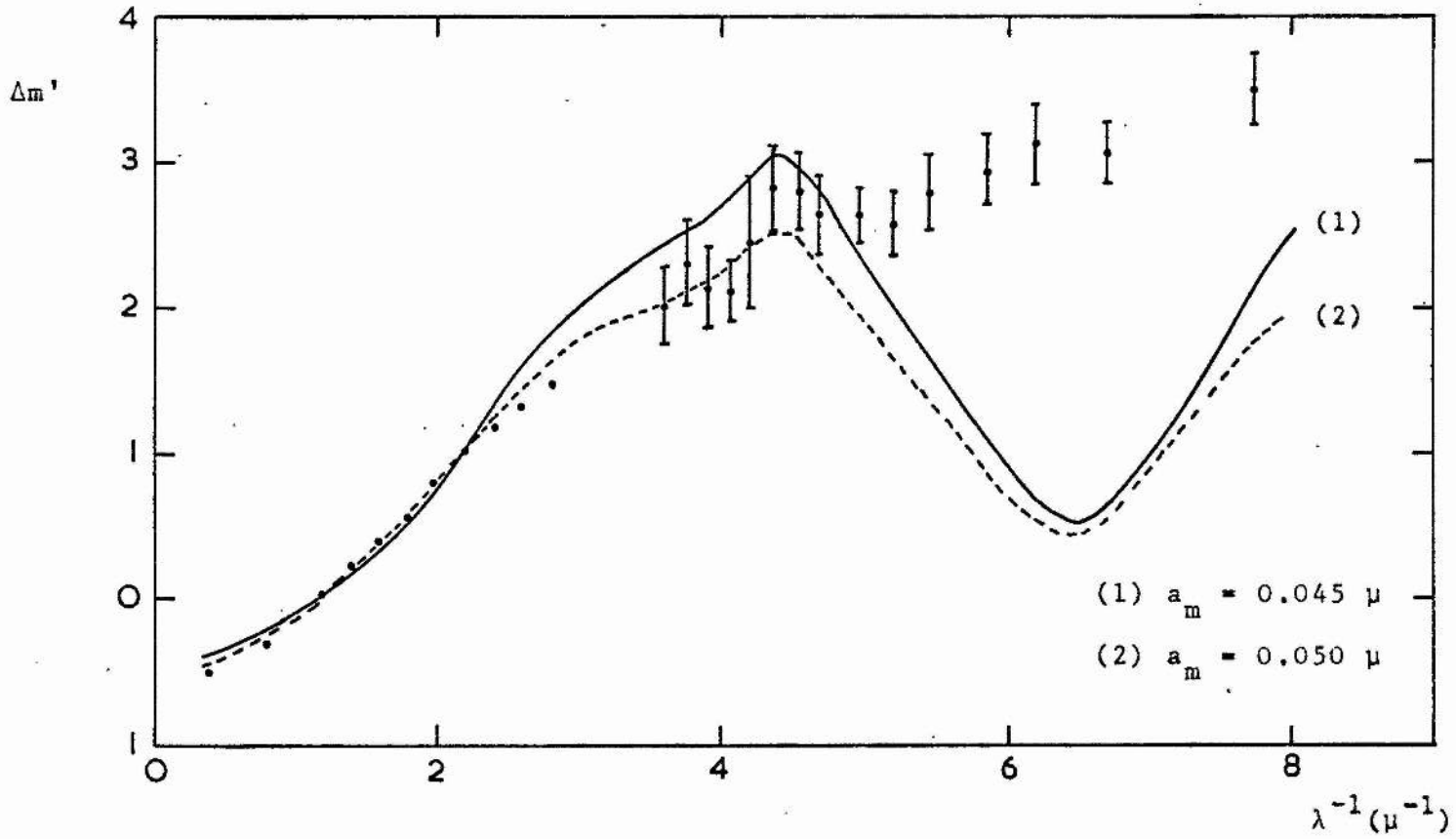

Fig. 2.4 Relative contributions of graphite, iron and silicates to the theoretical extinction (curve No. 9) of Wickramasinghe and Nandy (1971)

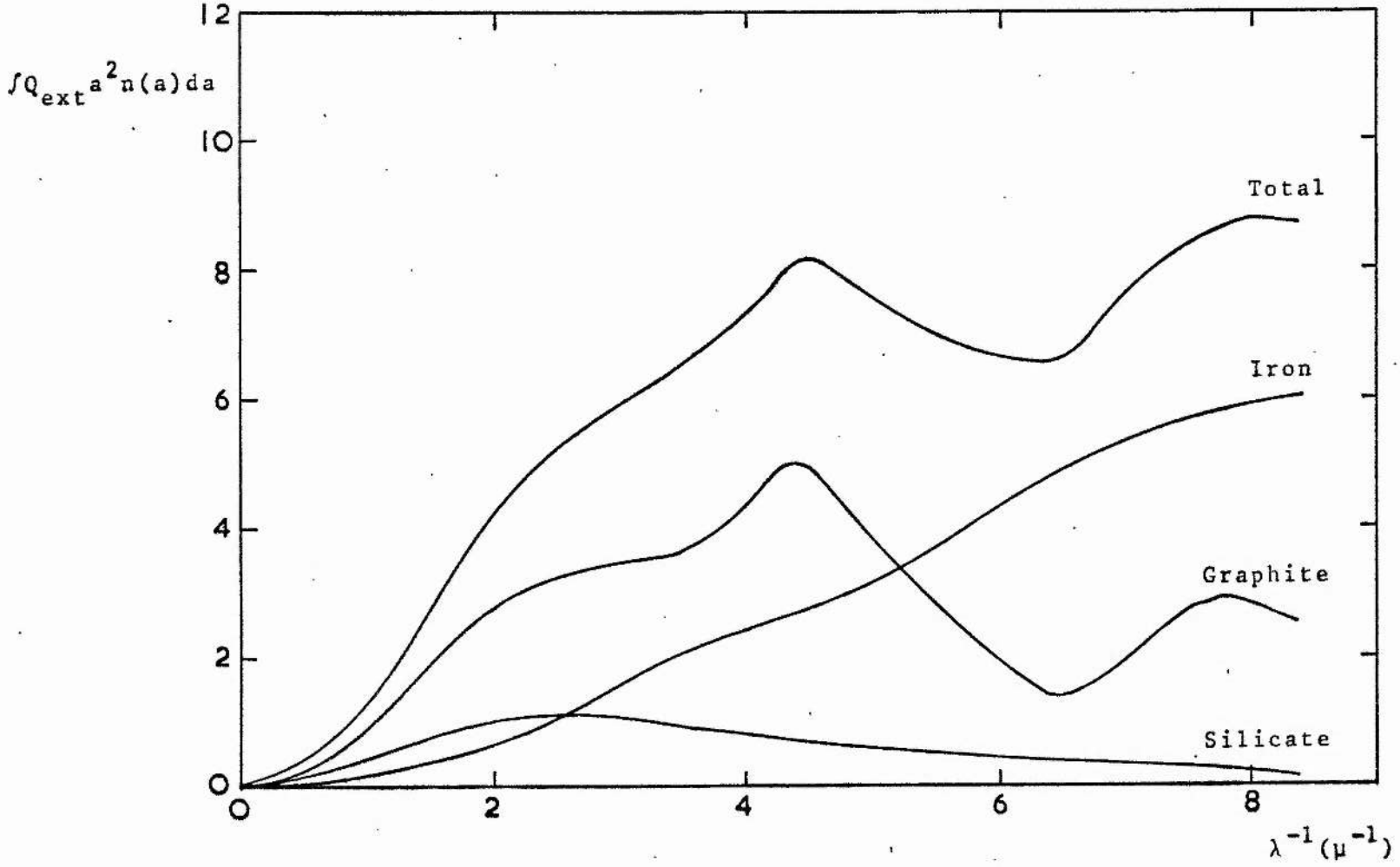

One possible criticism of the WN model is that the graphite hump tends to be rather broad compared with the observational data. Gilra (1971, 1972) has commented that graphite particles of radii close to 0.02 μ are necessary to give a peak of the required width, using the optical constants of Taft and Philipp (1965). Gilra obtained good fits to the observed extinction using a graphite-silicate-silicon carbide model. It is relevant to note that the measurements of Taft and Philipp were made at laboratory temperatures, and it is probable that the graphite feature would be narrower at temperatures appropriate to interstellar space. Also there is a doubt as to whether bulk optical constants are applicable to small particles (see Wickramasinghe et al, 1974). The results of Day and Huffman (1973) from direct laboratory measurements of extinction for graphite smoke differ significantly from the computed curves and produce a steeper rise in the far ultraviolet.

Chiao et al (1973) have carried out a Kramers-Kronig analysis on the observed wavelength-dependence of the extinction, using the method of Purcell (1969). This allows the required column densities to be evaluated for likely constituents of the grains and compared with cosmic abundance ratios. The results suggest that the cosmic abundance of silicon is too low to permit a major extinction contribution to be made by silicate grains. Iron and silicon carbide are underabundant with respect to the long-wavelength extinction but may contribute appreciably in the ultraviolet. The abundance of carbon is satisfactorily high.

It has recently been suggested by Wickramasinghe (1974, 1975) that formaldehyde (H_2CO) molecules may form in large quantities on interstellar grain surfaces and produce polymerised mantles around the grains. Formaldehyde is known to polymerise very easily into chains of the form

$$CH_2\text{-}O\text{-}CH_2\text{-}O\text{-}\ldots$$

producing a crystaline polymer called polyoxymethalene (POM). H_2CO is known to be present in interstellar clouds from radio observations of the spectral feature at 6 cm wavelength, and the constituent elements are sufficiently abundant to be capable of providing the main contribution to the mass density of the dust. By a strange coincidence, POM has a spectral feature centred at 10 μ, leading to an ambiguity in identification with the silicate band around that wavelength. As yet little data is available on the refractive index of POM, and thus detailed Mie calculations must await laboratory measurements of this over a wide range of wavelengths.

(2.6) Non-spherical Particles and Polarization

The discussion in the previous section is based on the implicit assumption that the extinction of real interstellar grains may be represented by that resulting from Mie computations for perfect homogeneous spheres. The fact that starlight is generally polarized implies that elongated particles or particles with non-homogeneous optical properties must be considered. The theory of light scattering by cylindrical particles has been discussed by van de Hulst (1957), Wait (1959) and Lind and Greenberg (1966); it has been

shown that the results for randomly orientated cylinders do not differ significantly from those for spheres of comparable size. If the cylinders are aligned in some way so that the axes tend to point in a preferred direction the transmitted light is in general partially plane polarized, and the ratio of total to selective extinction may vary with the degree of polarization (Wilson, 1960). Greenberg and Roark (1967) claim that spherical grains may be assumed in extinction computations without loss of generality provided polarization is not considered. Greenberg et al (1971) have investigated the optical properties of irregular particles and found that the extinction is very close to that of spheres with the same mean radius a if $2\pi a << \lambda$. Thus the use of spheres in the computation of extinction curves is justifiable; models involving non-spherical or non-homogeneous grains are required to explain the presence of interstellar polarization and its wavelength-dependence. Although the present work is not directly concerned with this aspect of the subject, for completeness the chapter is concluded with a brief discussion of polarization and grain alignment mechanisms.

Most theoretical investigations have been limited to the case of long cylindrical particles. Consider unpolarized light incident on a cylinder with length large compared with the radius, making angle θ with the cylinder axis. The extinction cross-section may be calculated for the two cases where the E-vector of the light is parallel or perpendicular to the plane defined by the cylinder axis and the direction of incidence (see, for example, van de Hulst, 1957). These cross-sections, C_1 and C_2, are functions of m, x and θ.

The total cross-section is

$$C = \tfrac{1}{2}(C_1 + C_2) \tag{2.42}$$

and the degree of polarization is defined as

$$p = \frac{C_1 - C_2}{C}. \tag{2.43}$$

Considering the simplest case where the cylinders are perfectly aligned at $\theta = 90^{\circ}$ to the incident light, the extinctions arising for the two directions of the E-vector are

$$\left.\begin{aligned} \Delta m_1 &= 1.086 N C_1(m, a, \lambda) \\ \Delta m_2 &= 1.086 N C_2(m, a, \lambda). \end{aligned}\right\} \tag{2.44}$$

These relations are analogous to equ. (2.32) for spheres. A normalized polarization

$$P = \frac{\Delta m_1(\lambda) - \Delta m_2(\lambda)}{\Delta m_1(\lambda_o) - \Delta m_2(\lambda_o)} \tag{2.45}$$

may be computed for given values of m and a, λ_o being a reference wavelength. The result is compared with the observed variation of polarization with wavelength, normalized in the same manner. This generally shows a broad maximum in P at $\lambda \sim 6500$ A (Coyne and Gehrels, 1967). Silicate needles of radius $a \sim 0.1$ μ give a satisfactory fit to the data (Wickramasinghe and Nandy, 1972). The degree of polarization for this model is $p \sim 0.8$ at $\lambda = 5000$ A, compared with an observed maximum of ~ 0.065 (Schmidt, 1958). Thus less than 10% alignment of the grains is required to explain the observations.

Graphite is intrinsically an efficient polarizer of light because of its anisotropic optical properties. The polarization of light by graphite flakes has been discussed by Greenberg (1966). Particles with sizes ~ 0.05 μ required to fit the

extinction data do not produce polarization of the correct wavelength-dependence. However, Wickramasinghe (1969) has shown that a mixture of graphite flakes and silicate needles give good results for several combinations of plausible sizes and degrees of alignment.

A number of theories have been proposed to explain why elongated grains should be aligned in space in order to produce the observed polarization (see, for example, Purcell and Spitzer, 1971). It was noted in chapter 1 that starlight is generally polarized with the E-vector for maximum transmission parallel to the plane of the Galaxy, and thus the grains are expected to be aligned with long axes predominantly normal to the plane.

The 'classical' alignment mechanism is that proposed by Davis and Greenstein (1951) which operates on dielectric grains spinning in the galactic magnetic field. Radio observations of Faraday rotation have shown that the direction of the field vector is generally parallel to the plane. The grains are assumed to have paramagnetic properties imparted by small quantities of metallic impurities; paramagnetic relaxation effects then tend to align the angular momentum of the grain parallel to the magnetic field, and its longer axis tends to become perpendicular to the angular momentum. The field strength necessary to produce sufficient alignment is $\sim 10^{-5}$ gauss, which is rather greater than that suggested by observational evidence (Verschuur, 1969). If significant quantities of iron are present, however, the grains are given ferromagnetic properties which considerably reduce the magnetic field strength required for alignment to occur (Jones and

Spitzer, 1967). Alternative theories involving directional gas streaming, cosmic rays and radiation pressure effects have not proved more successful, and it is now accepted by the majority of investigators that the magnetic field is responsible for the alignment.

CHAPTER 3

PHOTOELECTRIC SCANNER OBSERVATIONS

(3.1) Introduction

Application was made in the Autumn of 1971 for observing time at the Cerro Tololo Interamerican Observatory (CTIO) in Chile. Seven nights were allocated from 23 to 30 May, 1972 on the 36 inch (91 cm) telescope for use with a photoelectric scanning photometer. CTIO lies in the Andes at a height of about 7000 feet above sea level and at a latitude of 30° 10' South. The observatory is run by the Association of Universities for Research in Astronomy (AURA) and financed by the US National Science Foundation. The 36 inch telescope has a Cassegrain focus with a focal ratio of f/13.5. The scanner is described in the following section.

(3.2) The Photoelectric Scanning Photometer

The CTIO scanner is one of a pair developed under contract between AURA and Harvard College Observatory under the supervision of I. J. Danziger. (The other is at Kitt Peak National Observatory). The instrument employs a rotatable diffraction grating with a filter to separate the orders of diffraction. The optical plan was derived from that used for the Lick Observatory scanner (Wampler, 1966). A second channel was added to permit simultaneous observations of a star and the adjacent sky. The design and mode of operation of the instrument have been described by Hazen and Danziger (1972), and only a brief outline is given here.

A diagram of the optical components of the system is shown in fig. 3.1. Light from the telescope enters the scanner through a pair of diaphragms and the filter. The channel separation is 9.5 mm. Viewing mirrors may be inserted before or after the entrance diaphragms. The light then passes through a hole cored in the grating and onto a parabolic collimator mirror, where it is reflected in a parallel beam back onto the face of the grating. The grating is ruled with 600 lines per mm blazed for maximum intensity at 7500 A in the first order, and is mounted on a turntable driven by a permanent magnet stepping motor. The diffracted light passes through a set of parallel-plate baffles, which are aligned so that only light with a narrow range of diffraction angles (and hence a narrow range of wavelengths) is transmitted. It is then reflected by a flat mirror onto a second parabolic mirror, and re-imaged onto the exit slits through a hole in the flat mirror. The light then passes on to the beam separators and detectors.

The scanner was designed so that control and data handling may be carried out by a small digital computer housed in the dome. The computer interfacing was done by B. M. Lasker, and the driver programme was written by S. B. Bracker and P. S. Osmer. This permits the user to select a desired wavelength or series of wavelengths and carry out integrations by typing a set of simple instructions; the resulting pulse counts are typed out automatically. The range of the stepping motor gives wavelength limits of 2500 to 6650 A in the second order, and the bandpass, which is determined by the exit slit width, can be varied from 2 to 160 A in the second order. These limits are doubled in the first order.

Fig. 3.1 Diagram of the scanner optics

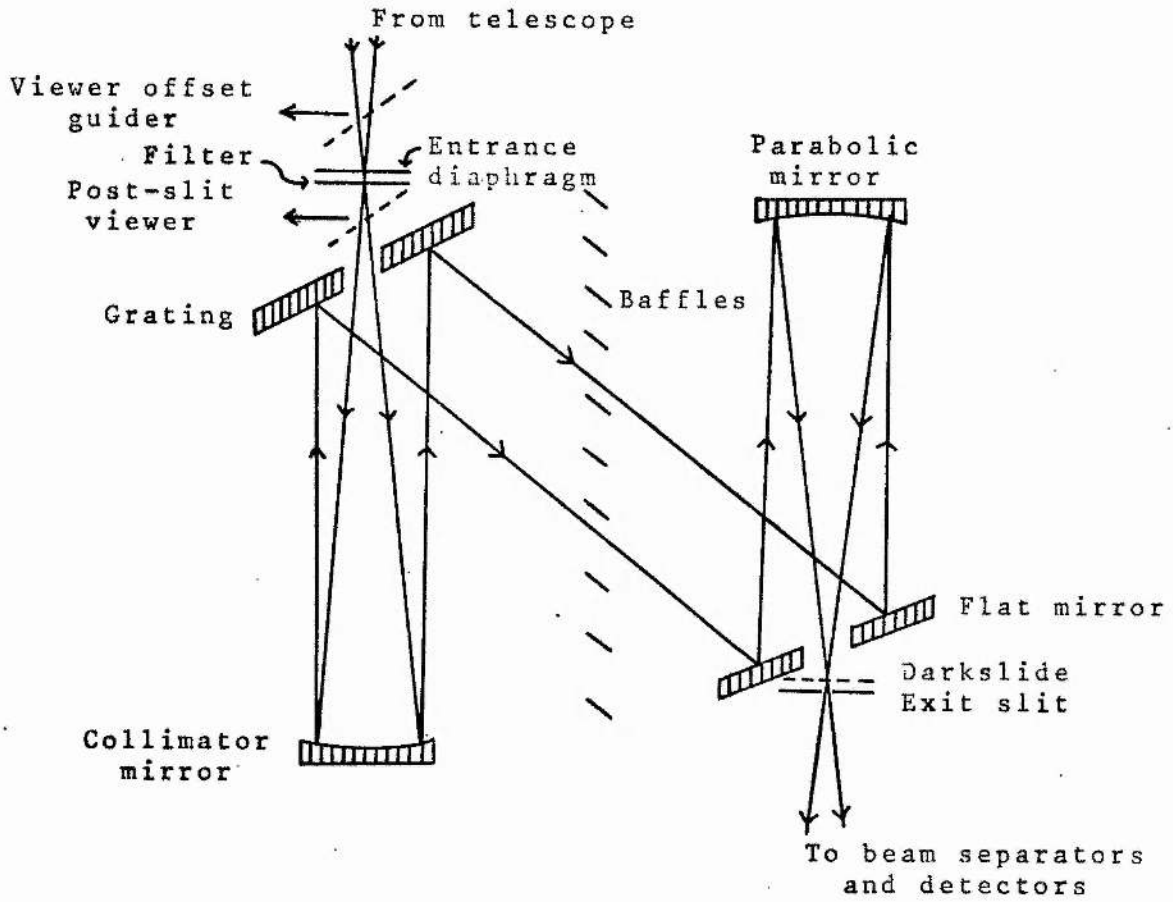

The advantages of this type of instrument are numerous. Its wide spectral coverage coupled with high photometric accuracy cannot be matched by any other method of observation. The narrowness of the bands enable full use to be made of the photometric accuracy inherent in the instrument when removing atmospheric extinction and when determining the effective wavelength of each spectral element. The two-channel facility enables star and sky to be observed simultaneously, with a consequent saving in observing time, and this coupled with computer control gives a high degree of efficiency and flexibility to the observing sequence. As noted in section 1.3, the scanner is particularly suitable for studies of interstellar reddening. Extinction curves can be deduced in detail over a wide range of wavelengths by direct comparison of scanner instrumental magnitudes for reddened and unreddened stars: there is no need to reduce the scans to an absolute scale of intensity. The data reductions for this type of observation are therefore relatively simple.

(3.3) The Observations

Stars for the observing programme were selected from lists of early-type stars (O9-A5) compiled from the photoelectric catalogue of the United States Naval Observatory (Blanco et al, 1968). These lists were kindly supplied by Dr K. Nandy. Some care was taken in assigning MK spectral types to the stars, using the catalogue of Jaschek et al (1964) and the paper of Hiltner et al (1969) as well as references cited in the USNO catalogue. Most of the stars

selected have well-established spectral types. Colour excesses E_{B-V} and E_{U-B} were determined for each star by comparing observed colours with the intrinsic colours given by Johnson (1963). The observing programme contained some 90 stars with visual magnitudes in the range 4.0-8.5. About a third of these were regarded as comparisons, having low reddening ($E_{B-V} \lesssim 0.3$). The reddened stars lie between galactic longitudes $\ell^{II} = 260^{o}$ and $\ell^{II} = 30^{o}$ and, with a few exceptions, within 5^{o} of the galactic plane.

The observations were carried out by Dr I. G. van Breda and the author using the scanner with S20 photomultipliers. The sky was clear enough for useful data to be obtained during about 40% of the allocated telescope time. Of the seven nights, one was completely clear and very stable; four were clear for approximately half the night, with varying degrees of stability; one night was clear for about 1½ hours only, and one was completely overcast.

The wavelength range covered by the observations was 3200-8040 A. This was divided into three sections, to allow for filter changes, as shown in table 3.1. In each case, the step wavelength between successive integrations was set equal to the resolution. The moderate values chosen for the step size/resolution represented a compromise between the desire to study any band structure in the extinction curves and the need to cover a wide spectral range in a reasonable length of time. The computer was programmed to carry out these scans by instructions punched on paper tape. A scan was commenced with an integration at the shortest wavelength and continued in sequence to the longest wavelength; the

sequence was then reversed and the pair of integrations for each wavelength summed. Thus the mean time for the measurements at each wavelength in a given scan was constant. In addition to the three standard scans in table 3.1, short 'tails' were sometimes added, in which the ultraviolet end of scan 1 or the infrared end of scan 3 was repeated. This was done to check on atmospheric stability, and also to gain greater accuracy when the observed star was particularly faint at these wavelengths.

The stars were generally observed in channel 1 of the scanner and the sky in channel 2. However, on the first night one star was observed in each channel in order to check for any wavelength-dependent difference between them. A reddened star and its assigned comparison were usually observed consecutively. A number of stars of similar spectral type were sometimes observed in sequence, alternating between reddened and unreddened, to allow intercomparison. The integration time used varied between 4 and 10 seconds, depending on the brightness of the star. Stars were observed as close as possible to a standard zenith distance of 30° in order to minimize atmospheric extinction corrections. Some of the brighter comparison stars were selected as standards for atmospheric extinction. The intention was to observe two of these at a number of zenith distances during each night, choosing one near the meridian at sunset and one near the meridian at midnight. Although cloud occasionally interrupted these observations, sufficient data was obtained for extinction coefficients to be computed with reasonable accuracy on the five useful nights. As far as possible, the observing

programme was arranged so that scans of extinction standards could also be used for comparison with reddened stars. In some cases the step wavelength was increased to 200 A (2nd order) and 400 A (1st order) to speed up the atmospheric extinction observations, coefficients at intermediate points being obtained by extrapolation.

Time and weather permitted observation of 38 stars from the original list. Of these, 25 were reddened stars (of which 8 were observed twice) and 13 were comparison stars (of which 10 were observed on two or more occasions). The HD numbers of the observed stars and their co-ordinates are listed in tables 3.2 (reddened) and 3.3 (comparison). Published UBV photometry, spectral classifications and the derived colour excesses are given in tables 3.4 and 3.5. Where more than one measurement of the magnitude and colours is available a mean is given, and this is placed in brackets if any of the individual values differ from the mean by more than $\pm 0^{m}.05$. Unless otherwise indicated in the remarks, the photometry and spectral types are taken from Blanco et al (1968).

Table 3.1

Details of the Scans

Scan No.	Wavelength range (A)	Step wavelength and resolution (A)	Order of diffraction	Filter
1	3200-4600	40	2nd	$CuSO_4$
2	4480-5240	40	2nd	Glass
3	5080-8040	80	1st	Kodak K2

Table 3.2

Right Ascension, Declination and Galactic Co-ordinates for Observed Reddened Stars

HD	α (1950)	δ	ℓ^{II} (1950)	b^{II}
	h m	o '	o	o
77581	9 00.2	-40 22	263.06	3.92
80558	9 17.1	-51 21	273.07	- 1.46
90706	10 25.1	-57 21	284.52	0.00
92964	10 40.7	-58 58	287.11	- 0.37
115842	13 17.5	-55 33	307.05	6.83
116119	13 19.6	-61 45	306.62	0.64
142468	15 53.5	-54 12	327.94	- 0.76
144969	16 07.1	-48 40	333.18	2.01
147084	16 17.6	-24 03	352.32	18.05
147889	16 22.4	-24 21	352.87	17.04
148379	16 26.1	-46 09	337.24	1.56
148688	16 28.2	-41 43	340.71	4.35
151346	16 44.7	-23 53	356.63	13.45
152235	16 50.5	-41 55	343.31	1.09
152236	16 50.5	-42 17	343.03	0.86
154043	17 01.6	-46 59	340.58	- 3.61
156201	17 14.4	-35 10	351.51	1.49
165319	18 03.1	-14 12	15.12	3.34
166628	18 09.3	-19 27	11.26	- 0.53
167838	18 14.8	-15 27	15.39	0.27
168571	18 18.2	-17 25	14.06	- 1.39
169454	18 22.4	-14 00	17.54	- 0.68
170938	18 29.8	-15 44	16.85	- 3.05
171012	18 30.2	-18 24	14.53	- 4.38
172488	18 38.1	- 8 46	23.97	- 1.64

Table 3.3

Right Ascension, Declination and Galactic Co-ordinates for Observed Comparison Stars

HD	α (1950)	δ	ℓ^{II} (1950)	b^{II}
	h m	o '	o	o
64760	7 51.8	-47 59	262.06	-10.44
93540	10 44.5	-64 15	289.98	- 4.83
96088	11 01.9	-57 41	289.06	1.99
99171	11 22.0	-42 23	286.33	17.38
106068	12 09.7	-62 40	298.51	- 0.40
110073	12 37.1	-39 43	300.52	22.83
136664	15 20.0	-36 41	333.84	16.74
146145	16 13.5	-52 58	330.98	- 1.81
148703	16 28.1	-34 36	345.94	9.23
150898	16 43.1	-58 15	329.99	- 8.47
166197	18 07.7	-33 49	358.47	- 7.12
172910	18 40.9	-35 41	359.81	-14.07
214080	22 33.4	-16 38	44.81	-56.91

Table 3.4

Published Photometry, Spectral Classifications and Colour Excesses for Observed Reddened Stars

HD	Sp	V	B - V	U - B	E_{B-V}	E_{U-B}	Rem.
77581	B0.5Ib	(6.88)	0.51	-0.49	0.73	0.52	(1)
80558	B7Iab	5.92	(0.53)	(-0.31)	(0.58)	(0.34)	(2)
90706	B2.5Ib	7.06	0.46	-0.43	0.61	0.43	(3)
92964	B3Ia	5.39	0.23	-0.71	0.36	0.16	
115842	B0.5Iab	6.02	0.29	-	0.51	-	
116119	B9I	7.91	0.71	-	0.71	-	
142468	B0.5I	7.85	0.58	-0.38	0.80	0.64	
144969	B0.5Ia	8.28	0.94	-0.08	1.16	0.96	
147084	A5II	4.54	0.84	(0.60)	0.73	-	
147889	B2V	7.89	0.86	-0.15	1.10	0.71	
148379	B2Ia	5.38	(0.55)	-0.56	(0.72)	0.40	
148688	B1Ia	5.32	0.32	-0.75	0.51	0.25	
151346	B8	7.90	0.41	-0.20	0.50	0.10	(4)
152235	B0.5Ia	6.32	0.54	-0.45	0.76	0.59	(5)
152236	B1Iae$^+$	4.76	(0.50)	(-0.58)	(0.69)	(0.42)	(6)
154043	B1Ik	7.08	0.62	-	0.81	-	
156201	B0.5Ia	7.90	0.65	-0.37	0.87	0.67	(7)
165319	B0Ia	7.94	0.59	-0.50	0.83	0.57	
166628	B3Ia	7.17	0.57	-0.29	0.70	0.58	
167838	B5Ia	6.73	0.46	-0.36	0.55	0.42	
168571	B1II	7.79	0.53	-0.40	0.77	0.60	
169454	B1Ia$^+$	6.61	0.94	-0.18	1.13	0.82	
170938	B1Ia	7.87	0.85	-0.25	1.04	0.75	
171012	B0.5Ia	6.82	0.45	-0.57	0.67	0.47	
172488	B0.5V	7.62	0.54	-0.40	0.82	0.61	

Table 3.4 - Remarks

(1) HD 77581: spectroscopic binary associated with X-ray source Vel X-1. V varies by ± 0.07 about the mean given; B - V and U - B are also slightly variable. (See Jones and Liller, 1973).

(2) HD 80558: there is a spread of about ± 0.1 in the published colour indices.

(3) HD 90706: spectral type from Lloyd Evans (1969). UBV photometry averaged from Blanco et al (1968), Feinstein (1969) and Lloyd Evans(1969).

(4) HD 151346: also classified B7p by Garrison (1967).

(5) HD 152235: UBV photometry averaged from Blanco et al (1968) and Schild et al (1969).

(6) HD 152236: UBV photometry averaged from Blanco et al (1968) and Schild et al (1969). There is a spread of about ± 0.1 in the colour indices.

(7) HD 156201: spectral type from Walborn (1973).

Table 3.5

Published Photometry, Spectral Classifications and Colour Excesses for Observed Comparison Stars

HD	Sp	V	B - V	U - B	E_{B-V}	E_{U-B}	Rem.
64760	B0.5Ib	4.24	-0.15	-0.99	0.07	0.02	(1)
93540	B7V	5.34	-0.10	-0.46	0.02	0.00	
96088	B3III	6.15	-0.17	-0.80	0.03	0.00	(2)
99171	B2IV-V	6.11	-0.19	-0.80	0.05	0.06	(3)
106068	B9Ia	5.92	0.30	-	0.30	-	
110073	B8IVp	4.64	-0.09	-0.44	0.00	0.00	
136664	B5V	4.53	-0.15	-0.61	0.01	0.00	
146145	A5	6.30	0.29	-	0.14	-	(4)
148703	B2IV	4.22	-0.18	-0.79	0.06	0.07	
150898	BOIab	5.56	-0.09	-1.02	0.15	0.04	
166197	B2IIIk	6.15	-0.16	-	0.08	-	
172910	B3V	4.87	-0.16	-0.70	0.04	0.01	
214080	B1Ib	6.80	-0.14	-0.92	0.05	0.04	(5)

Remarks

(1) HD 64760: spectral type from Hiltner et al (1969).

(2) HD 96088: UBV photometry averaged from Blanco et al (1968) and Feinstein (1969).

(3) HD 99171: spectral type from Hiltner et al (1969). Also classified BOIII (Blanco et al, 1968) and B2III (Hill, 1970).

(4) HD 146145: also classified A7V (Blanco et al, 1968).

(5) HD 214080: UBV photometry and spectral type from Hill (1970).

(3.4) The Scanner Data Reductions

The basic scanner data consisted of star and sky pulse counts, and allied data on the wavelengths, UT, integration time etc., typed out on teletype paper. This data was transferred to paper tape for computer processing. The reductions were carried out in two stages: firstly, the pulse counts were converted into instrumental magnitudes, and secondly, corrections for atmospheric extinction were applied.

The star HD 110073 was observed in each scanner channel; the ratio of channel 1 to channel 2, q, is shown plotted against λ in fig. 3.2. The variation of q with λ probably results from filter inhomogeneities or slight misalignment of the rotational axis of the grating relative to the plane intersecting the two parallel lines of sight. The instrumental magnitude $m(\lambda)$ for a star observed in channel 1 is defined

$$m(\lambda) = 17.5 - 2.5 \log\left(\frac{N_1(\lambda) - q(\lambda)N_2(\lambda)}{\Delta t}\right) \qquad (3.1)$$

where N_1 and N_2 are the pulse counts in the star and sky channels and Δt is the integration time in seconds. The arbitrary additive constant is assigned the value 17.5 as this gives magnitudes which are of the same order as wideband photometry. The highest count rates generally occurred between 5080 and 5560 A in the first order. The maximum count rate for the brightest star observed (HD 148703, V = 4.22) was $\sim 8\times10^4$ sec^{-1}, suggesting that deadtime errors are unlikely to be appreciable. As a check, visual magnitudes from tables 3.4 and 3.5 were plotted against instrumental magnitudes at λ = 5400 A for a number of stars which show

no sign of variability in V (fig. 3.3). There is no evidence for deviation from linearity at the bright end of the magnitude scales.

Atmospheric extinction coefficients $\kappa(\lambda)$ may be deduced by means of the relation

$$m(\lambda,z) = m_o(\lambda) + \kappa(\lambda) \sec z \qquad (3.2)$$

where $m_o(\lambda)$ is the magnitude above the atmosphere and z is the zenith distance in degrees. A plot of $m(\lambda,z)$ against air mass sec z for a given star observed at intervals during the night should thus be a straight line of slope $\kappa(\lambda)$ and intercept $m_o(\lambda)$. A least squares fit was derived to the data for the atmospheric standard stars of each night. Fig. 3.4 shows a plot of $\kappa(\lambda)$ against λ for three observations of HD 136664 made at mean air masses of 1.09, 1.27 and 1.53 on the night of 28/29 May, 1972. Also shown for comparison is a plot of mean wideband photometry coefficients given by Hardie (1966) for the Mount Wilson and McDonald Observatories. The altitude above sea level of these observatories is comparable with that of Cerro Tololo. The broken line fitted to these latter points follows closely the λ^{-4} law appropriate to molecular (Rayleigh) scattering. The CTIO data also follows the λ^{-4} law quite closely between 3500 and 5300 A. However, longward of this range there is appreciable structure in the scanner points and, in particular, a strong feature at about 7650 A. This is identified as an absorption band of molecular oxygen; other smaller features are also labelled in fig. 3.4 as being probable molecular bands of oxygen or water vapour (see Dufay, 1964). At the short wavelength end of the diagram there is an abrupt fall-off in the κ values.

This is caused by a leakage in the blue filter, which fails to remove red light of wavelength 2λ in the first order when observing in the second order at wavelengths λ shorter than about 3450 A. The proportion of unwanted light appearing is a function of both atmospheric and interstellar reddening, and the results given in chapter 5 are therefore truncated at the shortest unaffected scanner wavelength, which is 3480 A.

The extinction coefficients measured on the other nights show a similar wavelength-dependance to those plotted in fig. 3.4, although the total extinction at a given wavelength varies appreciably from night to night. On one night in particular the extinction was very high, but the atmosphere appeared to be reasonably stable. The strength of the 7650 A band was found to fluctuate considerably.

The instrumental magnitudes for each star were corrected to a standard zenith distance of 30° (equivalent to an air mass of sec z = 1.1547) using the measured coefficients as follows. Putting $z = 30^{\circ}$ in equ. (3.2),

$$m(\lambda,30) = m_{o}(\lambda) + 1.1547\kappa(\lambda). \qquad (3.3)$$

Subtracting equ. (3.2) from equ. (3.3) gives

$$m(\lambda,30) = m(\lambda,z) + (1.1547 - \sec z)\kappa(\lambda) \qquad (3.4)$$

The purpose of this correction is to equalise the effect of atmospheric extinction in each star so that it is removed when pairs of stars are differenced to give interstellar extinction curves. As the stars were, in any case, generally observed close to $z = 30^{\circ}$, the term (1.1547 - sec z) in equ. (3.4) is small and any errors in the values of $\kappa(\lambda)$ will have minimal effect on the corrected magnitudes.

Fig. 3.2 Variation in scanner channel ratio q with wavelength λ (HD 110073)

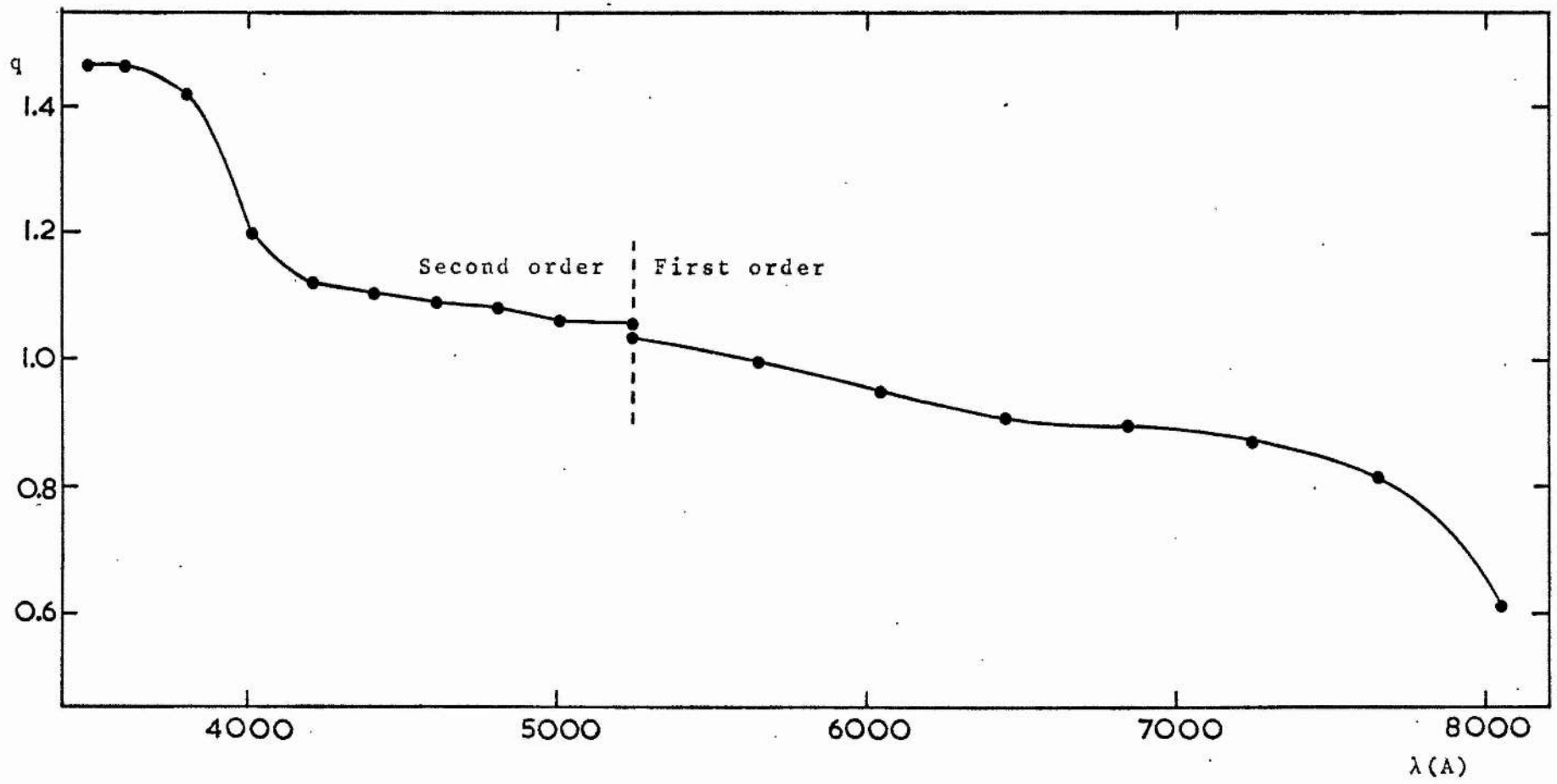

Fig. 3.3 Plot of instrumental magnitude m(5400) against V
The m values are adjusted to an air mass of 1.1547

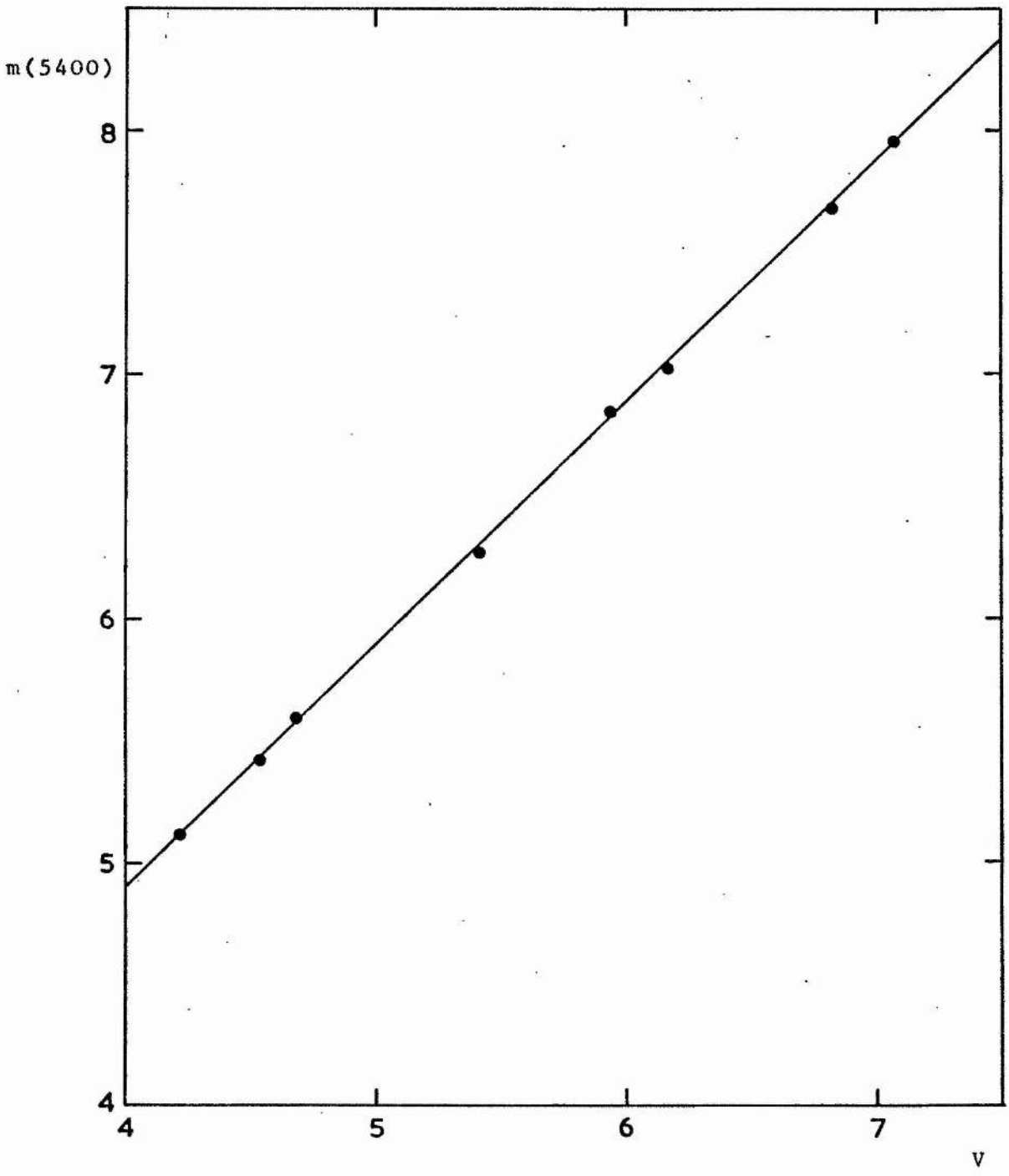

Fig. 3.4 Plot of atmospheric absorption coefficient against wavelength for the star HD 136664 scanned on the night of 28/29 May, 1972. Also shown are mean measurements for the Mount Wilson and McDonald Observatories (Hardie, 1962). Molecular absorption bands are identified from Dufay (1964).

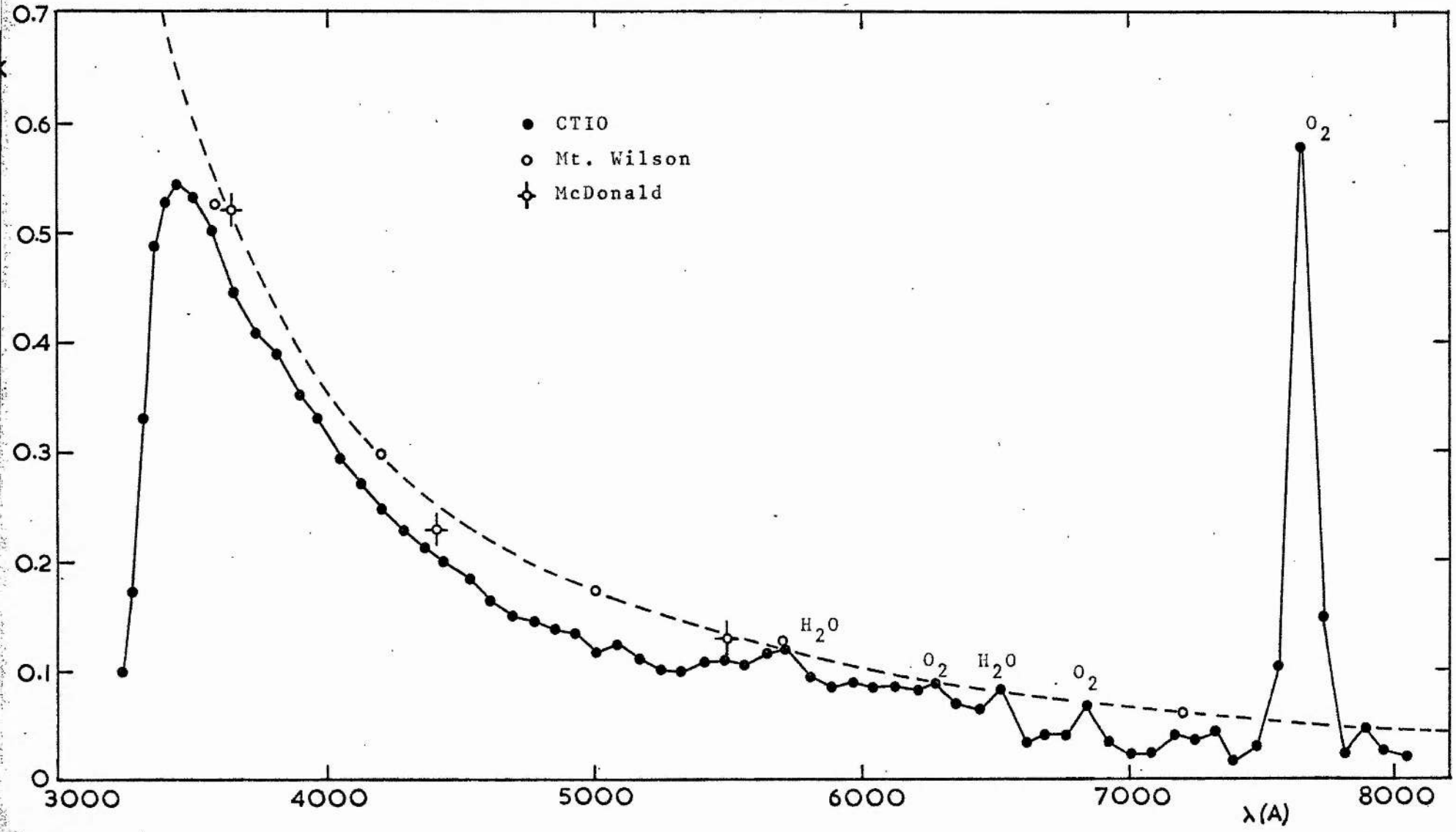

Fig. 4.1 Diagram of the infrared photometer design

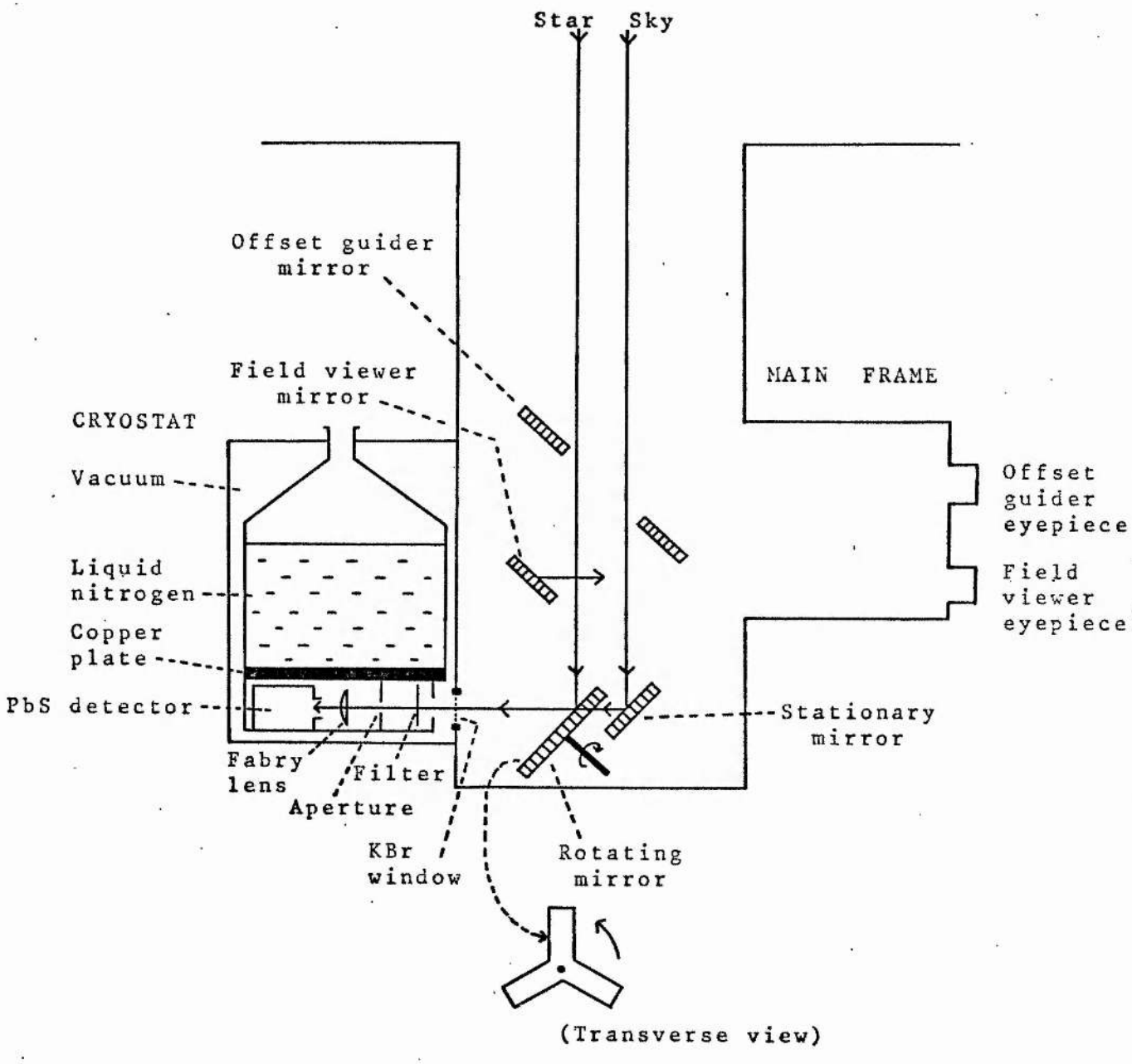

CHAPTER 4

WIDEBAND PHOTOMETRY

(4.1) Introduction

In order to extend the wavelength coverage of the observations, infrared photometry in the J, H, K and L bands was obtained for the same set of stars previously scanned at Cerro Tololo. In May, 1973, Dr I. S. Glass kindly observed three of the stars (two reddened, one comparison) with the 40 inch (1.02 m) telescope at the Sutherland site of the South African Astronomical Observatory (see van Breda, Glass and Whittet, 1974). The photometer used was designed and built by Dr Glass at the Royal Greenwich Observatory, and is described in the next section. The LTUP allocated five nights from 12 to 17 April, 1974 on the 40 inch telescope to enable the remainder of the programme stars to be observed.

In view of the time interval between the scanner and infrared observations, three nights were also allocated on the 20 inch (0.5 m) telescope at Sutherland to carry out monitoring in the V band as a check for variability (9 to 12 April, 1974). Observations were actually made with B, V, R and I filters. Dr A. W. J. Cousins also kindly included some of the programme stars in his lists for observation in UBV during May, 1973 (Cousins, 1973).

(4.2) The Infrared Photometer

The construction and use of the instrument have been discussed by Glass (1973) and only a brief description is given here. It is built in two sections: (i) the main frame,

containing star/sky chopper, offset guider and acquisition eyepiece, and (ii) the cryostat, containing the detector and coolant. The design is shown in fig. 4.1. The star/sky chopper consists of a propeller-like three-bladed mirror (also shown transversely in fig. 4.1) which rotates at a rate of 12.5 cycles per second, placed in front of a fixed plane mirror. The detector sees alternating images of star and sky reflected from the rotating and fixed mirrors respectively. A flat mirror may be inserted into the beam above the chopper for viewing purposes. The offset guider receives the outer part of the beam by reflection from a pierced 45° mirror. Light passes into the cryostat through a KBr window. The detector consists of a photoconductor (PbS) cell mounted behind a CaF_2 Fabry lens, an aperture wheel and a filter wheel, in an enclosure cooled to $77^{\circ}K$ by liquid nitrogen. An aperture diameter of 2 mm was used for the observations described in this chapter. The JHKL filters used have effective wavelengths of 1.25, 1.65, 2.20 and 3.50 μ respectively. Transmission curves for these filters are given by Glass (1973).

(4.3) JHKL Observations and Results

The results obtained in 1973 for three stars are given in table 4.1 (van Breda et al, 1974). The error limits quoted consist of the standard error due to statistical fluctuations combined with a nominal systematic uncertainty. The values of the latter are 0.06, 0.05, 0.04 and 0.04 magnitudes at J, H, K and L respectively (Glass, personal communication). The statistical part is usually smaller than the

systematic part, except for blue comparison stars at the L wavelength.

The 1974 observations were carried out jointly by Dr Glass, Dr van Breda and the author. The sky was clear for about 40% of the time during the five nights. All the remaining programme stars (tables 3.2 and 3.3) were observed on at least one occasion. In addition, the comparison star HD 96088 observed in 1973, was re-observed in order to improve the statistical accuracy, especially in the L band, by repeated integrations. Some difficulty was encountered in observing the B1Ib type comparison star HD 214080, as it did not reach an accessible altitude until after the twilight had begun. Moreover, it is very faint at L, and would have required repeated observations under good conditions to produce a meaningful result in this band. Because of this another star of the same spectral classification and very similar reddening, HD 91316 (ρ Leonis) was observed to give an indication of the expected colours. As this star is quite bright (V = 3.85) accurate photometry could be obtained without difficulty. Infrared standard stars were observed at regular intervals, generally after every two programme stars. These were taken from the list of Glass (1974).

The data reductions were carried out using a standard computer programme written by Dr Glass and run at the computing centre of the University of Cape Town. This converted the raw data into instrumental magnitudes, applied nominal corrections for the small degree of atmospheric extinction occurring at these wavelengths, and reduced the results to a standard system of magnitudes. The latter are given in tables 4.2 and 4.3.

An asterisk denotes stars that were observed twice, and in these cases a mean result is given.

Visual-infrared colour indices for HD 91316 and two other stars of similar reddening and spectral type are given in table 4.4(i). The values of V - J, V - H and V - K for HD 91316 lie between those of the other two stars, as is to be expected from the spectral types; in the case of V - L the uncertainty is large for HD 166197. It thus seems reasonable to adopt the colours of HD 91316 as being representative of a star of type B1Ib, and substitution of V = 6.83 for HD 214080 gives the values in table 4.4(ii). The uncertainty in these magnitudes is approximately ± 0.08 on the assumption that both stars are non-variable. The results are not inconsistent with the observed values in table 4.3, and are likely to be more reliable.

(4.4) BVRI Photometry and Checks for Variability

The BVRI observations were made using the SAAO 'People's' Photometer on the 20 inch telescope. This instrument has two channels, for use in (1) the blue/yellow and (2) the yellow/red regions of the spectrum. The second channel with an S20 photomultiplier was selected for these observations. Only about 25% of the time was clear on the three nights, and it was not possible to observe all the programme stars. On only one night was the sky clear during the hour before twilight when the reddened stars in the $\ell^{II} = 0^{o}$-30^{o} region of the Milky Way became accessible, and this group was therefore largely unobserved. Stars from the Harvard E and F regions (Cousins, 1972) were used as standards. Reductions were

carried out using a standard SAAO computer programme. As the E and F region stars are intended as standards for UBV photometry, zero point corrections were applied only to the B and V values. The R and I magnitudes must therefore be regarded as instrumental.

The V and B - V results for reddened stars are given in column III of table 4.5, compared with those of Cousins (1973) (column II) and a mean of earlier values compiled in table 3.4 (column I). Similarly table 4.6 shows results for comparison stars. It may be concluded that there is no evidence for significant variation in 20 of the 38 stars; a few show small fluctuations, and for the rest there is insufficient data.

The variations of HD 77581, associated with the X-ray source Vel X-1, are periodic and may thus be predicted. It has been shown that the X-ray source has a period of 8.95 ± 0.02 days (Foreman et al, 1973) and that the light of the star goes through a double cycle of amplitude $0^{m}.07$ in this time (Jones and Liller, 1973; Vidal et al, 1973). From the light curve given by Vidal et al it is noted that a maximum in light occurred at JD 2441740.4 ± 0.1. Assuming a period of half the X-ray period, the number of cycles elapsing between this event and the scanner, BVRI and JHKL observations are given in table 4.7. The approximate uncertainty in these values is ± 0.2. An integer value implies maximum light and a half-integer value minimum light. Of the scanner observations, (i) occurred near mean light and (ii) near maximum; the BVRI observations occurred near maximum light, consistent with the low value of V in column III of table 4.5; the JHKL observations

both occurred near mean light. As there is little variation in colour during the cycle (Jones and Liller) a correction of + $0^{m}.07$ is applied at each wavelength to the second set of scanner data, which is then regarded as referring to mean light.

The R and I relative magnitudes are listed in tables 4.8 and 4.9.

Table 4.1

Infrared Photometry for three Stars observed in May, 1973 (van Breda et al, 1974)

HD	J	H	K	L
92964	4.71 ± 0.06	4.62 ± 0.06	4.53 ± 0.05	4.47 ± 0.05
96088	6.51 ± 0.07	6.62 ± 0.06	6.69 ± 0.06	7.03 ± 0.32
147889	5.34 ± 0.06	4.83 ± 0.06	4.54 ± 0.05	4.39 ± 0.08

Table 4.2

Infrared Photometry for Reddened Stars observed in April, 1974

HD	J	H	K	L
77581*	5.85 ± 0.06	5.71 ± 0.05	5.60 ± 0.07	5.56 ± 0.10
80558*	4.57 ± 0.06	4.36 ± 0.05	4.25 ± 0.04	4.12 ± 0.06
90706	5.97 ± 0.06	5.80 ± 0.07	5.69 ± 0.06	5.84 ± 0.09
115842*	5.33 ± 0.06	5.23 ± 0.05	5.15 ± 0.04	5.11 ± 0.08
116119*	6.13 ± 0.06	5.87 ± 0.05	5.73 ± 0.04	5.68 ± 0.12
142468	6.60 ± 0.07	6.44 ± 0.06	6.32 ± 0.07	6.19 ± 0.11
144969	5.92 ± 0.06	5.58 ± 0.07	5.36 ± 0.04	5.13 ± 0.06
147084*	2.23 ± 0.06	1.85 ± 0.05	1.62 ± 0.04	1.45 ± 0.04
148379	4.01 ± 0.07	3.81 ± 0.06	3.67 ± 0.05	3.55 ± 0.06
148688	4.36 ± 0.06	4.23 ± 0.05	4.11 ± 0.05	4.03 ± 0.05
151346	6.63 ± 0.06	6.41 ± 0.06	6.30 ± 0.06	6.47 ± 0.13
152235	4.99 ± 0.06	4.83 ± 0.05	4.72 ± 0.05	4.61 ± 0.05
152236	3.47 ± 0.06	3.27 ± 0.05	3.11 ± 0.04	2.94 ± 0.05
154043	5.54 ± 0.06	5.36 ± 0.06	5.21 ± 0.05	5.12 ± 0.07
156201	6.30 ± 0.07	6.08 ± 0.05	5.95 ± 0.05	5.86 ± 0.10
165319	6.53 ± 0.07	6.35 ± 0.05	6.27 ± 0.05	6.21 ± 0.12
166628	5.75 ± 0.06	5.54 ± 0.05	5.41 ± 0.05	5.38 ± 0.07
167838	5.54 ± 0.06	5.37 ± 0.06	5.27 ± 0.05	5.20 ± 0.06
168571	6.46 ± 0.06	6.23 ± 0.06	6.07 ± 0.05	6.11 ± 0.11
169454	4.42 ± 0.06	4.08 ± 0.05	3.85 ± 0.05	3.69 ± 0.05
170938	5.76 ± 0.06	5.47 ± 0.06	5.29 ± 0.05	5.12 ± 0.06
171012	5.78 ± 0.06	5.67 ± 0.05	5.54 ± 0.05	5.40 ± 0.08
172488	6.49 ± 0.07	6.39 ± 0.06	6.28 ± 0.05	6.31 ± 0.12

Table 4.3

Infrared Photometry for Comparison Stars observed in April, 1974

HD	J	H	K	L
64760	4.59 ± 0.06	4.69 ± 0.06	4.74 ± 0.05	4.79 ± 0.06
91316	4.18 ± 0.06	4.22 ± 0.06	4.26 ± 0.05	4.27 ± 0.06
93540	5.49 ± 0.06	5.48 ± 0.06	5.51 ± 0.05	5.59 ± 0.10
96088	6.49 ± 0.06	6.51 ± 0.06	6.67 ± 0.05	6.79 ± 0.22
99171*	6.48 ± 0.06	6.60 ± 0.05	6.65 ± 0.06	6.83 ± 0.21
106068	5.12 ± 0.06	4.99 ± 0.05	4.91 ± 0.06	4.86 ± 0.07
110073	4.75 ± 0.06	4.77 ± 0.05	4.79 ± 0.05	4.75 ± 0.06
136664*	4.87 ± 0.06	4.93 ± 0.05	4.97 ± 0.04	5.03 ± 0.07
146145*	5.74 ± 0.06	5.60 ± 0.05	5.56 ± 0.04	5.63 ± 0.06
148703	4.54 ± 0.06	4.64 ± 0.05	4.68 ± 0.04	4.82 ± 0.05
150898*	5.68 ± 0.06	5.74 ± 0.05	5.77 ± 0.05	5.77 ± 0.09
166197*	6.41 ± 0.06	6.47 ± 0.05	6.50 ± 0.05	6.57 ± 0.12
192910	5.20 ± 0.06	5.27 ± 0.06	5.31 ± 0.05	5.40 ± 0.08
214080	7.09 ± 0.07	7.09 ± 0.09	7.17 ± 0.07	(6.5 ± 1.0)

Table 4.4

(i) Visual-infrared Colour Indices for three Stars of low reddening

HD	Sp	V	V - J	V - H	V - K	V - L
64760	B0.5Ib	4.24	-0.35	-0.45	-0.50	-0.55
91316	B1Ib	3.85	-0.33	-0.37	-0.41	-0.42
166197	B2III	6.15	-0.26	-0.32	-0.35	-0.42

(ii) Extrapolated Photometry for HD 214080 (B1Ib, V = 6.83) using indices for HD 91316 above

J	H	K	L
7.16	7.20	7.24	7.25

Table 4.5

Check for Variability (Reddened Stars)

HD	I		II		III		Rem.
	V	B - V	V	B - V	V	B - V	
77581	(6.88)	0.51	(6.88)	0.49	6.83	0.47	(2)
80558	5.92	(0.53)	-	-	-	-	
90706	7.06	0.46	7.10	0.48	7.09	0.45	(1)
92964	5.39	0.23	5.39	0.27	-	-	(1)
115842	6.02	0.29	6.02	0.31	6.02	0.26	(1)
116119	7.91	0.71	-	-	7.93	0.69	(1)
142468	7.85	0.58	-	-	7.89	0.59	(1)
144969	8.28	0.94	-	-	8.26	0.91	(1)
147084	4.54	0.84	-	-	4.55	0.82	(1)
147889	7.89	0.86	7.90	0.83	-	-	(1)
148379	5.38	(0.55)	-	-	5.36	0.53	
148688	5.32	0.32	-	-	5.30	0.32	(1)
151346	7.90	0.41	-	-	7.91	0.39	(1)
152235	6.32	0.54	6.29 6.34	0.42 0.53	6.31	0.49	(3)
152236	4.76	(0.50)	-	-	4.71	0.46	(4)
154043	7.08	0.62	7.09	0.63	7.08	0.59	(1)
156201	7.90	0.65	-	-	7.84	0.65	
165319	7.94	0.59	-	-	7.92	0.53	
166628	7.17	0.57	-	-	7.17	0.55	(1)
167838	6.73	0.46	-	-	6.72	0.41	
168571	7.79	0.53	-	-	-	-	
169454	6.61	0.94	-	-	-	-	
170938	7.87	0.85	-	-	-	-	
171012	6.82	0.45	-	-	-	-	
172488	7.62	0.54	-	-	-	-	

Key to column headings

I Blanco et al (1968) and other references cited in the remarks to table 3.4.
II Cousins (1973).
III SAAO 20 inch observations (April, 1974).

(Remarks - see next page).

Table 4.6

Check for Variability (Comparison Stars)

HD	I		II		III		Rem.
	V	B - V	V	B - V	V	B - V	
64760	4.24	-0.15	-	-	-	-	
93540	5.34	-0.10	-	-	-	-	
96088	6.15	-0.17	6.16	-0.17	6.14	-0.17	(1)
99171	6.11	-0.19	-	-	6.16	-0.19	
106068	5.92	0.30	-	-	5.94	0.26	(1)
110073	4.64	-0.09	-	-	4.65	-0.11	(1)
136664	4.53	-0.15	-	-	4.53	-0.15	(1)
146145	6.30	0.29	6.31	0.26	6.31	0.27	(1)
148703	4.22	-0.18	-	-	-	-	
150898	5.56	-0.09	-	-	5.57	-0.10	(1)
166197	6.15	-0.16	6.14	-0.14	6.12	-0.16	(1)
172910	4.87	-0.16	-	-	-	-	
214080	6.80	-0.14	6.82	-0.14	6.83	-0.14	(1)

(Column headings are the same as for table 4.5).

Tables 4.5 and 4.6 - Remarks

(1) Any variation likely to be small (< ± 0.05).

(2) HD 77581 varies between 6.81-6.95 in V with a period of 4.5 days (Jones and Liller, 1973). Also slightly variable in B - V (∿ ± 0.03).

(3) HD 152235 apparently underwent an abrupt change in May, 1973 (Cousins, 1973).

(4) HD 152236 varies by ∿ ± 0.05 in both V and B - V.

Table 4.7

Phase of HD 77581 Observations

Observation	JD (2440000.0+)	Cycles from maximum
Scanner (i)	1463.5	-61.9
Scanner (ii)	1464.5	-61.7
Maximum (Vidal et al)	1740.4	0.0
BVRI	2148.3	+91.1
JHKL (i)	2151.3	+91.8
JHKL (ii)	2153.3	+92.3

Table 4.8

R and I magnitudes (Reddened Stars)

HD	R	I
77581	6.42	8.62
90706	6.68	8.88
115842	5.73	8.03
116119	7.36	9.39
142468	7.42	9.57
144969	7.51	9.38
147084	3.86	5.78
148379	4.89	7.03
148688	4.96	7.22
151346	7.50	9.66
152235	5.85	8.02
152236	4.27	6.44
154043	6.57	8.65
156201	7.29	9.33
165319	7.44	9.55
166628	6.70	8.84
167838	6.33	8.53

Table 4.9

R and I magnitudes (Comparison Stars)

HD	R	I
96088	6.14	8.73
99171	6.16	8.76
106068	5.64	7.92
110073	4.59	7.12
136664	4.53	7.11
146145	6.07	8.42
150898	5.50	8.02
166197	6.10	8.66
214080	6.82	9.37

CHAPTER 5

THE EXTINCTION CURVES

(5.1) Corrections for MK Type Mismatching

The extinction curves are produced by plotting the magnitude difference between observational data for reddened and comparison stars at each wavelength against λ^{-1} (see equ. 2.35), overlapping points in the scans (table 3.1) being averaged. If the MK spectral types of the two stars are not closely matched, distortions appear in the curves: the effect is particularly noticable when there is a difference in luminosity class, and is more serious for later types. Of the 25 reddened stars 20 are supergiants. Only 4 of the 13 comparison stars are of this class, due to the scarcity of high-luminosity early-type stars of low reddening. Thus in most cases where mismatching occurs, a reddened supergiant is paired with a comparison star of lower luminosity. As an example, the extinction curve (unnormalized) of HD 166628 (B3Ia) compared with HD 172910 (B3V) is shown in fig. 5.1. The Balmer absorption lines of hydrogen are weaker in the more luminous reddened star, producing troughs in the curve. Points requiring correction are denoted by crosses. The magnitude D and wavelength λ_1 of the Balmer discontinuity are also dependent on MK type (Barbier and Chalonge, 1939; Chalonge and Divan, 1952; Chalonge, 1958; Divan, 1971.) The discontinuity is greater and occurs at a slightly longer wavelength in the less luminous comparison star, causing the trough at $\lambda^{-1} \sim 2.7\ \mu^{-1}$ in fig. 5.1. The points to the right of this trough are too low by the difference $(D_c - D_r)$ between the discontinuities of the two stars.

Fig. 5.1 Plot of Δm against λ^{-1} for HD 166628 compared with HD 172910, showing Balmer corrections.

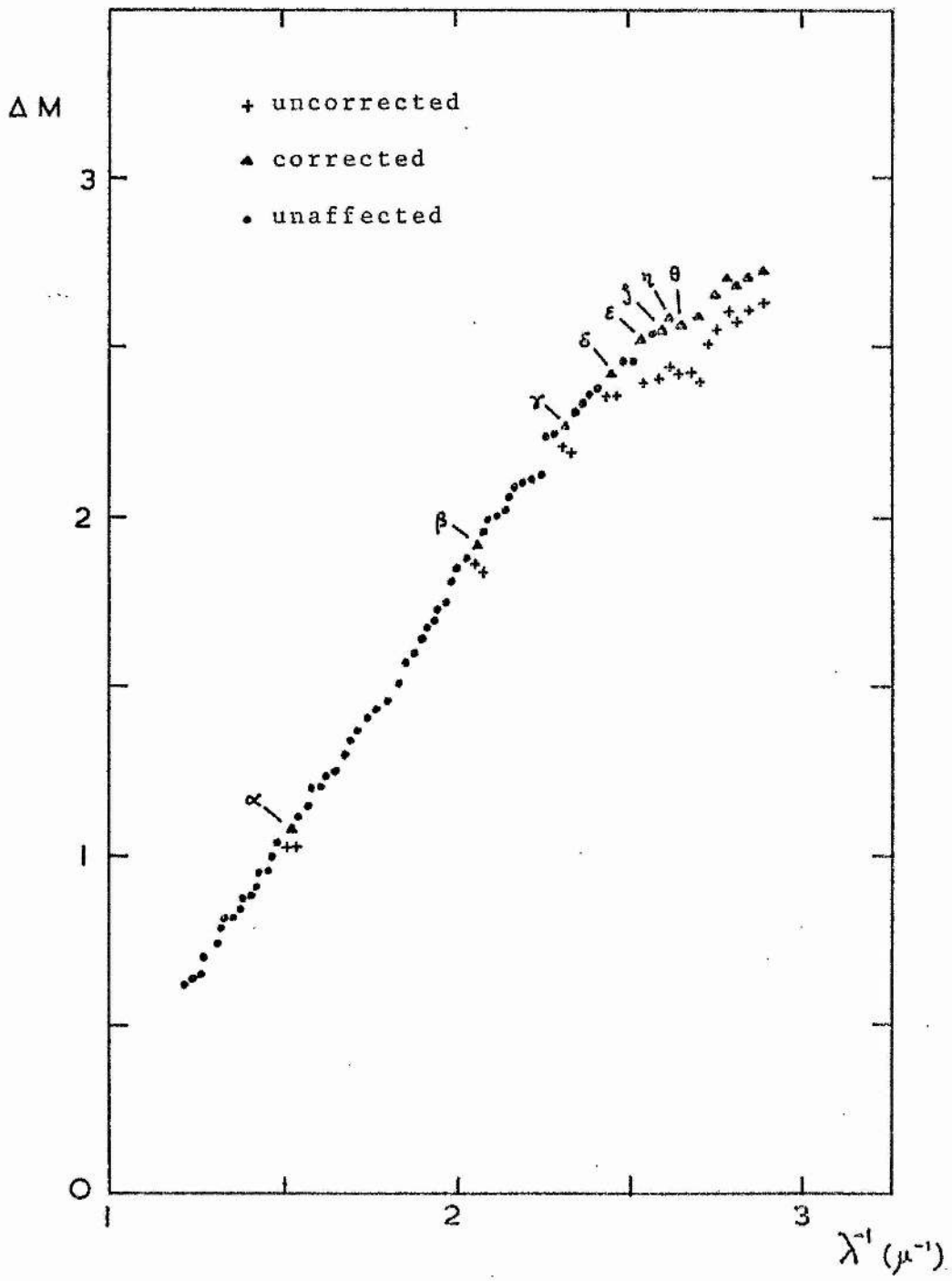

Fig. 5.2 Plot of mean Balmer line equivalent width w against spectral type for stars of class Ia

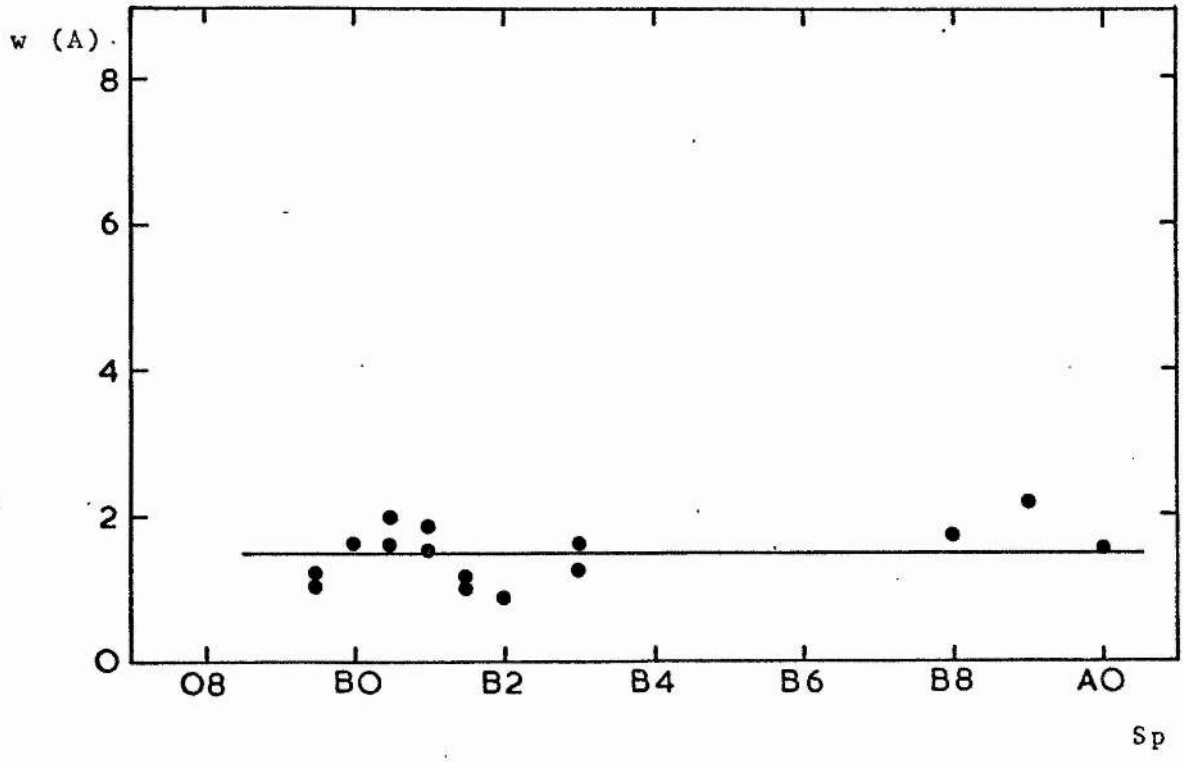

Fig. 5.3 Plot of mean Balmer line equivalent width w against spectral type for stars of classes Iab and Ib

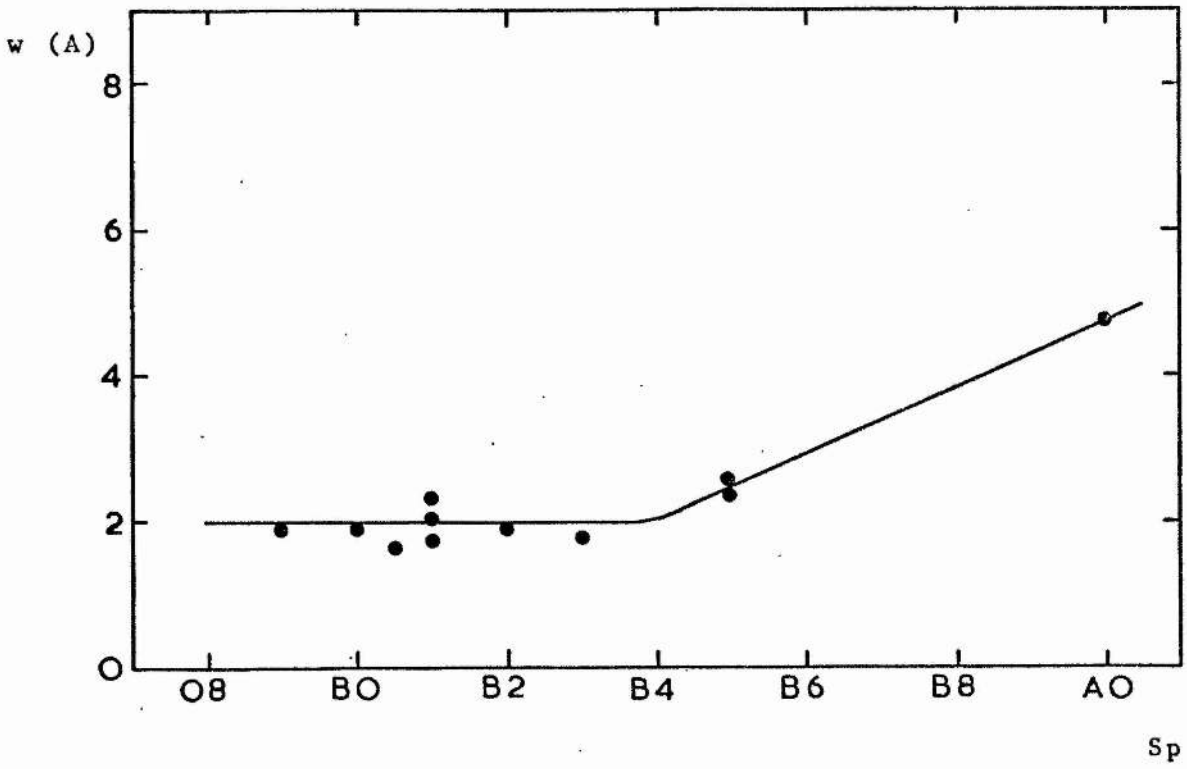

Fig. 5.4 Plot of mean Balmer line equivalent width w against spectral type for stars of classes II and III

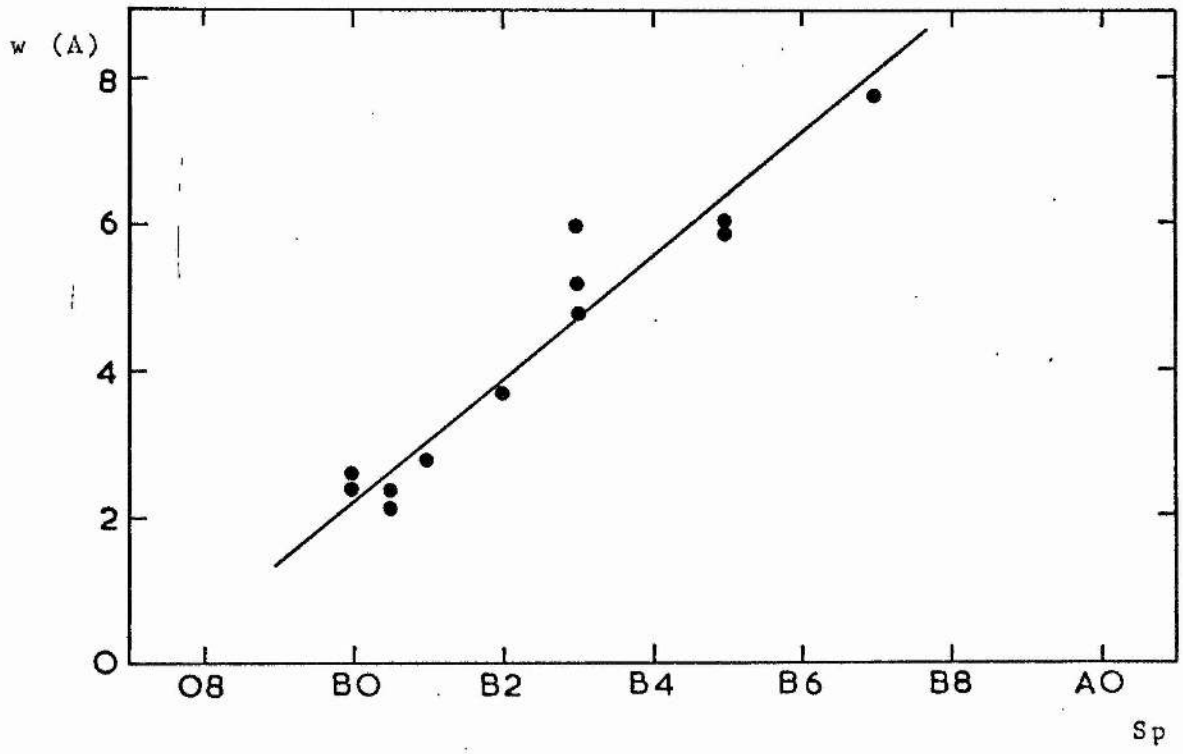

Fig. 5.5 Plot of mean Balmer line equivalent width w against spectral type for stars of classes IV and V

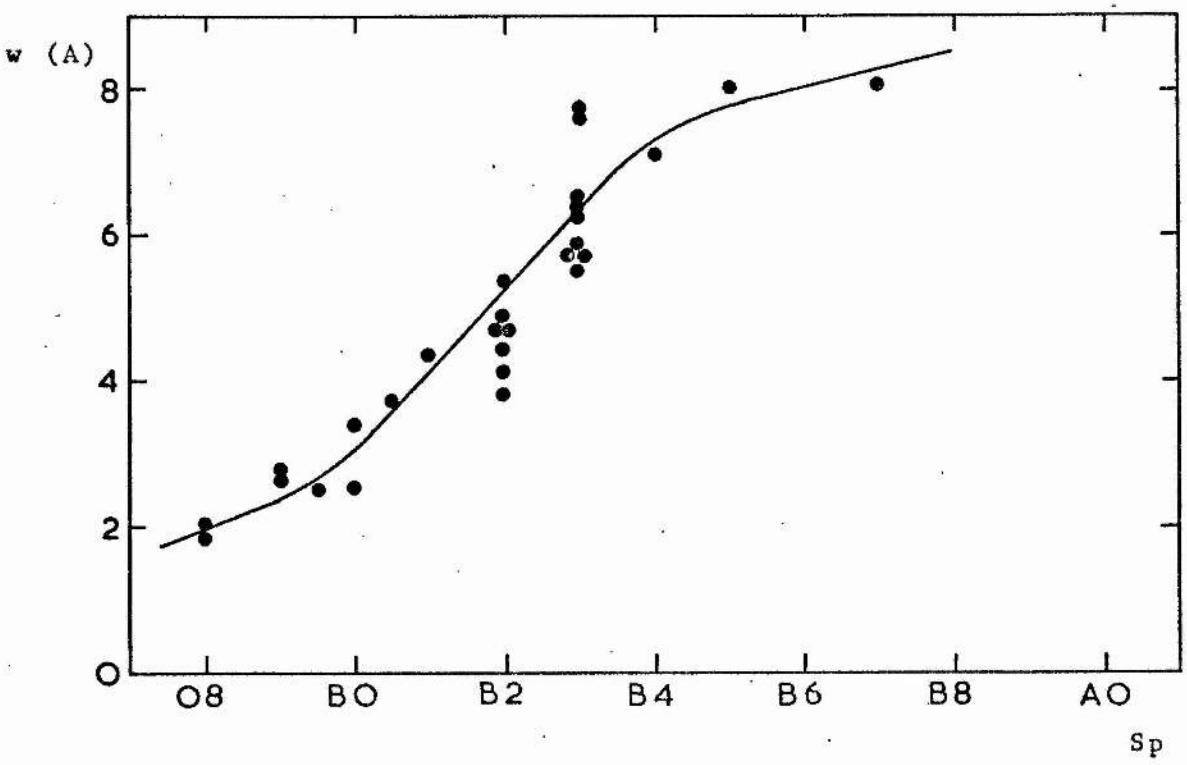

The equivalent widths w of the Balmer lines were measured by Williams (1936) for 84 early-type stars in the range O8-A0. Taking MK types from Jaschek et al (1964) the mean value of w for each star of class Ia is plotted against spectral type in fig. 5.2. Similarly, figs. 5.3-5.5 show plots for classes Iab/Ib, II/III and IV/V (there being insufficient numbers of stars classed Iab, II and IV to be usefully plotted separately). Approximate fits to the points are shown in the diagrams. The value of w is fairly constant for class Ia stars, and for types Iab-Ib it is constant from O9-B4 and then appears to increase. For the less luminous stars w rises roughly linearly towards later types. Table 5.1, giving w as a function of spectral type and luminosity class, is compiled from figs. 5.2-5.5.

The variation of the Balmer discontinuity parameters D and λ_1 with MK type is shown diagrammatically by Divan (1971); values of D are given in table 5.2.

Returning to fig. 5.1, the extinction curve may be corrected as follows, using the data in tables 5.1 and 5.2. When a Balmer line falls totally within a spectral element of width $\Delta\lambda$ the required correction to the extinction Δm is

$$C_h = 2.5 \log\left(\frac{\Delta\lambda - w_r}{\Delta\lambda - w_c}\right) \qquad (5.1)$$

where the subscripts r and c refer to reddened and comparison stars. In the case considered, w_r = 1.5 A and w_c = 6.4 A (table 5.1), thus for $\Delta\lambda$ = 40 A we have $C_h = +0^m.15$. The approximate uncertainty in this correction, deduced from the spread in w values at each spectral type in figs. 5.2-5.5, is $\pm 0^m.04$. In cases where the Balmer line overlaps into two spectral elements (e.g. the Hβ line affects the 4840 and 4880 A

scanner magnitudes), the elements are considered together and the correction for a band of width $2\Delta\lambda$ applied to the mean of the two Δm values. The corrected points are shown as triangles in fig. 5.1, and are labelled Hα-Hθ. The Balmer discontinuities are $D_r = 0^m.09$ and $D_c = 0^m.20$ for the two stars (table 5.2). The lowest point in the trough is raised by D_c, and the points shortward of this are raised by $D_c - D_r = 0^m.11$. It is difficult to correct the intermediate points in the trough, and these are therefore omitted. The uncertainty in the values of D_r and D_c is estimated from the diagram of Divan (1971) to be $\sim$ 20%. In the rarer case where the discontinuity occurs at a lower wavelength in the reddened star, the trough is replaced by a peak, which is lowered by D_r, and the shortward points are lowered by $D_r - D_c$.

The corrections applied in fig. 5.1 result purely from a difference in luminosity. In cases where the spectral type also differs, a further correction is required arising from the change in intrinsic colour-temperature of the stars at the Balmer limit. The parameter $\Delta\phi$, defined as the difference between the spectral gradient for $\lambda < \lambda_1$ and that for $\lambda > \lambda_1$ is a function of spectral type (Divan, 1971), and the dependence is given in table 5.3. A correction

$$C_\phi(\lambda) = (\Delta\phi_c - \Delta\phi_r)(\lambda_1/\lambda - 1) \qquad (5.2)$$

is applied to the points in the extinction curve shortward of the Balmer limit. The sense of these corrections is such that if the comparison star is too early the uncorrected curve is too steep.

As a check on the reliability of the corrections, several reddened stars were deliberately mismatched with comparison stars

over a range of spectral types and luminosities. For example, HD 92964 (B3Ia) was compared with HD 214080 (B1Ib), HD 96088 (B3III) and HD 136664 (B5V). With the appropriate corrections applied, the resulting extinction curves were the same in each case to within the error limits.

Table 5.1

Mean Equivalent Width of Balmer Lines (A)
as a Function of Spectral Type/Luminosity Class

Sp	Ia	Iab-Ib	II-III	IV-V
O9	1.5	2.0	-	2.4
B0	1.5	2.0	2.3	3.0
B0.5	1.5	2.0	2.7	3.4
B1	1.5	2.0	3.1	3.8
B2	1.5	2.0	3.9	4.8
B3	1.5	2.0	4.7	6.4
B5	1.5	2.5	6.3	7.8
B7	1.5	3.4	7.9	8.2
B8	1.5	3.9	-	8.4
B9	1.5	4.3	-	-
A0	1.5	4.8	-	-

Table 5.2

Balmer Discontinuity in Magnitudes as a
Function of Spectral Type/Luminosity Class

Sp	Ia	Ib	II	III	IV	V
O9	0.01	0.03	0.05	0.05	0.05	0.05
B0	0.02	0.04	0.06	0.07	0.07	0.08
B1	0.03	0.06	0.08	0.08	0.10	0.10
B2	0.05	0.09	0.10	0.13	0.14	0.14
B3	0.09	0.13	0.15	0.18	0.20	0.20
B5	0.11	0.19	0.20	0.22	0.26	0.26
B7	0.15	0.23	0.24	0.29	0.34	0.34
B8	0.18	0.26	0.28	0.33	0.39	0.39
B9	0.21	0.32	0.34	0.40	0.43	0.41
A0	0.28	0.40	0.41	0.50	0.51	0.48

Table 5.3

Change in Intrinsic Gradient at the Balmer Limit as a Function of Spectral Type

Sp Type	$\Delta\phi$
O9	-0.17
B0	-0.14
B1	-0.10
B2	-0.07
B3	-0.01
B5	+0.05
B7	+0.20
B8	+0.25
B9	+0.30
A0	+0.38

(5.2) Extinction Curves for the Individual Stars

The extinction curves were normalized by using standard wavelengths λ_1 = 4560 A and λ_2 = 7800 A in equ. (2.31). Thus

$$\Delta m'(\lambda) = \frac{\Delta m(\lambda) - \Delta m(7800)}{\Delta m(4560) - \Delta m(7800)} \qquad (5.3)$$

and we have $\Delta m'(4560) = 1$ and $\Delta m'(7800) = 0$. The factor

$$E = \Delta m(4560) - \Delta m(7800) \qquad (5.4)$$

is proportional to the difference ΔE_{B-V} in colour excess between reddened and comparison stars. The wavelengths λ_1 and λ_2 were chosen to be at roughly opposite ends of the quasi-linear region of the scanner curves. The wavelengths of stellar, interstellar and atmospheric bands were avoided.

The normalized extinction curves for the 25 reddened stars are presented in figs. 5.6-5.30. Where two scanner observations were made a mean is given (the comparison stars used for the first and second observations were not the same in every case). Second observations of two stars, HD 147889 and 172488, were not included in the final results as they were made during poor sky conditions; this was indicated by discrepancies in the overlap regions of the scans, and disagreement with BV photometry points. Corrections for mismatching described in the previous section are applied where possible and necessary. For the sake of clarity, error bars are not attached to the individual scanner points in the diagrams: the curves are divided into five segments and mean errors given in each case. These errors, shown displaced below the curves, represent the statistical uncertainty $\sqrt{n}$ combined for reddened and comparison stars, where n is the number of pulse counts. Viewing fig. 5.6 from left to right, the first and second

segments correspond to scan 3 in table 3.1, the third to scan 2 and the fourth and fifth to scan 1. The latter is divided at the Balmer limit, and the mean error given for the fifth segment includes the uncertainty in Balmer discontinuity corrections, where applicable. The infrared points are denoted by open circles with error bars; the systematic part of the uncertainty is omitted as it is assumed to be the same for reddened and comparison stars. Data points arising from UBVRI photometry, where available for both stars in a pair (tables 3.4, 3.5, 4.8 and 4.9), are represented by open circles in the diagrams. The U band is omitted in cases where Balmer discontinuity corrections are applied.

Two of the comparison stars, HD 106068 and HD 150898, have appreciable reddening. For the magnitude difference between a highly reddened star (a) and a moderately reddened star (b) to represent the true extinction law of (a), (b) must follow the same law. To check this we require a third star (c) of similar spectral type and negligible reddening: if the normalized curves arising from the configurations $m_a - m_b$, $m_a - m_c$ and $m_b - m_c$ are the same to within the errors we may conclude that (a) and (b) have the same extinction law. This condition was found to hold in the case of HD 116119 and HD 106068 using HD 110073 as the third star. The extinction curve of HD 106068 is shown in fig. 5.31, and is similar to fig. 5.11. However, the curve of HD 169454 compared with HD 150898 was found to be rather steeper at the ultraviolet end and less steep in the infrared than that obtained using HD 214080 as comparison. The curve of HD 150898 compared with HD 214080, shown in fig. 5.32, is quite flattened at the

ultraviolet end. Corrections have been applied to remove this effect in the relevant cases.

As noted in section 3.4, the data is truncated at 3480 A to remove points affected by red leak in the blue filter. Very slight systematic discrepancies were found between the scanner magnitude differences measured in the first and second orders at 5080 and 5160 A, and it seems reasonable to suppose that these result from filter leakages influencing the first order magnitudes. No discrepancy is apparent at 5240 A. The effect is to produce dips of depth $\sim 0^{m}.005$ at 5080 and 5160 A in the normalized extinction curves, which have been corrected by disregarding the first order data at these wavelengths.

The extinction curve for HD 147084 (A5II) compared with HD 146145 (fig. 5.14) shows a remarkable peak between wavenumbers 2.7 and 2.9 μ^{-1}. The classification of the comparison star is not well established; the Balmer discontinuity is large for types as late as A5, and even a small difference in MK type could produce a distortion of this magnitude in the curve, although the Balmer lines seem to be quite well matched. It may be assumed with some confidence that this feature is of stellar rather than interstellar origin.

The luminosity class of HD 151346 (B8) is unknown, but the Balmer lines appear to correspond quite closely to those of its comparison, HD 110073 (B8IV). The matching is also good with HD 93540 (B7V) but poor with HD 106068 (B9Ia), and it is thus very likely that HD 151346 is of class IV or V.

Key to Figures 5.6-5.32

Closed circles:	scanner data unaffected by luminosity mismatching.
Triangles:	scanner data with Balmer corrections applied.
Open circles: (without error bars)	UBV photometry, also RI photometry where available for both stars in a pair. U points are omitted in cases where Balmer corrections are applied.
Open circles: (with error bars)	JHKL infrared photometry.
Scanner errors:	mean statistical uncertainties in scanner data points are denoted by error bars placed below the extinction curve; broken lines indicate the segment of the curve to which they apply. The 2.65-2.90 μ^{-1} segment error includes the uncertainty in the Balmer discontinuity corrections, where appropriate.

Fig. 5.6 HD 77581 compared with (1) HD 64760 and (2) HD 99171 (mean of two observations).

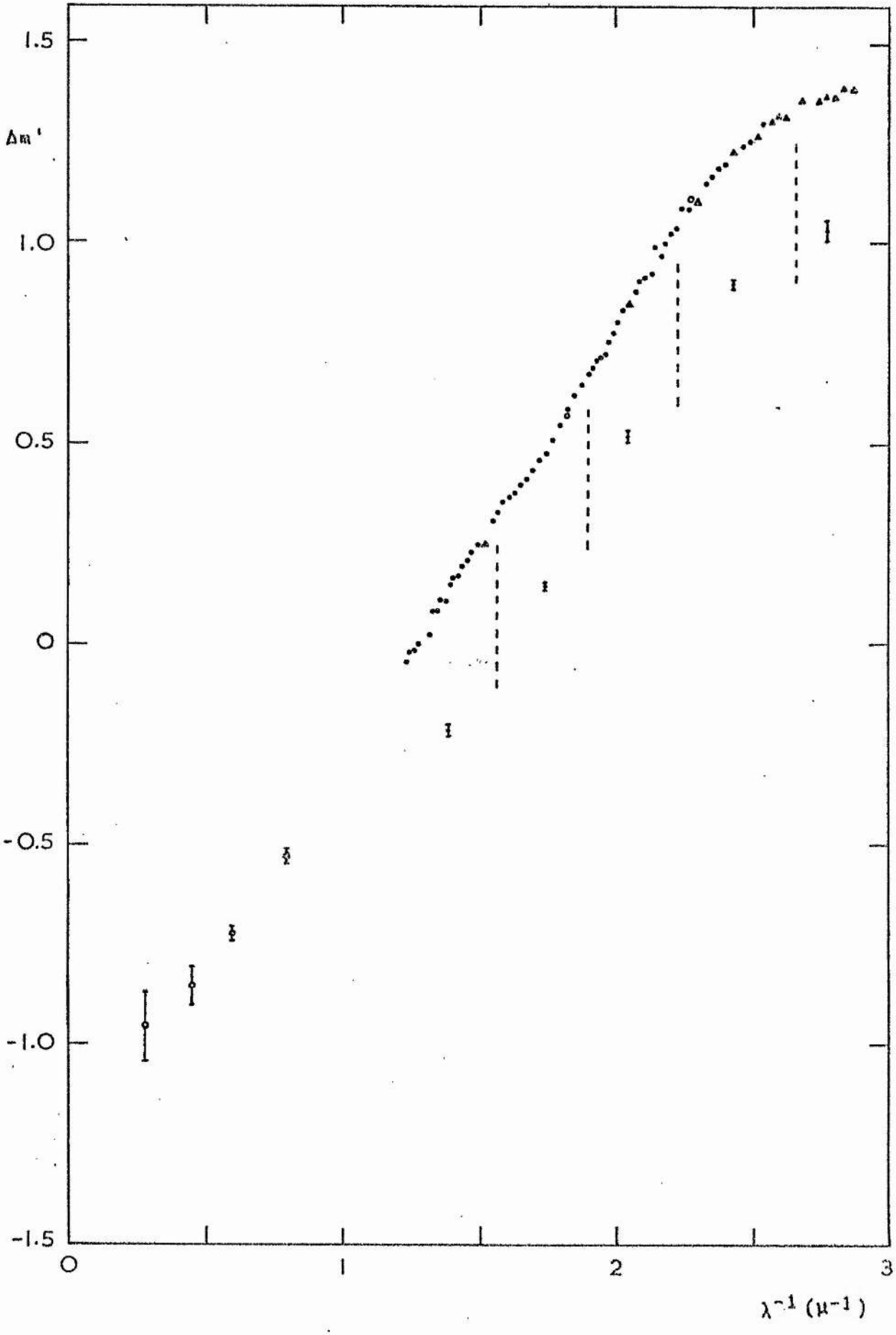

Fig. 5.7 HD 80558 compared with HD 93540.

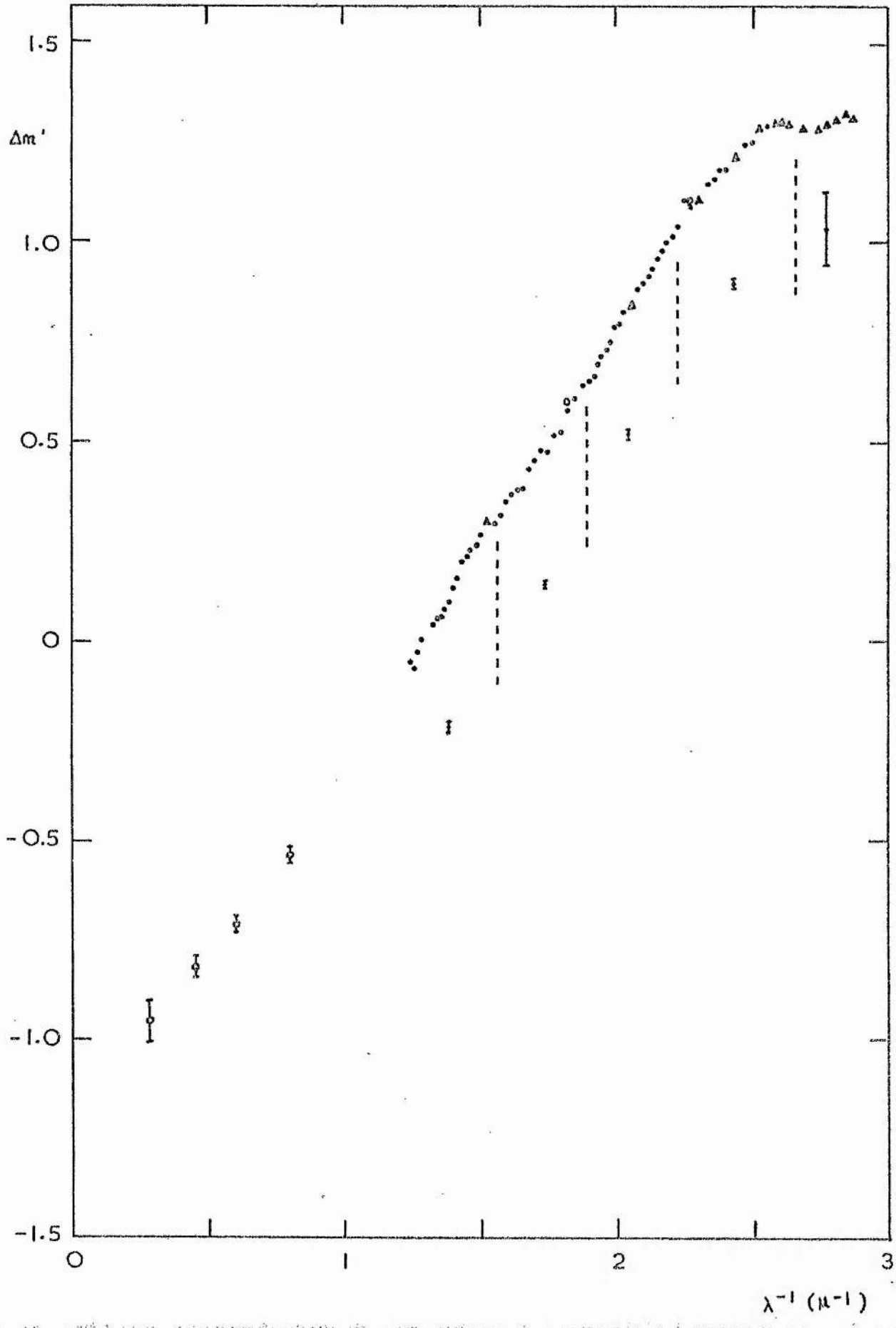

Fig. 5.8 HD 90706 compared with HD 96088.

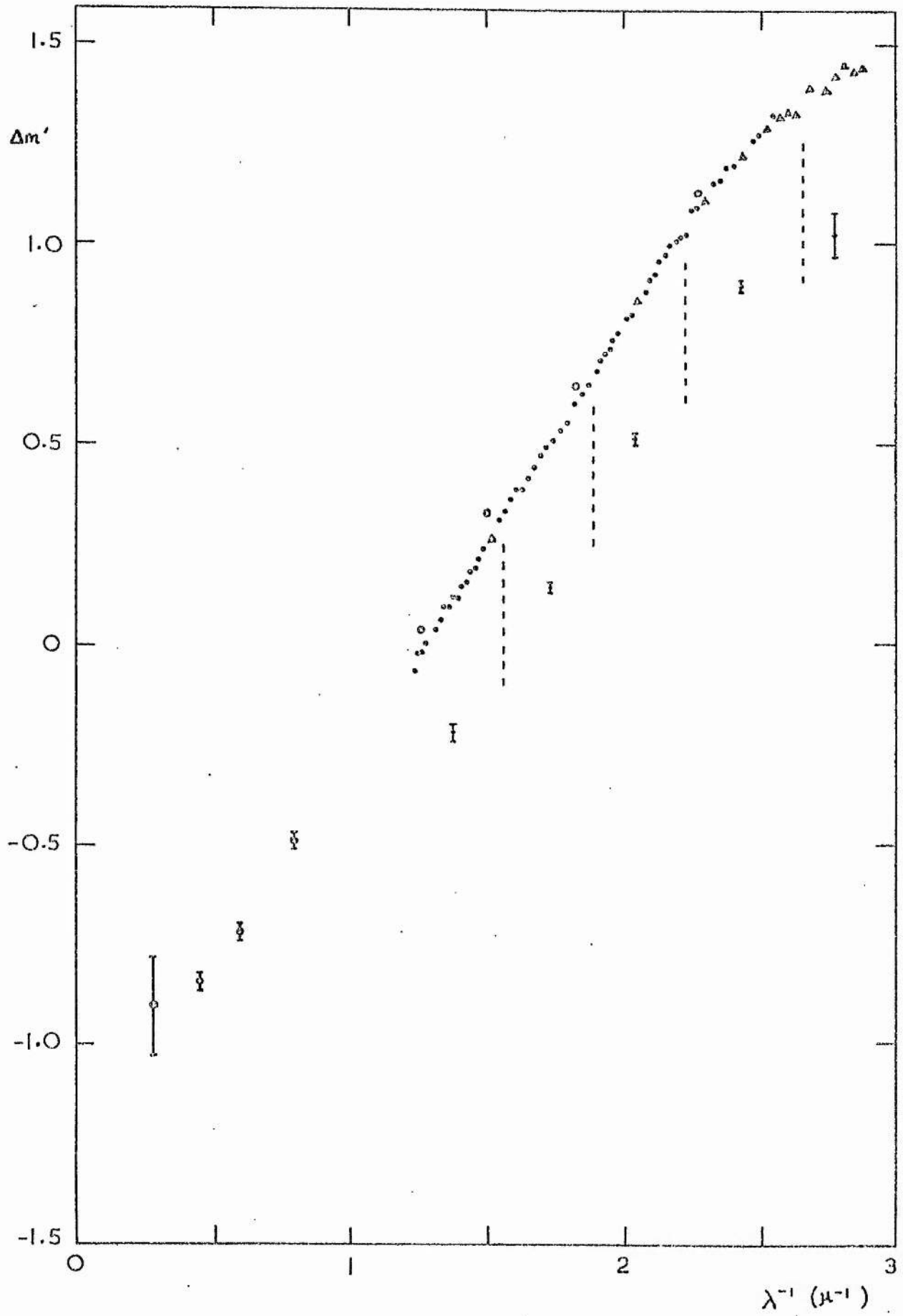

Fig. 5.9 HD 92964 compared with HD 96088.

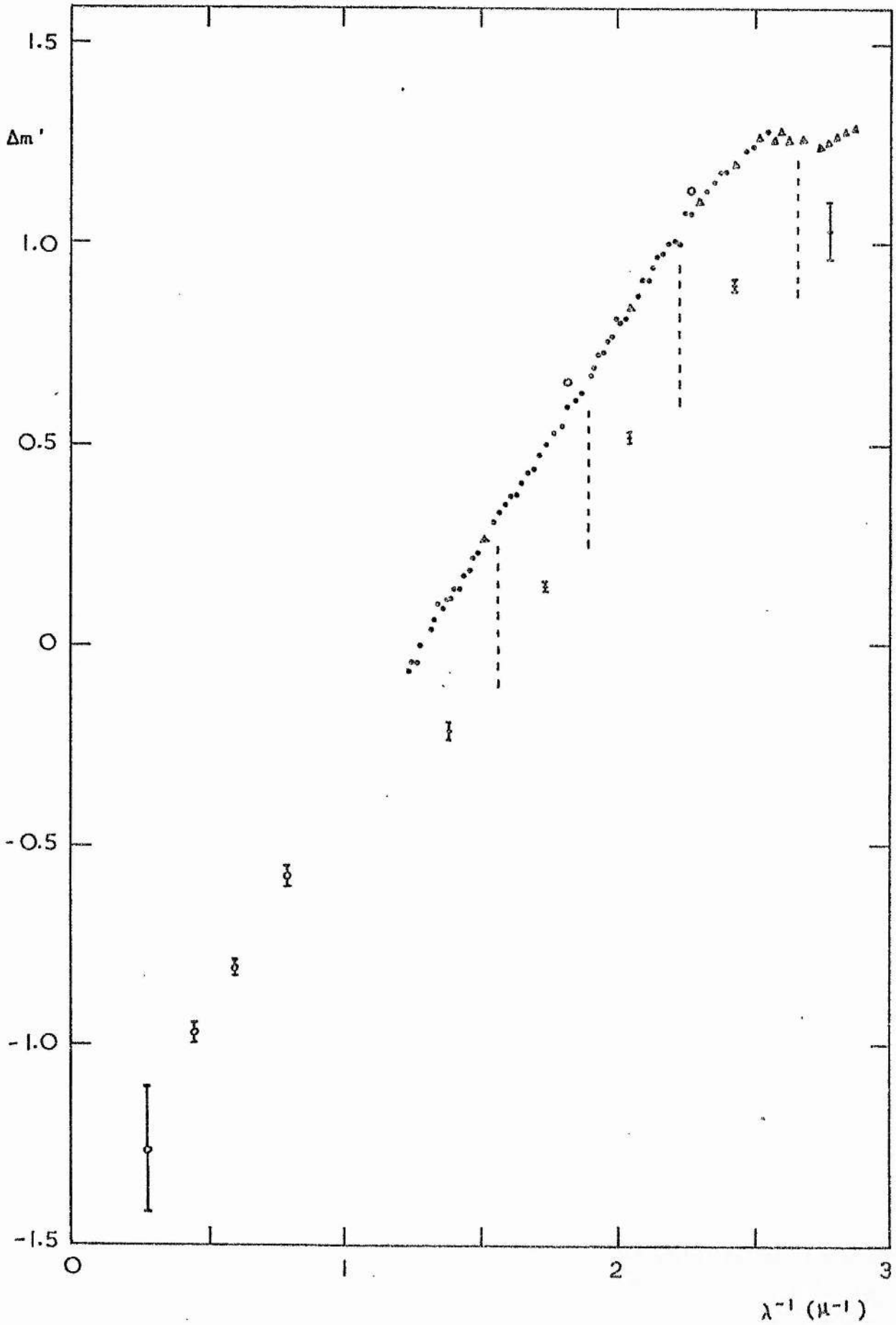

Fig. 5.10 HD 115842 compared with (1) 64760 and (2) 99171 (mean of two observations)

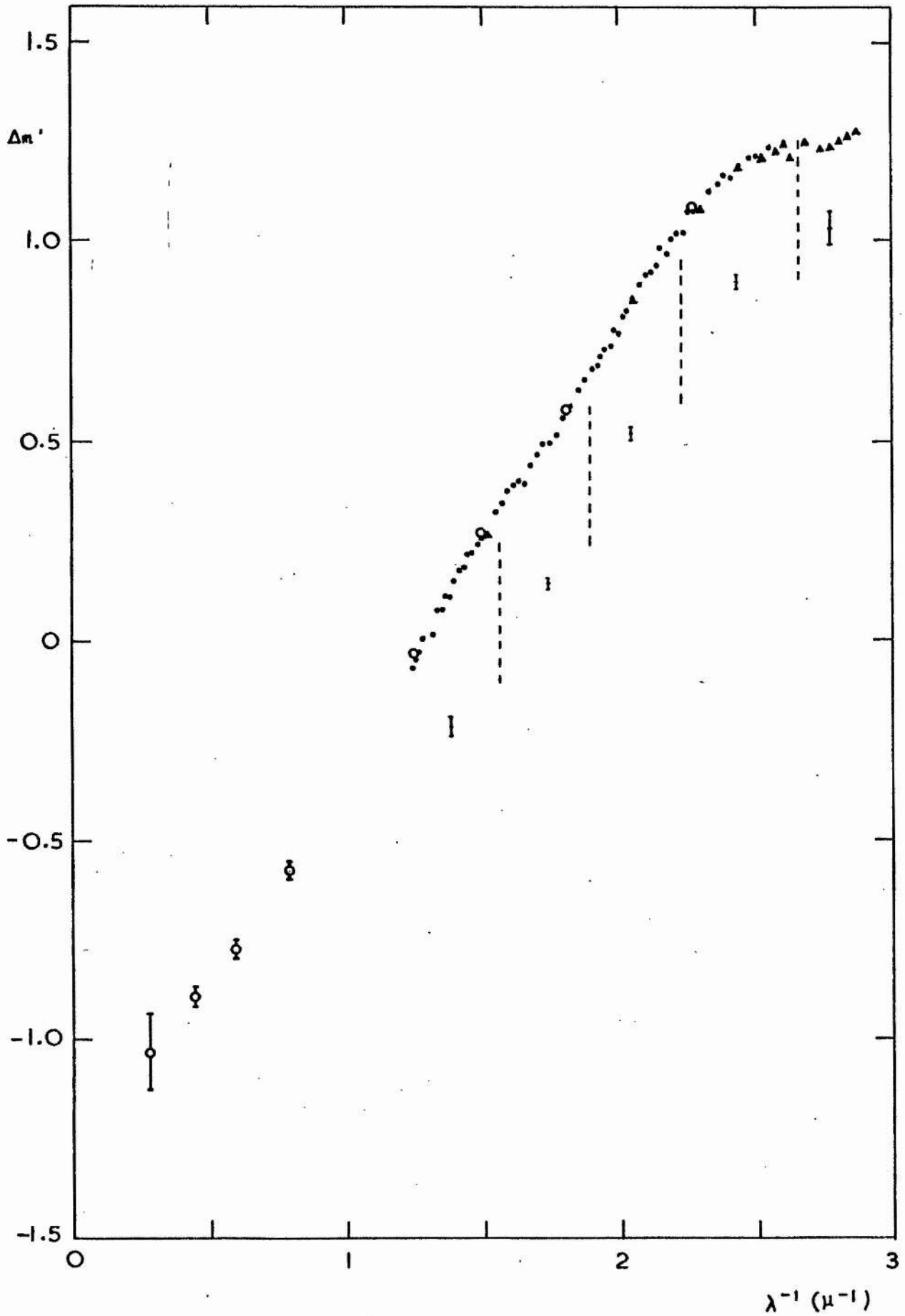

Fig. 5.11 HD 116119 compared with 106068

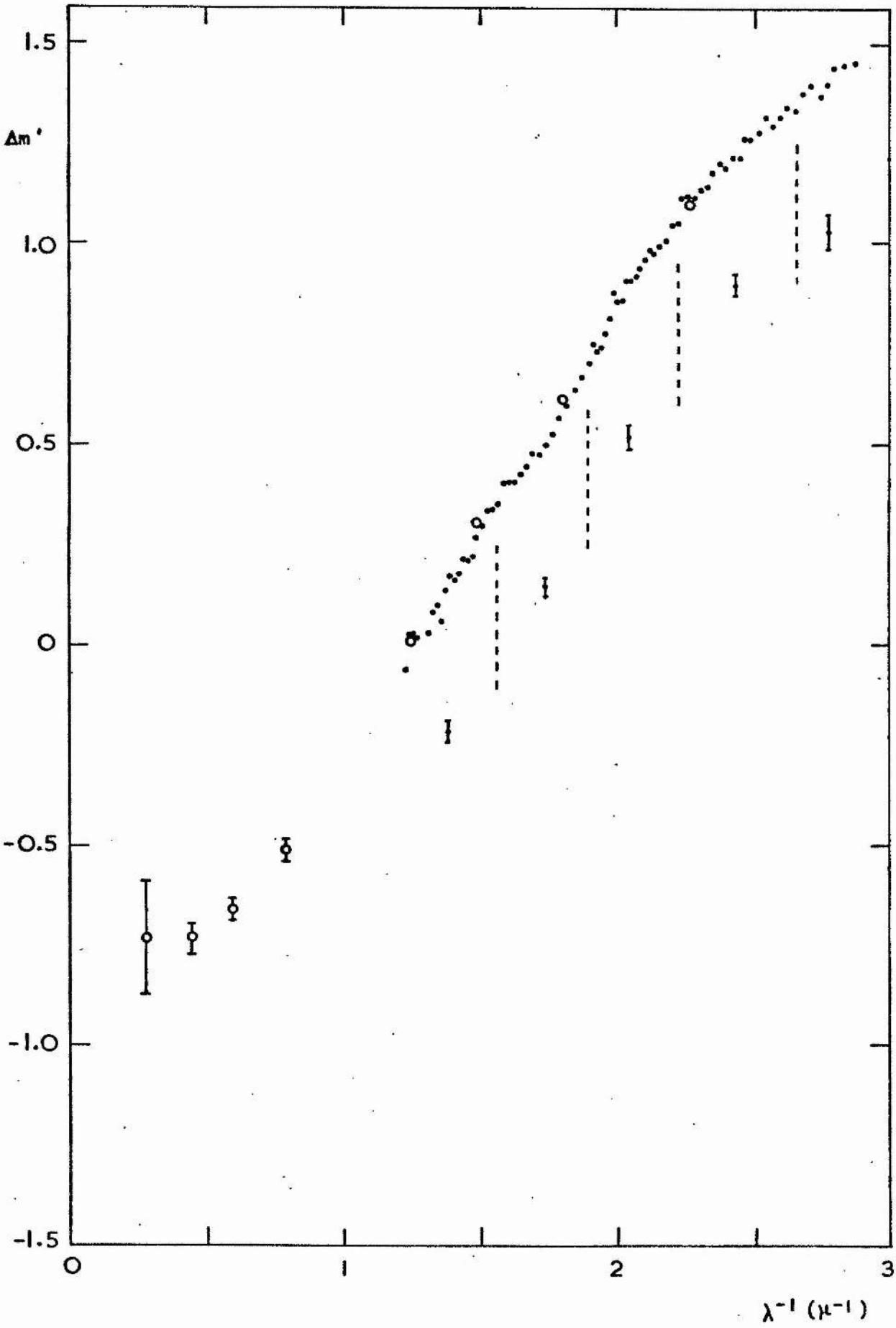

Fig. 5.12 HD 142468 compared with 99171

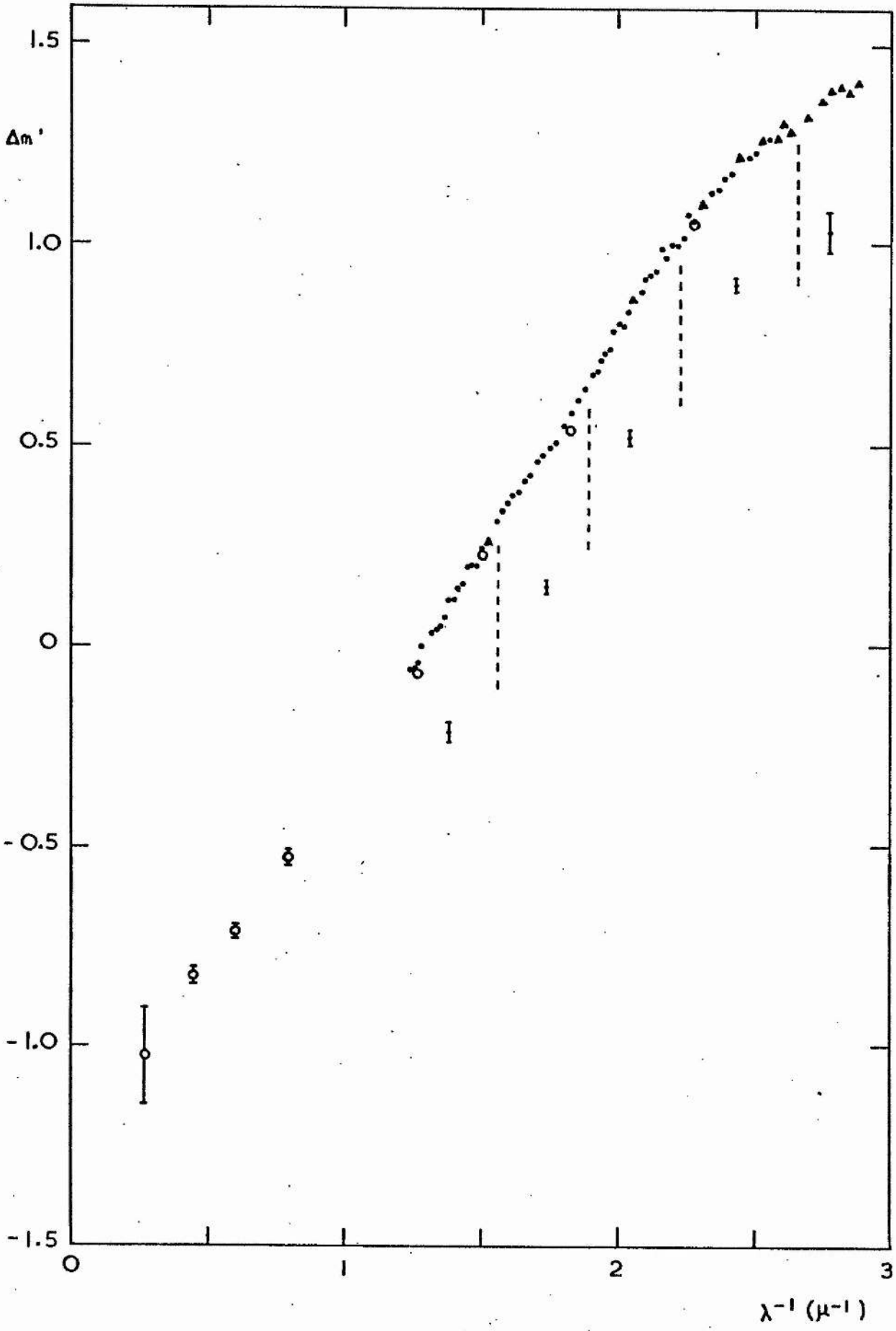

Fig. 5.13 HD 144969 compared with (1) 99171 and (2) 150898 (mean of two observations)

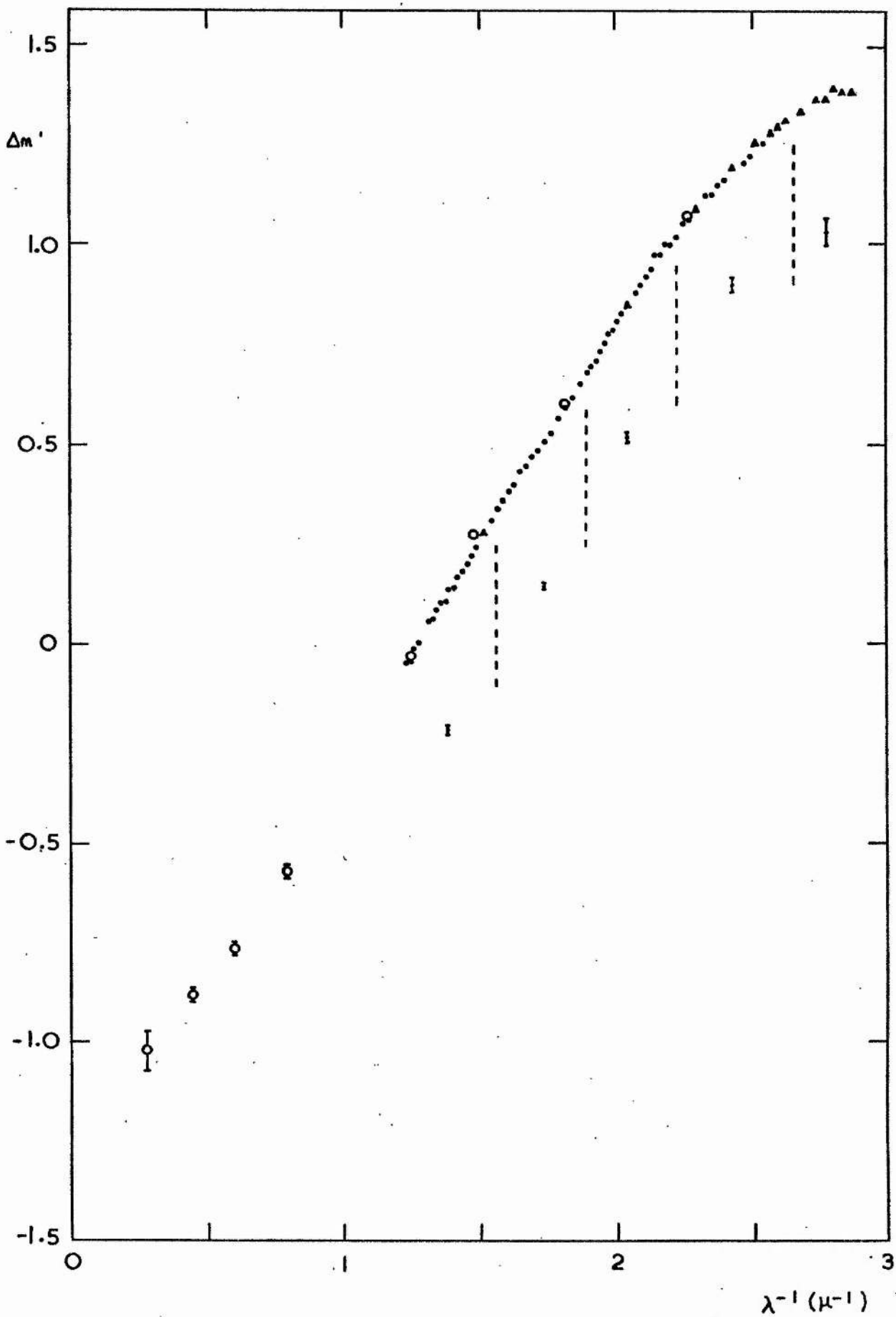

Fig. 5.14 HD 147084 compared with 146145
(mean of two observations)

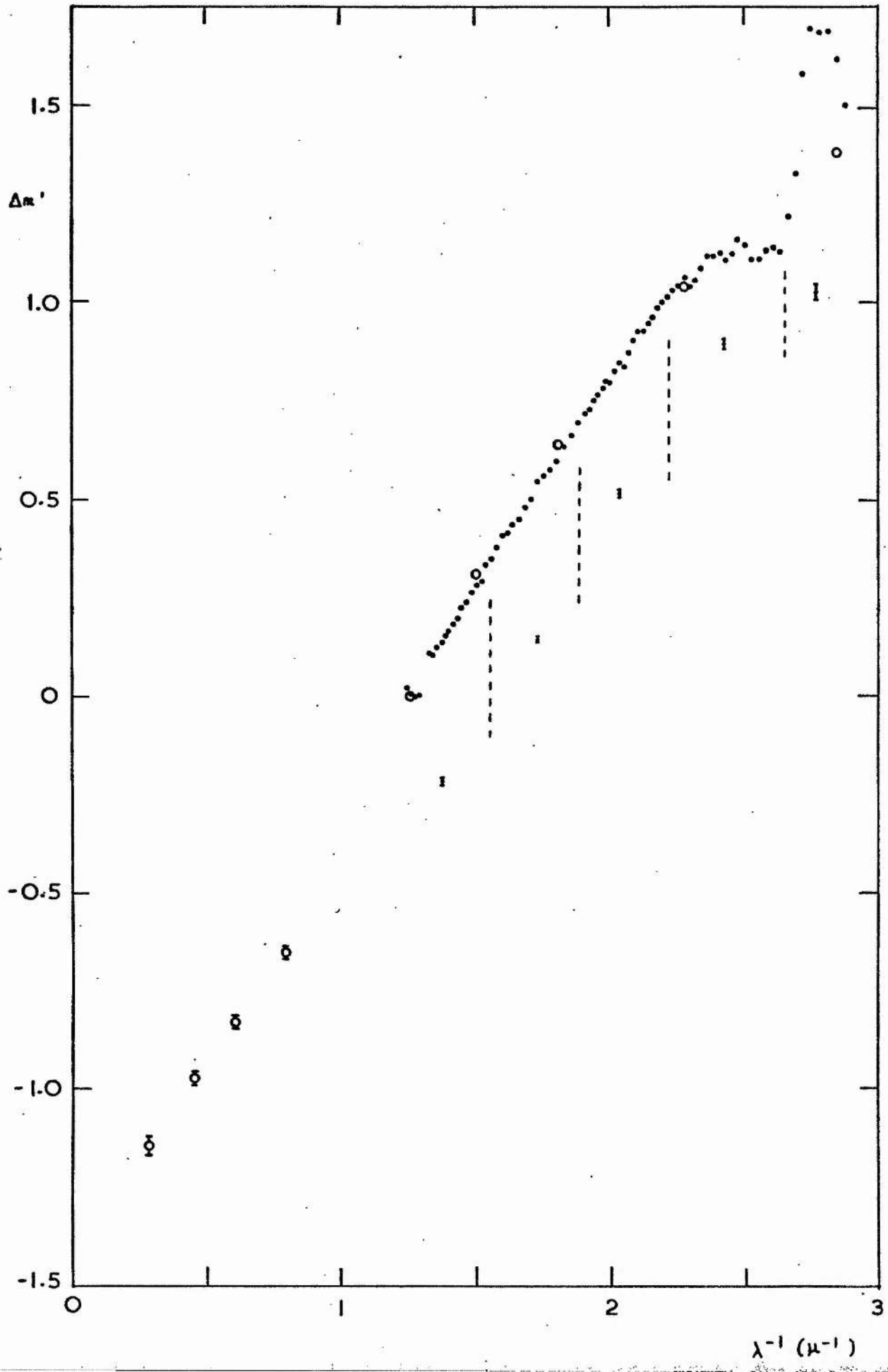

Fig. 5.15 HD 147889 compared with HD 148703.

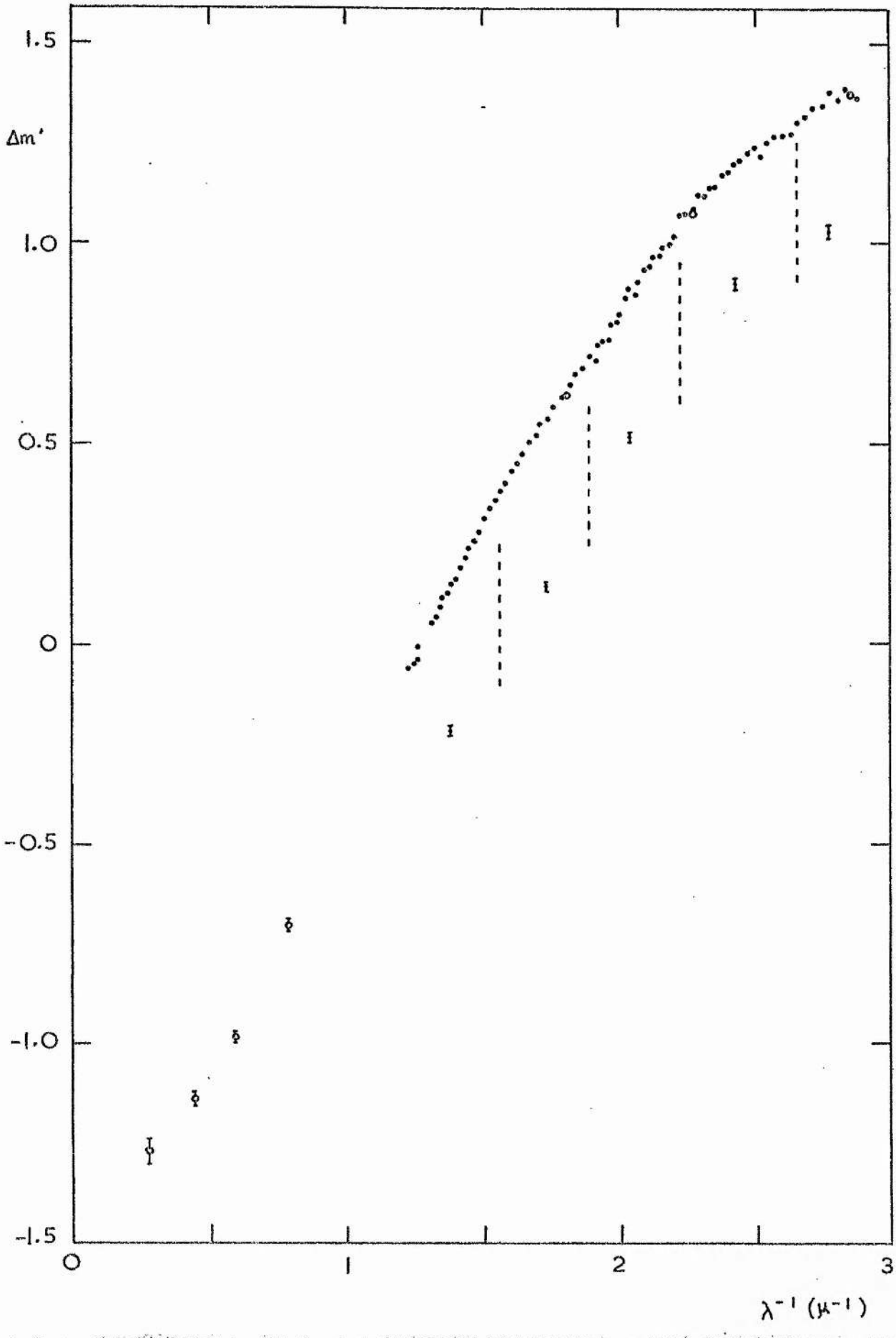

Fig. 5.16 HD 148379 compared with 166197

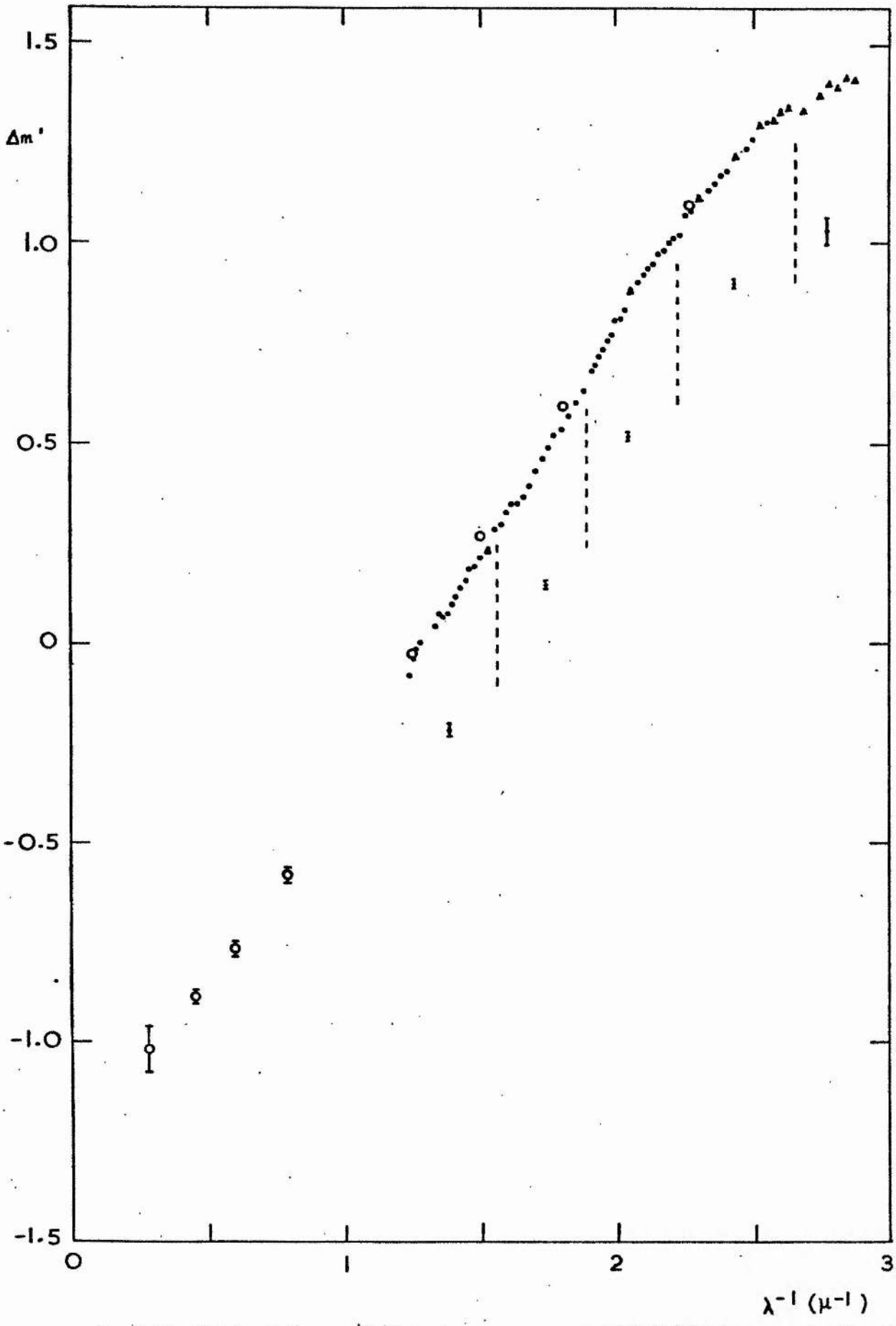

Fig. 5.17 HD 148688 compared with 214080

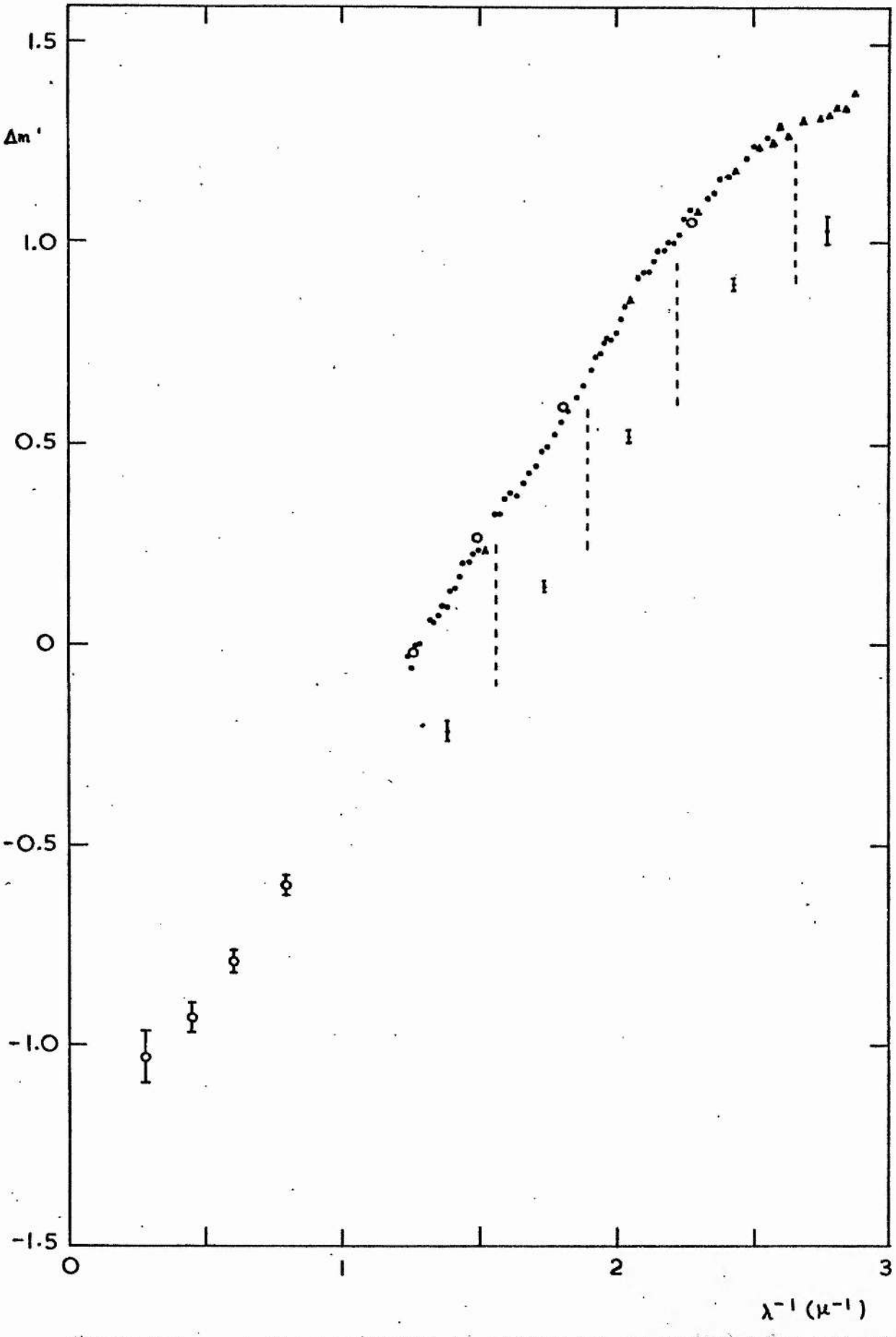

Fig. 5,18 HD 151346 compared with 110073

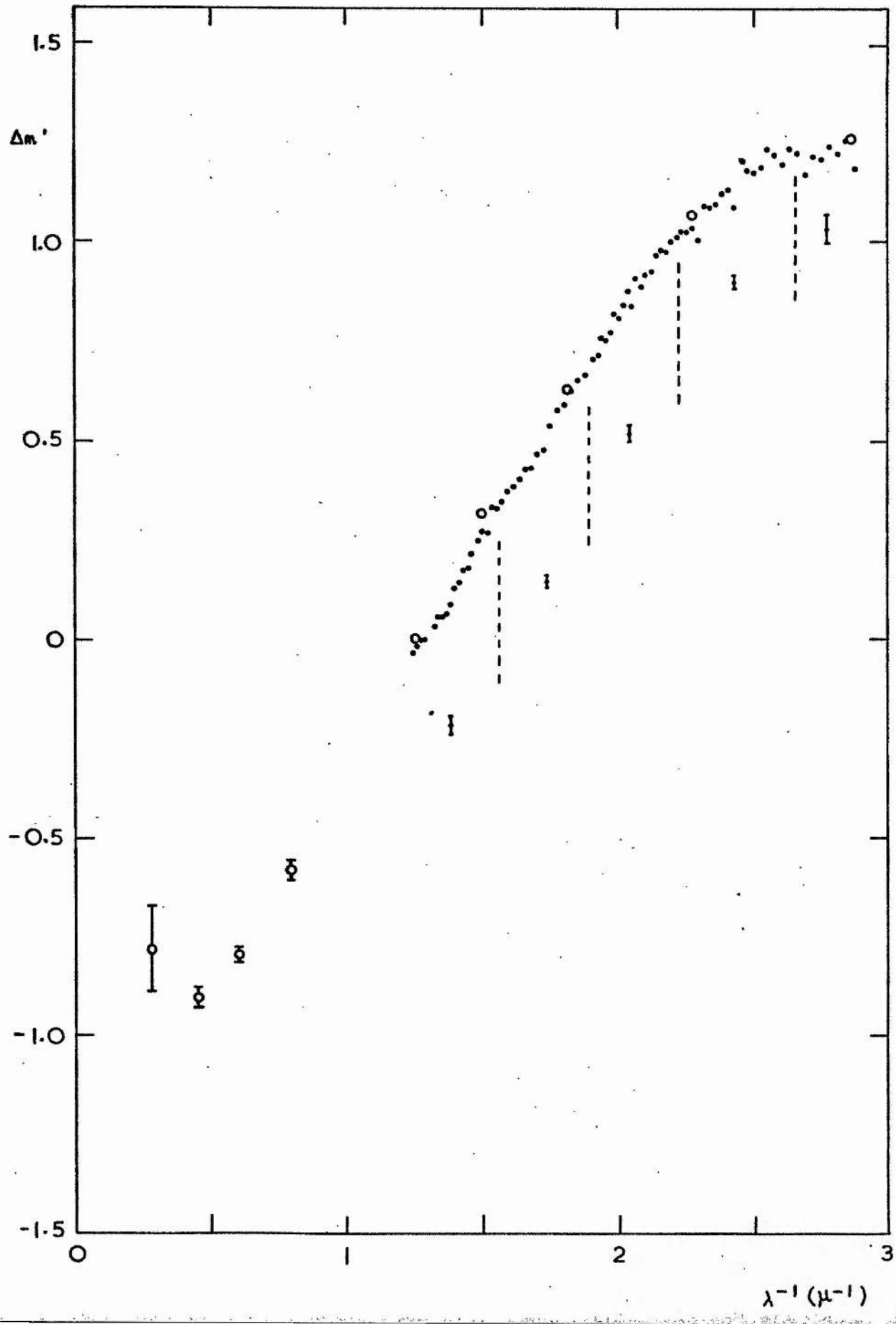

Fig. 5.19 HD 152235 compared with 150898

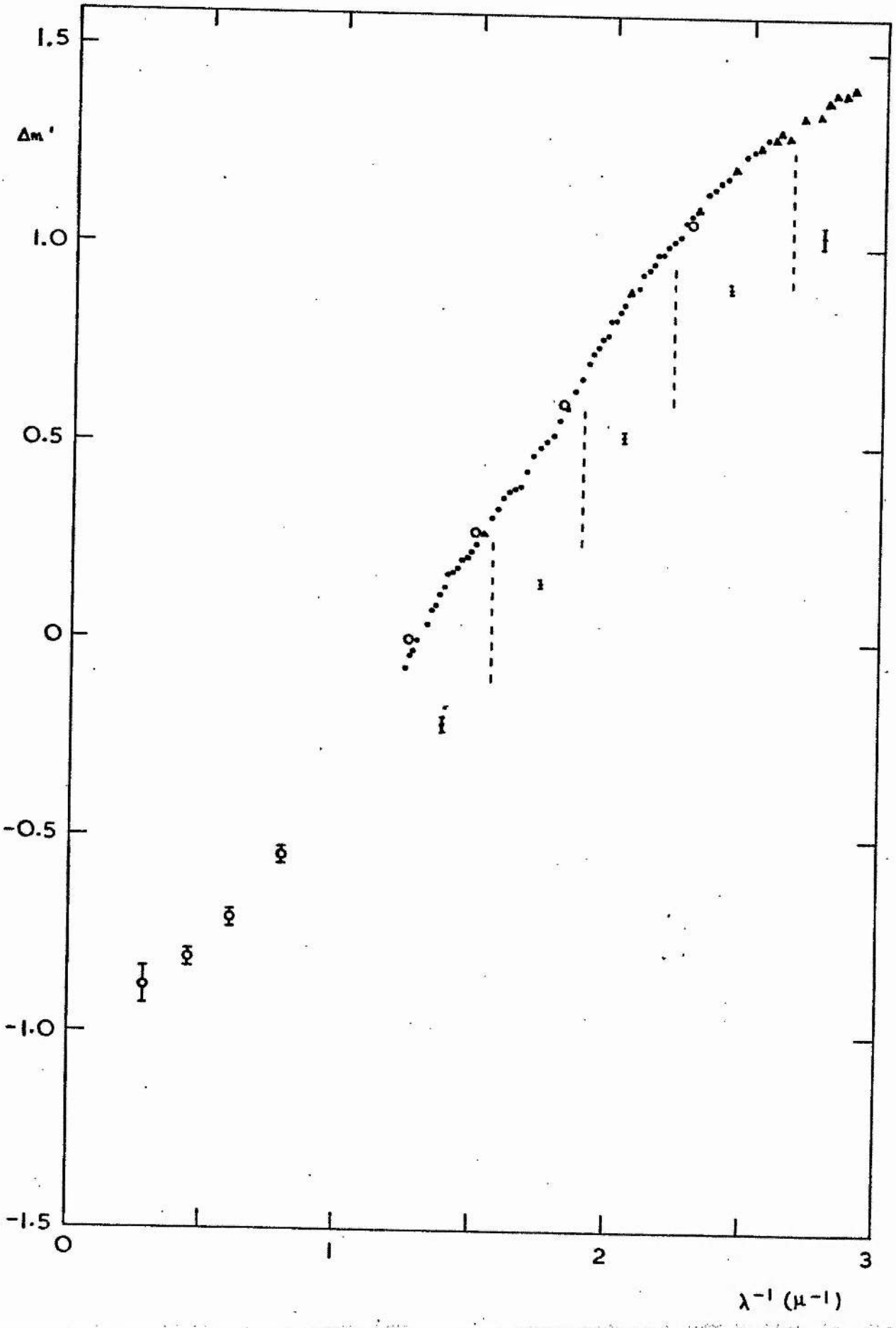

Fig. 5.20 HD 152236 compared with 214080

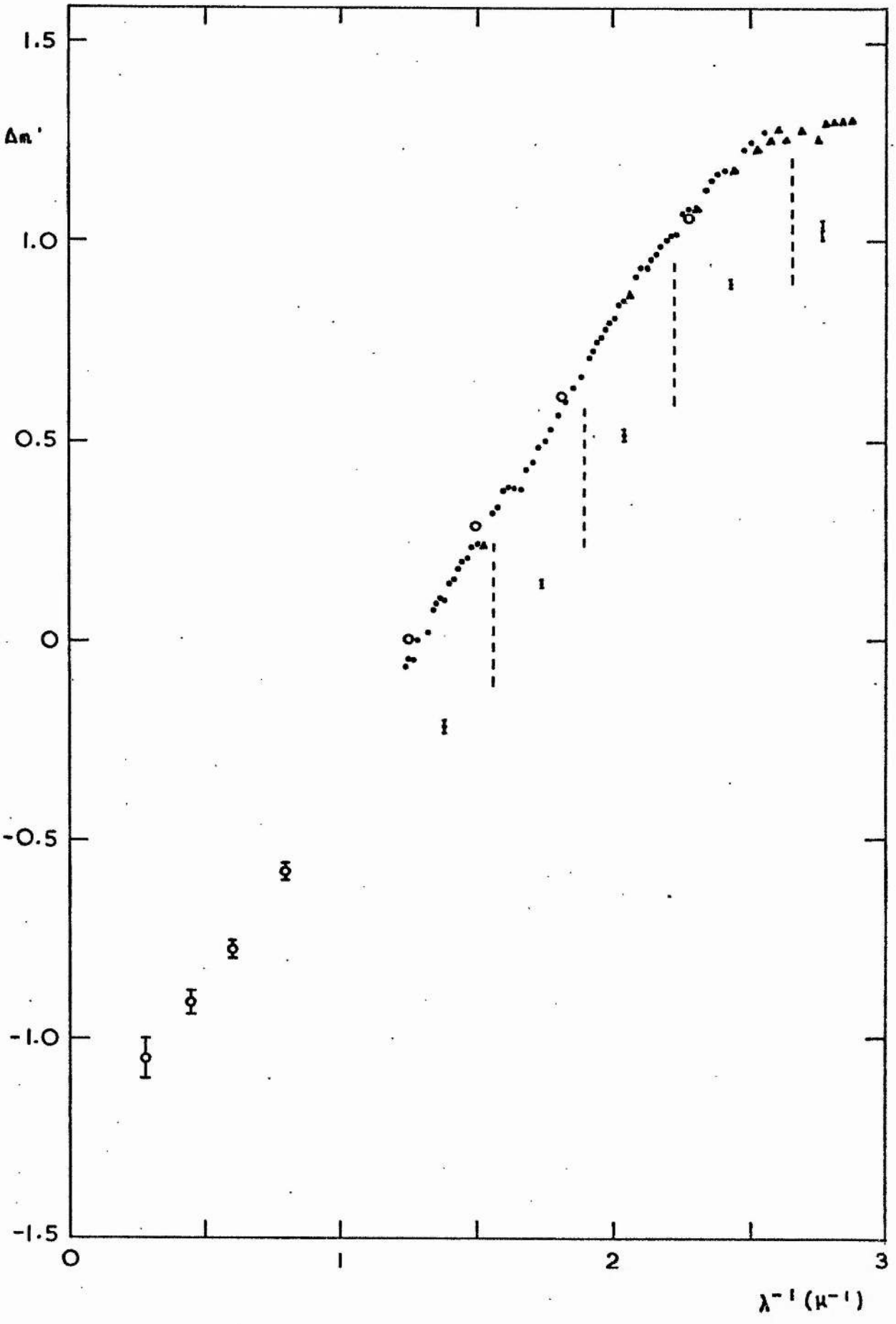

Fig. 5.21 HD 154043 compared with 214080

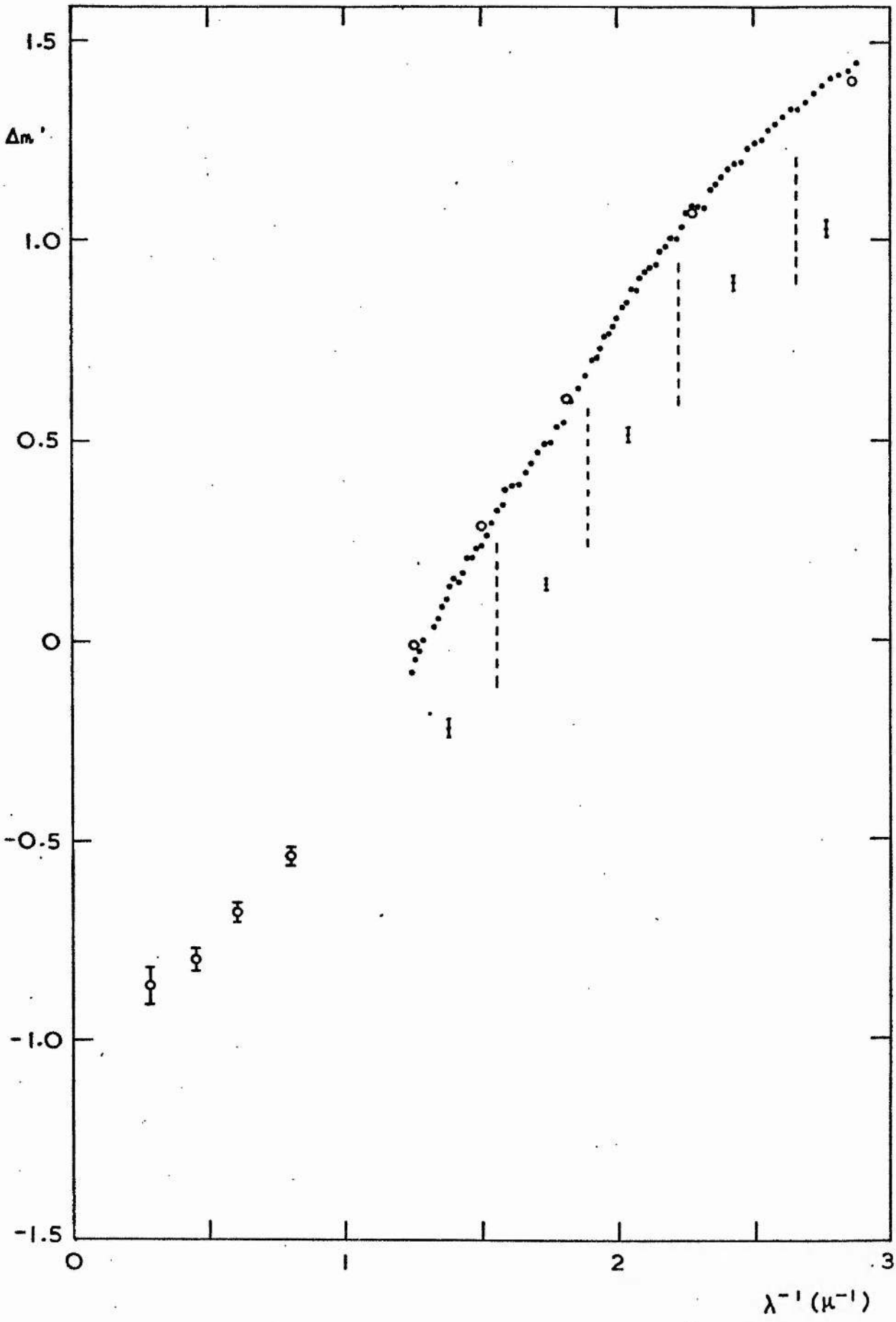

Fig. 5.22 HD 156201 compared with 214080

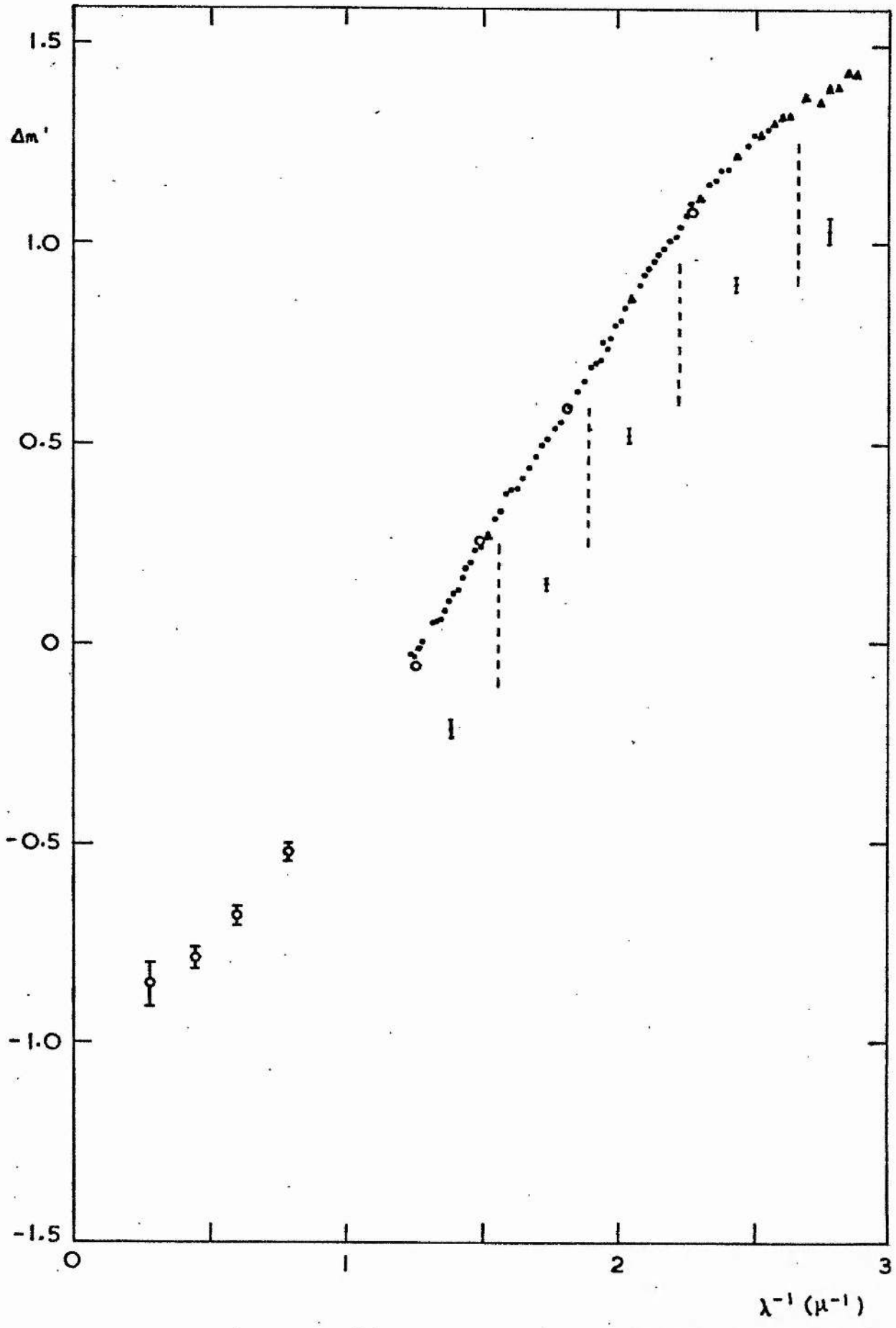

Fig. 5.23 HD 165319 compared with 150898

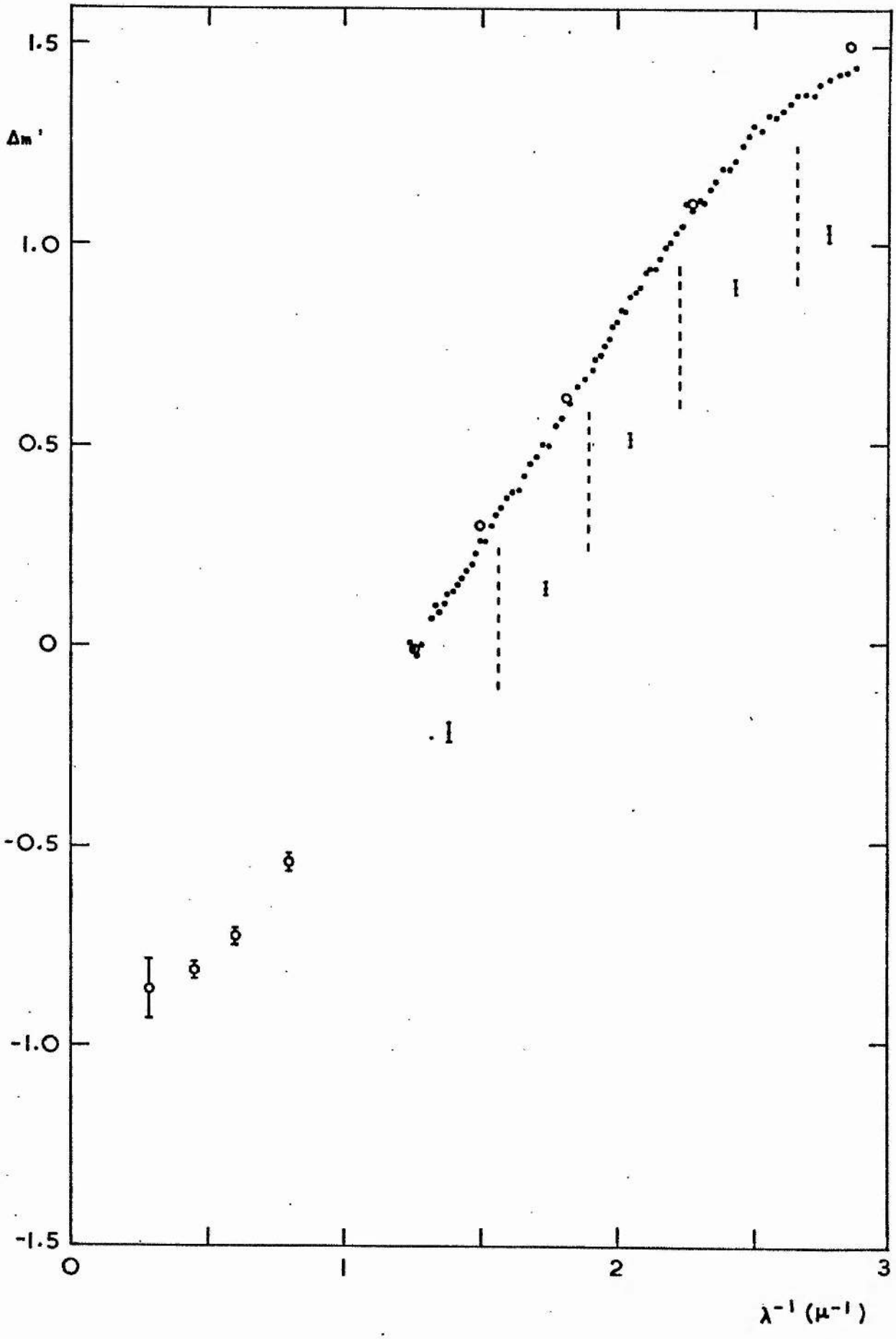

Fig. 5.24 HD 166628 compared with 172910

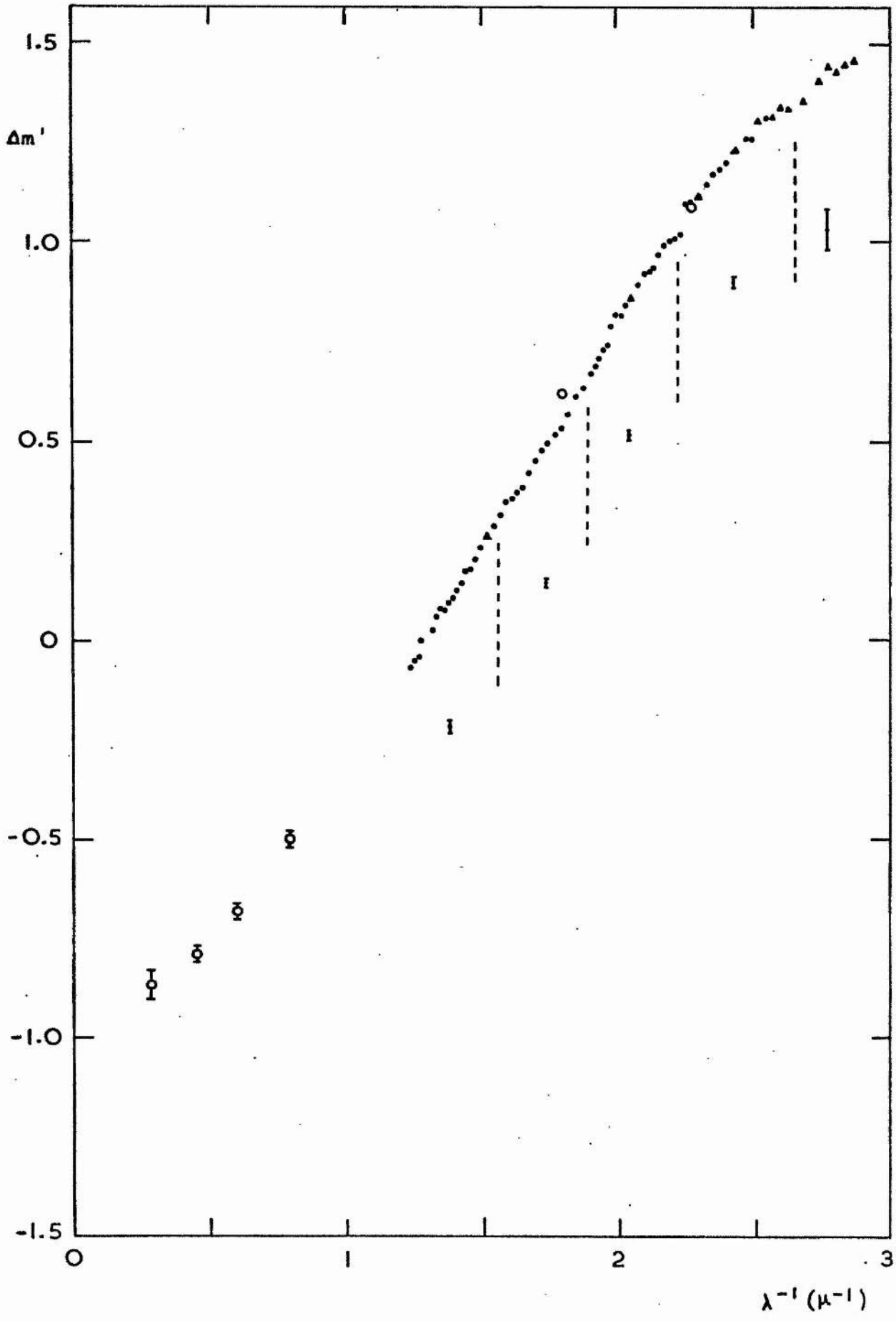

Fig. 5.25 HD 167838 compared with 136664

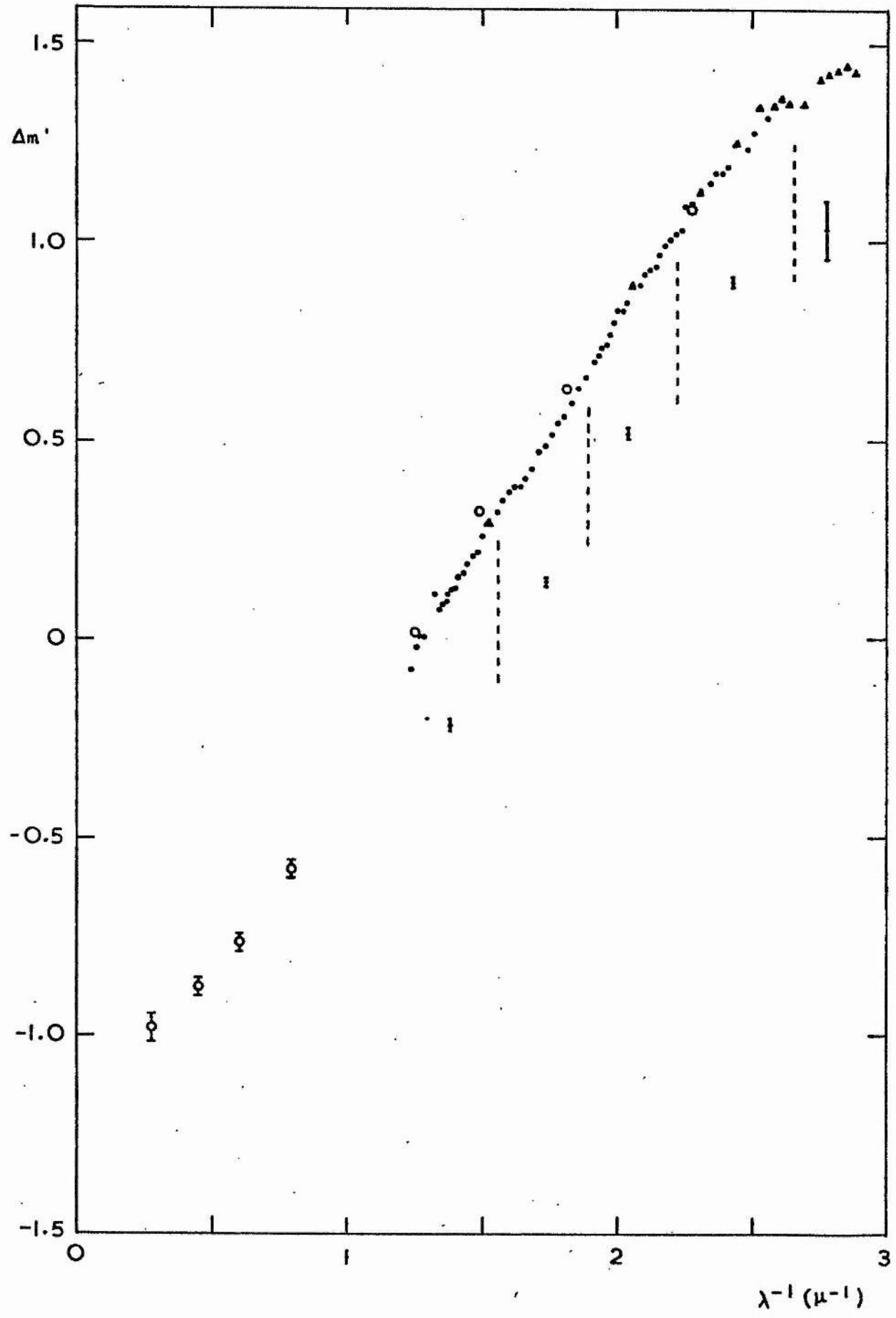

Fig. 5.26 HD 168571 compared with 214080

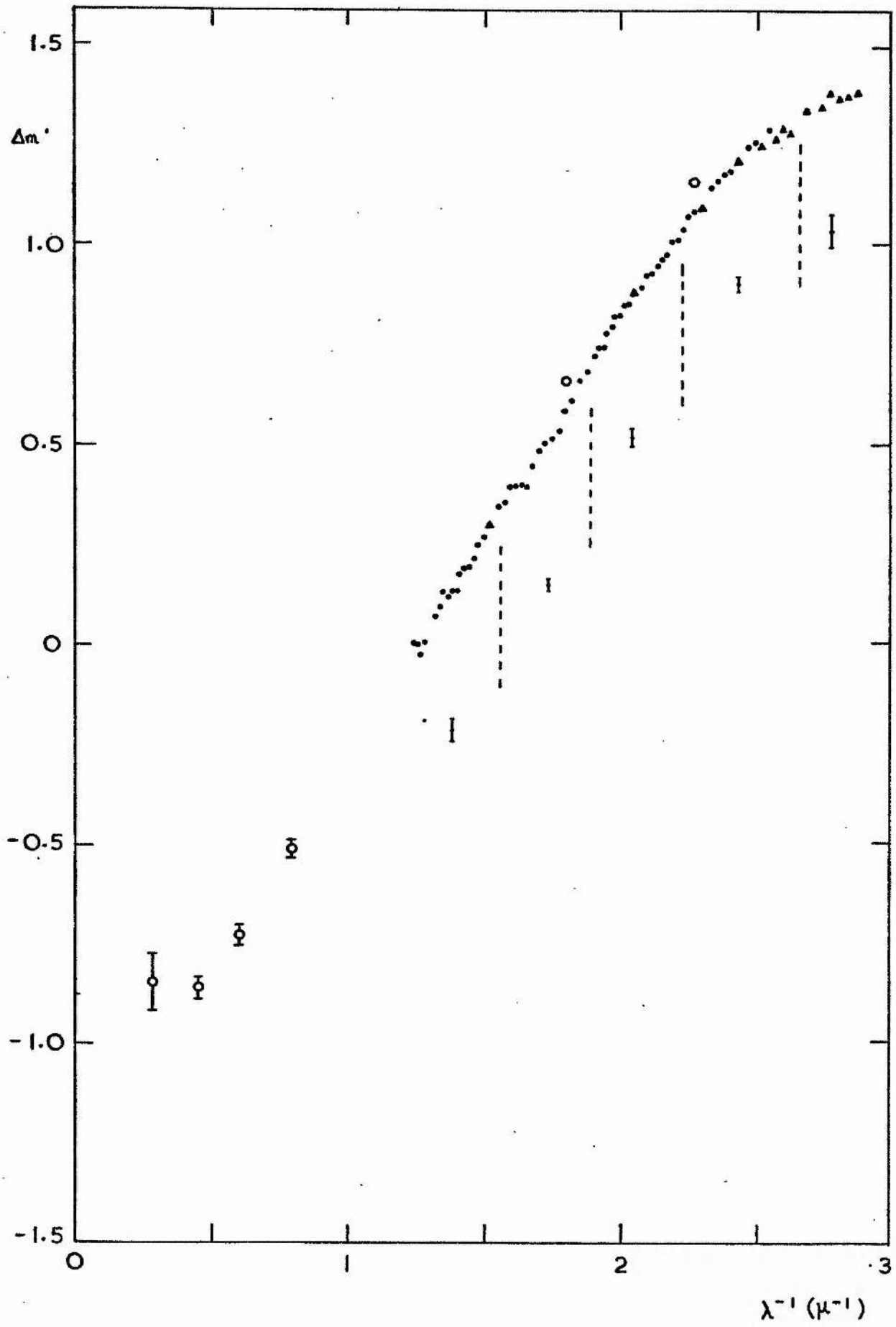

Fig. 5.27 HD 169454 compared with (1) 150898 and (2) 214080 (mean of two observations)

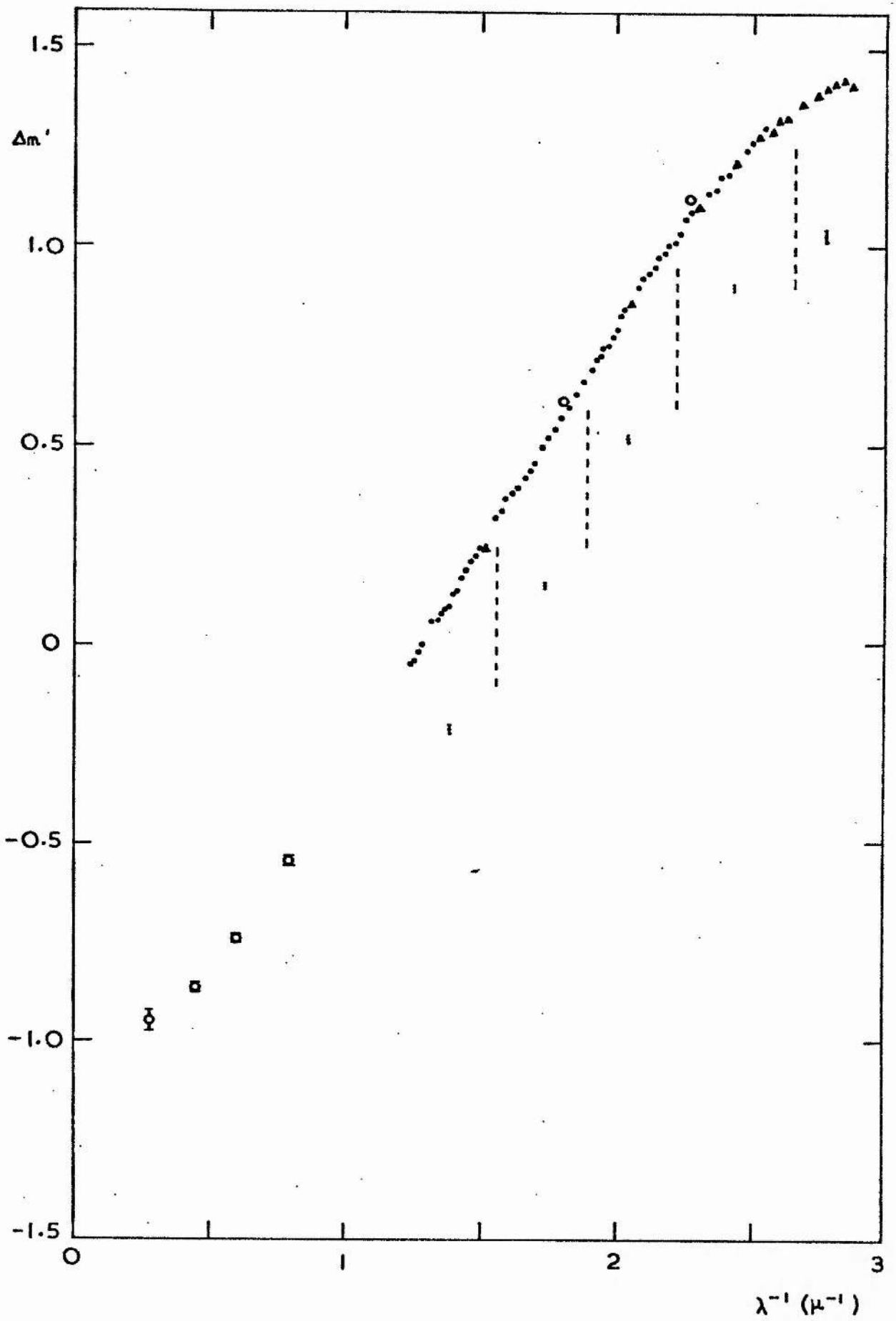

Fig. 5.28 HD 170938 compared with 214080

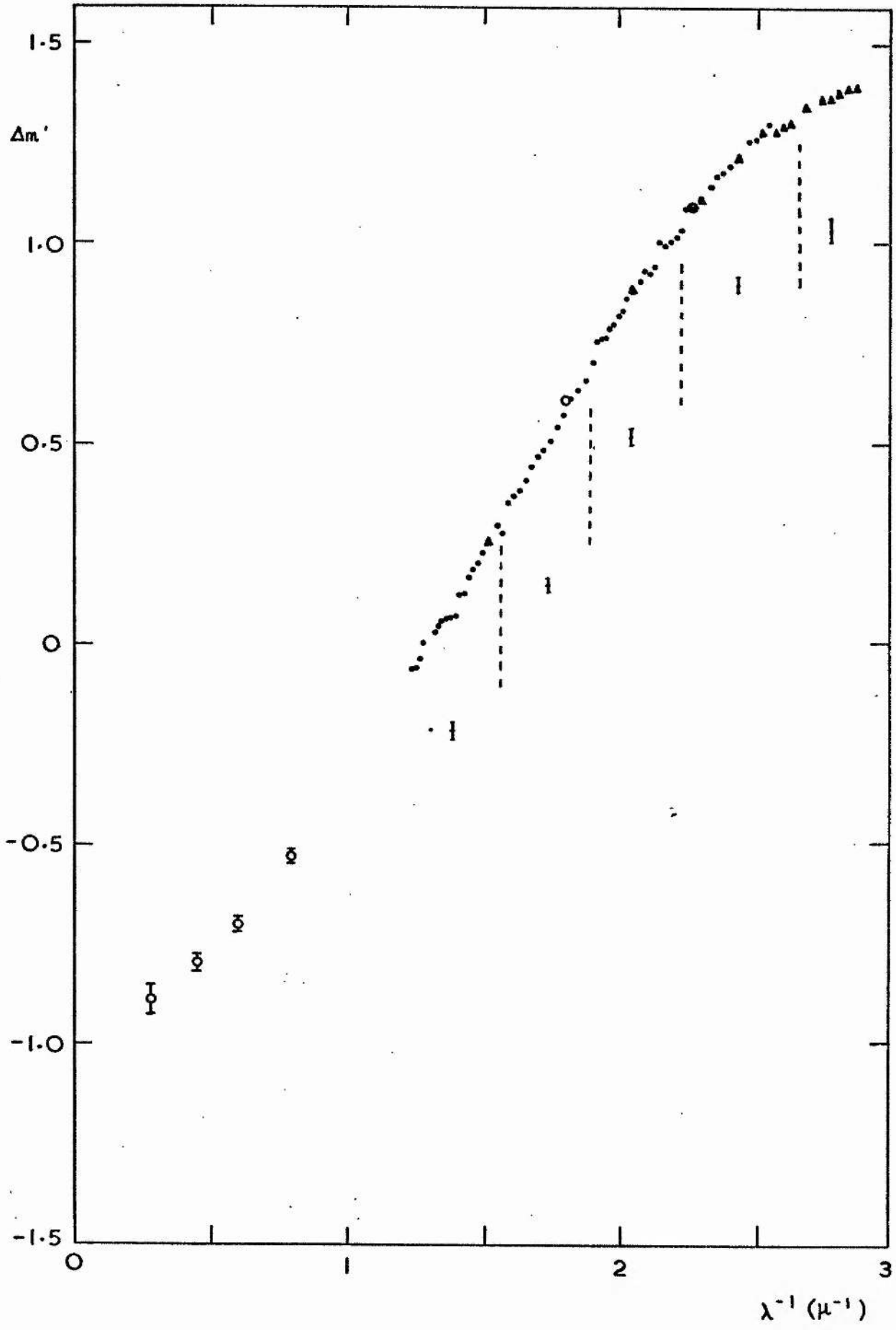

Fig. 5.29 HD 171012 compared with 214080
(mean of two observations)

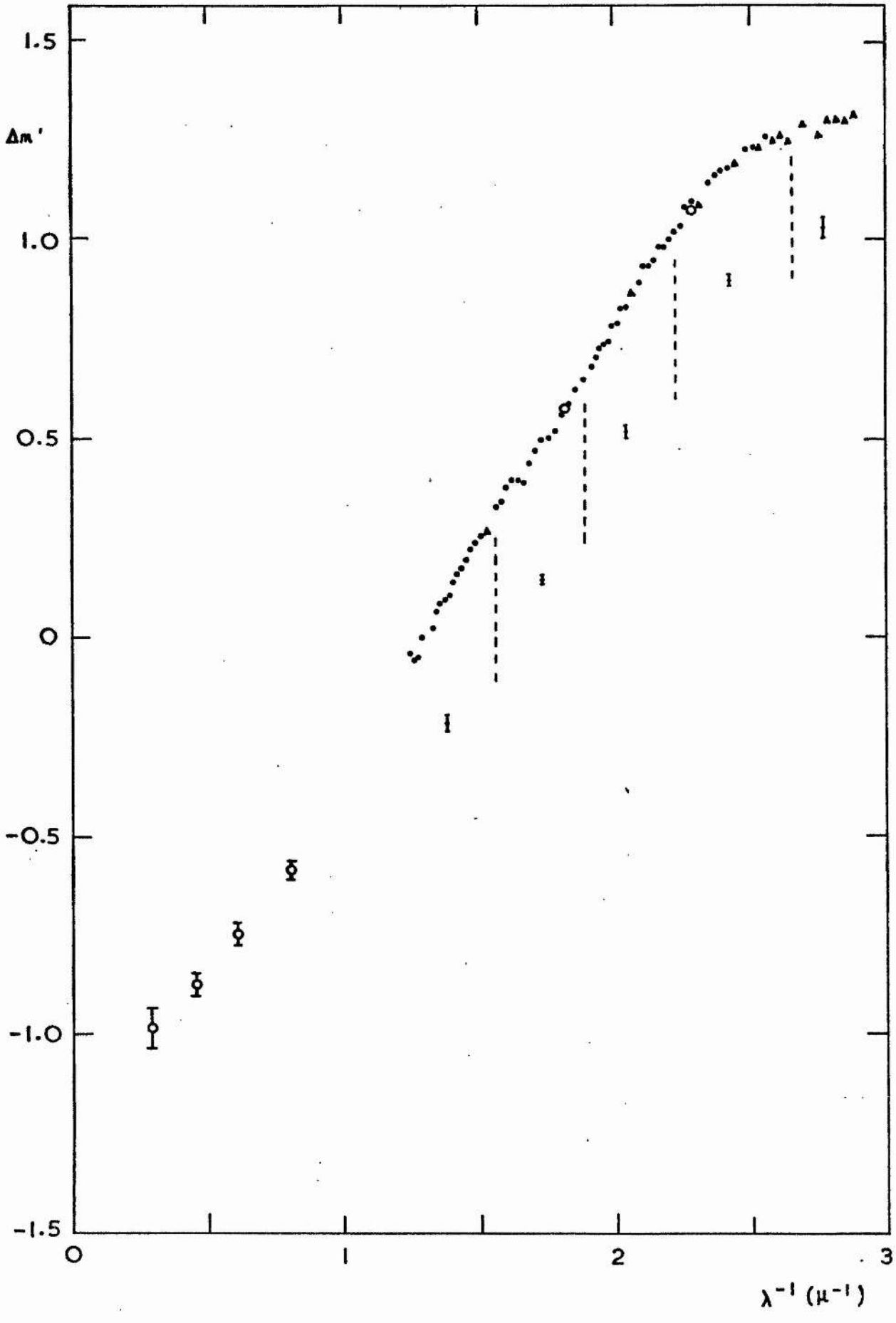

Fig. 5.30 HD 172488 compared with 214080

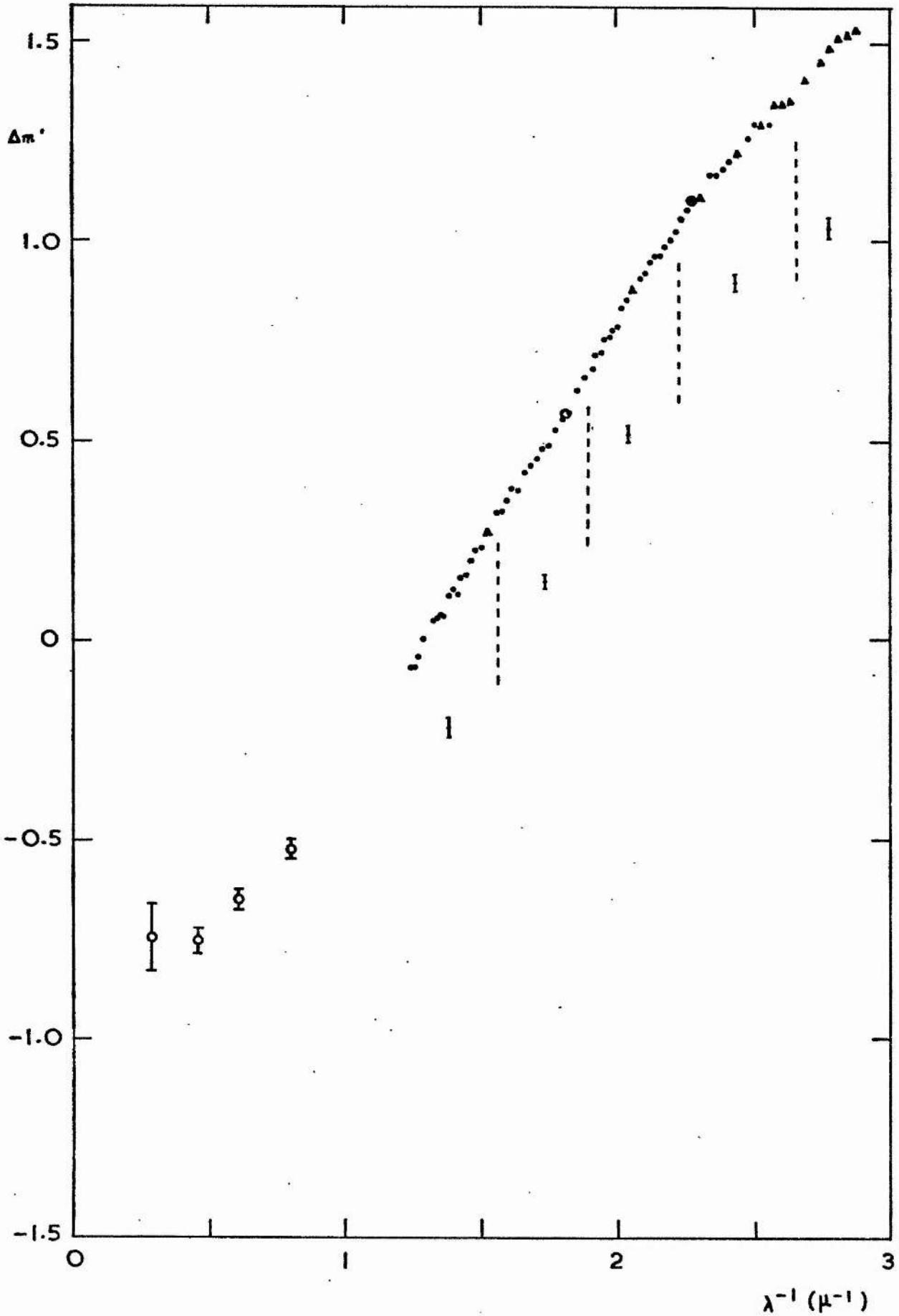

Fig. 5.31 HD 106068 compared with 110073

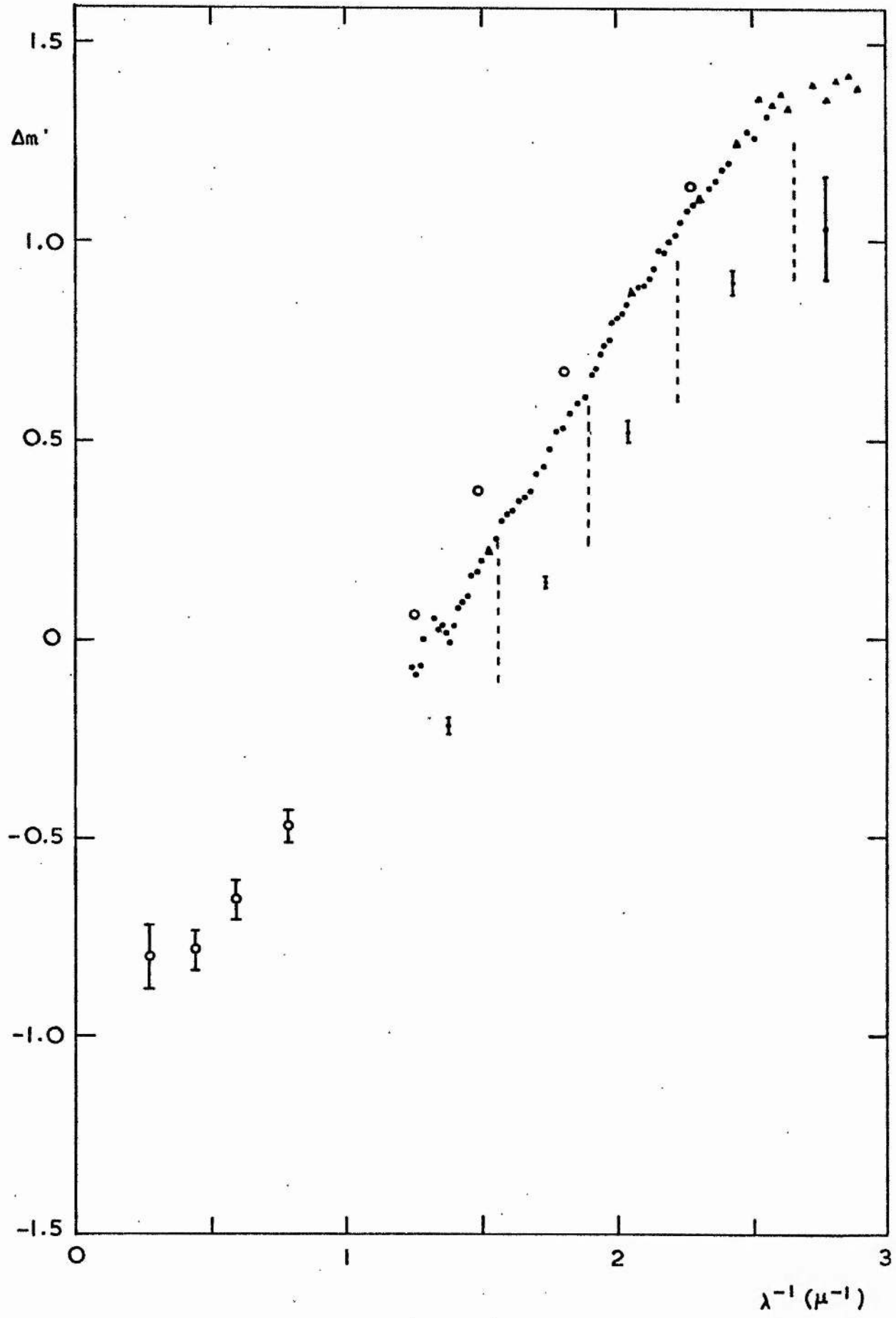

Fig. 5.32 HD 150898 compared with 214080

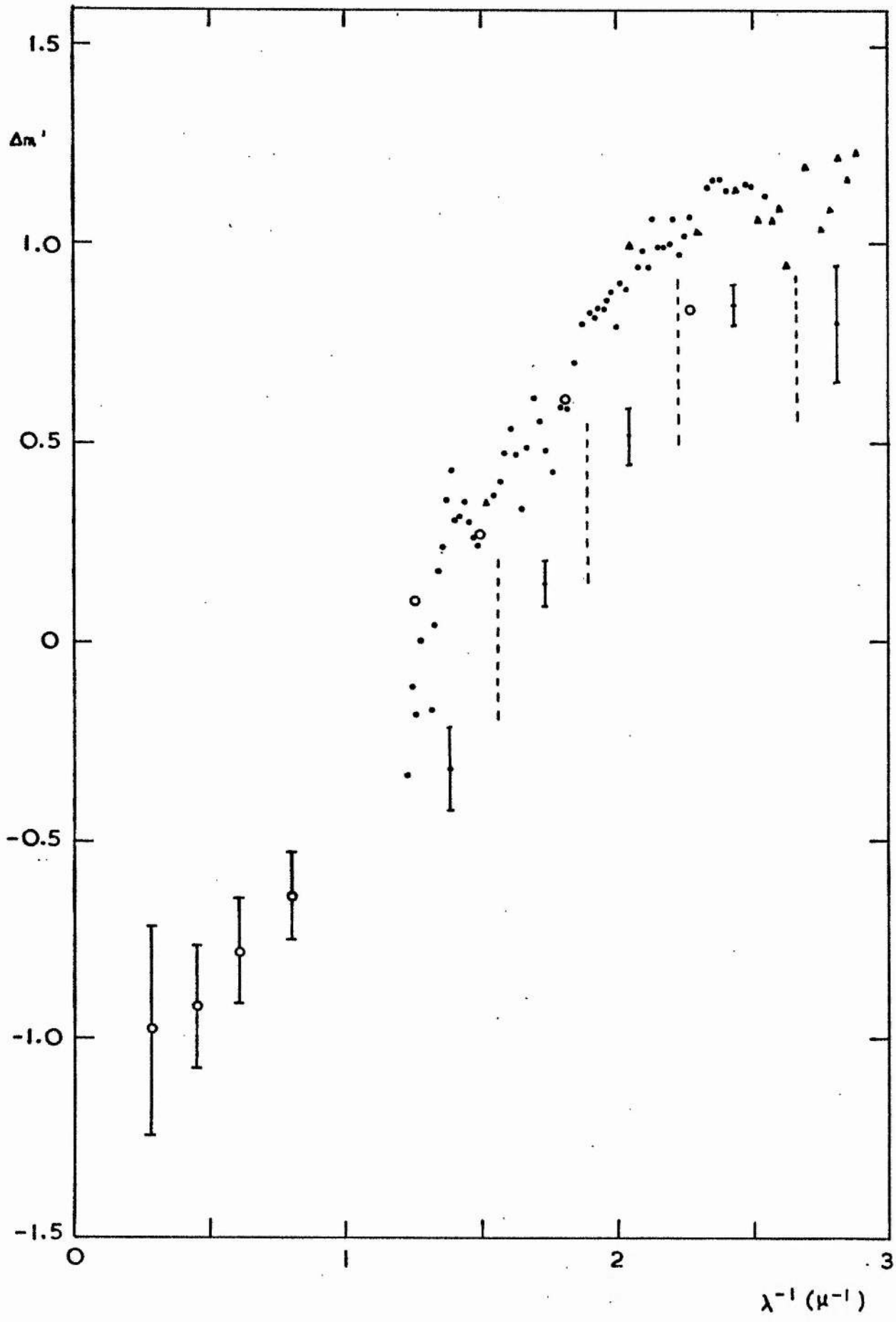

(5.3) Classification of the Curves

The extinction curves in figs. 5.6-5.30 were divided into groups of similar overall shape. The groups have been labelled A, B, C, D, E, F by Whittet, van Breda and Nandy (1973) according to the slope at the ultraviolet end of the scanner curves. In general there is a tendency for the infrared slope to correlate inversely with the ultraviolet slope. The grouping of the stars is shown in table 5.4, and a composite diagram showing the superposed mean extinction curves for each group appears in fig. 5.33. The infrared points and scanner data are linked by straight lines to aid identification. The grouping adopted here is not identical to that reported by Whittet et al for 22 reddened stars. For instance, no significant difference was found between curves D and E when the infrared data was considered. Also a revised classification was adopted for HD 99171 (comparison) with more consistent results. It should be emphasised that this classification of the curves is not unique; in fact, there appears to be a continuous sequence of curves between A and D in fig. 5.33.

Three of the stars, HD 147084, 147889 and 151346 lie in a group at considerably higher galactic latitude than the remainder, and this difference is reflected in their extinction curves. The curves of these stars, which are in the region of Upper Scorpius, are labelled S1 (147084 and 151346) and S2 (147889). (The sharp rise in the curve of HD 147084 is omitted, the points for $\lambda^{-1} > 2.7\ \mu^{-1}$ in the mean curve being due to HD 151346 only). The S2 curve does not follow the general uv/ir slope correlation as it approximates to law C in the ultraviolet, but dips much lower than any of the other curves in the infrared.

Table 5.4

Star Pairs grouped according to Extinction Curve

Curve	Reddened Star (HD)	Sp	Comparison Star (HD)	Sp	
A	116119	B9I	106068	B9Ia	
	172488	B0.5V	214080	B1Ib	*
B	90706	B2.5Ib	96088	B3III	*
	152235	B0.5Ia	150898	B0Iab	†
	154043	B1Ik	214080	B1Ib	
	156201	B0.5Ia	214080	B1Ib	*
	166628	B3Ia	172910	B3V	*
C	142468	B0.5I	99171	B2IV-V	*
	144969	B0.5Ia	99171	B2IV-V	*
			150898	B0Iab	†
	148379	B2Ia	166197	B2III	*
	165319	B0Ia	150898	B0Iab	†
	167838	B5Ia	136664	B5V	*
	168571	B1II	214080	B1Ib	*
	169454	B1Ia+	150898	B0Iab	†
			214080	B1Ib	*
	170898	B1Ia	214080	B1Ib	*
D	77581	B0.5Ib	64760	B0.5Ib	
			99171	B2IV-V	*
	80558	B7Iab	93540	B7V	*
	92964	B3Ia	96088	B3III	*
	115842	B0.5Iab	64760	B0.5Ib	
			99171	B2IV-V	*
	148688	B1Ia+	214080	B1Ib	*
	152236	B1Ia+	214080	B1Ib	*
	171012	B0.5Ia	214080	B1Ib	*
S1	147084	A5II	146145	A5(?)	
	151346	B8(IV or V?)	110073	B8IVp	
S2	147889	B2V	148703	B2IV	

* corrections applied for Balmer mismatching.
† corrections applied for reddening in comparison star.

Fig. 5.33 Superposed extinction curves for the groups given in table 5.4.

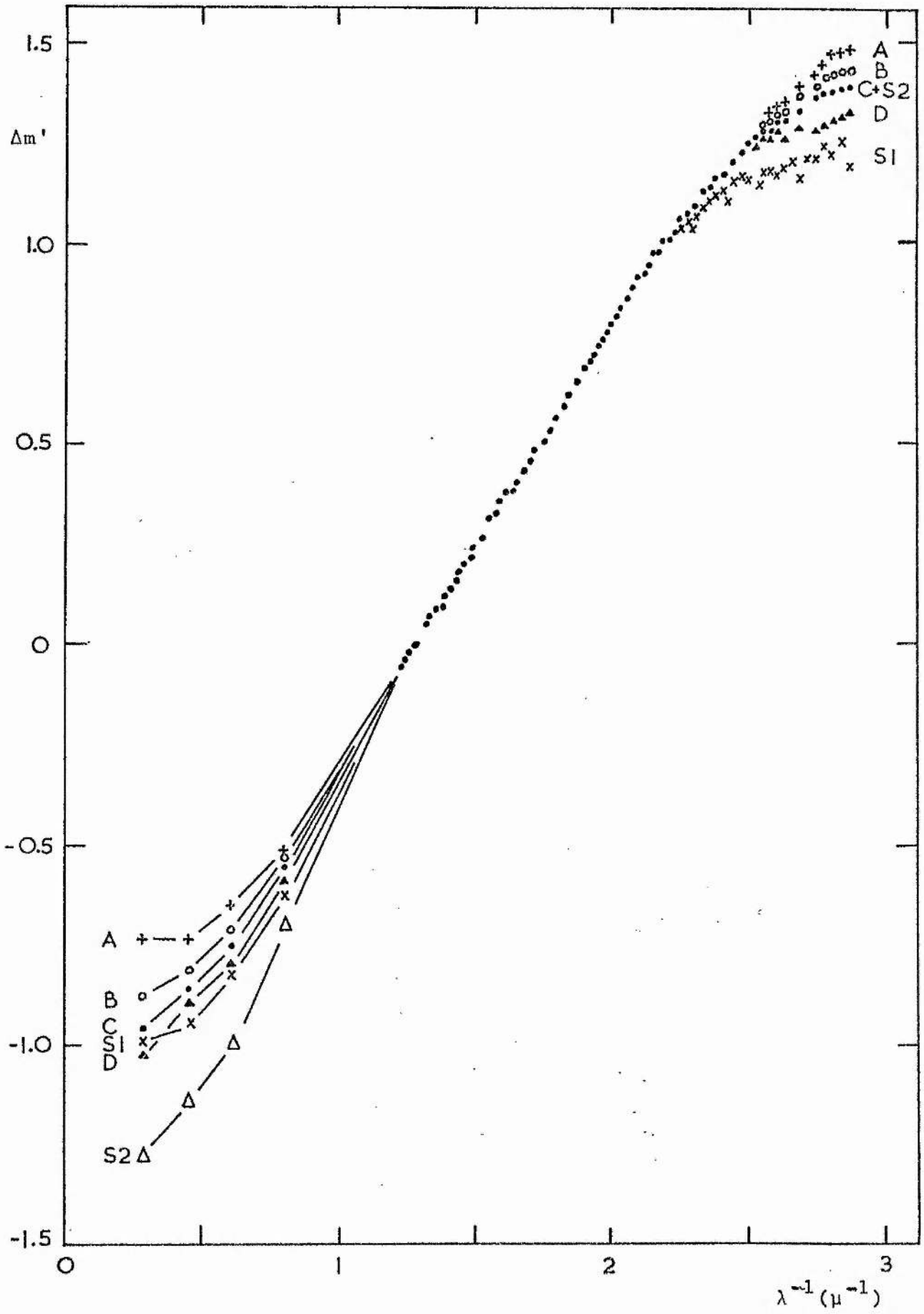

(5.4) Discussion

The distribution of the reddened stars in the galactic plane is shown in fig. 5.34. The positions of dark clouds and bright nebulae are taken from the Atlas Coeli of Becvar. There is no obvious correlation between position and type of extinction curve; indeed, there are cases where stars close together in angular position seem to follow distinctly different laws. HD 90706 and 92964, with extinction laws B and D respectively, lie in the same region of sky as the η Carinae Nebula. HD 152235 (law B) and 152236 (law D) are probable members of the Sco OB-1 association (Braes, 1967; Schild et al, 1969). Most of the stars in the $\ell^{II} = 0^{o}$-30^{o} region show extinction close to curve C, but curves A, B and D also occur.

As already noted, the curves of the three stars in Upper Scorpius do not correspond to any of those found nearer to the galactic plane. HD 147084 and 147889 lie towards the compact dust cloud associated with the multiple star ρ Ophiuchi, and HD 151346 lies in a dust lane which extends from this cloud towards the galactic equator (fig. 5.34). The distance of the obscuring matter is ∿ 200 pc (Bok, 1956) and the latitude is $b^{II} \sim 17^{o}$, thus most of the reddening is likely to occur in the cloud itself, within a few parsecs of the stars. HD 147889 lies in emission nebulosity near the centre of the cloud (Struve and Rudkjobing, 1949); its extinction curve (S2) is markedly different from that of HD 147084 (S1) although their separation is only ∿ 75', equivalent to 4.4 pc at a distance of 200 pc.

Fig. 5.34 Locations of the reddened stars in the galactic plane.

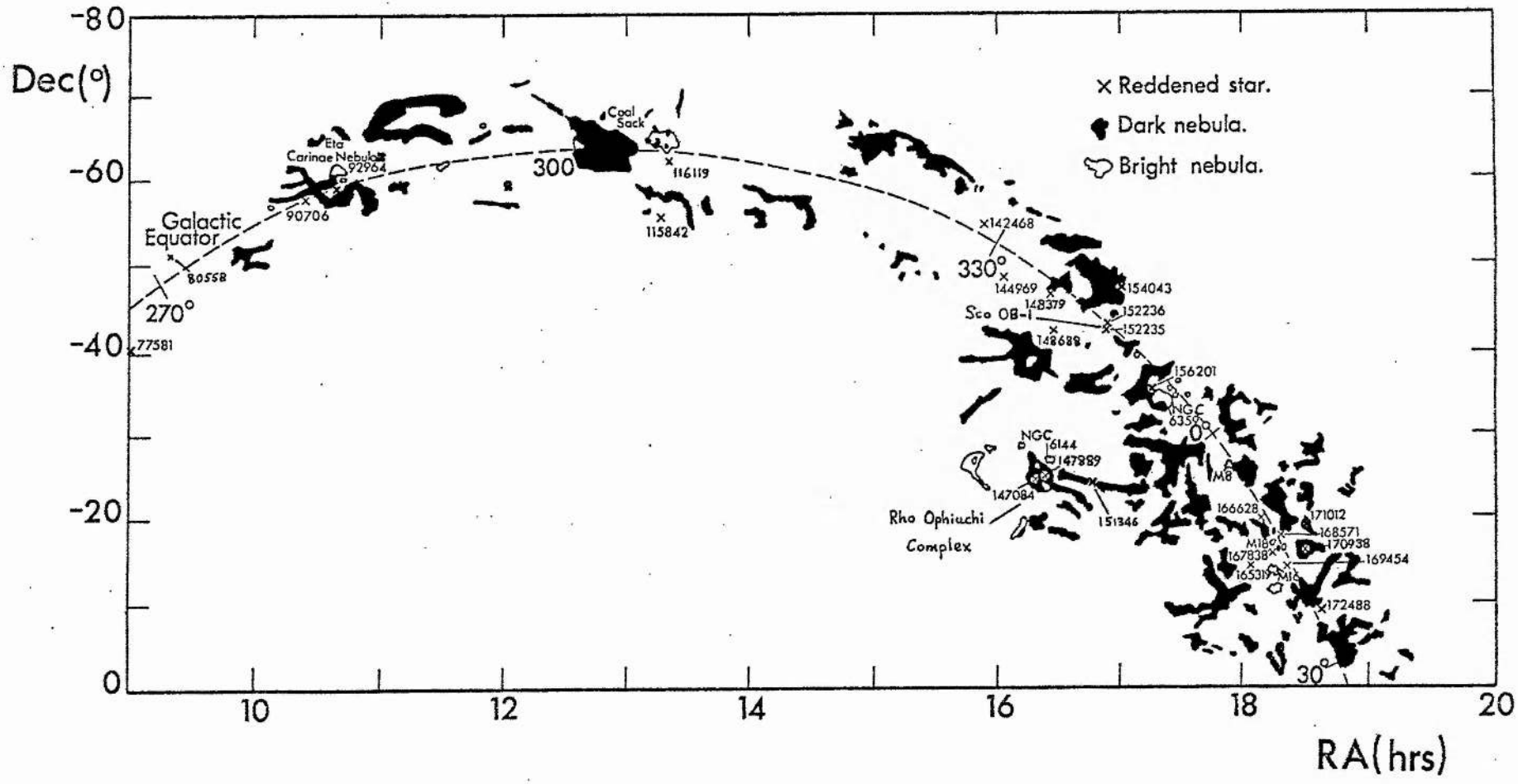

It is likely that variations in the conditions prevailing in the local dust clouds are responsible for these differences in the extinction curves. In general, models involving progressively larger grains are required to produce the increased flattening in the ultraviolet and the corresponding dip in the infrared for curves B to S1 compared with A in fig. 5.33. In view of the lack of correlation between extinction law and longitude, a systematic variation in the particle size distribution along the galactic plane seems to be ruled out. Radiation pressure is likely to play an important role in the motions of dust clouds, and differential effects may modify the size distribution of the grains (see, for example, Dufay, 1957, p. 243-245). The radiation of luminous early-type stars imbedded in dust clouds may cause the smaller particles to be swept away or evaporated, resulting in an increase in the mean size of the distribution. This argument was first used by Baade and Minkowski (1937) to explain the anomalous extinction in the Orion Nebula. If curve A is taken to result from the general 'galactic' extinction, curves B, C and D may be explained by assuming that a progressively greater contribution to the extinction is made by a 'local' component in which the size distribution of the grains is modified by the stars themselves. The case of the Upper Scorpius stars is rather different as here virtually all the extinction appears to be 'local'; this region is discussed further in chapter 7.

The range of variation in the extinction curves in fig. 5.33 is similar to that found for Northern Milky Way stars. The mean curves for the Cygnus, Perseus and Orion regions

(Nandy, 1964, 1965a; Nandy and Wickramasingh, 1971) correspond roughly to curves A, C and S1 over the scanner wavelength range. However, it is noted that the process of averaging over considerable regions of sky masks any local variations of the magnitude found in this work.

A shallow depression between wavenumbers 1.6 and 1.9 μ^{-1} is apparent in many of the individual extinction curves, and is present to some extent in almost all of them. It is particularly noticable in figs. 5.6, 5.7, 5.12 and 5.26. The mean depth of the depression is $\sim 0^{m}.04$, which is significant compared with the photometric error ($\lesssim 0^{m}.01$) in this spectral region. Whiteoak (1966) noticed a similar feature in his extinction curves for Northern Milky Way stars, and it thus seems to be a fairly widespread phenomenon. The curve of HD 147889 has a cusp-like depression at $\lambda^{-1} = 1.97\ \mu^{-1}$ which divides the curve into two distinct sections. The presence of this feature was first noted by Dr van Breda and is described by van Breda et al (1974). Its appearance is rather different from that of the 1.6-1.9 μ^{-1} depression. These and other broadband features in the curves are discussed further in chapter 8.

CHAPTER 6

THEORETICAL MODEL FITTING AND THE VALUE OF R

(6.1) Introduction

The development of theoretical work on the composition of interstellar grains and the matching of theoretical and observed extinction curves is reviewed in section 2.5. Models involving graphite, silicates and iron or silicon carbide are found to be reasonably consistent with observational data on the extinction and albedo over the whole of the accessible wavelength range. No unique model for the grains has emerged, however; the only component which is regarded with some confidence is graphite, in view of the relatively high cosmic abundance of carbon and the identification of the π electron transition at 2200 A with the broad ultraviolet hump in the curve. Thus the fitting of theoretical models, using currently available laboratory data on the optical properties of likely solids, to new observational data on the extinction curve is not expected to produce further insight into the composition of the grains. (An advance in this direction is likely to require more detailed laboratory measurements of optical constants under simulated interstellar conditions.) The prime motivation for model fitting in the context of the present work is to provide a theoretical basis for the extrapolation of the curves to infinite wavelength, in order to deduce the ratio of total to selective extinction. It also provides a test for the suggestion made in section 5.4 that the variations found in the curves from star to star are explicable in terms of local variations in the distribution of grain sizes.

It was noticed that one of the curves computed by Wickramasinghe and Nandy (1971) for graphite-iron-silicate grain mixtures resembles the observational curve A in fig. 5.33. The two curves are shown superposed in fig. 6.1; the theoretical curve is re-normalized to the standard wavelengths used in section 5.2. The relative contributions of the three components to this theoretical curve are illustrated in fig. 2.4 and discussed in section 2.5. The good agreement suggested that this curve would make a suitable starting point for model fitting, and that Mie computations along the lines followed by WN should be capable of providing good fits to the other observational curves.

Fig. 6.1 Comparison of WN curve 9 (see fig. 2.4) with observational curve A. Mean errors are given using the same convention as in section 5.2.

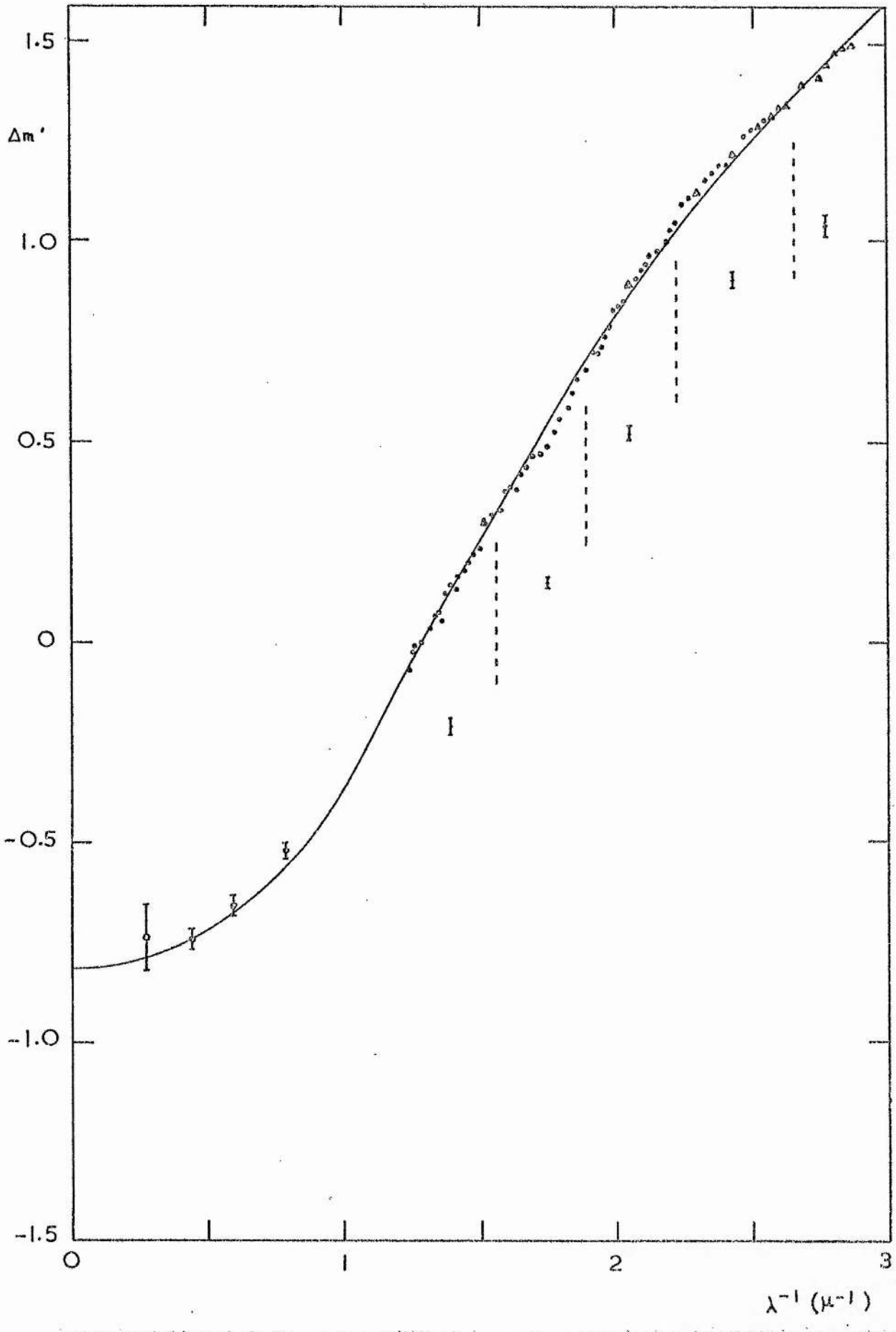

(6.2) Optical Constants

Before proceeding with Mie computations we require values of the complex refractive index $m = n - ik$ for the materials involved. The quantities n and k, called the optical 'constants', are in general functions of wavelength. They are related to the real and imaginary parts of the dielectric constant $\varepsilon = m^2 = \varepsilon_1 - i\varepsilon_2$ by the equations

$$\left.\begin{aligned} \varepsilon_1 &= n^2 - k^2 \\ \varepsilon_2 &= 2nk. \end{aligned}\right\} \qquad (6.1)$$

A complication arises when considering the optical properties of graphite as it is highly anisotropic. There are in general two refractive indices, m_1 and m_2, applying to light with electric vector parallel and perpendicular to the crystal axis. The imaginary component of m_1 is small and the crystal behaves like a dielectric, while m_2 is appropriate to a metal. Lenham and Treherne (1966a) have measured n and k independently for the two cases. Their values for 'dielectric' graphite contain a feature between wavenumbers 1.6 and 2.0 μ^{-1} which can produce a dip in the extinction curve similar to that found by Whiteoak (1966) and by the present author (see Borg, 1967). However, their values of n and k for 'metallic' graphite are in marked disagreement with those of other investigators (Taft and Philipp, 1965; Carter et al, 1965) and their results must therefore be regarded with suspicion. Wickramasinghe (1967, p. 110) has noted that if the graphite particles are in the form of thin flakes randomly orientated in space, the extinction arising from light with electric vector parallel to the crystal axis will be small. The net extinction may therefore be represented by that of spherical, isotropic graphite particles

with refractive index m_2. The results of Taft and Philipp (1965) are adopted for this analysis, in accordance with most previous investigations. The wavelength-dependence of the dielectric constant was used with equ. (6.1) to give the n and k values shown plotted against λ^{-1} in fig. 6.2. For completeness, the ultraviolet data is included in the diagram, although here we are concerned only with wavenumbers below 3.0 μ^{-1}. The structure between 3.5 and 5.5 μ^{-1} produces the characteristic graphite hump in the theoretical extinction curves of WN.

The optical constants of iron have been measured by Lenham and Treherne (1966b) in the wavelength range 0.3-6.0 μ, and are plotted against λ^{-1} in fig. 6.3. The agreement with values measured by Yolken and Kruger (1965) in the visual region is good for n, but a discrepancy of about 0.8 occurs in the k values. There is a hump between wavenumbers 1.5 and 2.0 μ^{-1} in the n curve of fig. 6.3, which produces a slight dip in the extinction curve for iron grains of radii 0.01 μ computed by Borg (1967).

The WN model assumed a constant real value (m = 1.66) for the refractive index of the silicate component in the wavelength range 0.3-3 μ. Pollack et al (1973) have since published measurements of optical constants for various silicate rock samples ranging from the far infrared, including the spectral features around 10 and 20 μ, to the ultraviolet. These results have been the subject of Mie computations by Bromage et al (1973). The n and k values for obsidian are taken for the purposes of the present work as being representative of silicates. Obsidian is a glassy igneous rock composed mainly of feldspars

such as $NaAlSi_3O_8$ mixed with quartz (SiO_2). Its composition and physical properties are not unlike those of the glassy spherules found in lunar rock samples and meteoritic material. The refractive index follows a normal dispersion relation for a dielectric outside the region of the absorption bands, and is virtually constant between $\lambda^{-1} = 0.3$ and $3\ \mu^{-1}$. The variation of n and k for $\lambda^{-1} < 0.3\ \mu^{-1}$, shown in fig. 6.4, is dominated by the two characteristic bands.

The effect of errors in the optical constants of graphite, iron and silicate grains on the computed extinction curves has been investigated by Morgan and Nandy (1974). They considered the effect of 10% changes in the measured values of n and k and found that the transmitted errors are wavelength-dependent. The errors incurred are greatest in the far ultraviolet for graphite and in the near ultraviolet for silicates; for iron they are quite small at all wavelengths. In the infrared and visual regions the extinction curve is fairly insensitive to small changes in n and k.

Fig. 6.2 Optical constants for graphite plotted against λ^{-1} (Taft and Philipp, 1965)

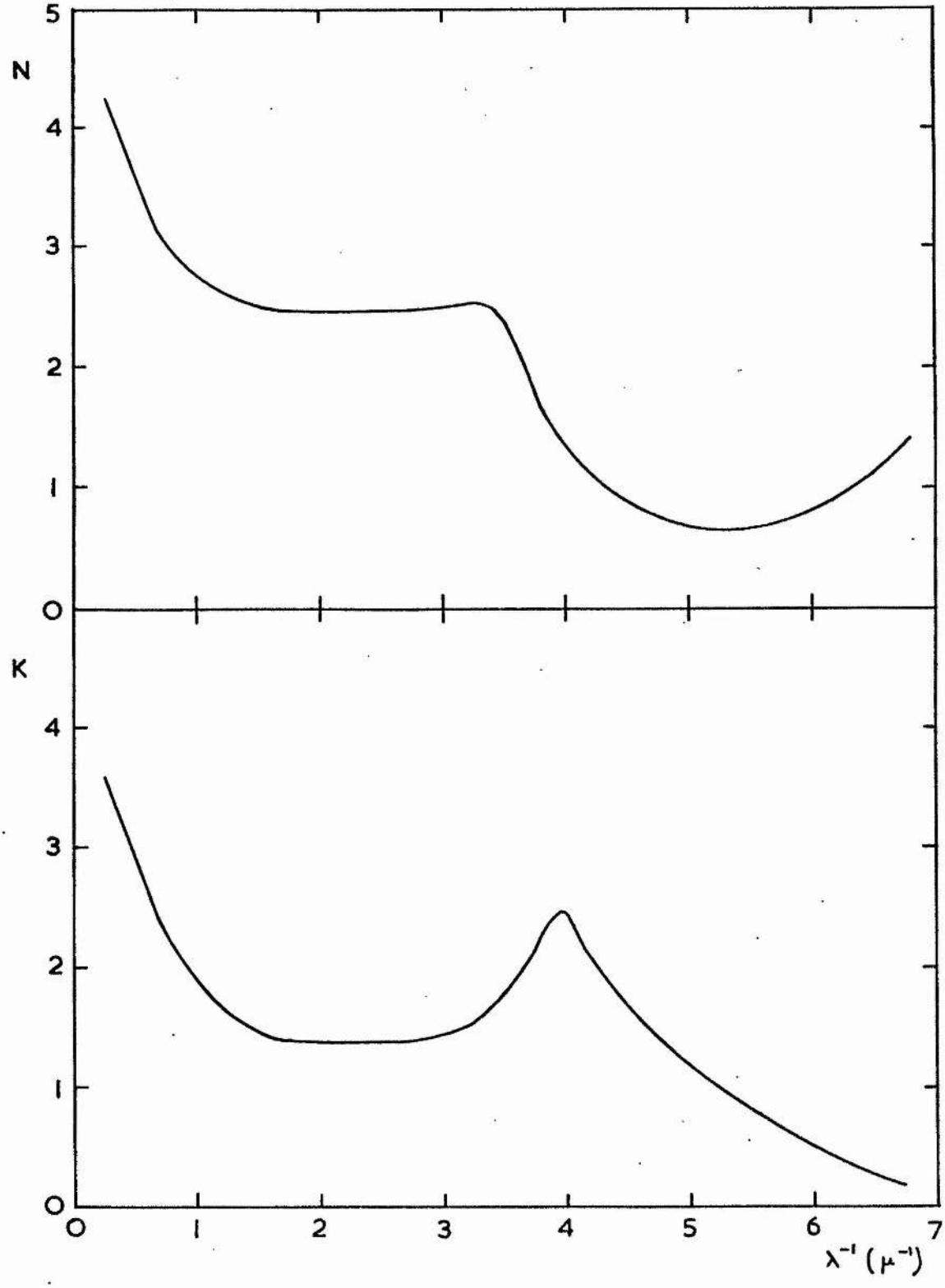

Fig. 6.3 Optical constants for iron plotted against λ^{-1} (Lenham and Treherne, 1966b)

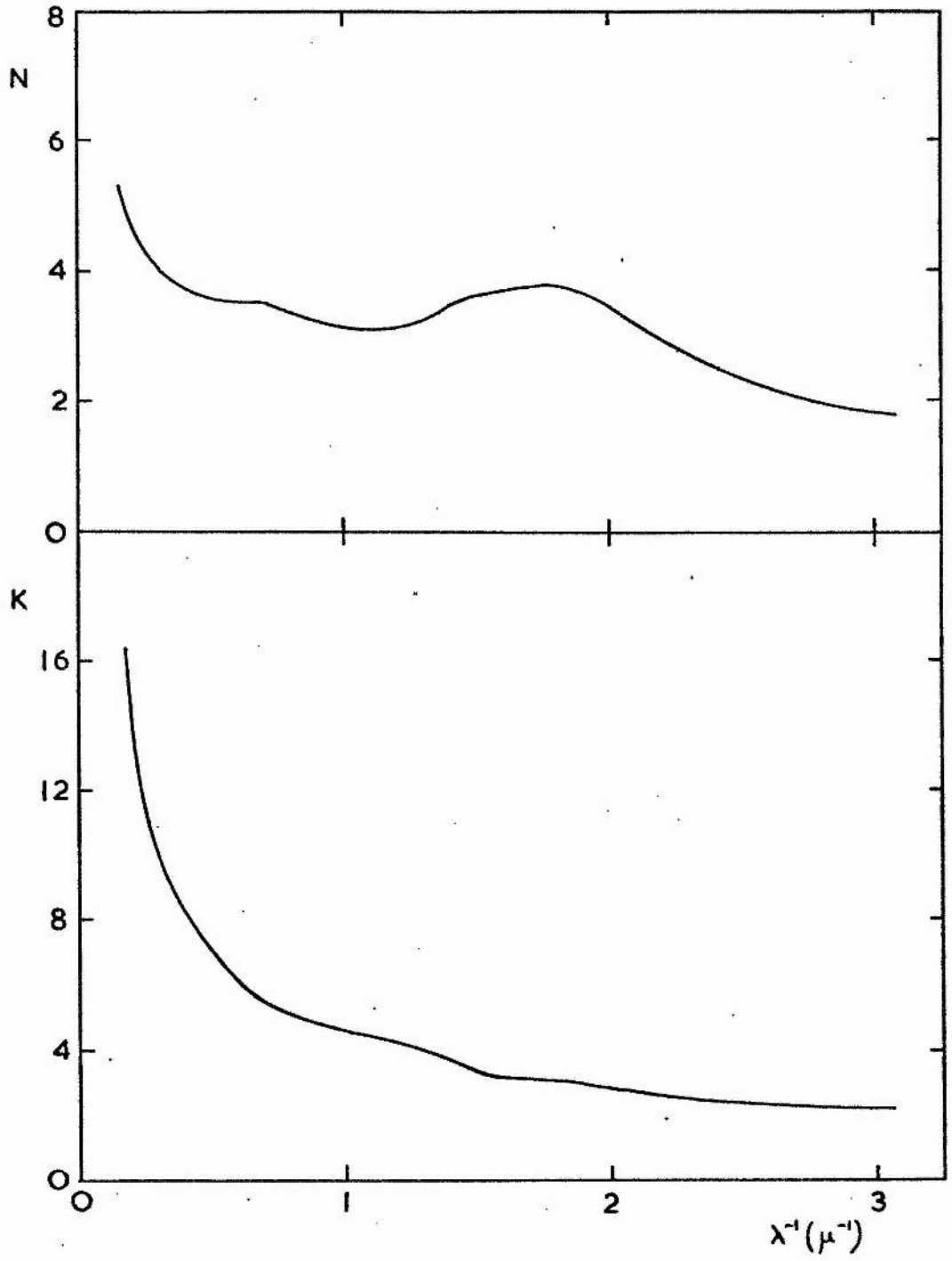

Fig. 6.4 Optical constants for obsidian in the infrared plotted against λ^{-1} (Pollack et al, 1973)

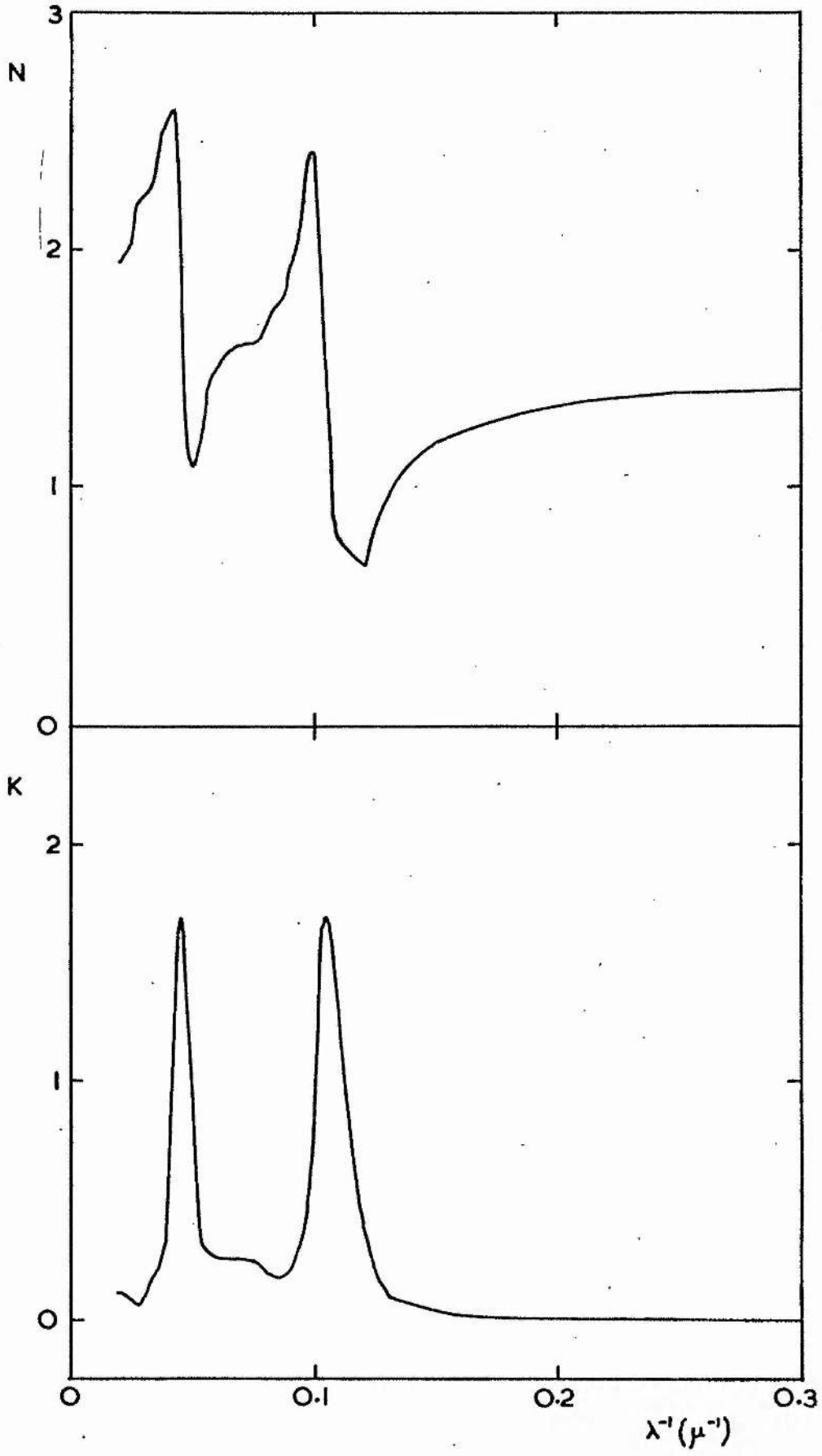

(6.3) Computational Method

The computational method follows closely that of WN. A Fortran IV programme was written to compute Q_{ext} from the Mie formula (equ. 2.9) and carry out integrations over the grain size distribution. The programme appears in the appendix. The procedure for evaluating the coefficients a_n and b_n is described in section 2.2. The series in equ. (2.9) was summed until the n^{th} term differed from the $(n-1)^{th}$ term by less than 0.01%. The number of terms required for convergence to this order of accuracy is shown as a function of $x = 2\pi a/\lambda$ in fig. 6.5.

The grain size distribution adopted is of the form given in equ. (2.41). Using the values of the constants α and β assumed by WN we have

$$n^{(i)}(a) = A^{(i)} a^{\frac{3}{2}} \exp\{-\tfrac{1}{2}(a/a_m^{(i)})^3\} \qquad (6.2)$$

where i = 1, 2, 3 refer to graphite, iron and silicate grains. The distribution function for each component is thus characterised by the mean radius $a_m^{(i)}$ and a relative weighting factor $A^{(i)}$. The extinction at each wavelength for each component is given by equ. (2.37):

$$\Delta m^{(i)} = 1.086\pi \int_0^\infty a^2 Q_{ext}^{(i)} n^{(i)}(a)\,da. \qquad (6.3)$$

The integral in equ. (6.3) was evaluated by Simpson's Rule, with the integrand truncated to zero for $a < a_o = 10^{-3}\ \mu$ and for $a > 3a_m$. The range of integration is divided into N elements of width h, as illustrated in fig. 6.6. Simpson's Rule gives the integral of a function f(a) as

$$\int_{a_o}^{a_o+Nh} f(a)\,da = \frac{h}{3}\{f(a_o) + 4\left[f(a_1) + f(a_3) + \ldots + f(a_{N-1})\right] + 2\left[f(a_2) + f(a_4) + \ldots + f(a_{N-2})\right] + f(a_N)\} \qquad (6.4)$$

where N is an even number and $a_1, a_2, \ldots, a_N$ are the values of a at each division. Q_{ext} is a function of m, λ and a, and m is a function of λ; thus for a given material and a given λ value Q_{ext} depends only on a. We may therefore put

$$f(a) = a^2 Q_{ext}(a) n(a) \qquad (6.5)$$

in equ. (6.4) and evaluate the integral in equ. (6.3) at each required λ value and for each type of grain. The number of elements was increased until the resulting integral did not change its value by more than 0.05%.

In order to specify the relative proportions of the three grain species, the weights $A^{(i)}$ were replaced by two parameters, x_{gr} and x_{ir}. These are defined as the ratios of the extinction due to graphite and iron to that due to silicate, all measured at λ = 4560 A. Thus the extinction contributions of the graphite, iron and silicate grains are in the proportion $x_{gr} : x_{ir} : 1$ at this wavelength. Setting the quantities $A^{(i)}$ to unity in equ. (6.2), the total extinction of the mixture may be represented by

$$\Delta m_{tot}(\lambda) = x_{gr} \frac{\Delta m^{(1)}(\lambda)}{\Delta m^{(1)}(4560)} + x_{ir} \frac{\Delta m^{(2)}(\lambda)}{\Delta m^{(2)}(4560)} + \frac{\Delta m^{(3)}(\lambda)}{\Delta m^{(3)}(4560)} . \qquad (6.6)$$

The programme was used to compute $\Delta m_{tot}(\lambda)$ at a set of 30 wavelengths between 0.34 and 4 μ, to give the theoretical extinction curves for input values of $a_m^{(i)}$, x_{gr}, x_{ir} and the optical constants. The curves were normalized in the usual way (section 5.2) to allow direct comparison with the observational curves by superposition. To test the reliability of the programme, the curves computed by WN were reproduced (using m = 1.66 for silicates) with satisfactory results.

Fig. 6.5 Number of terms required for convergence of Mie series plotted against $x = 2\pi a/\lambda$ (for truncation error < 0.01% between last two terms)

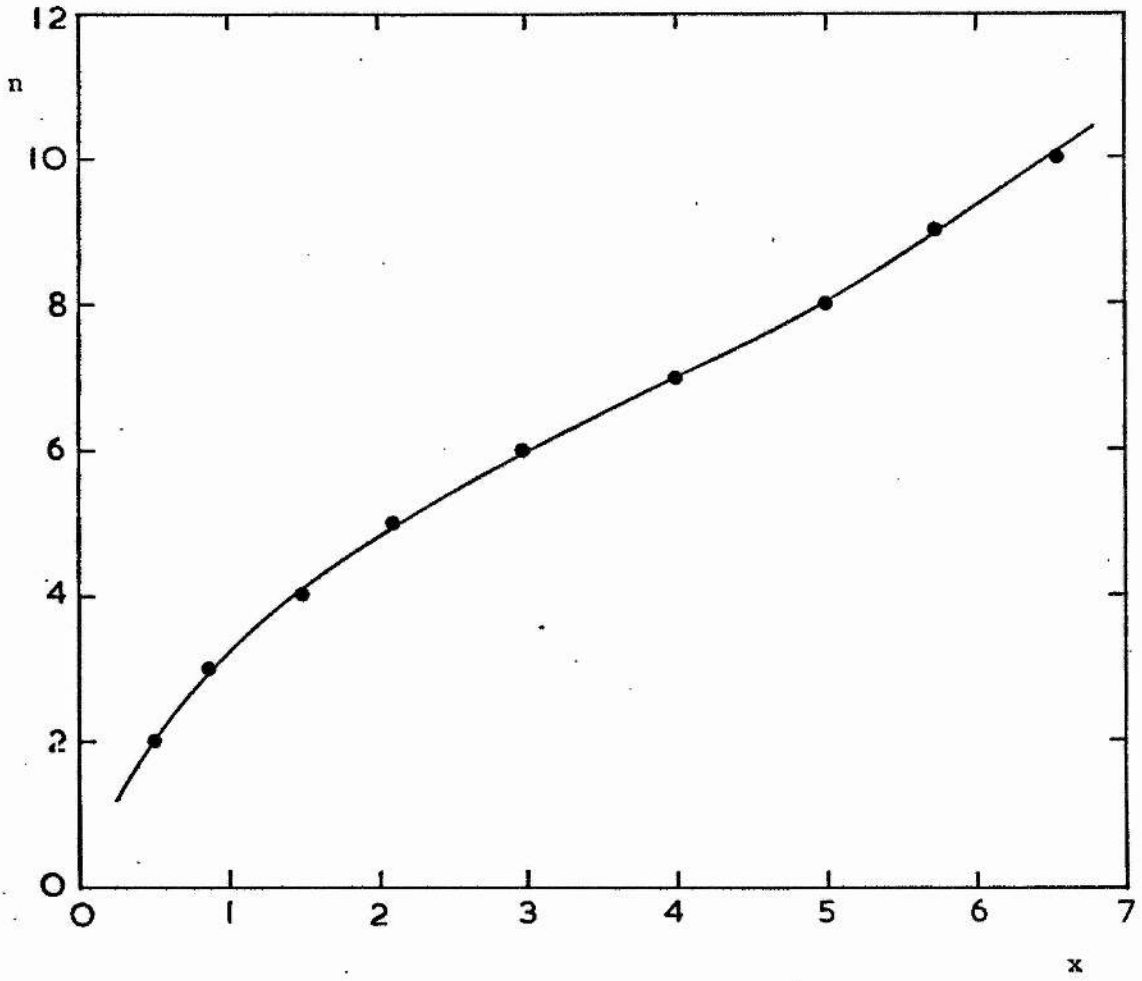

Fig. 6.6 Plot of size distribution function against a, showing method of integration (for a_m = 0.057 μ)

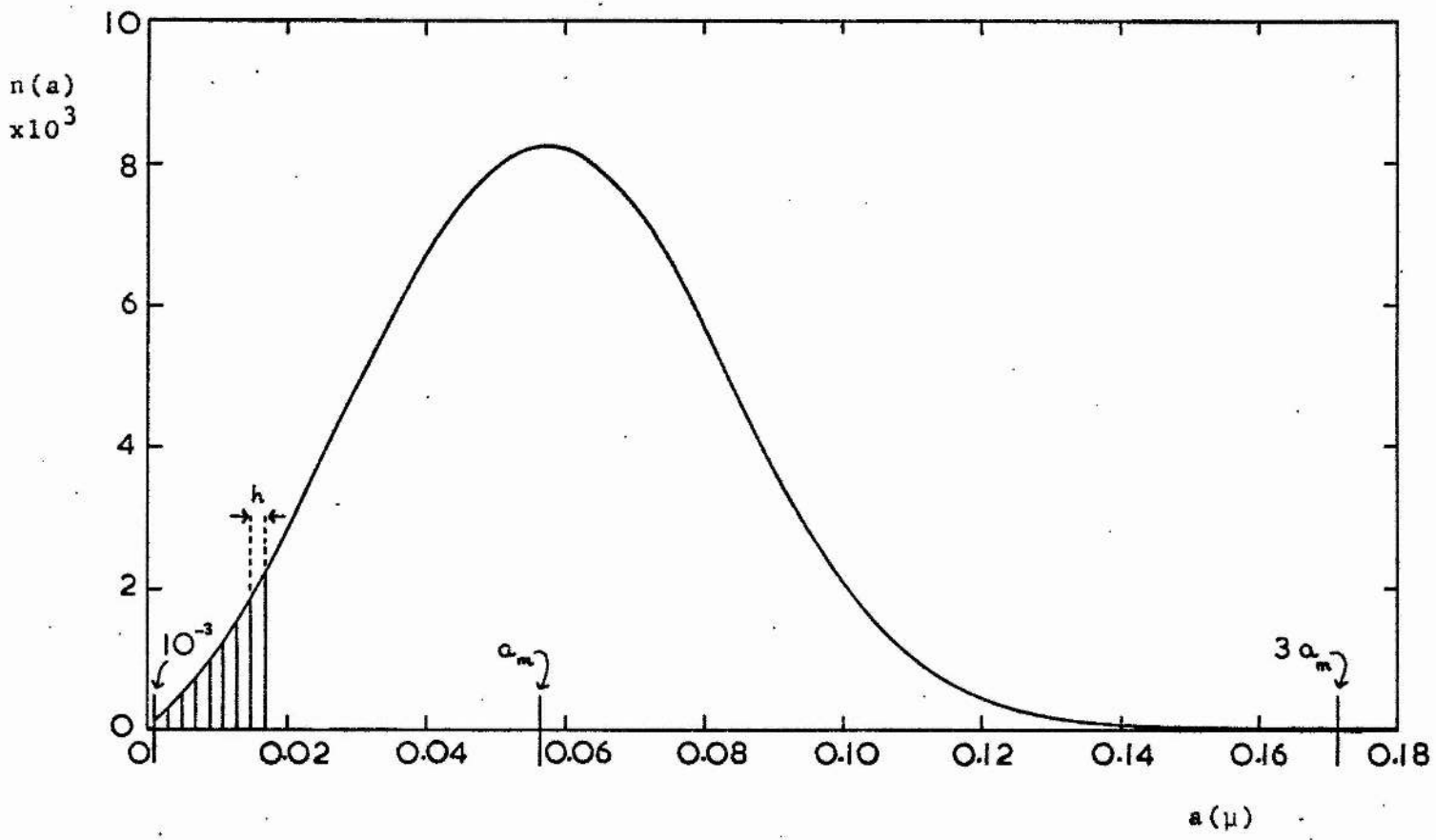

(6.4) Curve-fitting Procedure and Results

The WN curve shown in fig. 6.1 uses the following values of the programme input parameters:

$$a_m(gr) = 0.05\ \mu, \quad a_m(ir) = 0.02\ \mu, \quad a_m(si) = 0.15\ \mu, \quad x_{gr} = 3.0, \quad x_{ir} = 0.611,$$

When the constant real refractive index assumed by WN for the silicate component in the wavelength range considered is replaced by the measured values for obsidian, $a_m(si)$ must be increased to 0.21 μ to give a closely similar curve. It has been argued that graphite grains of radii close to 0.02 μ are required to match the ultraviolet extinction curve in the 4-5 μ^{-1} region (see section 2.5). With this value of $a_m(gr)$ it was difficult to obtain good fits to the observational curves simultaneously in the infrared and near ultraviolet using feasible values of the other input parameters. Curves were computed over a range of the characteristic sizes, and best results were generally obtained for values within the following limits:

$$a_m(gr) = 0.04\text{-}0.06\ \mu,$$
$$a_m(ir) = 0.015\text{-}0.04\ \mu,$$
$$a_m(si) = 0.18\text{-}0.26\ \mu.$$

Results are presented here for the combination:

$$a_m(gr) = 0.045\ \mu,$$
$$a_m(ir) = 0.025\ \mu,$$
$$a_m(si) = 0.22\ \mu.$$

WN found that x_{gr} and x_{ir} values which produced good fits to the general trend in the observed extinction curves followed a relationship of the form

$$c_1 x_{ir} = x_{gr} + c_2 \qquad (6.7)$$

where c_1 and c_2 are constants. The curve in fig. 6.1 arises from the case where $c_1 = 6$ and $c_2 = 2/3$. Using these values of the constants, good fits to the observational curves A, B and C were obtained with x_{gr} equal to 2.2, 1.3 and 1.0 respectively. Smaller values of x_{gr} were not capable of giving fits to curve D as the blue end of the curve tended to be too steep when the matching was satisfactory in the infrared, and vice versa. The iron component of the mixture contributes mainly at the blue end, suggesting that c_1 should be decreased to give a more rapid fall in x_{ir} with x_{gr} in equ. (6.7). Values of $c_1 = 5$ and $c_2 = 0.5$ with x_{gr} in the range 2.1-0.55 produced good fits to curves A, B, C, D and S1. An approximate fit to curve S2 could be obtained for $\lambda^{-1} < 1.8\ \mu^{-1}$ by decreasing x_{gr} to about 0.2, but this curve was much too low in the ultraviolet. It was noted that the infrared slope of the curve is sensitive to the characteristic size of the silicate grain distribution: by increasing $a_m(si)$ from 0.22 μ to 0.26 μ the curve could be made to dip low in the infrared in the manner of curve S2, while the ultraviolet extinction remained relatively high. A good overall fit to curve S2 was obtained with $x_{gr} = 1.0$ and $a_m(si) = 0.26\ \mu$. The values of x_{gr}, x_{ir} and $a_m(si)$ for the fits to each observational curve are listed in table 6.1. The matching of the theoretical results (continuous curves) with the mean observational extinction curves is illustrated in figs. 6.7-6.12.

In order to compute R values we need to know the way in which the curve approaches the $\lambda^{-1} = 0$ axis. The curves used in the model-fitting process extended to $\lambda^{-1} = 0.25\ \mu^{-1}$ in the infrared. The extinction for wavenumbers from 0.25 to

0.02 μ^{-1} was computed using measured values of the optical constants for obsidian (Pollack et al, 1973; fig. 6.4). In the case of graphite, the plots in fig. 6.2 were extrapolated graphically towards $\lambda^{-1} = 0$. The contribution of graphite to the total extinction is quite small in the far infrared, and any errors in the n and k values will have little effect. The extinction due to the iron component is vanishingly small for $\lambda^{-1} < 0.25\ \mu^{-1}$ and may be neglected. The computed infrared extinction for the theoretical model to curve C is shown in fig. 6.13. The peaks at $\lambda^{-1} \sim 0.11$ and $0.05\ \mu^{-1}$ are produced by the characteristic silicate bands. The broken line shows the extinction arising when the refractive index of obsidian is assumed to be real and constant (equal to 1.47) in the far infrared, as it is to a first approximation in the visual region. Clearly the presence of these bands does not affect the extrapolation of the curve to $\lambda^{-1} = 0$; they are merely superposed on the smooth total curve, which follows a λ^{-4} law in the far infrared as $\lambda >> a$. The theoretical curves in figs. 6.7-6.12 are shown extrapolated in this way with the silicate features omitted.

The values of R are given in table 6.2, deduced directly from the normalized extinction curves in figs. 6.7-6.12. R is given by

$$R = \frac{\Delta m(\lambda_V) - \Delta m(\infty)}{\Delta m(\lambda_B) - \Delta m(\lambda_V)} \qquad (6.8)$$

where $\lambda_B = 4400$ A and $\lambda_V = 5530$ A are the effective wavelengths of the B and V filters. $\Delta m(\lambda_B)$ and $\Delta m(\lambda_V)$ are measured from the observational curve and $\Delta m(\infty)$ is measured from the theoretical curve. The presence of the 1.6-1.9 μ^{-1} trough in the

observational curves causes the R values to be lower than would be obtained if $\Delta m(\lambda_V)$ were measured from the theoretical curve. The uncertainties in the results are estimated by considering the range of theoretical curves which could be said to fit the infrared points in each case, giving limiting values of $\Delta m(\infty)$.

Table 6.1

Values of the Parameters x_{gr}, x_{ir} and $a_m(si)$ for the best fits to each Observational Curve. ($a_m(gr)$ = 0.045 μ and $a_m(ir)$ = 0.025 μ in each case.)

Curve	x_{gr}	x_{ir}	$a_m(si)$ (μ)
A	2.10	0.52	0.22
B	1.25	0.35	0.22
C	0.90	0.28	0.22
D	0.70	0.24	0.22
S1	0.55	0.21	0.22
S2	1.00	0.30	0.26

Table 6.2

Values of R for the Mean Extinction Curves.

Curve	R	error
A	2.7	0.2
B	3.0	0.2
C	3.2	0.2
D	3.4	0.2
S1	3.9	0.3
S2	4.3	0.3

Fig. 6.7 Theoretical model fitted to observational curve A.

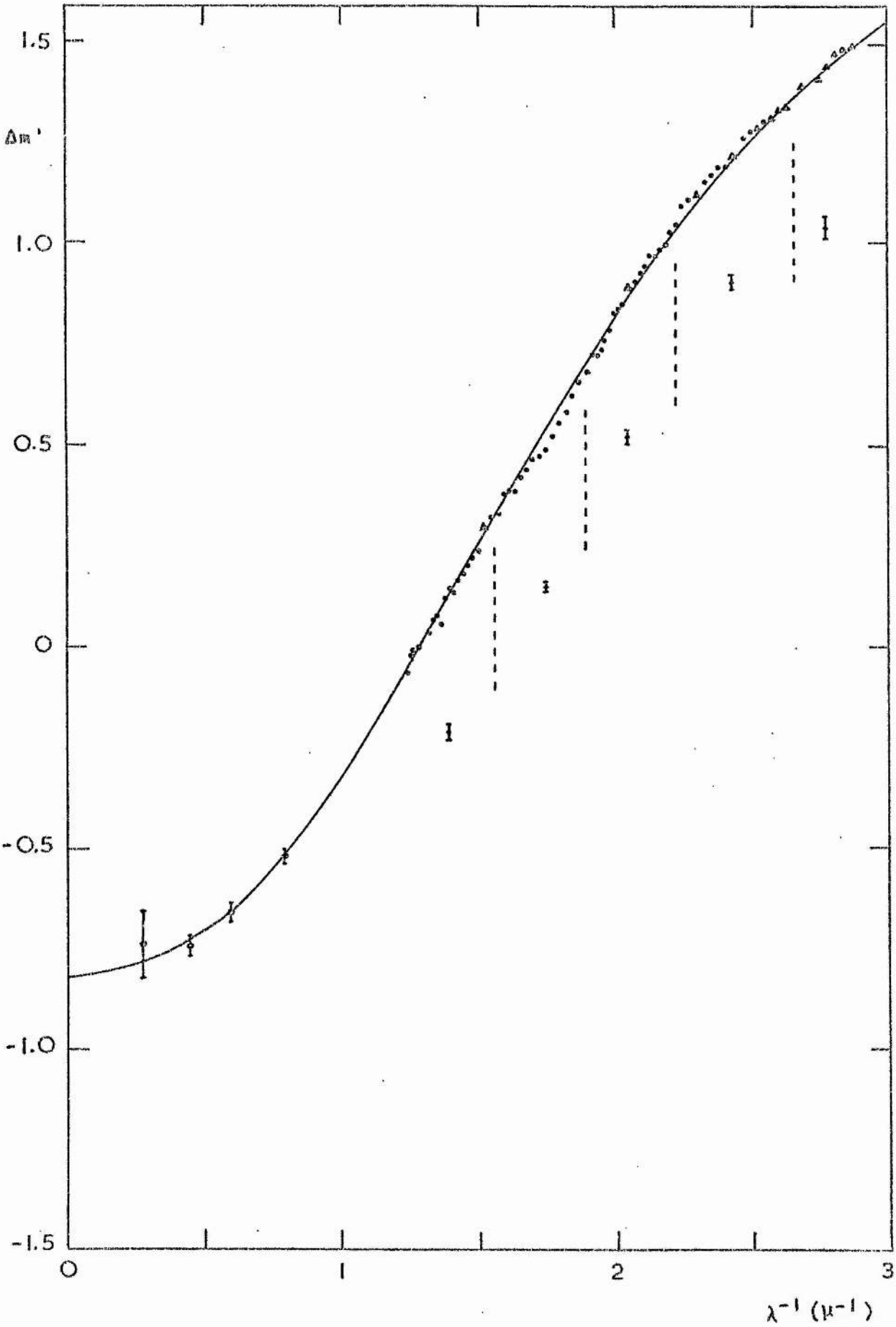

Fig. 6.8 Theoretical model fitted to observational curve B.

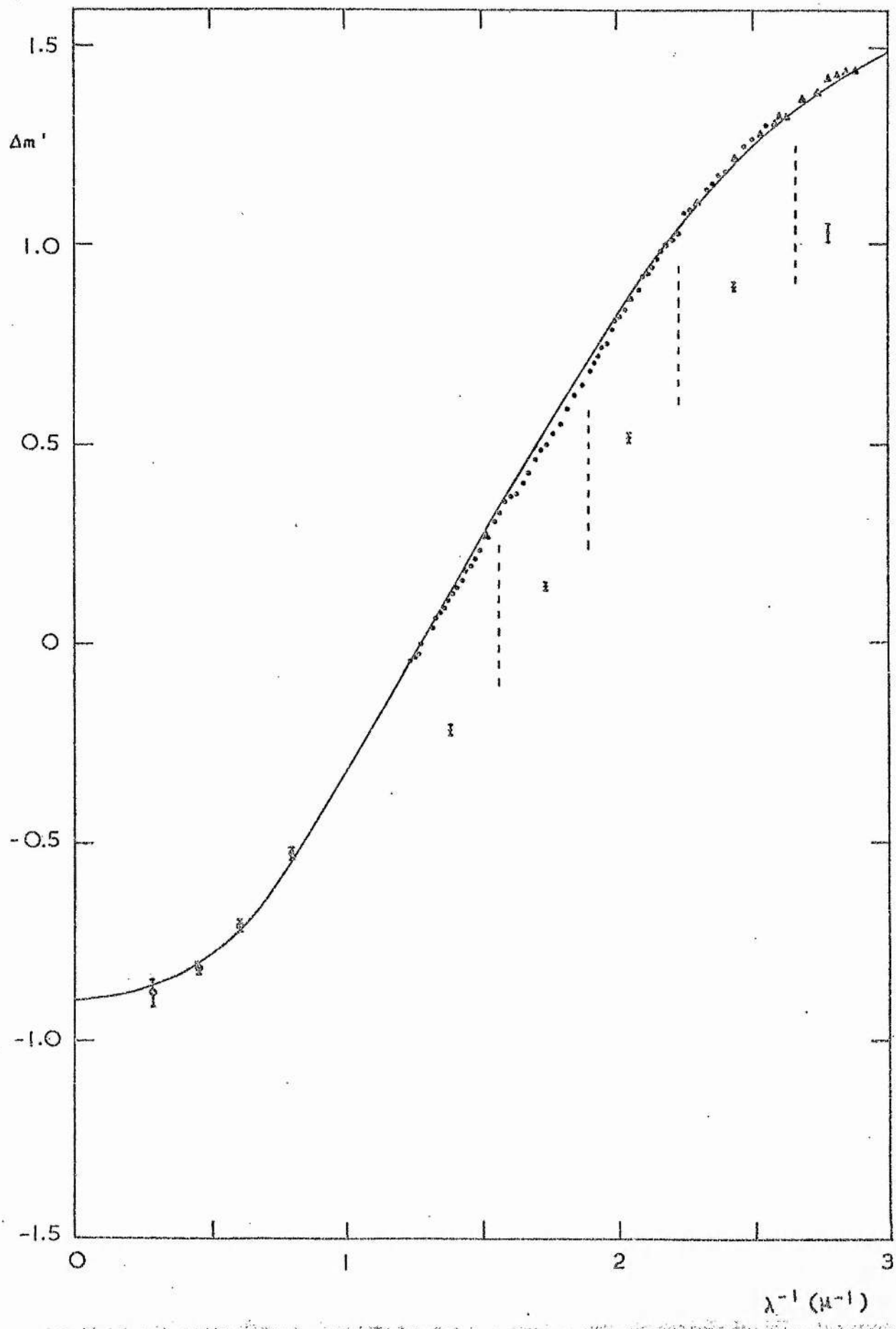

Fig. 6.9 Theoretical model fitted to observational curve C.

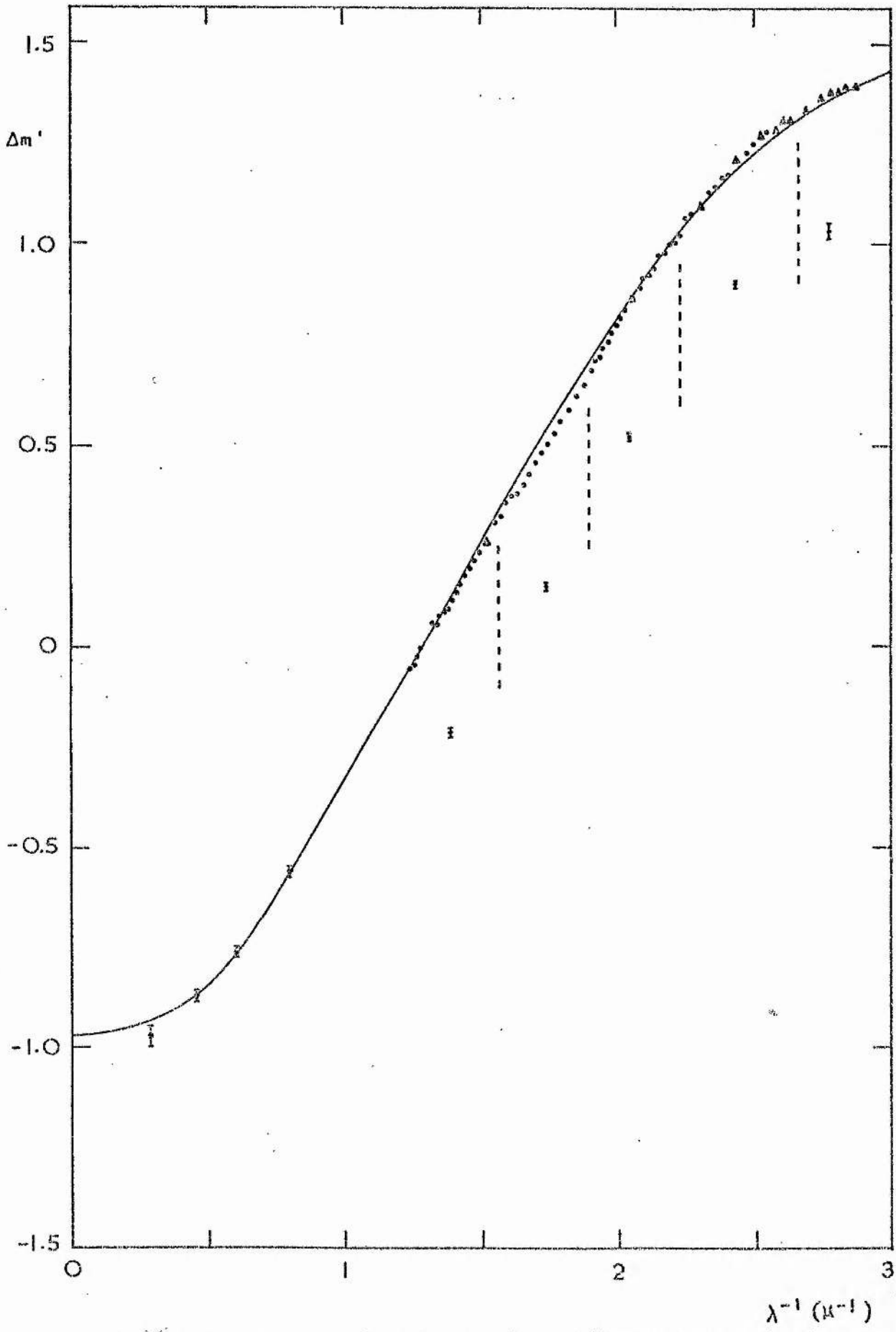

Fig. 6.10 Theoretical model fitted to observational curve D.

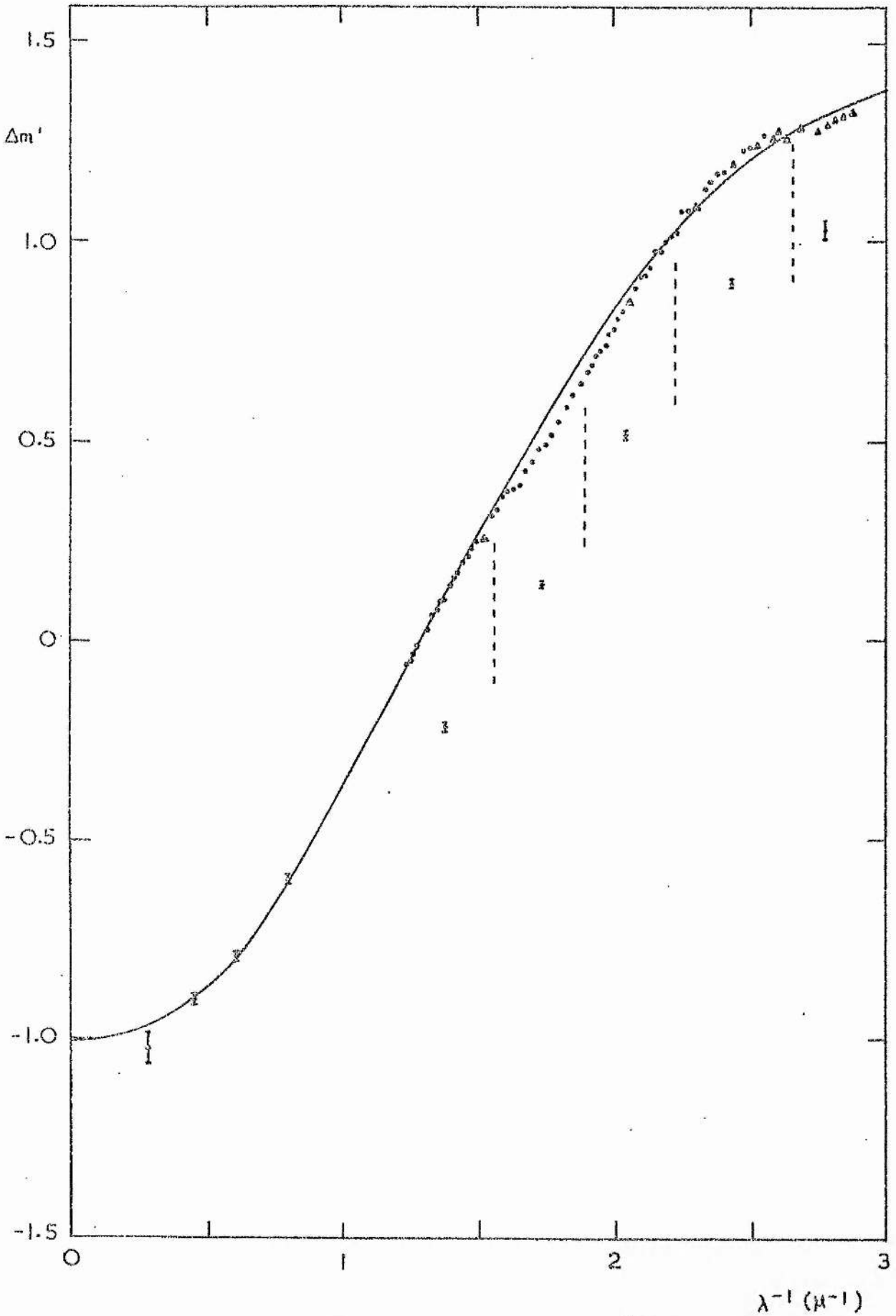

Fig. 6.11 Theoretical model fitted to observational curve S1.

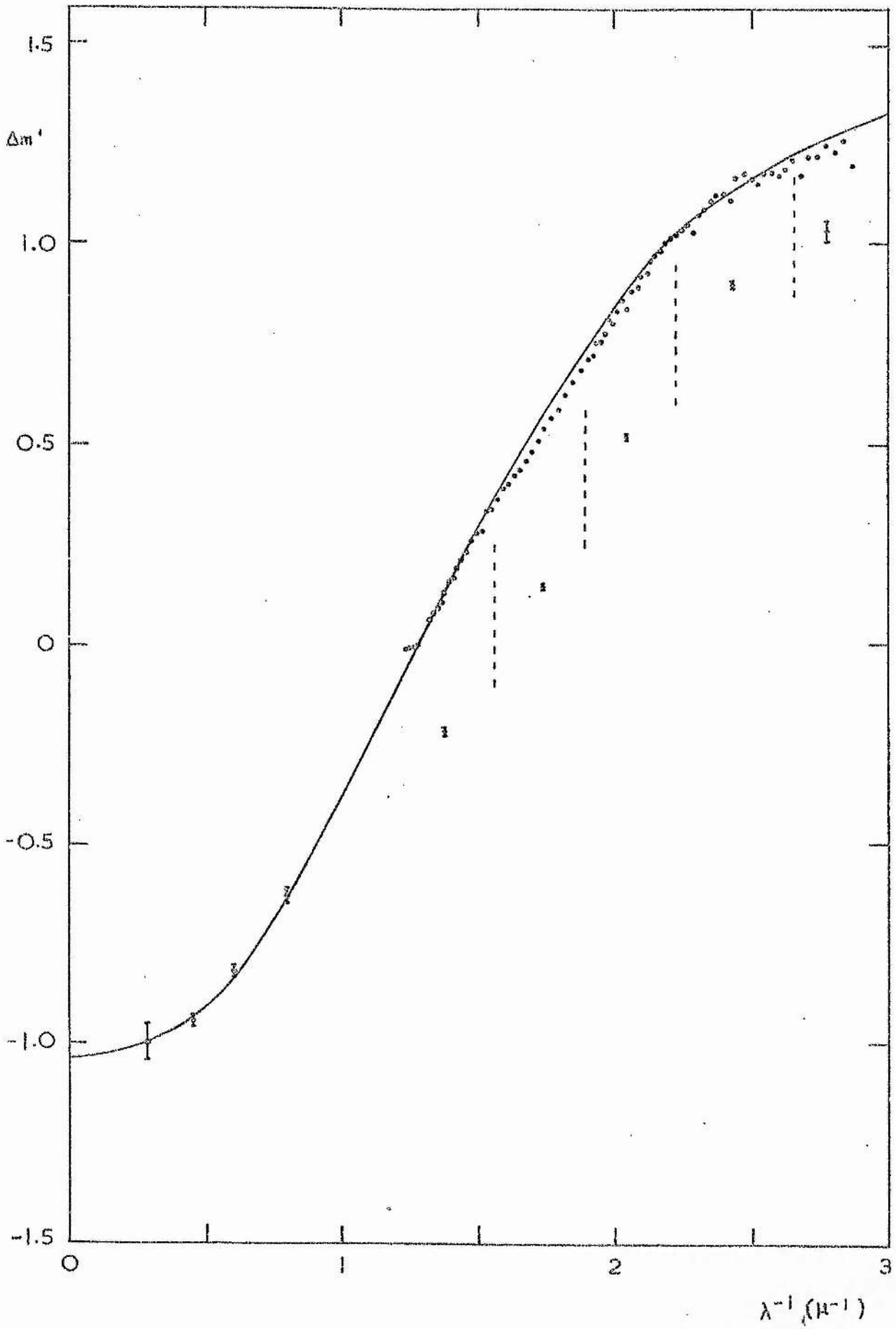

Fig. 6.12 Theoretical model fitted to observational curve S2.

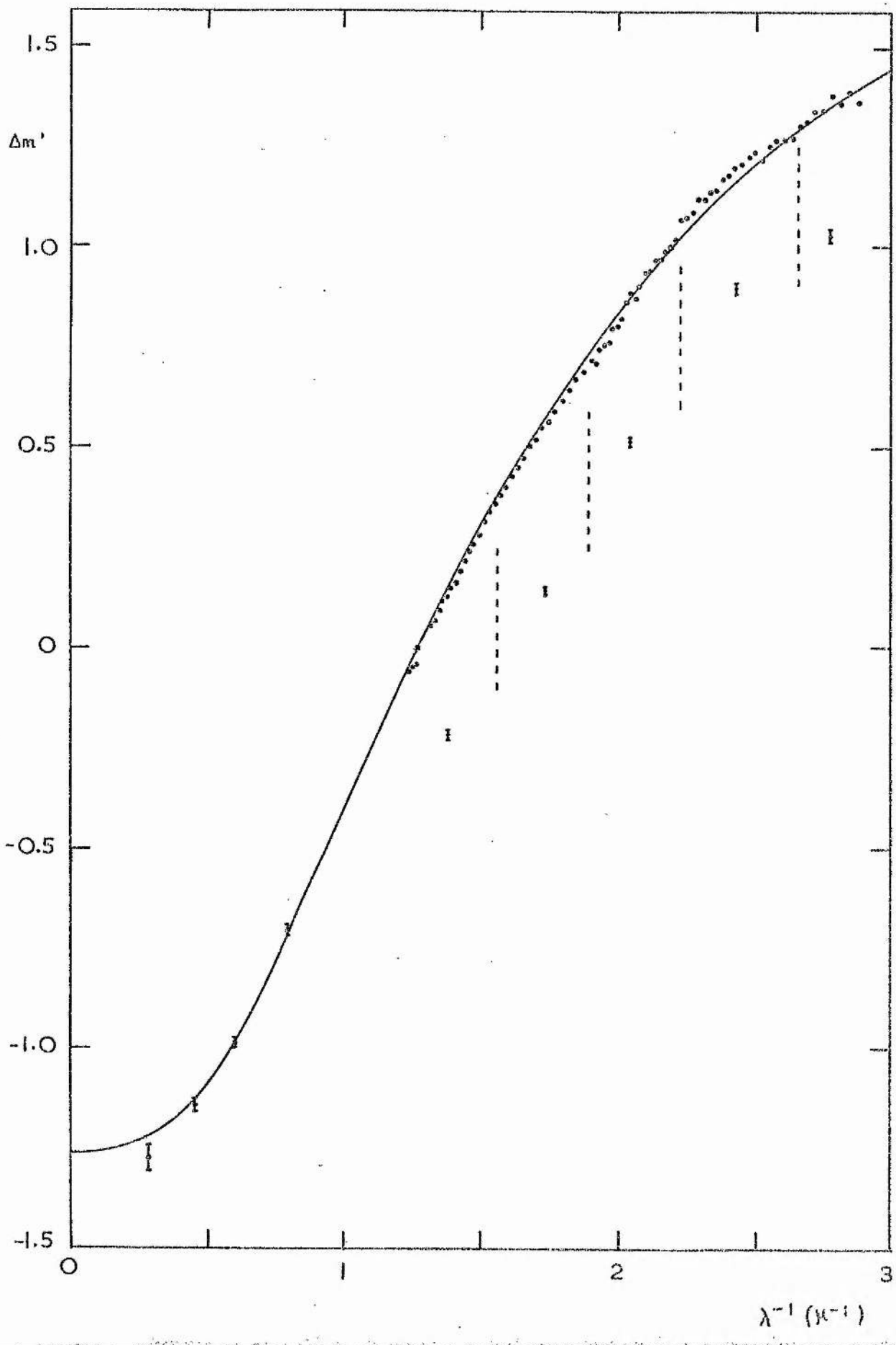

Fig. 6.13 Computed infrared extinction (curve C) showing silicate bands
Broken line shows curve deduced for a constant value (m = 1.47)
for the refractive index of the silicate component

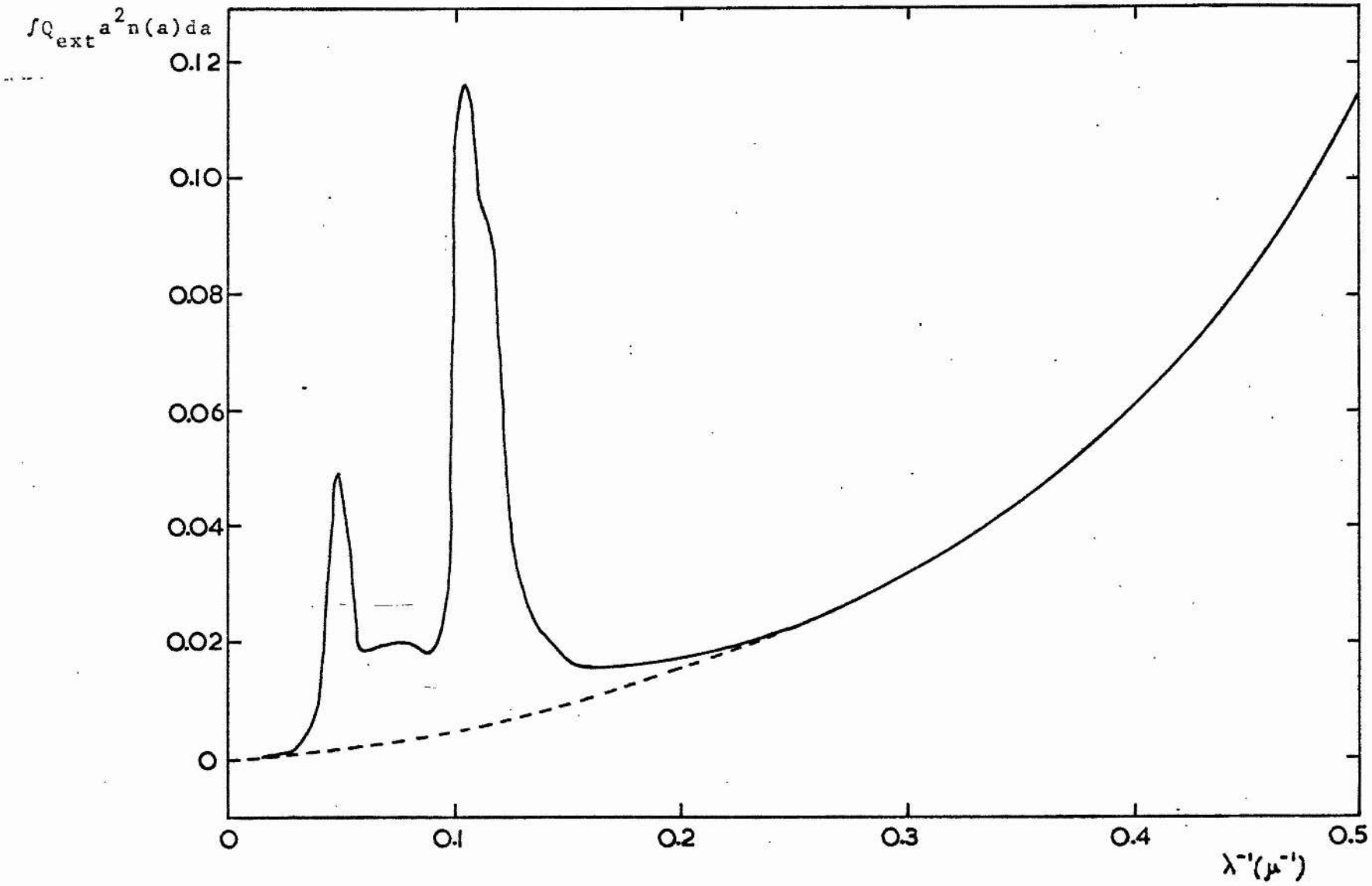

Fig. 6.14 Plot of relative radiation pressure ($Q_{pr}/\rho a$) against grain radius (a) at λ = 1500 A

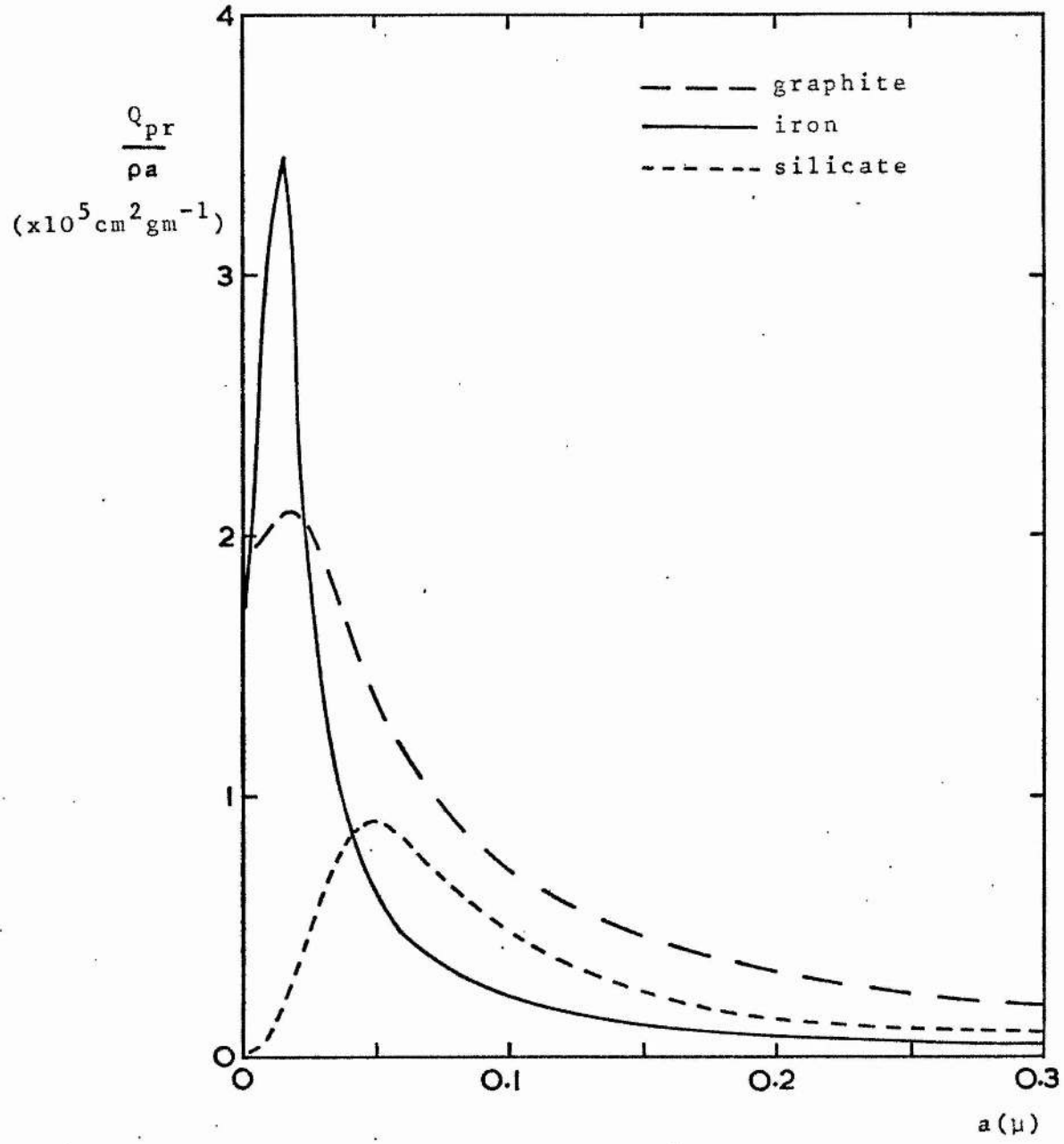

(6.5) Radiation Pressure

In view of the discussion in section 5.4 it is of interest to evaluate Q_{pr}, the efficiency factor for radiation pressure, for graphite, iron and silicate grains. Q_{pr} is defined in section 2.1 (equ. 2.18) and may be computed from the Mie theory (see also Wickramasinghe, 1967, 1973). The force of repulsion due to photons of wavelength λ on a grain at distance d from a star is, from equ. (2.19),

$$F_R = \frac{\ell(\lambda) S}{4\pi d^2} \cdot \frac{\pi a^2}{c} \cdot Q_{pr}(a, m, \lambda) \qquad (6.9)$$

where $\ell(\lambda)$ is the spectral luminance of the star per unit wavelength interval, and S is its surface area. This force is opposed by gravitational attraction given by

$$F_G = \frac{GM(\frac{4}{3}\pi a^3 \rho)}{d^2} \qquad (6.10)$$

where M is the mass of the star and ρ is the density of the grain material. Thus the net force $(F_R - F_G)$ applied to the grain varies inversely with the square of the distance. The ratio of these forces is, from equ. (6.9) and (6.10),

$$\frac{F_R}{F_G} = \frac{3\ell(\lambda) S}{16\pi GMc} \left(\frac{Q_{pr}}{\rho a} \right), \qquad (6.11)$$

which is independent of distance, and thus at a given wavelength,

$$\frac{F_R}{F_G} \propto \frac{Q_{pr}}{\rho a}. \qquad (6.12)$$

The wavelength of maximum emission for an early-type star of surface temperature $T \sim 2 \times 10^4$ °K is, by Wien's law, $\lambda_m \sim 1500$ A. Q_{pr} was computed at this wavelength for the three grain types over a range of radii, using extrapolated values of the optical constants for iron and silicate and

measured values for graphite (fig. 6.2). The extrapolation for iron was carried out on the assumption of constant conductivity (see WN, 1971). $Q_{pr}/\rho a$ is shown plotted against a in fig. 6.14. The curve for iron shows a sharp maximum at a $\sim$ 0.015 μ, and the graphite and silicate curves show broader peaks at a $\sim$ 0.02 μ and 0.05 μ respectively. Thus the net outward force is dependent on grain size and is greatest for grains of these radii in the three cases.

(6.6) Discussion

Figures 6.7-6.12 illustrate that a graphite-iron-silicate grain model is capable of producing theoretical curves which match the overall shape of the observational curves reasonably closely. A detailed fit is not possible as the model cannot reproduce broadband structure in the curves such as the trough between wavenumbers 1.6 and 1.9 μ^{-1}. It should be noted that the curves fitted are in no way unique, as numerous combinations of the input parameters could produce similar results. Also the choice of normalization wavelengths influences the way in which the models fit the data. It is unlikely, however, that combinations using values of the characteristic grain sizes far outside the limits quoted in section 6.4 could give a consistent set of curves matching the data over the whole wavelength range. The value of $a_m(gr)$ is restricted to some extent by the position of the 'knee' at $\lambda^{-1} \sim 2.2\ \mu^{-1}$, and the fact that the curve must be fairly linear in the 1.0-2.0 μ^{-1} region sets limits on $a_m(ir)$ and $a_m(si)$. With $a_m(gr) = 0.045\ \mu$ the model gives a smooth, continuous change in slope in the 2.0-2.5 μ^{-1} region, and is not capable of producing the sharp 'corner' suggested by the observations of Harris (1969).

Harris' claim that the change in slope occurs in a very narrow wavelength range ($\sim$ 6 Å) and that the 2.0-2.7 μ^{-1} extinction is best represented by two intersecting straight lines is not supported by the observational evidence presented here. Nevertheless, there are clear discrepancies in this region, the theoretical curves tending to fall below the observational points at $\lambda^{-1} \sim 2.3\ \mu^{-1}$ (see particularly figs. 6.7 and 6.12). This problem is discussed further in chapter 8.

The decreasing values of the parameters x_{gr} and x_{ir} required to fit curves B, C, D and S1 compared with curve A are interpreted as a progressive depletion of the smaller grain species due to differential radiation pressure effects. Evaporation is not a viable cause of depletion for this grain model as the substances are highly refractory. For significant depletion to occur we require $F_R/F_G >> 1$ in equ. (6.10). It has been shown by several investigators that this condition can occur in the region of luminous OB stars (Schoenberg and Jung, 1932; Greenstein, 1937; Schalen, 1939; Pecker, 1972). Fig. 6.14 indicates that depletion is more probable for iron and graphite grains of radii 0-0.05 μ than for silicate grains of radii 0.2-0.3 μ by an order of magnitude. In the case of HD 147889 (S2) an increase in the characteristic size of the silicate grain distribution was needed to fit the observational curve. This is consistent with the suggestion of Carrasco et al (1973) that the grains in the dense central region of the ρ Ophiuchi cloud increase their size by accretion of the heavier elements from the interstellar gas. Significant numbers of the smaller grain species are also required to explain the relatively high ultraviolet extinction. Considerable depletion may be

expected to occur near a B2V star in so compact a cloud, but as there is nebulosity surrounding the star photoelectric charging may cause retention of the smaller particles (see Mathews, 1967; Wickramasinghe and Nandy, 1972).

The values of R given for the mean curves A, B, C and D in table 6.2 do not greatly differ from the 'classical' value of R = 3, while in Upper Scorpius a value of R ∿ 4 seems to apply. The R values for the individual stars are given in table 6.3 (column 2). These were deduced by means of the theoretical model giving the best fit to the curve for each star, and are not in general identical to the R value of the appropriate mean curve. The depth of the 1.6-1.9 μ^{-1} trough and the optimised matching of the theoretical curve with the J, H and K infrared data points determined the precise value of R in each case. The L data point was given low weight in the model fitting, as it may be affected by circumstellar dust emission. Column 3 of table 6.3 gives the absolute magnitude $M_V(Sp)$ determined from the spectral type (table 3.4) using the calibration of Blaauw (1963). The visual absorption $A_V = R.E_{B-V}$ is listed in column 4, and column 5 gives the distance in kpc from the relation

$$5 \log d - 5 = V - M_V(Sp) - A_V. \qquad (6.13)$$

Columns 6 and 7 give the absorption per kpc (A_V/d) and the distance from the plane of the Galaxy

$$z = d \sin(b^{II}) \qquad (6.14)$$

in parsecs.

The A_V/d values for stars in Upper Scorpius are anomalously high due to the high density of local dust in this region. The mean value of A_V/d for the other stars in table 6.3 is $1^m.6$/kpc,

which is close to the mean given by Allen (1973) for the interstellar medium near the galactic plane. Table 6.4 lists average values of R, A_V/d and $|z|$ for stars of extinction laws A-D. There is little variation in $\langle A_V/d \rangle$, while columns 2 and 4 indicate a tendency for R to increase with distance from the plane. There are clearly exceptions to this general trend (HD 92964 and 152236, for instance, have relatively high R and low z), and the spread in individual $|z|$ values for each extinction law is considerable. This may possibly be the result of local depletion effects superposed on a general R-z correlation.

Wilson (1960) suggested that the value of R should vary with the degree of linear polarization p according to the relationship

$$R(p) = 2.1\{1 + 3.4(p/E_{B-V})\}. \qquad (6.15)$$

The polarization is here defined as

$$p = 2.5 \log(I_{max}/I_{min}) \qquad (6.16)$$

where I_{max} and I_{min} are the intensities for maximum and minimum transmission through the analyser. The catalogue of Mathewson and Ford (1970) includes polarization measures for ten of the stars in table 6.3, and also for the two appreciably reddened comparison stars HD 106068 and 150898 (for which model fitting to figs. 5.31 and 5.32 gives approximate R values of 2.9 and 3.6 respectively). Mathewson and Ford assumed the following definition of polarization:

$$p' = \frac{I_{max} - I_{min}}{I_{max} + I_{min}}. \qquad (6.17)$$

Thus, from equ. (6.16) and (6.17),

$$p = 2.5 \log\left(\frac{1 + p'}{1 - p'}\right). \qquad (6.18)$$

Fig. 6.15 shows a plot of extinction curve R values, R(ext), against R(p) from equ. (6.15) for the 12 stars with p' measurements. There is a suggestion of correlation between these parameters, although the sample is too small to draw firm conclusions. The uncertainty (± 0.2) in R(ext) is capable of explaining most of the scatter in the points relative to the straight line shown.

The model fitting for individual stars allows tentative identification and measurement of any infrared excess radiation influencing the curves. Such excess could result from circumstellar dust emission, which would be expected to produce a downward trend in the observational curves for wavelengths greater than about 2 μ. Table 6.5 gives measures of the infrared excess at the L band (3.5 μ), taken as the magnitude difference between the observed and theoretical curves, in cases where such a downward trend is detectable. (There does not appear to be any appreciable excess at the K (2.2 μ) wavelength.) The error limits given in table 6.5 are those arising from the statistical uncertainties in the L magnitudes. Although these errors are generally of the same order as the measured excesses, it is unlikely that this number of stars could show low extinction at L by chance. (Only two stars show L points lying appreciably above the theoretical curve). It is notable that no stars following extinction laws A or B show a measurable infrared excess, while five of the seven law D stars do so. This is consistent with the hypothesis that an increasing role is played by local dust as we progress from law A to law D. No infrared excess is detected for HD 77581, in agreement with the results of Hyland and Mould (1973).

Table 6.3

R Values and Associated Data for Individual Stars

HD	R	M_V(Sp)	A_V	d(kpc)	A_V/d	z(pc)
77581	3.3	-5.8	2.4	1.13	2.1	77
80558	3.2	-6.4	1.9	1.24	1.5	-32
90706	3.1	-5.7	1.9	1.49	1.3	0
92964	3.5	-6.8	1.3	1.54	0.8	-11
115842	3.4	-6.2	1.7	1.25	1.4	149
116119	2.9	-6.5	2.1	2.95	0.7	32
142468	3.2	-6.2	2.6	1.97	1.3	-27
144969	3.2	-6.4	3.7	1.56	2.4	55
147084	3.9	-2.7	2.8	0.08	35.0	25
147889	4.3	-2.5	4.7	0.14	33.8	41
148379	3.1	-6.8	2.2	0.98	2.3	26
148688	3.4	-6.6	1.7	1.09	1.6	83
151346	3.8	-0.4	1.9	0.19	10.0	44
152235	3.1	-6.4	2.4	1.18	2.0	22
152236	3.5	-8.2	2.4	1.28	1.9	19
154043	3.0	-6.2	2.4	1.48	1.6	-93
156201	3.0	-6.4	2.6	2.18	1.2	57
165319	3.1	-6.2	2.6	2.06	1.3	119
166628	3.0	-6.8	2.1	2.37	0.9	-22
167838	3.3	-7.0	1.8	2.41	0.8	12
168571	3.1	-5.0	2.4	1.20	2.0	-29
169454	3.2	-8.2	3.6	1.73	2.1	-21
170938	3.2	-6.6	3.3	1.69	2.0	-90
171012	3.4	-6.4	2.3	1.54	1.5	-113
172488	2.6	-4.0	2.1	0.79	2.7	-22

Table 6.4

Mean Values of R, A_V/d and $|z|$
for Extinction Laws A, B, C and D

Law	<R>	$<A_V/d>$ (mag/kpc)	$<\|z\|>$ (pc)
A	2.8	1.7	27
B	3.0	1.4	39
C	3.2	1.8	47
D	3.4	1.6	69

Table 6.5

Stars with Infrared Excess at 3.5 μ

HD	Law	Excess with stat. error
		m m
80558	D	0.04 ± 0.04
92964	D	0.28 ± 0.16
115842	D	0.07 ± 0.10
142468	C	0.12 ± 0.13
144969	C	0.10 ± 0.05
147084	S1	0.15 ± 0.03
147889	S2	0.05 ± 0.03
148379	C	0.09 ± 0.06
148688	D	0.08 ± 0.07
152236	D	0.08 ± 0.05
167838	C	0.03 ± 0.03

Fig. 6.15 Plot of R(ext) values from table 6.3 against R(p) from equ. (6.15) for 12 stars

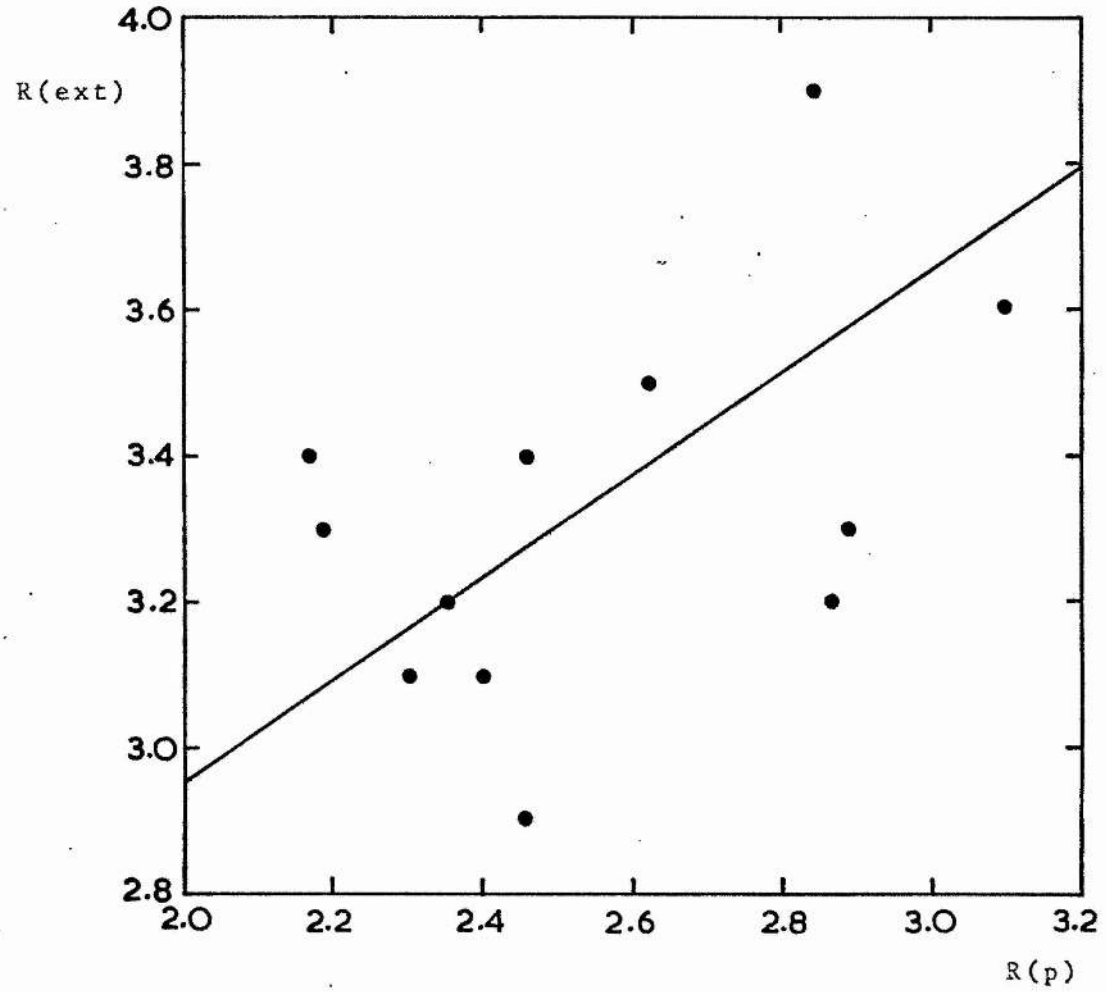

Fig. 6.16 Positions of reddened stars projected onto the galactic plane

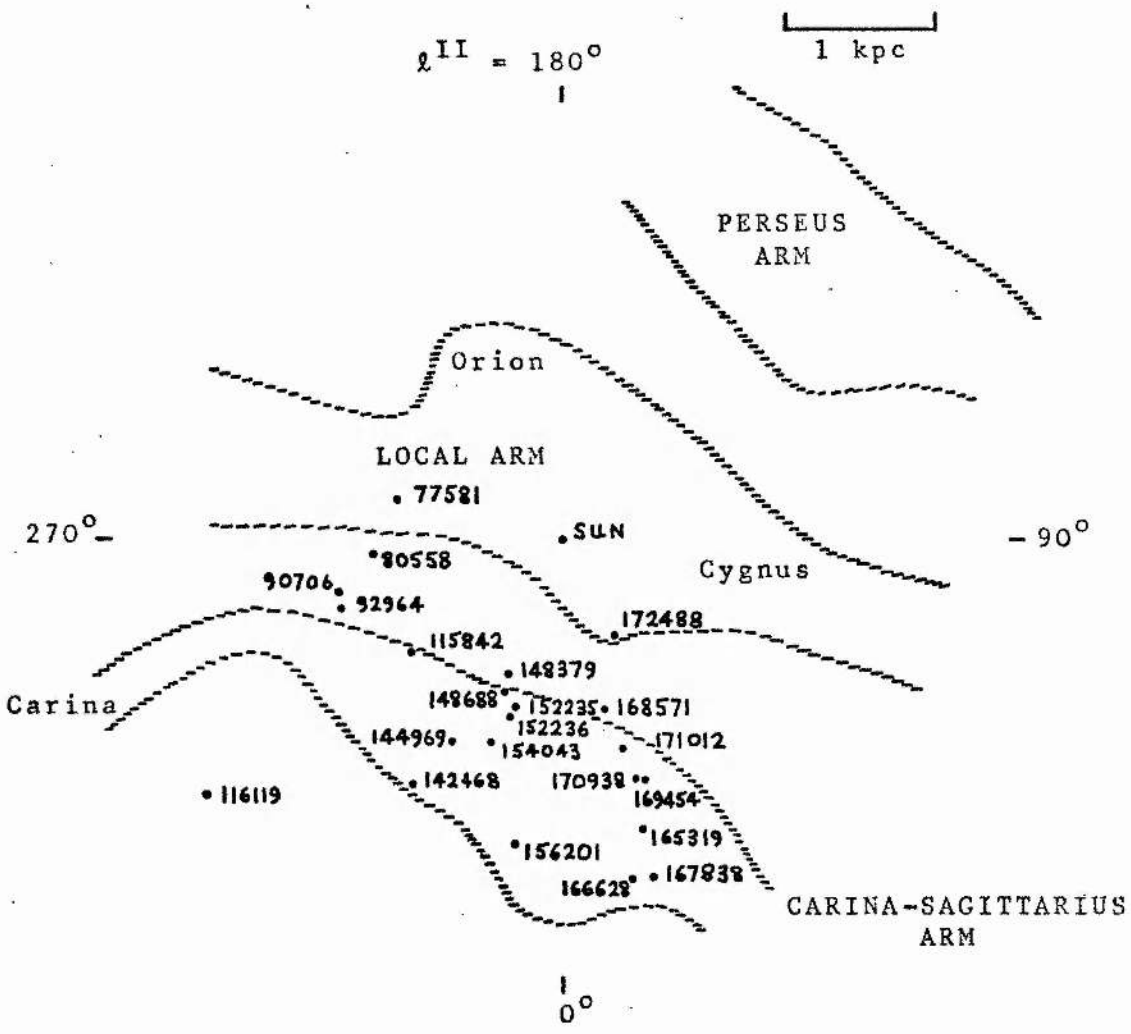

The positions of the stars projected onto the galactic plane are shown in fig. 6.16 (the Upper Scorpius stars being omitted). The boundaries of the spiral arms are taken from the diagram of Nandy (1965b). The lines of sight to two of the stars, HD 77581 and 172488, lie completely within the local arm, which is consistent with the relatively high values of A_V/d for these stars in table 6.3. Crézé (1972) has suggested that R varies between 4.0 and 1.5 according to the proportion of the line of sight lying within spiral arms. There is clearly no support for this hypothesis in the results given here.

The most distant star studied, HD 116119 ($d \sim 3$ kpc), lies well beyond the Carina-Sagittarius arm. The line of sight passes close to the nearby Coal Sack (see fig. 5.34), for which Rodgers (1960) derived a distance of 174 pc and a mean absorption of $A_V \sim 1^m$ by a statistical analysis of photometric data. Behind the cloud there is a clear region extending to ~ 0.8 kpc from the Sun, corresponding roughly to the gap between spiral arms in fig. 6.16; beyond this Rodgers deduced a mean absorption of $0^m.85$/kpc out to 6 kpc, which is similar to the value of A_V/d given in table 6.3 for HD 116119.

The stars HD 90706 and 92964 ($d \sim 1.5$ kpc) lie in front of the η Carinae complex, which is ~ 2.5 kpc distant (Faulkner, 1963). The extinction of these stars may be partially due to a dark cloud ~ 0.8 kpc from the Sun studied by Bok (1932), for which Graham (1971) deduced a reddening contribution of $E_{B-V} \sim 0.22$ and a value of R unlikely to be much greater than 3. This cloud has a filamentary structure, as shown in fig. 5.34. HD 90706 is a member of the open cluster IC 2581 (Lloyd

Evans, 1969), which is associated with nebulosity. Turner (1973) deduced R ∿ 5.5 for this cluster by variable extinction, a result which is disputed by Moffat (1974). Turner's values for R and the cluster distance imply that M_V ∿ -7.5 for HD 90706, which is inconsistent with the spectral classification (B2.5Ib) given by Lloyd Evans. The observed infrared extinction for this star would have to be in error by over a magnitude on the normalized scale (fig. 5.8) for Turner's value of R to apply.

It was noted in section 5.4 that HD 152235 and 152236 are regarded as probable members of Sco OB-1, a densely populated young association containing a high proportion of O stars. The distances derived for this pair of stars are similar (∿ 1.2 kpc) and much less than the value of 2.4 ± 0.2 kpc deduced for the association by Schild et al (1971) on the assumption that R = 3. This discrepancy probably arises, at least in part, from a systematic error in the absolute magnitudes. Blaauw's (1963) calibration is subject to considerable uncertainty, particularly in the domain of early-type supergiants. M_V values from the O star calibration of Walborn (1973) differ by $-0^m.8$ from those of Blaauw for O9-B0 Ia stars. Such a correction applied to the absolute magnitudes of HD 152235/6 would increase their distances to ∿ 1.8 kpc. If the R value used in the cluster distance determination is increased from 3 to 4, the distance drops from 2.4 to 1.8 kpc. The central region of Sco OB-1 is immersed in emission nebulosity (Morgan et al, 1953); thus an R value of 4 would not be particularly surprising, although Schild et al suggest that most of the reddening occurs in the local spiral arm.

HD 152235/6 lie about 1^{o} and 2^{o} from the centre of the association, respectively, outside the boundaries of the nebulosity.

HD 152236 (ζ_1 Sco) is, itself, a particularly interesting object. It is described by Crawford et al (1971) as 'one of the intrinsically brightest stars in our Galaxy'. Jaschek and Jaschek (1973) have reported variations in HeI, NII and OII spectral line strengths which they attribute to turbulence in the outer layers of the star, possibly associated with mass loss. Jaschek and Brandi (1973) also studied the adjacent star HD 148688, and again found indications of possible mass loss. This may be expected to produce excess radiation at infrared and radio wavelengths due to thermal free-free emission from circumstellar ionized gas (see Wright and Barlow, 1975, and the references therein). The results of table 6.5 suggest that these stars may have small excesses at 3.5 μ. Jaschek and Brandi deduced a distance of 1100 pc for HD 148688, in good agreement with that given in table 6.3.

CHAPTER 7

THE VALUE OF R IN THE RHO OPHIUCHI COMPLEX

(7.1) Introduction

The non-typical nature of the extinction curves found for two stars in the ρ Oph complex (and a third nearby) suggested that this region is worthy of more detailed study. The complex lies towards the inner region of the Sco OB-2 association in Upper Scorpius, which it partially obscures, and several of the more luminous stars are surrounded by emission and reflection nebulosity. This indicates that they are imbedded in the dust rather than seen through it. The most densely obscured region lies within the asterism formed by ρ Oph, σ Sco, α Sco and 22 Sco (see Garrison, 1967). Bok (1956) deduced by the star count method that the distribution of the dust is spherically symmetric to a first approximation, and that the grain density increases exponentially towards the centre where it is $\sim 10^3$ times greater than the interstellar mean. The degree of reddening thus varies markedly from star to star. Photometric data and spectral classifications are available for Sco OB-2 stars from a number of sources, as it is a sub-group of the well-studied Scorpio-Centaurus association, suggesting that the value of R may be determined by the variable extinction method. Such an analysis is the principal subject of this chapter and of a paper by Whittet (1974). It will be useful to begin by reviewing briefly the relevant literature.

Interest in the ρ Oph complex has been stimulated in recent years by the discovery of molecular emission (Heiles, 1970; Penzias et al, 1972; Encrenaz, 1974) and a group of 2 μ

infrared point sources (Grasdalen et al, 1973; Vrba et al, 1975) in the central region. An intense source of CO emission lies close to the position of HD 147889 (Encrenaz). One of the 2 μ points is also associated with this star, which is thought to be the brightest member of a very highly reddened young cluster responsible for the infrared sources. Most of these are not identified with visual objects, suggesting that the visual extinction may be as high as $\sim 30^m$ in some cases.

Bless and Savage (1972) have presented extinction curves for ρ Oph (A + B) and σ Sco which include ultraviolet satellite data. They deduce, in agreement with the present observations, that the extinction in this region is appreciably different from that in the general interstellar medium. It is interesting to compare these curves with that for θ Ori, also given by Bless and Savage (see fig. 1.3). The far ultraviolet extinction is much lower than the interstellar mean in each case; the 4.5 μ^{-1} hump, quite prominent in the ρ Oph and σ Sco curves, is very weak in Orion. This suggests that the smallest component of the grains (i.e. the iron component of the WN model) is depleted in both regions, while depletion of graphite grains occurs with greater efficiency in Orion.

There has been controversy for some time on the value of R appropriate to the ρ Oph dust cloud. The extinction curves of Bless and Savage suggest that R may be intermediate between the Orion value of about 6 and the normal interstellar value of 3, which is in accordance with the findings of Carrasco et al (1973) and results given in chapter 6. This contradicts an earlier estimate by Garrison (1967) who derived a 'normal'

R value by variable extinction. His result is based on only two stars, HD 147889 and 22 Sco, which are both classified B2V: if their distances and absolute magnitudes are taken to be the same the ratio of the differences in visual magnitude and reddening gives R = 3.1. Hardie and Crawford (1961) found an anomalous position for HD 147889 on the colour-magnitude diagram of Sco OB-2, and deduced that either it is subluminous or the value of R is significantly greater than 3. Gutierrez-Moreno and Moreno (1967) plotted E_{B-V} against V for stars of similar spectral type in Upper Scorpius and found that the line for R = 6 appeared to fit the points rather better than that for R = 3. The analysis reported here uses data for a larger number of stars in the inner region, with a calibration of the absolute magnitudes.

The variable extinction method is liable to give an inflated value of R if field stars are included, as pointed out by Becker (1966). This is due to the fact that foreground and background stars generally have low and high reddening respectively compared with true cluster members, and they thus tend to tilt the line fitted to the $E_{B-V}/(V - M_V)$ plot towards higher R values (see Garrison, 1970; Moffat, 1974). Membership of Sco OB-2 is probable for most of the stars used here (Bertiau, 1958; Hardie and Crawford, 1961; Garrison, 1967). It is relatively easy to eliminate field stars in this case; foreground stars are expected to be almost completely unreddened, and background stars are unlikely to be detectable through the denser regions of the cloud; it is a simple matter to identify peripheral background stars with intermediate or low reddening from the $E_{B-V}/(V - M_V)$ diagram.

The spread in kinematical distances for cluster members is small, thus the error due to intrinsic scatter should not be appreciable. The main source of uncertainty is the absolute magnitude calibration.

(7.2) The Data and Absolute Magnitude Calibration

Table 7.1 lists data for HD stars of types F3 and earlier lying within about 2° of the cloud centre. (Peculiar A stars are omitted). The MK classifications, V-magnitudes and E_{B-V} values (columns 2-4) are taken from Garrison (1967) unless otherwise indicated in the remarks. Absolute magnitudes $M_V(\alpha)$ deduced from Hα line strengths measured by Andrews (1968) are available for 6 of the stars and are given in column 5 of table 7.1. Hβ indices have been published for about half of the stars (Hardie and Crawford, 1961; Gutierrez-Moreno and Moreno, 1967; Glaspey, 1971, 1972). These were used to estimate absolute magnitudes $M_V(\beta)$ by means of the Crawford (1973) calibration, and the results are listed in column 6. The calibration of Blaauw (1963) giving absolute magnitude $M_V(Sp)$ in terms of MK spectral type is separated into two distinct sections according to whether the stars were selected by (1) space density or (2) apparent magnitude. The values of $M_V(Sp_1)$ and $M_V(Sp_2)$ from the two sections are given in columns 7 and 8 of table 7.1. The sections overlap for main sequence stars in the range B8-A1, where two differing sets of data are available. Fig. 7.1 shows a plot of Hα or Hβ M_V values against $M_V(Sp_1)$ for types B1-A1, and similarly fig. 7.2 shows $M_V(\beta)$ against $M_V(Sp_2)$ for types B8-F3. Note that the stars with $M_V(\alpha)$ values are all earlier than B8 and do not therefore appear

in fig. 7.2; stars having both $M_V(\alpha)$ and $M_V(\beta)$ data appear twice in fig. 7.1, and those with $M_V(\beta)$ values of types B8-A1 appear in both figures. The line of exact agreement in fig. 7.1 fits the points reasonably well. In fig. 7.2, however, a line displaced by $0^m.6$ to the right appears to fit the points rather better than the line through the origin, which suggests the relation:

$$M_V(Sp_1) = M_V(Sp_2) + 0.6. \qquad (7.1)$$

In order to obtain a homogeneous set of data, absolute magnitudes $M_V(Sp)$ were adopted from section 1 using this adjustment for main sequence stars later than A1; $V - M_V(Sp)$ values thus deduced are listed in column 9 of table 7.1. A correction by this amount was used by Andrews and Thackeray (1973) as it gives consistent results in the overlap region. The fact that it is also consistent with Balmer line photometry gives further justification for its use.

Table 7.1

Data for Stars in the Direction of the ρ Oph Cloud

HD	Sp	V	E_{B-V}	M_V (α)	(β)	(Sp_1)	(Sp_2)	$V - M_V(Sp)$	Rem.
145792	B5V	6.41	0.19	-	-0.5	-1.0	-	7.41	
146001	B7IV	6.04	0.17	-0.83	-0.7	-1.2	-	7.24	
146029	B9V	7.38	0.14	-	+0.2	+0.6	0.0	6.78	
146284	B8IV	6.70	0.27	-	-0.5	-0.7	-	7.40	
146285	B8V	7.94	0.34	-	+0.6	+0.1	-0.5	7.84	
146416	B9V	6.60	0.09	-	+0.7	+0.6	0.0	6.00	
146706	B9V	7.55	0.21	-	+0.7	+0.6	0.0	6.95	
146899	A7V	10.22	0.43	-	+2.8	-	+2.0	7.62	
147012	B9V	9.75	0.59	-	-	+0.6	0.0	9.15	
147013	AOV	9.10	0.45	-	-	+1.0	+0.5	8.10	
147084	A5II	4.54	0.74	-	-	-2.7	-	7.24	(1)
147165A	B1III	3.07	0.39	-4.37	-4.1	-4.4	-	7.47	(2)
147165B	B9V	8.48	0.36	-	-	+0.6	0.0	7.88	(3)
147196	$B8V_p$	7.05	0.33	-	-0.5	+0.1	-0.5	6.95	
147283	A3V	10.27	0.72	-	-	-	+1.5	8.17	
147343	A1V	9.36	0.63	-	+2.3	+1.5	+0.8	7.86	
147384	B9.5V	8.62	0.45	-	+1.0	+0.8	+0.25	7.82	
147592	A1V	8.90	0.27	-	+1.0	+1.5	+0.8	7.40	
147648	B8V	9.42	0.89	-	-	+0.1	-0.5	9.32	
147649	A7V	9.60	0.24	-	-	-	+2.0	7.00	
147701	B5V	8.35	0.72	-	-	-1.0	-	9.35	
147702	A3V	9.14	0.37	-	-	-	+1.5	7.04	
147703	B9V	7.47	0.25	-	-	+0.6	0.0	6.87	
147809	A1V	8.60	0.39	-	+1.0	+1.5	+0.8	7.10	
147888	B5V	7.11	0.47	-1.31	-0.7	-1.0	-	8.11	(4)
147889	B2V	7.86	1.08	-	-1.8	-2.5	-	10.36	(5)
147932	B5V	7.27	0.47	-	-	-1.0	-	8.27	
147933	B2IV	4.59	0.47	-3.91	-	-3.3	-	7.89	(6)
147934	B2V	5.02	0.47	-3.38	-	-2.5	-	7.52	(6)
147955	B9.5V	8.07	0.29	-	-	+0.8	+0.25	7.27	
148118	A5V	9.45	0.30	-	-	-	+1.8	7.05	
148302	A7V	10.01	0.29	-	-	-	+2.0	7.41	
148334	B9V	9.96	0.29	-	-	+0.6	0.0	9.36	
148352	F3V	7.51	0.00	-	+3.3	-	+2.9	4.01	
148562	A3V	7.81	0.09	-	+1.9	-	+1.5	5.71	
148563	A2V	8.62	0.20	-	+1.0	-	+1.2	6.82	
148579	B9V	7.34	0.35	-	+0.7	+0.6	0.0	6.74	
148605	B2V	4.79	0.11	-2.46	-1.8	-2.5	-	7.29	
148624	A7IV	10.38	0.20	-	-	+1.7	-	8.68	
148822	FOV	9.65	0.19	-	-	-	+2.4	6.65	
148842	A1V	10.62	0.23	-	-	+1.5	+0.8	9.12	
149069	A1V	10.50	0.18	-	-	+1.5	+0.8	9.00	

Table 7.1 – Remarks

(1) HD 147084 (σ Sco) : V may be slightly variable (Garrison, 1967); extinction curve gives R = 3.9 ± 0.3 (chapter 6); see also discussion in text.

(2) HD 147165A (σ Sco A) : β CMa variable; spectroscopic binary (Huang and Struve, 1955; Struve et al, 1955) with ΔV ≃ 2.2 (Nather et al, 1974); correction of +0.14 is applied to V.

(3) HD 147165B (σ Sco B) : lies about 21" from A; Sp, V and E_{B-V} from Andrews and Thackeray (1973).

(4) HD 147888 (ρ Oph D) : visual binary with ΔV ≃ 1.0; correction of +0.36 is applied to V.

(5) HD 147889 : extinction curve gives R = 4.3 ± 0.3 (chapter 6).

(6) HD 147933/4: (ρ Oph A/B) visual binary; individual V magnitudes from Andrews (1968).

Fig. 7.1 Plot of $M_V(\alpha \text{ or } \beta)$ against $M_V(Sp_1)$ for stars of types B1-A1 from table 7.1.

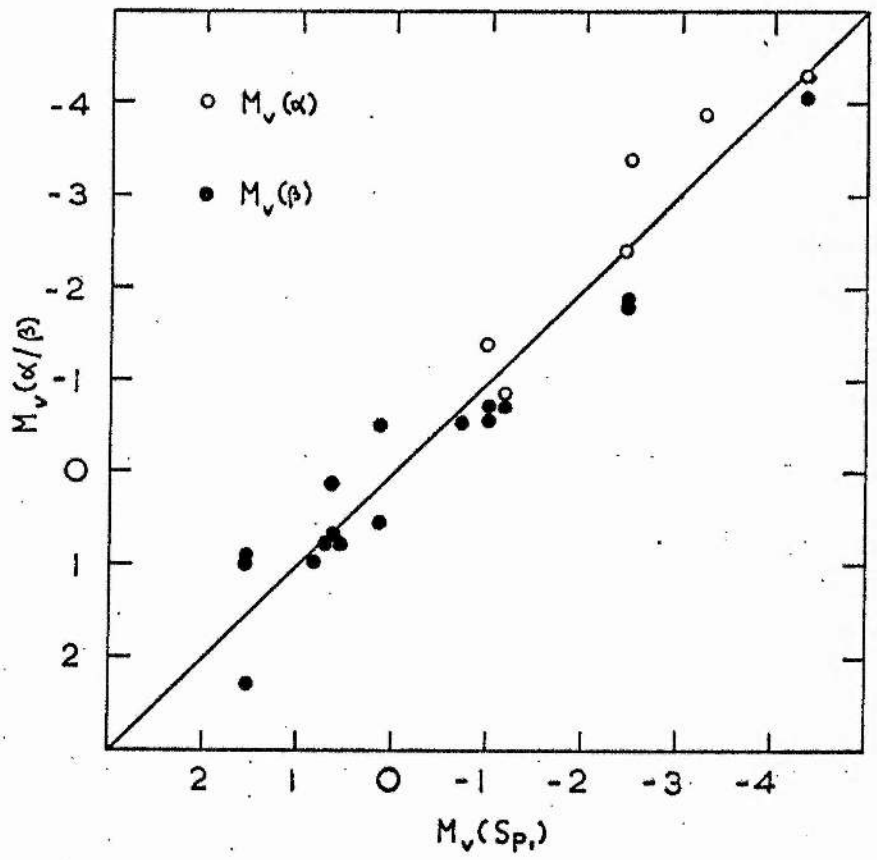

Fig. 7.2 Plot of $M_V(\beta)$ against $M_V(Sp_2)$ for stars of types B8–F3 from table 7.1.

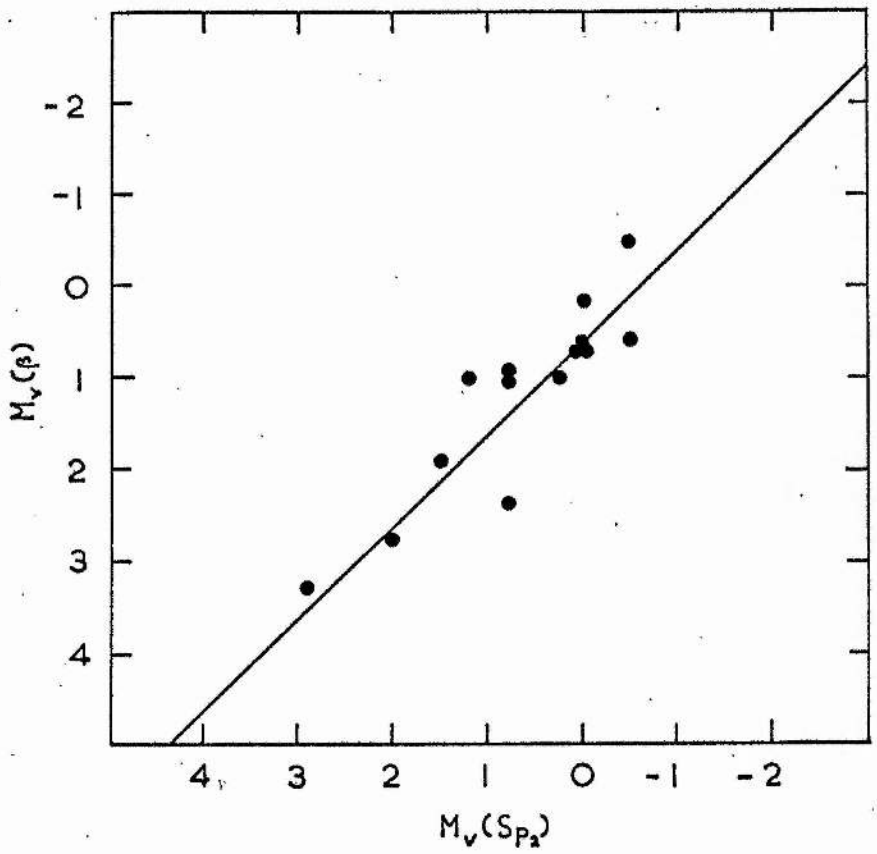

(7.3) Results and Discussion

A plot of E_{B-V} against $V - M_V(Sp)$ for the stars in table 7.1 is shown in fig. 7.3. Ideally this should be a straight line given by

$$E_{B-V} = \frac{1}{R} \{V - M_V(Sp) - D\} \qquad (7.2)$$

where D is the distance modulus of the association. A fairly linear correlation is apparent for most of the stars. There is one completely unreddened foreground star (HD 148352); four stars appear to be grouped behind a less obscured region of the association, having relatively low E_{B-V} and high $V - M_V$. The $V - M_V$ value for HD 147084 is surprisingly low in view of its high reddening. The absolute magnitude of this star is particularly uncertain; the spectral type (A5II) gives -2.7, but Bertiau (1958) deduced -3.6 from the kinematical distance assuming R = 3. (Higher R gives greater luminosity). It is notable that the Blaauw calibration gives a difference of 2.1 in M_V between stars of types A5II and A5Ib.

A least squares analysis was applied to the data points in fig. 7.3, omitting the field stars and HD 147084 for the reason given above. The straight line fitted is drawn on the diagram. The slope and intercept give the results with standard errors:

$$R = 3.7 \pm 0.3$$

$$D = 6.1 \pm 0.1.$$

Of the 36 stars used to give this result, 14 are in the direction of nebulosity, listed in table 7.2. If these stars are omitted from the least squares analysis, the results are

$$R = 3.3 \pm 0.3$$

$$D = 6.2 \pm 0.1.$$

A least squares fit for the stars in table 7.2 gives

$$R = 4.2 \pm 0.5$$

$$D = 6.0 \pm 0.2.$$

The distributions and lines fitted are shown in figs. 7.4 and 7.5. It is notable that the values of D derived in the three cases are consistent both with each other and with the mean kinematical value of 6.18 (Bertiau, 1958), which lends weight to the R values deduced.

Thus the value of R appears to be normal for stars not associated with nebulosity. The result for stars in table 7.2 is in good agreement with that of 4.3 ± 0.3 derived in chapter 6 for HD 147889, the most highly reddened of the group. This value considerably improves the position of this star on the Sco OB-2 colour-magnitude diagram of Hardie and Crawford (1961). If HD 147889 is omitted from the least squares fit R increases to 4.5 with a standard error of 0.9. The value of R = 3.9 ± 0.3 derived from the extinction curve of HD 147084 is rather high for a star not apparently in nebulosity, and implies an absolute magnitude of -4.3 if the kinematical distance is correct.

It has been suggested that there may be anomalies in the colours of HII region stars which lead to a spuriously high value of R. These may take the form of infrared excesses due to circumstellar dust emission or the presence of late-type companions (see, for example, the discussion of Anderson, 1970). As dust emission is unlikely to have any effect at wavelengths $\lambda \lesssim 2\ \mu$ it cannot affect the distribution of points on the $E_{B-V}/V - M_V$ diagrams. Of the stars in table 7.2, HD 147165A is a spectroscopic binary and HD 147888 is a visual binary; a correction to V was applied in these cases (see the appropriate

remarks to table 7.1). The colours of these stars do not seem to be unusual, and they yield E_{B-V} values similar to those of stars around them. Possible variations in the radial velocities of HD 147889 and 148605 suggest that they may be spectroscopic binaries (Abt and Biggs, 1972). Radial velocities are not available for the other stars in table 7.2, but it seems unlikely that red companions luminous enough to produce a significant modification of the V and B magnitudes are generally present in view of the good agreement between the derived cluster distance modulus and the kinematical value. Results of $R \sim 4$ have been deduced for the diffuse nebulae IC 1805 (Ishida, 1969) and NGC 2244 (Dufour and Lee, 1970) by comparing radio surface brightness with Balmer line intensities for the gas itself, a method which cannot be influenced by such anomalous effects. It is thus concluded that the results presented here represent a genuine departure from normal interstellar extinction in the environment of HII regions and reflection nebulae.

Table 7.2

Stars from Table 7.1 lying towards Nebulosity

Central Star/System	Nebula	Stars included
σ Sco	Sharpless (1959) No. 9.	HD 147012
		HD 147013
		HD 147165A
		HD 147165B
HD 147889	IC 4603	HD 147889
ρ Oph	IC 4604	HD 147888
		HD 147932
		HD 147933
		HD 147934
22 Sco	IC 4605	HD 148562
		HD 148579
		HD 148605
α Sco	IC 4606	HD 148302
		HD 148563

Fig. 7.3 Plot of E_{B-V} against $V - M_V(Sp)$ for all stars in table 7.1.

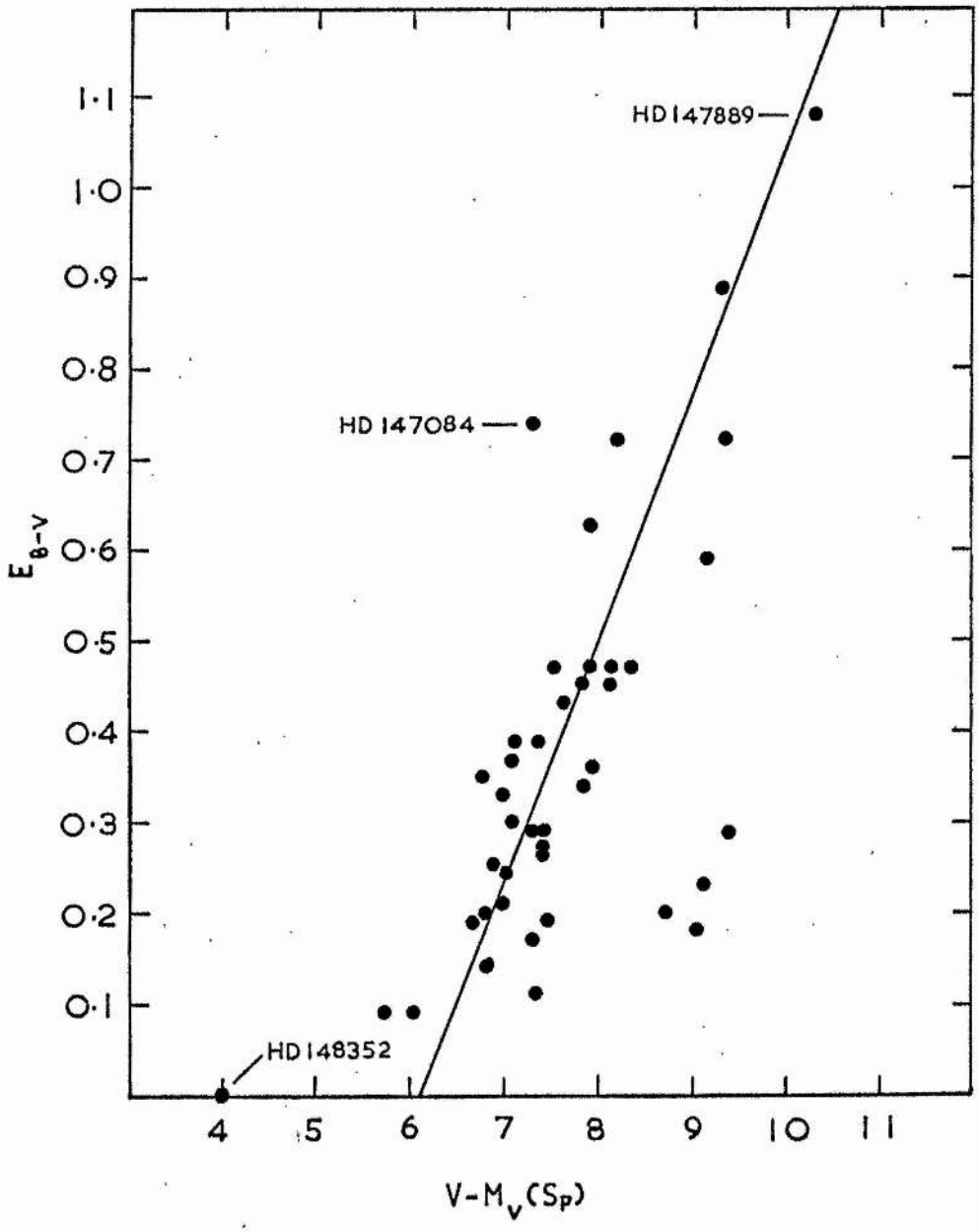

Fig. 7.4 Plot of E_{B-V} against $V - M_V(Sp)$ for stars not associated with nebulosity (field stars omitted).

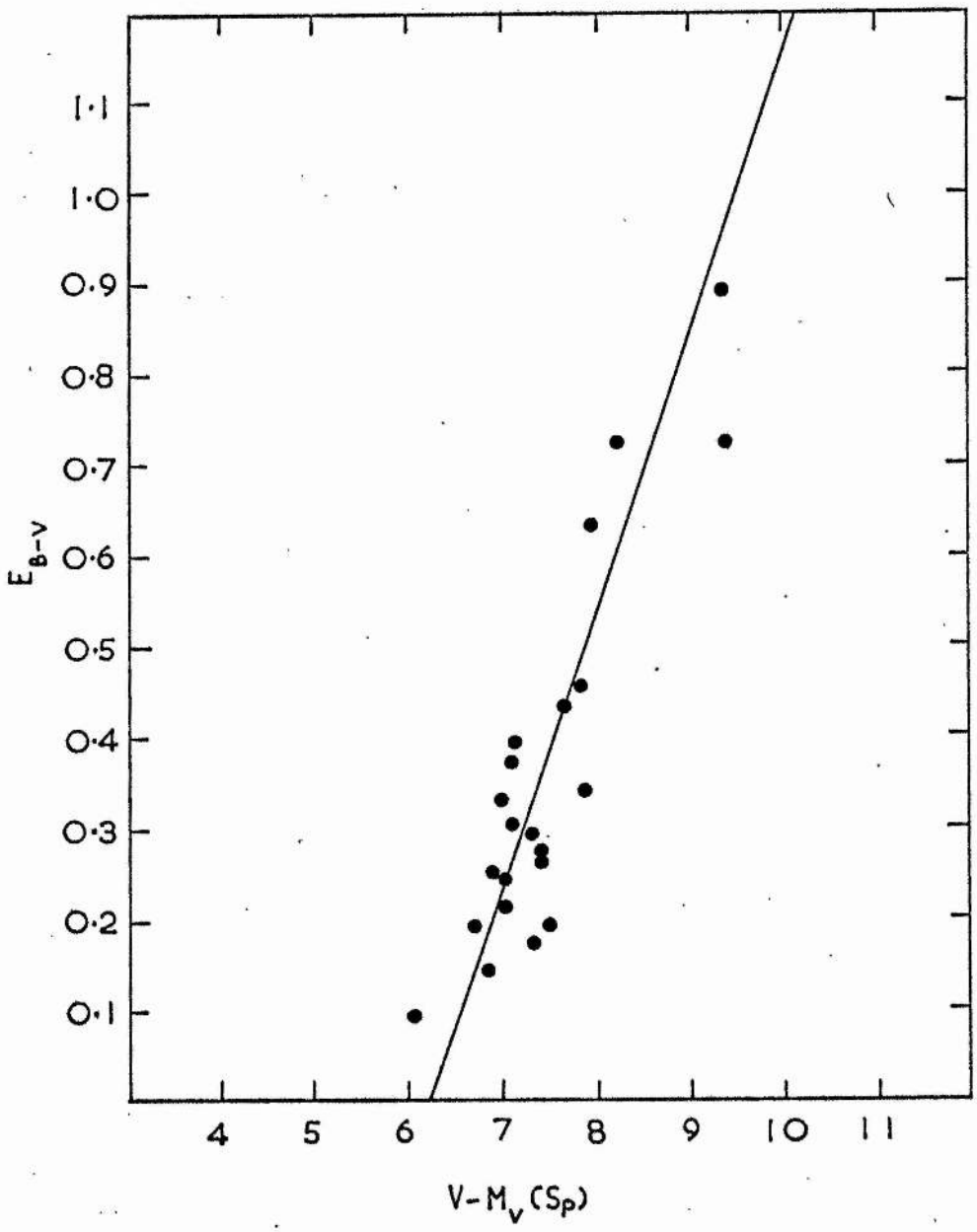

Fig. 7.5 Plot of E_{B-V} against $V - M_V(Sp)$ for stars associated with nebulosity (table 7.2).

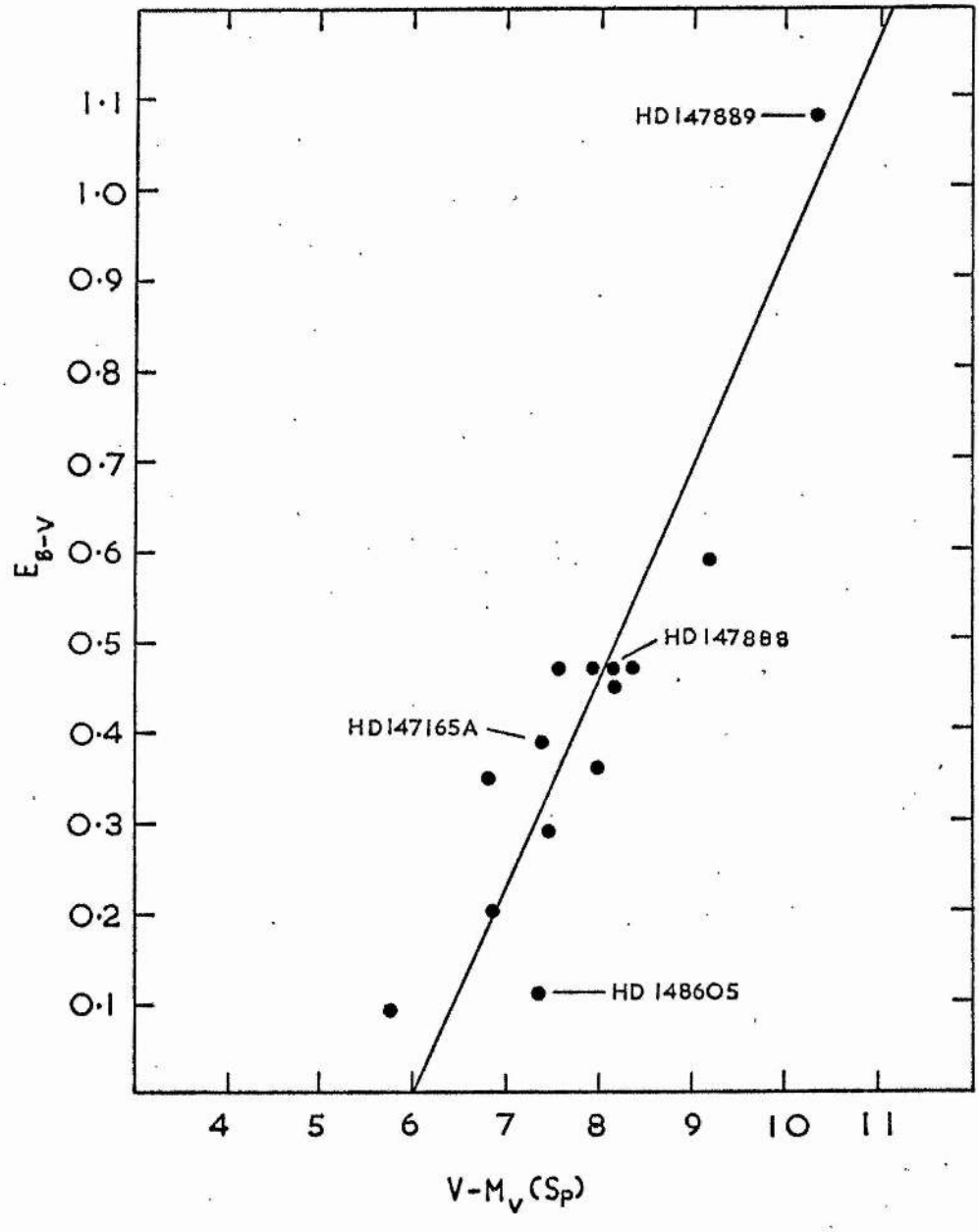

CHAPTER 8

BROADBAND STRUCTURE IN THE EXTINCTION CURVES

(8.1) The Extinction Residuals

It was noted in section 5.4 that the quasi-linear section of the scanner extinction curves contain appreciable structure. This may be illustrated by plotting deviations from a linear fit to the curves in the visual region against λ^{-1} on expanded scales. The quantity $\Delta m_R(\lambda)$ is defined as the residual extinction produced when the straight line drawn through the normalization points is removed from the curve, and is given by

$$\Delta m_R(\lambda) = \Delta m'(\lambda) - \left(\frac{\lambda^{-1} - \lambda_2^{-1}}{\lambda_1^{-1} - \lambda_2^{-1}} \right) \qquad (8.1)$$

where $\Delta m'(\lambda)$ is the normalized extinction; λ_1 = 4560 A and λ_2 = 7800 A, as in section 5.2. Plots of $\Delta m_R(\lambda)$ against λ^{-1} in the range 1.25-2.50 μ^{-1} for the mean curves are shown in figs. 8.1 (A, B, C) and 8.2 (D, S1, S2). Also shown are the models fitted to these curves (figs. 6.7-6.12), reduced in the same way. (Curve S1 is truncated at 2.3 μ^{-1} to avoid confusion with S2). The error bars given for the individual points represent mean photometric errors, combined with uncertainties in the Balmer corrections for the affected points (triangles). The standard deviations of the $\Delta m_R(\lambda)$ values for the individual stars averaged to give each mean plot are in general of the same order as the photometric errors.

The points in figs. 8.1 and 8.2 are joined by straight lines to give a clearer picture of the structure in the curves. The sense of the residuals is such that more positive values indicate enhanced absorption. The sections at the top of the

diagrams give the central wavelengths in Angstroms of the principal diffuse interstellar absorption features (see, for example, York, 1971). The underlined numbers refer to diffuse bands (half-widths 20-40 A) and the remainder to diffuse lines (half-widths 5-10 A). Several of these features can be discerned in one or more of the plotted curves. A maximum corresponding to the 4430 band is clearly visible in each case, with the notable exception of curve S1, and the 4760 band is also in evidence in curves B, D and S2. The peak in the 1.56-1.62 μ^{-1} region of the curves may result from the combined absorptions of the 6180 band and the 6284 line.

In addition to diffuse features of widths comparable with the resolution, the residual plots clearly also contain broader structure. The trough between wavenumbers 1.6 and 1.9 μ^{-1}, previously commented upon, is prominent in all the curves except S2, where it appears to have been shifted towards shorter wavelength. The departure of the observational data from the theoretical models in this region is striking. The trough appears to have an asymmetric profile, being steeper at the long wavelength end, and contains a hump about 250 A wide centred at 1.7 μ^{-1} (5900 A). This feature is prominent in curve D and absent in curve S1 (fig. 8.2). It may be partly due to a combination of the 5780 and 5797 lines and diffuse bands at 5830 and 5850 A reported by York (1971), which would not be resolved in these observations. Hayes et al (1973) have studied the trough in the extinction curves of Whiteoak (1966) and found that the depth correlates with reddening. The 1.7 μ^{-1} feature and the sharp edge at 1.62 μ^{-1} are not apparent in the Whiteoak data, which has a resolution of 100 A.

Fig. 8.1 Plot of Extinction Residuals Δm_R against λ^{-1} for Mean Curves A, B and C

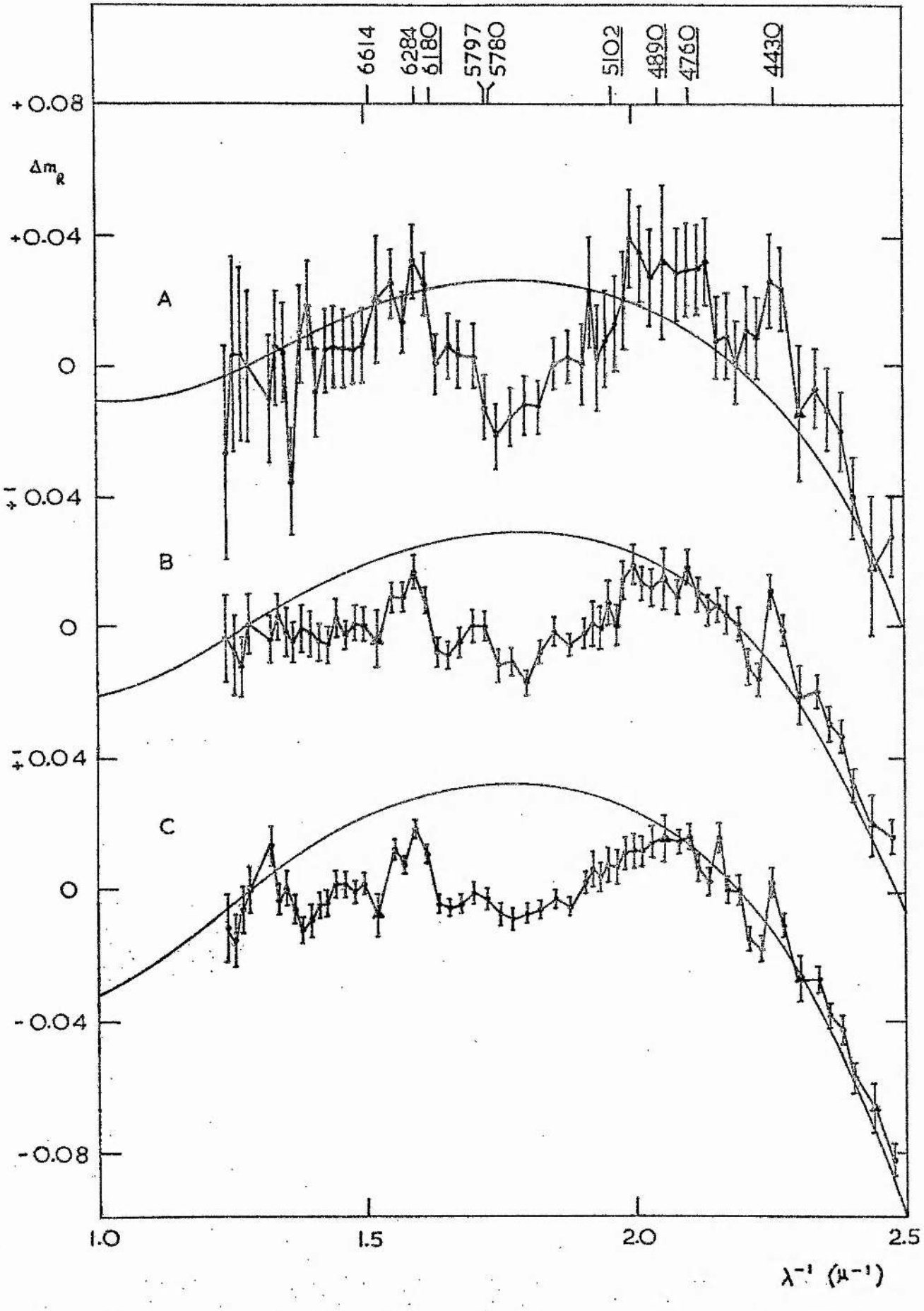

Fig. 8.2 Plot of Extinction Residuals Δm_R against λ^{-1} for Mean Curves D, S1 and S2

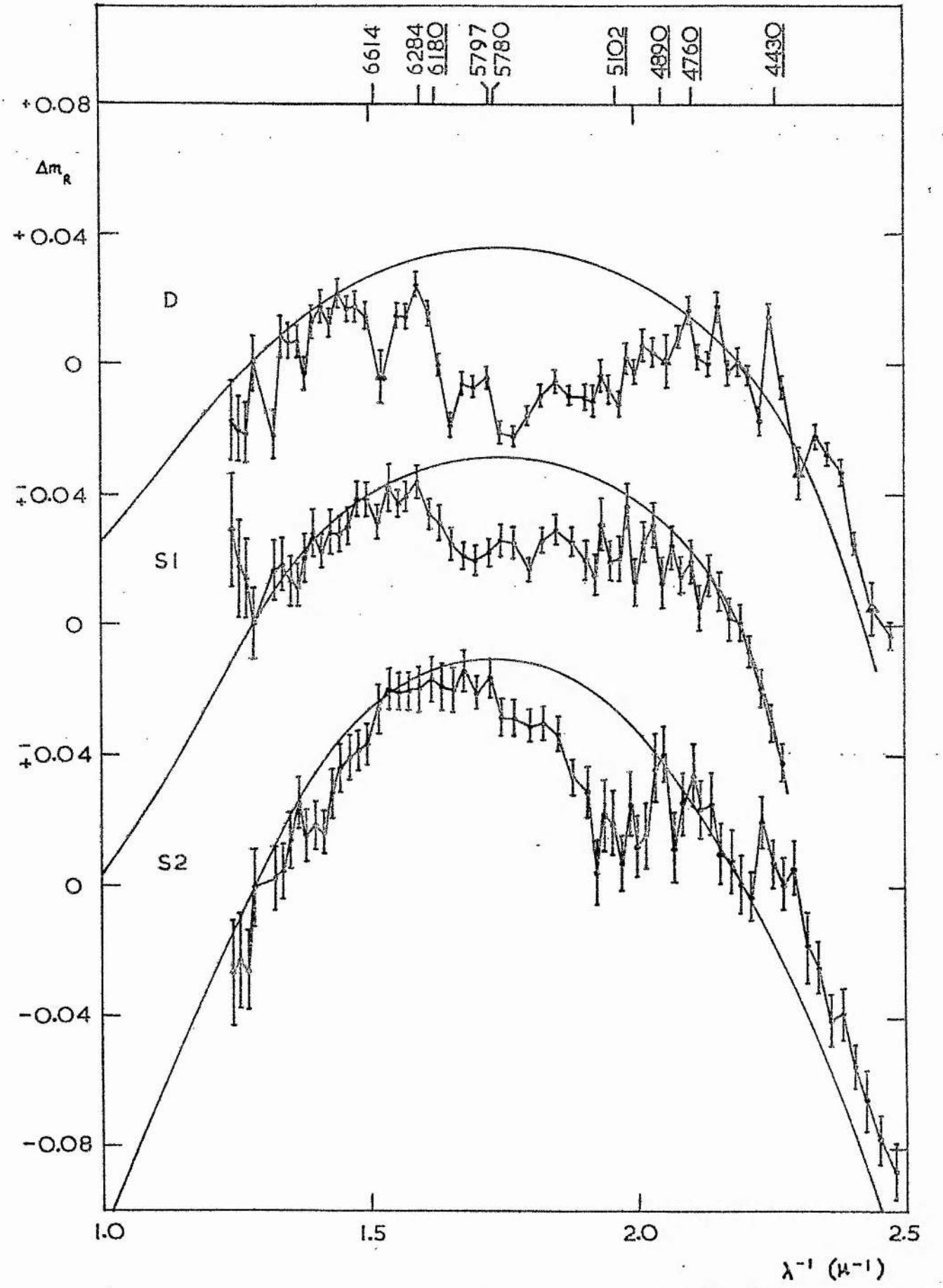

Fig. 8.3 Plot of Extinction Residuals Δm_R against λ^{-1} for HD 77581 and 152236

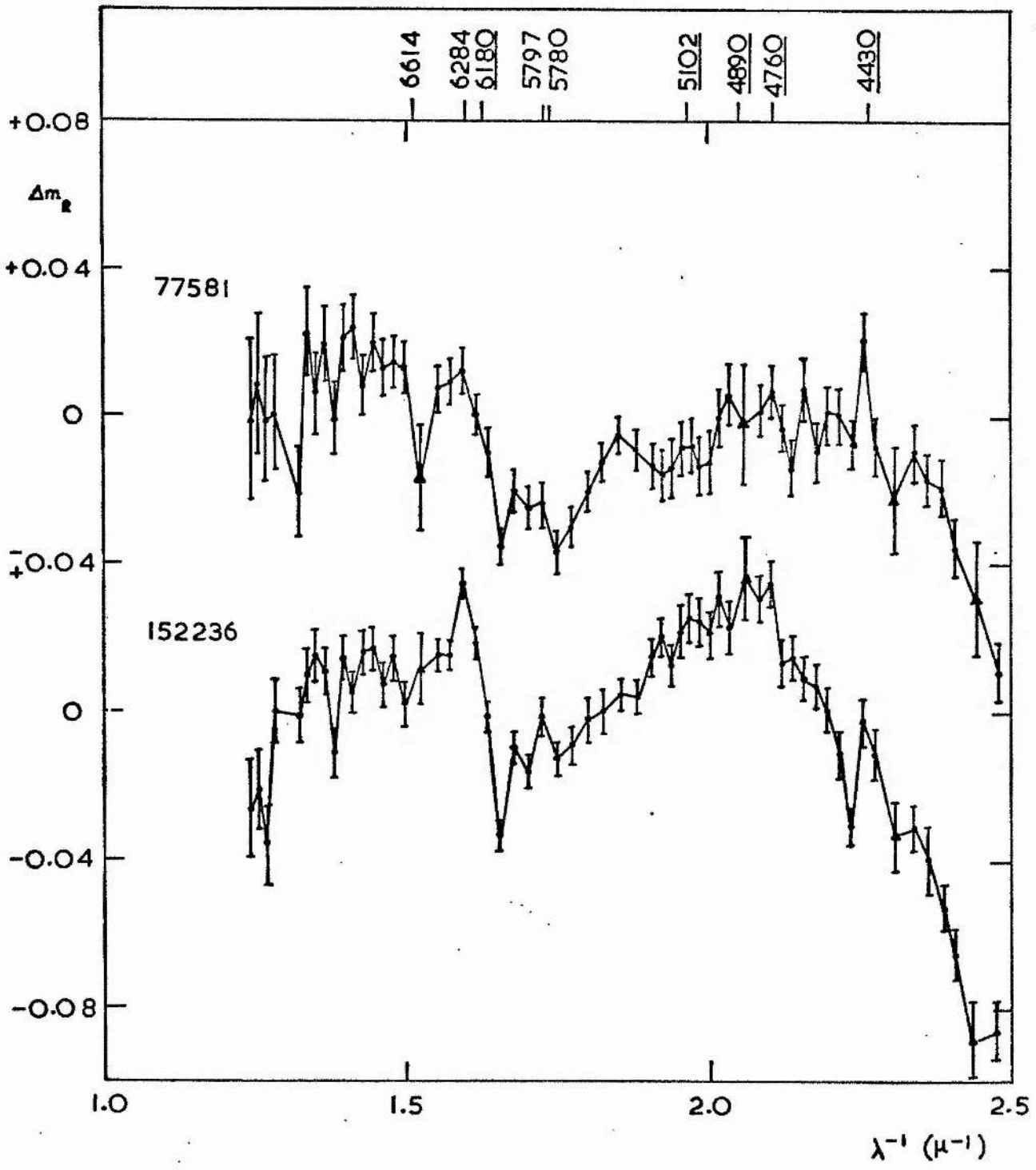

Another problem arising from a study of figs. 8.1 and 8.2 is the difficulty in assigning a definite wavelength to the change in slope at the blue end of the curves. According to Harris (1969) the knee should occur at 2.29 μ^{-1} (4360 A). There seems to be little evidence in the data to suggest that the extinction undergoes a fundamental change in slope near this wavenumber, although the situation is complicated by the close proximity of the 4430 band and the Hγ stellar line with associated corrections. There is a slight discontinuity at 2.38 μ^{-1} (4200 A) which may be due to an absorption feature noted by Walker et al (1968) at this wavelength. Hayes et al (1973) have argued that the knee occurs at $\lambda^{-1} \sim 2.09\ \mu^{-1}$, which is near the point where the residuals begin to show a downward trend in the diagrams, viewing figs. 8.1 and 8.2 from left to right.

Fig. 8.3 shows residuals plotted for two individual stars of particular interest, HD 77581 (associated with Vel X-1) and the superluminous HD 152236 (possibly undergoing mass loss). These stars are included in the law D mean curve. The 1.6-1.9 μ^{-1} trough is quite deep in both cases, and the 5900 A feature is particularly well defined in the 77581 curve. The Balmer lines of HD 77581 are weak for a star of its spectral type, causing the corrected points to be rather low. The sharp peak at 2.16 μ^{-1} (4640 A) in the 77581 curve appears only in cases where HD 99171 is used as comparison star, implying that it is not of interstellar origin. The plots in fig. 8.3 are not otherwise remarkable, suggesting that the reddening and intrinsic energy distributions of these stars are 'normal'.

Table 8.1

Heights of the 4430 and 5900 A Bands
and Central Depth of the 5300-6100 A Trough,
measured in Thousandths of a Magnitude

HD	m(4430)	m(5900)	m(D)
77581	45	26	67
80558	52	24	59
90706	51	18	38
92964	48	10	32
106068	25	12	25
115842	31	20	40
116119	42	38	54
142468	61	15	61
144969	59	35	83
147084	-	-	15
147889	59	-	-
148379	38	17	45
148688	29	12	33
151346	6	-	39
152235	38	19	50
152236	38	34	42
154043	35	27	68
156201	33	16	49
165319	47	34	61
166628	86	31	63
167838	45	23	41
168571	26	55	57
169454	55	32	66
170938	51	16	47
171012	26	36	50
172488	20	22	52

Fig. 8.4 Plot of m(4430) against relative strengths measured by Walker (1963) for 7 stars

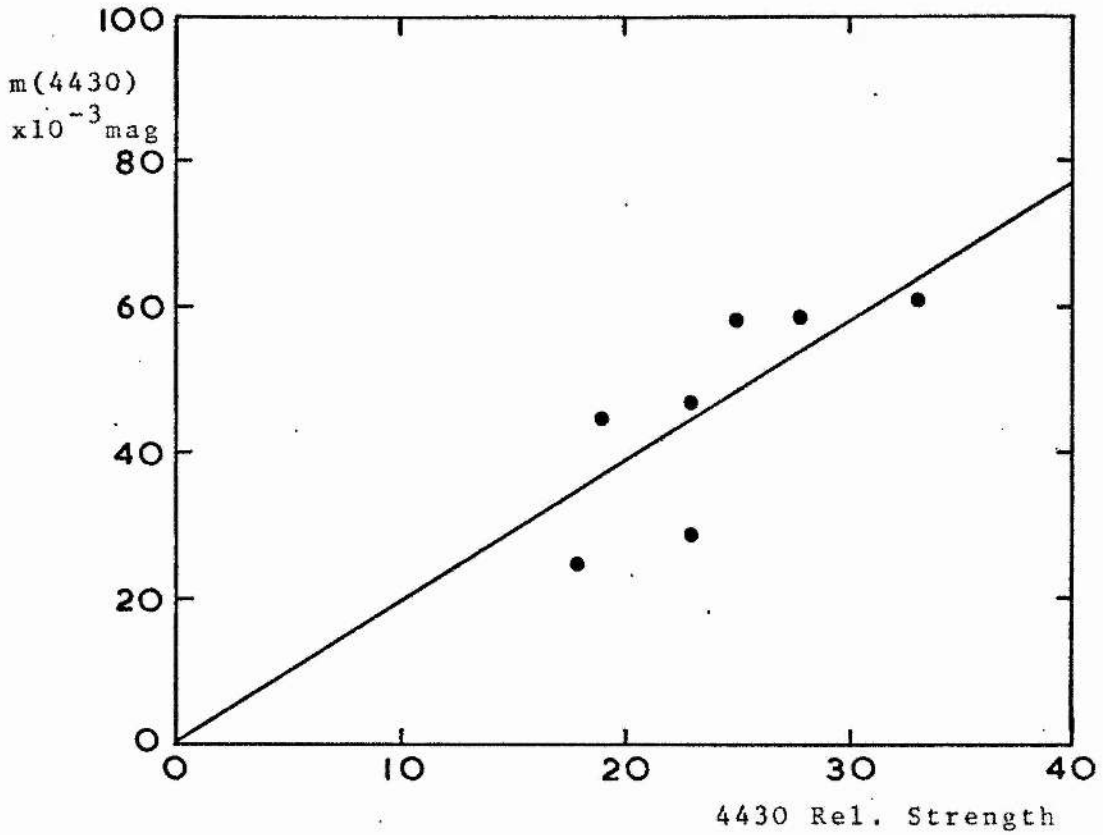

Fig. 8.5 Correlation of m(4430) with m(5900)

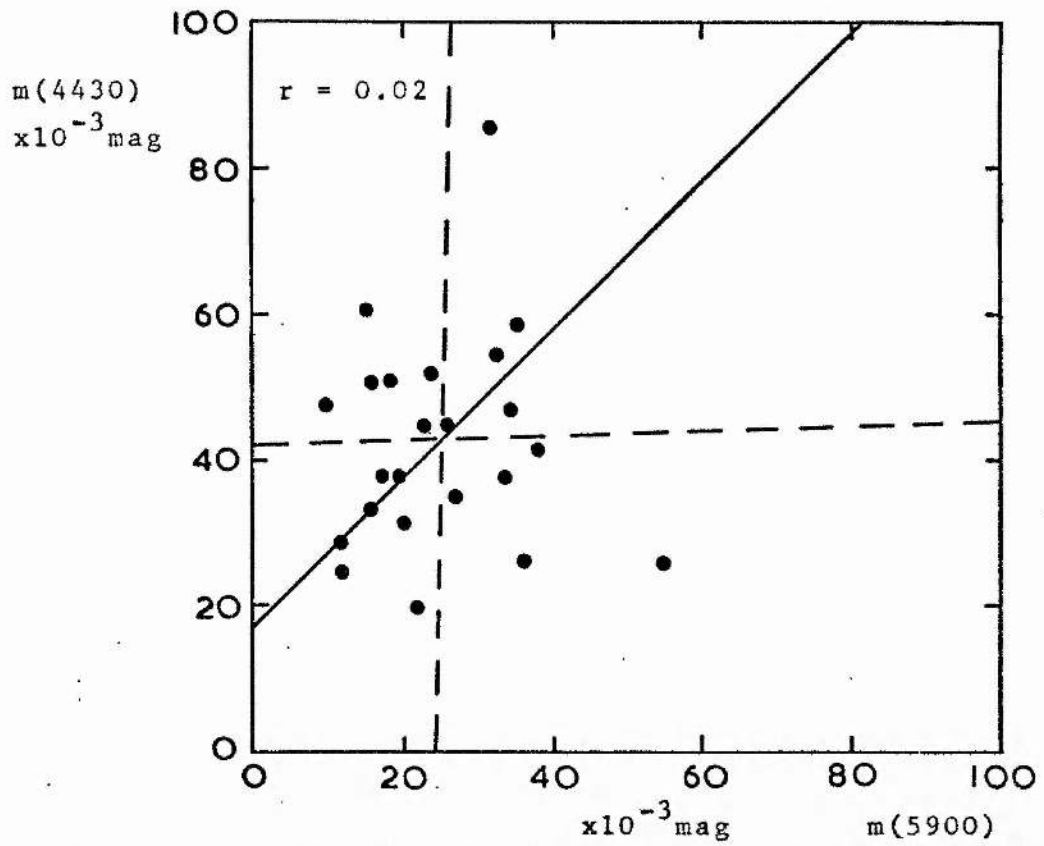

Fig. 8.6 Correlation of m(4430) and m(5900) with m(D)

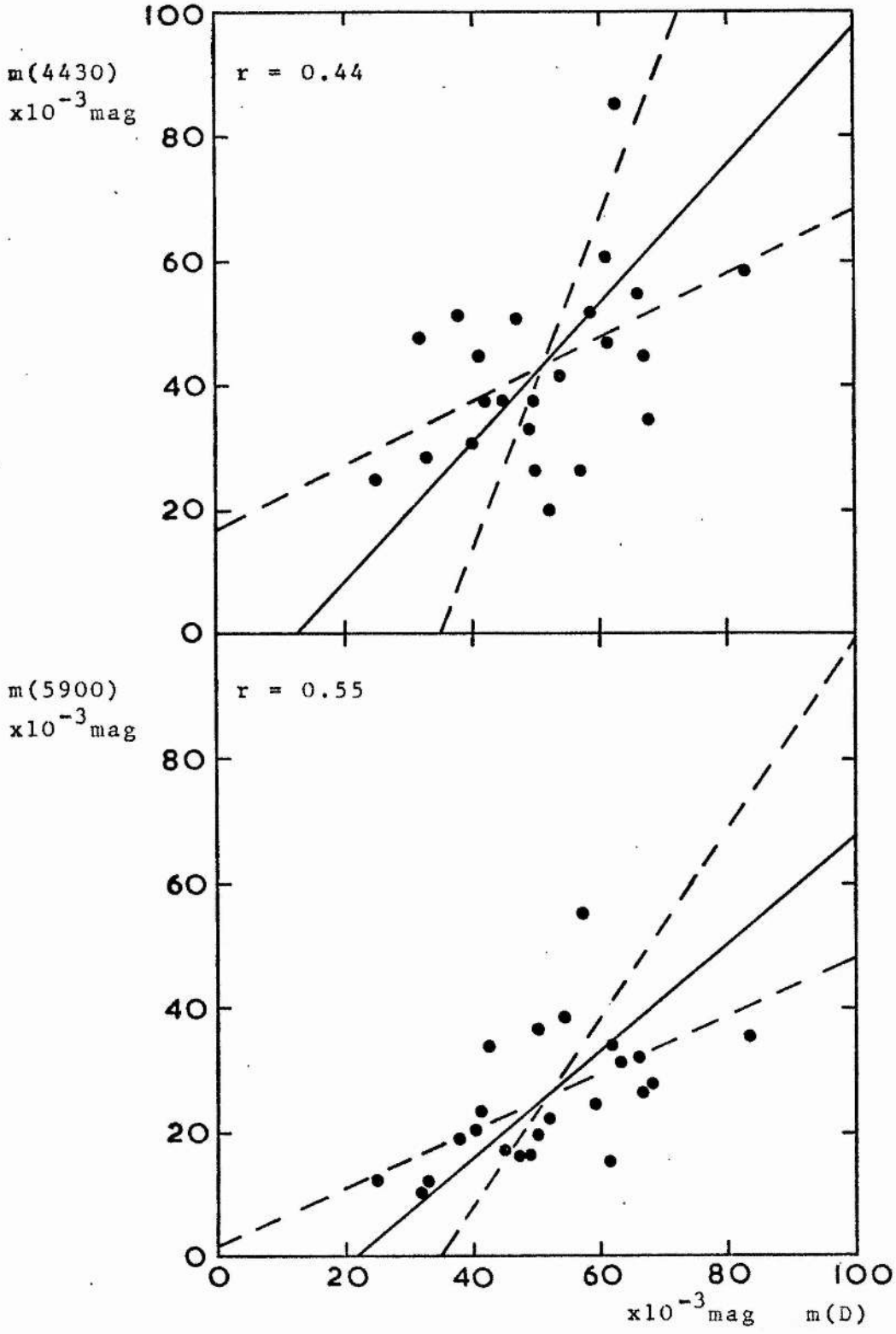

Fig. 8.7 Correlation of band parameters with colour excess

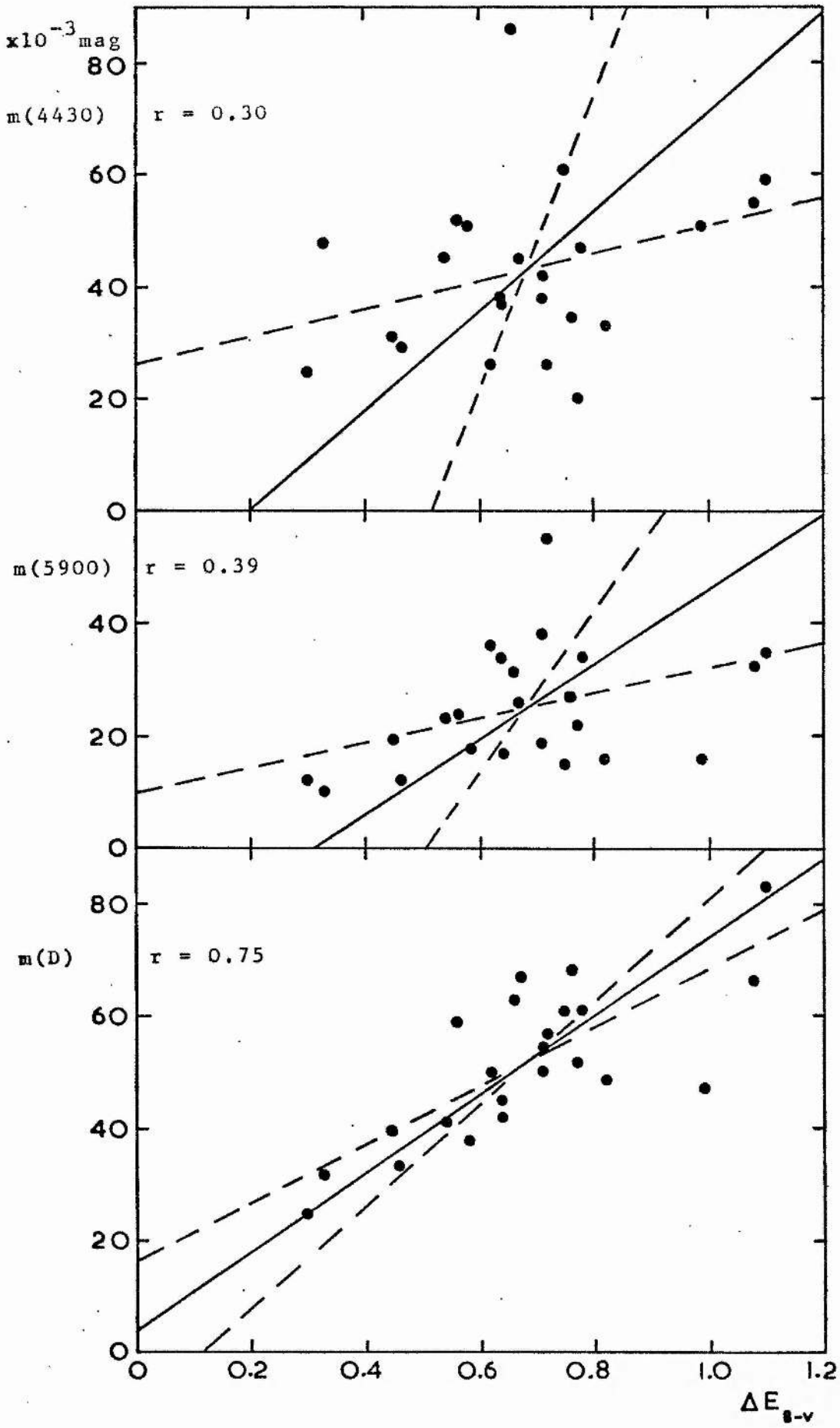

Fig. 8,8 Ratio of band parameters to colour excess plotted against galactic longitude

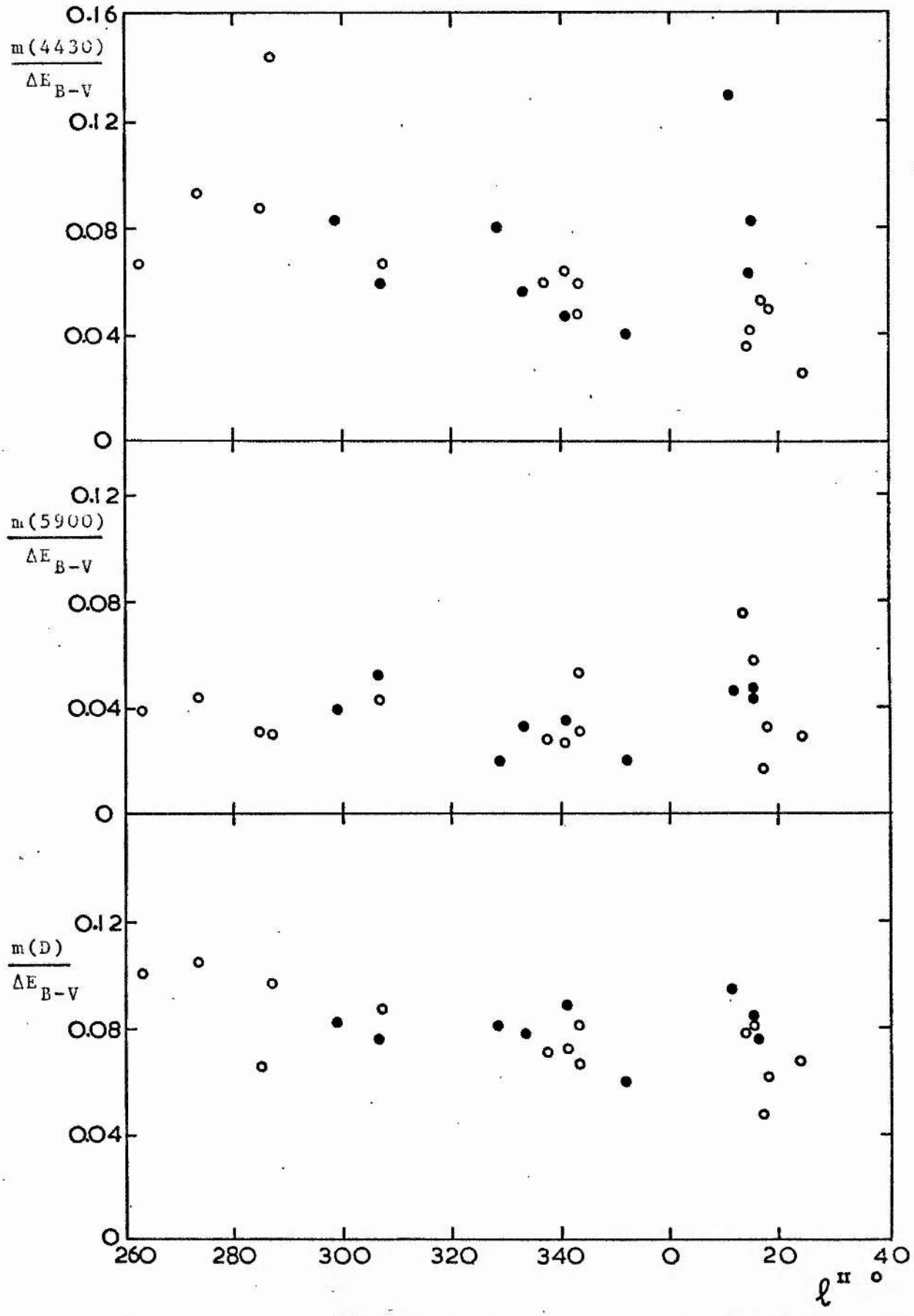

(8.2) Analysis of Band Heights

The residuals derived for the individual stars were used to measure three parameters relating to the band structure in the curves: these were the heights in magnitudes of the 4430 band and the feature at 5900 A, and the central depth m(D) of the 1.6-1.9 μ^{-1} dip. The heights m(4430) and m(5900) were measured using the generally well defined minima occurring to the left of these bands as the reference level (see, for example, curve D in fig. 8.2), and m(D) was measured from the minimum at $\lambda^{-1} \sim 1.75\ \mu^{-1}$ to the mean level of the plateaux which occur in the regions 1.5-1.6 μ^{-1} and 1.95-2.05 μ^{-1}. Results deduced for the individual stars are given in units of thousandths of a magnitude in table 8.1. The measured values have been multiplied by the appropriate normalization factors (equ. 5.4) and the results thus represent absolute measures of the band absorption for each star. The comparison star HD 106068 is included in table 8.1 as it is sufficiently reddened to give measurable band structure. The results for HD 116119 were deduced using HD 110073 as comparison star instead of HD 106068, as the unnormalized band measures are anomalously low when the comparison star is appreciably reddened. Similarly, HD 150898 was replaced by an alternative comparison star (usually HD 214080).

The uncertainties in the measured values in table 8.1 are high, varying from $\sim$ 20% for the brightest star pairs to $\sim$ 100% for the faintest and those with low ΔE_{B-V}. The 5900 feature is ill defined in some cases, and is absent in the Upper Scorpius stars. Walker (1963) has published photoelectric measures of the 4430 relative band strength for a large number of stars, including seven of those in table 8.1. A plot of m(4430) against

his values is shown in fig. 8.4. The degree of agreement is reasonable in view of the uncertainties in m(4430).

An analysis was carried out to test the correlation of the three band parameters with each other and with the degree of reddening. The three Upper Scorpius stars were excluded as the band structure is clearly anomalous in this region. Fig. 8.5 gives a plot of m(4430) against m(5900), showing the lines of regression (broken lines) and the line of best fit (continuous). The coefficient of correlation, r, given in the top left-hand corner of the diagram, is very low in this case, indicating an almost random distribution. The correlations of m(4430) and m(5900) with m(D), shown in fig. 8.6, are considerably higher. Fig. 8.7 shows plots of the band parameters against ΔE_{B-V}. The degree of correlation is high for m(D), in agreement with the results of Hayes et al (1973), and is intermediate for m(4430) and m(5900). This difference may be largely due to greater errors in the measurements of the 4430 and 5900 band heights. Snow (1973) also found only moderate correlation between 4430 strength and reddening. Walker (1963) suggested possible variations in the $4430/E_{B-V}$ relationship with galactic longitude, and noted that the band is generally weak in the Southern Milky Way, particularly towards the Galactic Centre. Fig. 8.8 shows plots of the band heights per unit reddening versus ℓ^{II}; stars whose reddening appears to occur predominantly in the local spiral arm (referring to fig. 6.16) are denoted by open circles. There is a tendency for $m(4430)/E_{B-V}$ to decrease with ℓ^{II} for local arm reddening, and this ratio is notably greater for the more distant stars in the $\ell^{II} = 0^{o}$-30^{o} region. There is also a suggestion of a slight

decrease in $m(D)/E_{B-V}$ with ℓ^{II}, and in this case no difference is apparent between local and non-local reddening. There is no discernible systematic variation in $m(5900)/E_{B-V}$ with ℓ^{II}.

(8.3) Interpretation

The results of the preceeding section suggest that the central trough in the residuals originates in the grains responsible for the extinction, or in interstellar material closely associated with them. Borg (1967) has suggested a possible identification of this feature (as observed by Whiteoak) with structure in the dispersion curves of graphite given by Lenham and Treherne (1966a) for the case where the incident light is parallel to the crystal axis. In view of the comments in section 6.2, confirmation of the reality of this structure is required before any further progress can be made with this model. Hayes et al (1973) proposed a model in which two adjacent, very broad absorption bands are superposed on the smooth curve from the Mie theory, producing a trough in the region between them. The bands are assumed to result from transitions associated with impurity sites or defects in the grain lattice, known as colour centres. These may be caused by irradiation of the grains by the galactic background flux of high energy particles and photons (Wolstencroft et al, 1969). In the case of a defect, a lattice ion is displaced to give an interstitial particle and a lattice vacancy; an impurity occurs when the lattice ion is replaced by a foreign particle. The most widely studied colour centres are those occurring in alkali halides (see Schulman and Compton, 1963) which result from transitions associated with electrons trapped at lattice

vacancies (F centres). The bands produced are very broad, having widths typically $\sim$ 1000 A, due to coupling of the electronic transitions with lattice vibrations.

The depth of the observed feature permits an estimation of the defect population that would be required to produce it. From fig. 8.8 we see that the mean value of $m(D)/E_{B-V}$ is $\sim 0^m.08$, thus the depth is $\sim 0^m.03$ per magnitude of visual extinction for R = 3. If each grain along the line of sight contains N colour centres, the ratio of band absorption to extinction is

$$\frac{NC_B}{C_{ext}} = 0.03, \qquad (8.1)$$

where C_B is the absorption cross-section at the band centre. This is given by

$$C_B = \frac{4\pi e^2 f}{\gamma m_e c}, \qquad (8.2)$$

where f is the oscillator strength and $\gamma = \Delta(c/\lambda)$ is the half-width of the band in units of frequency (Wickramasinghe et al, 1968). Taking f $\sim$ 1 appropriate to an F centre producing a band of width $\sim$ 1000 A in the visual region, equ. (8.2) gives

$$C_B \sim 10^{-15} \text{ cm}^2.$$

The extinction cross-section of the grains is, from equ. (2.2),

$$C_{ext} = \pi a^2 Q_{ext}. \qquad (8.3)$$

Considering graphite spheres of radii 0.05 μ, $Q_{ext} \sim 1.5$ and thus

$$C_{ext} \sim 10^{-10} \text{ cm}^2.$$

Substituting these values in equ. (8.1), we obtain

$$N \sim 3 \times 10^3.$$

The total number of atoms per grain is $\sim 10^8$, thus a defect population of 0.003% would be sufficient to explain the observed

feature, which is considerably less than that predicted by Wolstencroft et al (1969).

Colour centres have also been invoked to explain the presence of the knee. Nandy et al (1968) suggest that it could result from an absorption band of width $\sim$800 A centred at 4350 A, superposed on an appropriate Mie curve. The position of the band required is subjective, as it depends on the choice of normalization wavelengths. The theoretical curve fitted to the data of Nandy et al is constrained to pass through the depressed 1.6-1.9 μ^{-1} region and consequently passes below the data in the 2.0-2.5 μ^{-1} region (refer to fig. 8.1). In the present analysis, the theoretical curves pass above the depression and fit the data quite well between 2.0 and 2.5 μ^{-1}. Fig. 8.9 shows a plot of the difference between the observational and theoretical curves against λ^{-1} between 2.0 and 2.9 μ^{-1}, averaged for all the observed stars. Features corresponding to the 4760 and 4430 diffuse bands and the 4200 feature noted by Walker et al (1968) are labelled. There is also apparent band structure in the 2.4-2.6 μ^{-1} region. It thus seems plausible that the extinction in the region of the elusive knee can be explained in terms of the Mie theory, using a suitable grain size distribution, combined with diffuse band structure produced by colour centres. Extension of the data into the ultraviolet would place tighter constraints on the model fitted, and hence give a better indication of the positions of the possible bands.

In a recent paper Herbig (1975) has presented an extensive correlation analysis of spectroscopic data on all of the principal diffuse interstellar features, and has shown that

in general they correlate very closely in strength with each other and with reddening. This seems to leave very little margin for doubt that they have a common origin in the grains. Herbig also concludes that the band strengths are ∿ 30% weaker than average in Cygnus and Sco-Oph. It has been shown by several investigators that the bands tend to be deficient in dense clouds and near luminous stars (Stoeckly and Dressler, 1964; Wampler, 1966; Snow and Wallerstein, 1972; Snow and Cohen, 1974). This has led to the suggestion that band formation is associated with the smallest grains, which may be depleted in such regions. The theoretical work of Bromage (1972) also tends to support this view. Herbig finds significant correlation of band strength with the slope of the extinction curve in the near ultraviolet, which is sensitive to the proportion of small grains. The apparently anomalous 4430 strengths found for the three stars observed in Upper Scorpius may be understood if this band originates in the smallest grains. HD 147889, lying at the centre of the dust complex, shows a normal amount of 4430 absorption (curve S2, fig. 8.2) while the two periferal stars (S1) show virtually none. By assuming that the small grains are abundant in the centre and depleted in the outer regions of the ρ Oph cloud, we may explain both the 4430 strength and the slope of the ultraviolet extinction for these stars. This result combined with the high value of R for HD 147889 implies that both very large and very small particles must be abundant near this star. (See also the discussion in section 6.6).

The possibility that the colour centres suggested as a cause of ultra-broad structure in the extinction may also be

capable of explaining the diffuse bands has been discussed by Wickramasinghe et al (1968). The widths of the bands produced by F centres in alkali halides are temperature-dependent, but are not expected to fall below $\sim$ 300 A at temperatures appropriate to the grains. Transitions associated with impurity ions at lattice sites can give bands of widths 10-100 A. Huffman (1970) and Manning (1970a,b) have shown that absorption features found in terrestrial silicates impregnated with Fe^{3+} (garnets) bear a striking resemblance to the diffuse bands. However, these features are very numerous, and identification of an individual transition with a given interstellar band becomes too easy to be convincing in any particular case. The possible presence of iron impurities in the grains is nevertheless attractive in view of the discussion in section 2.6 regarding grain alignment by the magnetic field.

Johnson et al (1973) have found that the wavelengths of several diffuse bands coincide with transitions occurring in the complex molecule dipyridyl magnesium tetrabenzporphin. As molecules are expected to form in dense dust clouds and are likely to be destroyed when exposed to the flux of ultraviolet radiation in the Galaxy, molecular diffuse bands should be strongest in the dark clouds and weak in the general interstellar medium. This is the converse of what is observed.

Fig. 8.9 Plot of difference between observational and theoretical curves against λ^{-1} in the region of the knee (average for all stars)

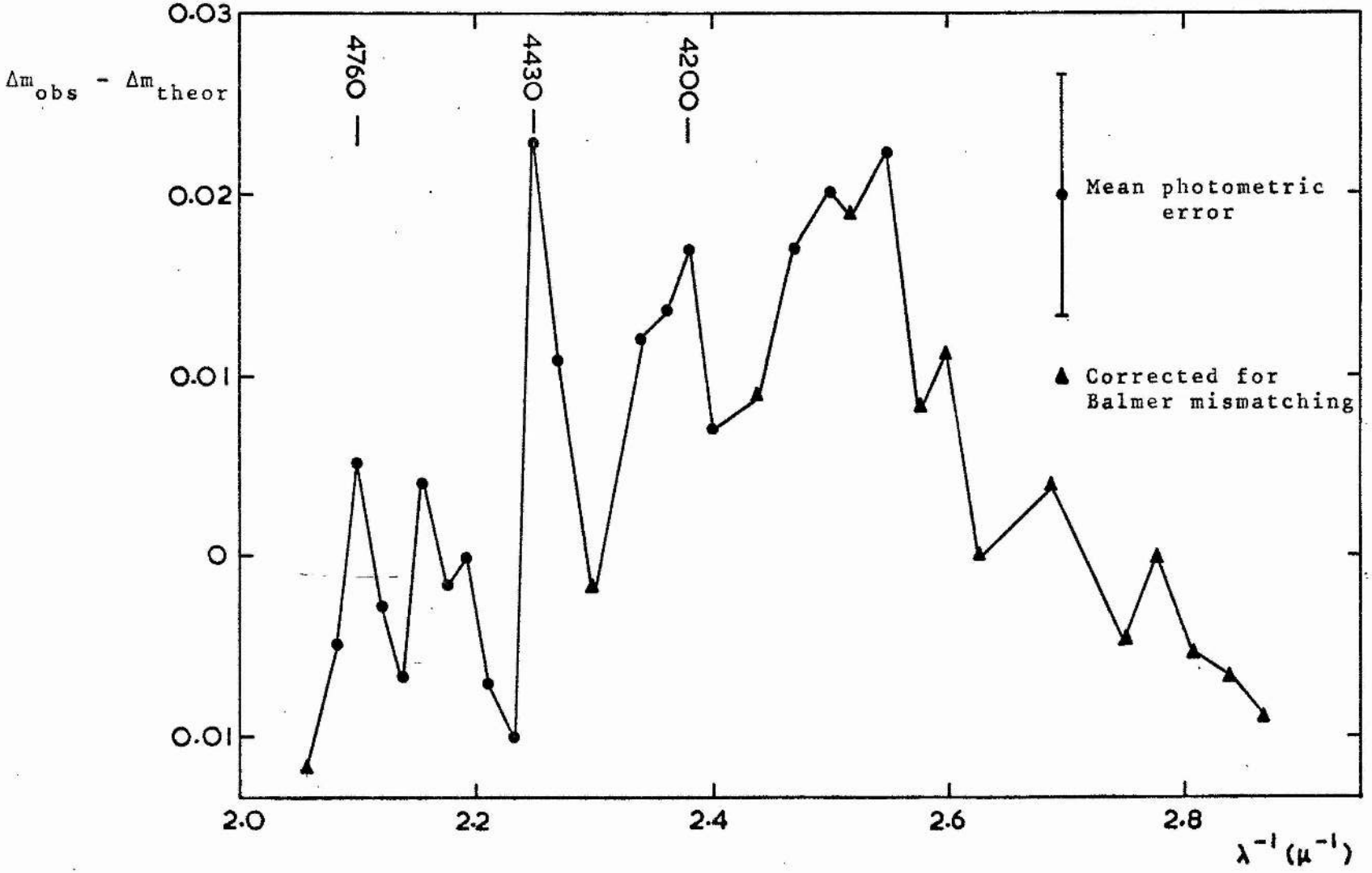

CHAPTER 9

CONCLUSION

(9.1) Summary and Discussion of Principal Results

We have seen from a study of 25 reddened stars in the Southern Milky Way that there is no apparent systematic variation in the extinction law with position in the galactic plane. In several cases stars quite close together in the sky show appreciably different laws, suggesting that fluctuations in the grain size distribution are occurring on a fairly localized scale. The extinction curves are extrapolated to $\lambda^{-1} = 0$, with the aid of model fitting, to give values of the ratio of total to selective extinction. For stars lying within 10° of the galactic equator R is found to vary between 2.6 and 3.5, with a mean value of 3.2. This mean result is in good agreement with those of extensive statistical determinations by Martin (1971) and Harris (1973), and is close to the value generally assumed in photometric studies of galactic structure. Thus no systematic error in the distance scale of the Galaxy is implied; local variations tend to average out, and widespread application of R = 3 (or better R = 3.2) is unlikely to lead to any major misconstruction provided that anomalous regions are avoided.

Upper Scorpius is clearly one such anomalous region: the R values deduced for three stars in this area of sky are notably higher (3.8-4.3) than for more distant stars close to the galactic plane. A variable extinction analysis applied to members of the Sco OB-2 association indicates a significantly higher value of R for those lying towards nebulosity in the

ρ Oph cloud. It seems probable that two distinct processes are responsible for this effect. The stars contained in the nebulae surrounding ρ Oph, σ Sco, 22 Sco and α Sco (table 7.2) lie in the outer regions of the cloud and have relatively low reddening. In these cases depletion of the smaller grains by radiation pressure may be a feasible explanation for the observed increase in R. The extinction curve of σ Sco is highly flattened in the near ultraviolet and does not show a steep rise in the far ultraviolet (Bless and Savage, 1972; see fig. 1.3), which is consistent with this interpretation. Near the cloud centre the local grain density is much greater, and hence the optical depth of the dust to ultraviolet radiation which could cause depletion is high. Moreover, the discussion in sections 6.6 and 8.3 suggest an abundance of small grains in the line of sight to HD 147889. The model proposed by Carrasco et al (1973) in which the grains grow by an accretive process seems more appropriate to explain the high R value in this case. The supply of small particles could be produced by an influx from the surrounding regions; thus the two suggested processes are compatible. It is predicted that the 4.5 μ^{-1} feature associated with graphite will be found to be weak in the ultraviolet extinction of HD 147889, as Gilra (1972) has shown that the feature is obliterated if the graphite grains acquire mantles.

In a very recent paper Serkowski, Mathewson and Ford (1975) present measures of the wavelength of maximum polarization, λ_{max}, for a large sample of stars, and note a correlation between λ_{max} and colour excess ratios. From this they deduce that R is directly proportional to λ_{max}. Such a

dependence, if verified, would be of considerable practical value: it would provide a simple method of measuring R for individual stars by means of observations in the visual and near infrared regions only, avoiding the difficulties involved in extrapolating the extinction curves to $\lambda^{-1} = 0$. Measurements of λ_{max} are given by Serkowski et al for 12 of the reddened stars in this analysis. Fig. 9.1 shows a plot of extinction curve R values from table 6.3 against λ_{max} in microns for these stars. There is a fair degree of correlation. The broken line in the diagram represents the relation

$$R = 5.5\ \lambda_{max} \qquad (9.1)$$

suggested by Serkowski et al. The solid line gives the best fit to the points, which is

$$R = 4.4\ \lambda_{max} + 0.83. \qquad (9.2)$$

In the case of HD 147889, $\lambda_{max} = 0.8\ \mu$, and equ. (9.1) and (9.2) give R values of 4.4 and 4.35 respectively, in excellent agreement with the extinction curve value.

The presence of considerable band structure is noted in the scanner extinction curves, and this cannot be reproduced by the theoretical model considered. A depressed region between 1.6 and 1.9 μ^{-1} is a common feature of the observational curves. Its depth correlates well with reddening, suggesting that it is produced by two adjacent, very broad absorption bands which originate in the grains. The bands could result from defects in the grain crystal structure, and a defect population considerably less than that predicted by Wolstencroft et al (1969) would be sufficient to give the observed depth of $\sim 0^{m}.03$ per magnitude of visual extinction.

Fig. 9.1 Plot of R against λ_{max}

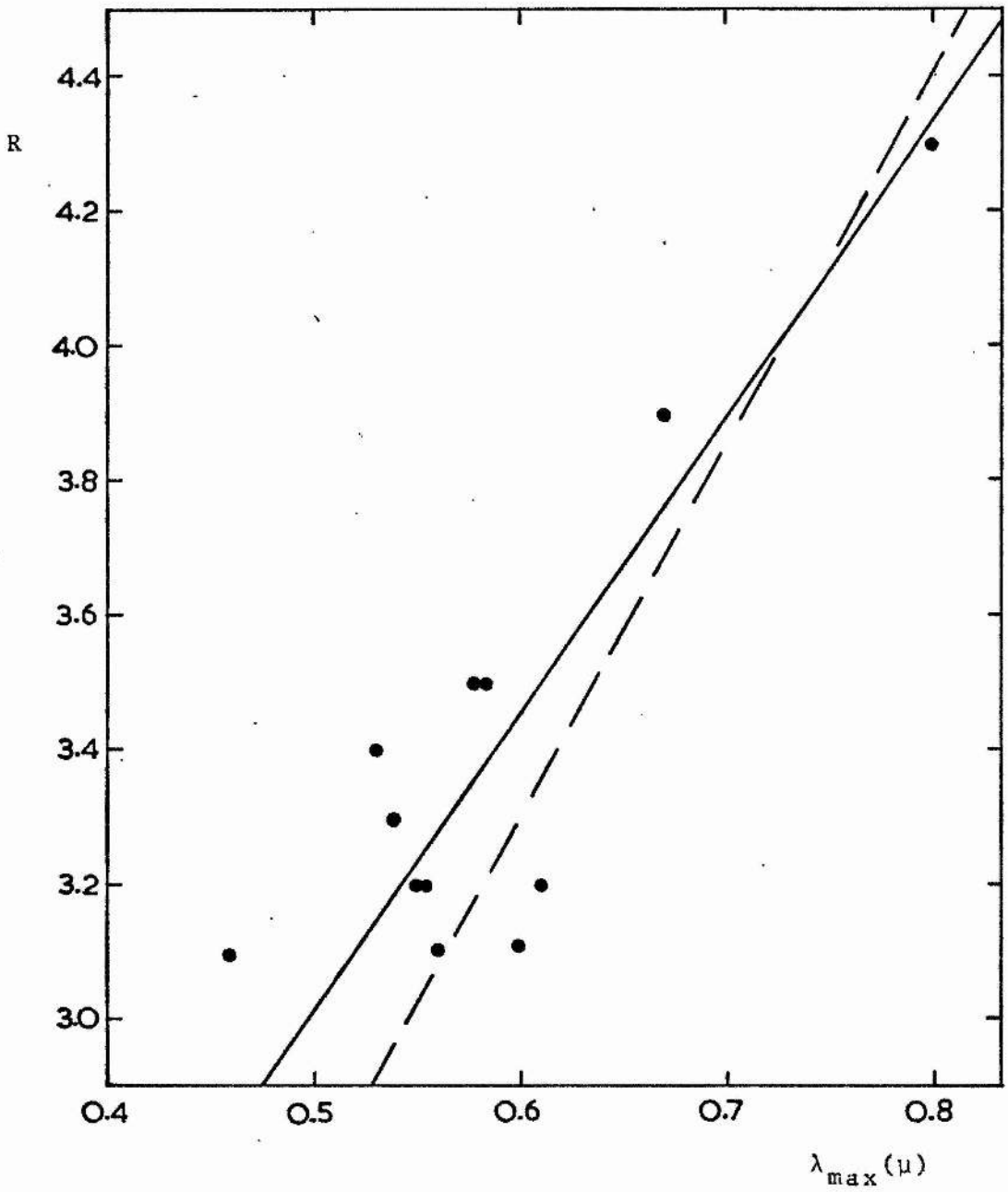

The ratio of 4430 band height to colour excess shows signs of systematic variation with longitude for stars whose reddening occurs mainly in the local spiral arm; the band is relatively stronger for more distant stars towards Sagittarius.

(9.2) Suggestions for further Research

Many possibilities for future research are suggested by the results. These may conveniently be divided into three broad categories: (1) observations, (2) laboratory experiments, and (3) theoretical studies.

In view of the variations found in the extinction law within relatively small areas of sky, there is clearly a need to obtain detailed observational curves for a much larger sample of stars. This applies not only to the Southern Milky Way, but equally to the North where little work of comparable resolution and photometric accuracy has been reported. The efficiency with which this can be achieved using a photoelectric scanner becomes apparent when one realises that all the scanner data reported here resulted from only about 30 hours of usable observing time. Choice of stars for future observing programmes is a matter of some importance. There is a temptation to concentrate on stars in 'interesting regions' such as dark clouds, nebulosity and young associations; Aannestad and Purcell (1973) have made the pertinent comment that there is a need for widespread observations of stars <u>not</u> in such regions before the mean interstellar extinction curve can be considered to be well determined. The possibility of variations with galactic latitude as well as longitude should also be considered. The reliability of the results could be improved

by discriminating against Ia type supergiants in the selection procedure, as it is almost impossible to find suitable comparison stars. Corrections give a fair indication of the true curve when mismatching occurs, but the uncertainty is considerably increased beyond the Balmer limit. It is suggested that a system of standard comparison stars should be set up for extinction observations; intercomparison of standards would then provide a means of eliminating any that possess individual peculiarities.

Extension of the individual extinction curves into the satellite ultraviolet would be of considerable interest. The possibility of regional variations in the strength of the 4.5 μ^{-1} feature has already been mentioned in connection with the ρ Oph cloud. Previous investigations have concentrated for obvious reasons on bright stars of relatively low reddening. It should be possible in future projects to obtain satellite data for the stars in the present observing programme.

The optical data for solids used in Mie theory calculations have generally been determined without any thought to a possible astrophysical application. Thus they usually apply only to pure materials in bulk form, and at laboratory temperatures. Even with these limitations there are notable discrepancies in the published results of different authors, and the spectral resolution of the laboratory data is generally inferior to that of the astronomical observations. Only recently have experimentalists begun to investigate situations more appropriate to interstellar space (see Day and Huffman, 1973; Huffman and Stapp, 1973). Study of the optical effects of radiation damage in likely grain constituents is particularly important in view of the discussion in section 8.3.

Given realistic and reliable data on the optical constants for various likely solids, the theoretician will be able to proceed with the problem of identifying the main chemical constituents of the grains. Hopefully a unified, unambiguous model will then emerge. To be entirely satisfactory, the model must be capable of explaining the observations relating to the extinction, polarization, albedo and diffuse bands, and must be consistent with cosmic abundance ratios. There is almost unlimited scope for theoretical work on the processes occurring in the interstellar medium. For example, a wealth of observational data has been accumulated in recent years on the dense dust-molecule complexes such as those associated with ρ Oph, M42 and Sgr B2. The chemical evolution of such objects is a problem which should keep theoreticians busy for some time.

This list of research prospects is by no means exhaustive, but merely serves to illustrate the possibilities.

APPENDIX

A FORTRAN IV COMPUTER PROGRAMME

```
C
C
C       PROGRAM COMPUTES THEORETICAL EXTINCTION CURVES USING THE MIE
C       FORMULA FOR A SIZE-DISTRIBUTION OF SPHERICAL GRAINS.
C
C       DCB WHITTET      ASTRONOMY DEPARTMENT    JULY 1974 .
C
C
C       L1= NO OF WAVELENGTHS AT WHICH QEXT IS TO BE COMPUTED (MAX:32)
C       L2= NO OF MODELS FOR WHICH QEXT IS TO BE COMPUTED (MAX:6)
C       L3= NO OF DISCRETE GRAIN SIZES IN DISTRIBUTION (MAX:1000)
C
C       MAX NO OF TERMS SUMMED IN SERIES= 30
C       REQUIRED PRECISION: 0.01%
C
C
C
      COMPLEX CMPLX,CCOS,CSIN,C,D
      COMPLEX AA(32),ZETA(32),A(30),B(30),M(32),Y(32)
      DIMENSION R1(32),R2(32),W(32),R(1000),DIST(1000)
      DIMENSION RATIO(6),X(32),RM(6),EXT(32,7)
      DIMENSION XX(20),YY(20),ZZ(20)
      DIMENSION S(7),T(7)
C
      DO 80 II=1,32
      DO 80 KK=1,7
      EXT(II,KK)=0.0
   80 CONTINUE
C
C
      READ(5,100) L1,L2,L3
  100 FORMAT(2I3,I5)
      L4=L2+1
C
      READ(5,105)(RATIO(N),N=1,6)
      READ(5,105)(RM(N),N=1,6)
  105 FORMAT(6F5.3)
C
      READ(5,120)(W(N),N=1,32)
      DO 110 N=1,L1
      W(N)=1.0/W(N)
  110 CONTINUE
C
      DO 360 K=1,L4
      IF(K.EQ.L4) GOTO 270
C
      DO 140 J=1,L3
      P=FLOAT(J)
      R(J)=0.001+(P-1.0)*(RM(K)*3.0-0.001)/FLOAT(L3-1)
      DIST(J)=(R(J)**1.5)*EXP(-0.5*(R(J)/RM(K))**3.0)
  140 CONTINUE
C
      READ(5,120)(R1(N1),N1=1,32)
      READ(5,120)(R2(N2),N2=1,32)
```

```
  120 FORMAT(16F5.3,/,16F5.3)
C
  122 WRITE(6,300)
      WRITE(6,305) K
      WRITE(6,150)
  150 FORMAT(' OPTICAL CONSTANTS ')
      WRITE(6,230)
  230 FORMAT(5X,' 1/W        N        K ')
      DO 130 N=1,L1
      F=1.0/W(N)
      WRITE(6,240) F,R1(N),R2(N)
  240 FORMAT(5X,F5.3,3X,F6.3,2X,F6.3)
      M(N)=CMPLX(R1(N),-R2(N))
  130 CONTINUE
C
      DO 260 I=1,L1
C
      DO 250 J=1,L3
C
      X(I)=2.0*3.142*R(J)/W(I)
      Y(I)=M(I)*X(I)
      SUM=0.0
      AA(1)=0
      AA(2)=CCOS(Y(I))/CSIN(Y(I))
      ZETA(1)=CMPLX(COS(X(I)),-SIN(X(I)))
      ZETA(2)=CMPLX(SIN(X(I)),COS(X(I)))
      NTEST=1
C
      DO 220 N=1,30
      IF(NTEST.EQ.0) GOTO 220
      N1=N+2
      P=FLOAT(N)
      AA(N1)=-P/Y(I)+(1.0/(P/Y(I)-AA(N1-1)))
      ZETA(N1)=((2.0*P-1.0)/X(I))*ZETA(N1-1)-ZETA(N1-2)
      C=(AA(N1)/M(I)+P/X(I))*ZETA(N1)-ZETA(N1-1)
      A(N)=((AA(N1)/M(I)+P/X(I))*REAL(ZETA(N1))-REAL(ZETA(N1-1)))/C
      D=(M(I)*AA(N1)+P/X(I))*ZETA(N1)-ZETA(N1-1)
      B(N)=((M(I)*AA(N1)+P/X(I))*REAL(ZETA(N1))-REAL(ZETA(N1-1)))/D
      TERM=(2.0*P+1.0)*REAL(A(N)+B(N))
      IF(SUM.EQ.0.0) GOTO 200
C
C     PRECISION CHECK
      RAT=ABS(TERM/SUM)
      IF(RAT.LT.0.0001) GOTO 210
C
  200 SUM=SUM+TERM
      GOTO 220
  210 NTEST=0
  220 CONTINUE
C
      QEXT=SUM*2.0/(X(I)*X(I))
      JF=2*INT((FLOAT(J))/2.0)
      IF(J.EQ.JF) NUMB=2.0
      IF(J.NE.JF) NUMB=4.0
```

```
109         IF(J.EQ.1) NUMB=1.0
110         IF(J.EQ.L3) NUMB=1.0
111         H=(RM(K)*3.0-0.001)/FLOAT(L3-1)
112         EXT(I,K)=EXT(I,K)+R(J)*R(J)*DIST(J)*QEXT*NUMB*H/3.0
113 C
114     250 CONTINUE
115 C
116     260 CONTINUE
117 C
118         GOTO 290
119     270 DO 280 I=1,L1
120         DO 280 K1=1,L2
121         EXT(I,K1)=RATIO(K1)*EXT(I,K1)/S(K1)
122         EXT(I,K)=EXT(I,K)+EXT(I,K1)
123     280 CONTINUE
124 C
125     290 S(K)=EXT(8,K)
126         T(K)=EXT(21,K)
127 C
128 C
129 C
130         WRITE(6,300)
131     300 FORMAT('1')
132         IF(K.EQ.L4) GOTO 315
133         WRITE(6,305) K
134     305 FORMAT(' MODEL ',I3)
135         WRITE(6,306) RATIO(K)
136     306 FORMAT(' WEIGHT= ',F5.3)
137         WRITE(6,304) L3
138     304 FORMAT(' NO OF DISCRETE SIZES= ',I4)
139         WRITE(6,310) RM(K)
140     310 FORMAT(4X,' AM= ',F6.3,' MICRONS ',//)
141         GOTO 319
142     315 WRITE(6,316)
143     316 FORMAT(' MEAN EXTINCTION ',//)
144     319 WRITE(6,320)
145     320 FORMAT(5X,' 1/W      EXT ')
146         DO 340 I1=1,L1
147         F=1.0/W(I1)
148         IF(K.NE.L4) G=EXT(I1,K)/S(K)
149         IF(K.EQ.L4) G=(EXT(I1,K)-T(K))/(S(K)-T(K))
150         WRITE(6,330) F,G
151     330 FORMAT(5X,F5.3,2X,F6.3)
152 C
153     340 CONTINUE
154 C
155     360 CONTINUE
156 C
157         WRITE(6,300)
158         STOP
159         END
```

ACKNOWLEDGMENTS

I am indebted to my supervisor, Dr I. G. van Breda, for guidance and collaboration on all aspects of the work described in this thesis. His personal involvement in the development of the research, and, in particular, his contribution to the efficiency of the observing programme, were of immense value. I am also indebted to the Directors and staff members of the University Observatory, St. Andrews, the Cerro Tololo Interamerican Observatory, Chile, and the South African Astronomical Observatory, for advice, assistance and personal kindness. I wish particularly to thank Dr I. S. Glass (SAAO, now at Herstmonceux) for his interest and involvement in the infrared photometry observations; Dr P. S. Osmer (CTIO) for instruction on use of the scanner; Sr K. Czuia (CTIO) for assistance at the telescope; Dr A. W. J. Cousins (SAAO) for carrying out UBV monitoring observations, and Mrs R. M. Banfield (SAAO) for reducing the BVRI observations. Thanks are due to Dr K. Nandy (Royal Observatory, Edinburgh) for guidance in the choice of programme stars and collaboration on the interpretation of results, and also to Drs D. Kilkenny and R. W. Hilditch (St. Andrews), Mr B. D. Kelly (St. Andrews and SAAO), Dr N. R. Walborn (CTIO), and Professor N. C. Wickramasinghe and Dr D. P. Gilra (University College, Cardiff) for useful discussion on various aspects of the research.

I am obliged to the Director of CTIO and the Large Telescope Users Panel for allocation of observing time, and to the Science Research Council for provision of travel and subsistance funds for the visits to Chile and South Africa. I am also grateful to the SRC for award of a Research Studentship

for the academic years 1971-72 and 1972-73, and to the University of St. Andrews for financial support during the academic year 1973-74. I am grateful to the University of St. Andrews Computing Laboratory and the South-Western Universities Computing Network (Cardiff) for use of facilities.

Finally, my thanks are due to my wife, Marian, for continual encouragement and for typing the script. We both wish to thank the Applied Physics Department, UWIST, Cardiff for use of typing facilities.

REFERENCES

Aannestad, P. A. & Purcell, E. M., 1973. Ann. Rev. Astr. Astrophys., 11, 309.

Abt, H. A. & Biggs, E. S., 1972. Bibliography of Stellar Radial Velocities (Latham Process Corp., New York).

Allen, C. W., 1973. Astrophysical Quantities, 202. (University of London, Athlone Press, 3rd edition).

Allen, D. A. & Penston, M. V., 1974. Nature, 251, 110.

Anderson, C. M., 1970. Astrophys. J., 160, 507.

Andrews, P. J., 1968. Mem. R. Astr. Soc., 72, 35.

Andrews, P. J. & Thackeray, A. D., 1973. Mon. Not. R. Astr. Soc., 165, 1.

Baade, W. & Minkowski, R., 1937. Astrophys. J., 86, 123.

Barbier, D. & Chalonge, D., 1939. Ann. Astrophys., 2, 254.

Barnard, E. E., 1919. Astrophys. J., 49, 1.

Barnard, E. E., 1927. Atlas of the Selected Regions of the Milky Way (Carnegie Inst., Washington).

Becker, W., 1966. Z. Astrophys., 64, 77.

Becklin, E. E. & Neugebauer, G., 1967. Astrophys. J., 147, 799.

Bell, R. A. & FitzGerald, M. P., 1971. Proc. 3rd Colloq. Astrophys. Supergiant Stars, 168.

Bertiau, F. C., 1958. Astrophys. J., 128, 533.

Binnendijk, L., 1952. Astrophys. J., 115, 428.

Blaauw, A., 1963. Basic Astronomical Data, 383, ed. K. Aa. Strand (University of Chicago Press).

Blanco, V. M., 1956. Astrophys. J., 123, 64.

Blanco, V. M., Demers, S., Douglass, G. G. & FitzGerald, M. P., 1968. Publ. U.S. Naval Obs., 21.

Bless, R. C., Code, A. D. & Houk, T. E., 1968. Astrophys. J., 153, 561.

Bless, R. C. & Savage, B. D., 1972. Astrophys. J., 171, 293.

Boggess, A. & Borgman, J., 1964. Astrophys. J., 140, 1636.

Bok, B. J., 1932. Harvard Reprints Series I, No. 77.

Bok, B. J., 1956. Astr. J., 61, 309.

Borg, K., 1967. Medd. Lund Obs. Ser., 2, No. 151.

Braes, L. L. E., 1967. Bull. Astr. Soc. Neth. Suppl., 2, 1.

Bromage, G. E., 1972. Astrophys. Space Sci., 15, 426.

Bromage, G. E., Nandy, K. & Khare, B. N., 1973. Astrophys. Space Sci., 20, 213.

Carrasco, L., Strom, S. E. & Strom, K. M., 1973. Astrophys. J., 182, 95.

Carter, J. G., Huebner, R. H., Hamm, R. N. & Birkhoff, R. D., 1965. Phys. Rev., 137, A639.

Chalonge, D., 1958. Ric. Astr. Vaticano, 5, 345.

Chalonge, D. & Divan, L., 1952. Ann. Astrophys., 15, 201.

Chiao, R. Y., Feldman, M. J. & Parrish, P. T., 1973. IAU Symposium No. 52, 59.

Cousins, A. W. J., 1972. Mon. Not. Astr. Soc. Sth. Afr., 31, 127.

Cousins, A. W. J., 1973. Mon. Not. Astr. Soc. Sth. Afr., 32, 117.

Coyne, G. V. & Gehrels, T., 1967. Astr. J., 72, 887.

Crawford, D. L., 1973. IAU Symposium No. 54, 93.

Crawford, D. L., Barnes, J. V., Hill, G. & Perry, C. L., 1971. Astr. J., 76, 1048.

Crézé, M., 1972. Astr. Astrophys., 21, 85.

Danielson, R. E., Woolf, N. J. & Gaustad, J. E., 1965. Astrophys. J., 141, 116.

Davis, L. & Greenstein, J. L., 1951. Astrophys. J., 114, 206.

Day, K. L. & Huffman, D. R., 1973. Nature Phys. Sci., 243, 80.

Debye, P., 1909. Ann. Phys., 30, 59.

Diermendjian, D., 1969. Electromagnetic Scattering on Spherical Polydispersions (American Elsevier Publ. Co., New York).

Divan, L., 1971. Astr. Astrophys., 12, 76.

Dufay, J., 1957. Galactic Nebulae and Interstellar Matter (Hutchinson & Co.).

Dufay, J., 1964. Introduction to Astrophysics: The Stars (George Newnes Ltd.).

Dufour, R. J. & Lee, P., 1970. Astrophys. J., 160, 357.

Duke, D., 1951. Astrophys. J., 113, 100.

Encrenaz, P. J., 1974. Astrophys. J. Lett., 189, L135.

Faulkner, D. J., 1963. Publ. Astr. Soc. Pacific, 75, 269.

Feinstein, A., 1969. Mon. Not. R. Astr. Soc., 143, 273.

Fernie, J. D. & Malborough, J. M., 1963. Astrophys. J., 137, 700.

Foreman, W., Jones, C., Tananbaum, H., Gursky, H., Kellogg, E. & Giacconi, R., Astrophys. J. Lett., 182, L103.

Garrison, R. F., 1967. Astrophys. J., 147, 1003.

Garrison, R. F., 1970. Astr. J., 75, 1001.

Gillett, F. C. & Forrest, W. J., 1973. Astrophys. J., 179, 483.

Gilman, R. C., 1969. Astrophys. J. Lett., 155, L185.

Gilra, D. P., 1971. Nature, 229, 237.

Gilra, D. P., 1972. Scientific Results from the Orbiting Astronomical Observatory, 295, ed. A. D. Code (NASA).

Glaspey, J. W., 1971. Astr. J., 76, 1041.

Glaspey, J. W., 1972. Astr. J., 77, 474.

Glass, I. S., 1973. Mon. Not. R. Astr. Soc., 164, 155.

Glass, I. S., 1974. Mon. Not. Astr. Soc. Sth. Afr., 33, 53.

Gould, R. J. & Salpeter, E. E., 1963. Astrophys. J., 138, 393.

Graham, J. A., 1971. Dark Nebulae Globules and Protostars, 27, ed. B. T. Lynds (University of Arizona Press).

Grasdalen, G. L., Strom, K. M. & Strom, S. E., 1973. Astrophys. J. Lett., 184, L53.

Greenberg, J. M., 1966. Astrophys. J., 132, 672.

Greenberg, J. M., 1968. Nebulae and Interstellar Matter, 221, eds. B. M. Middlehurst & L. H. Aller (University of Chicago Press).

Greenberg, J. M. & Roark, T. P., 1967. Astrophys. J., 147, 917.

Greenberg, J. M., Wang, R. T. & Bangs, L., 1971. Nature Phys. Sci., 230, 110.

Greenstein, J. L., 1937. Harvard Obs. Circular No. 422.

Gutierrez-Moreno, A. & Moreno, H., 1967. Astrophys. J. Suppl., 15, 459.

Hackwell, J. A., Gehrz, R. D. & Woolf, N. J., 1970. Nature, 227, 822.

Hall, J. S., 1949. Science, 109, 166.

Hall, J. S., 1950. Publ. U.S. Naval Obs., 17, Part 1.

Hardie, R. H., 1962. Astronomical Techniques, 178, ed. W. A. Hiltner (University of Chicago Press).

Hardie, R. H. & Crawford, D. L., 1961. Astrophys. J., 133, 843.

Harris, D. H., 1973. IAU Symposium No. 52, 31.

Harris, J. W., 1969. Nature, 223, 1046.

Hayes, D. S., Mavko, G. E., Radick, R. R., Rex, K. H. & Greenberg, J. M., 1973. IAU Symposium No. 52, 83.

Hazen, N. L. & Danziger, I. J., 1972. Proc. Soc. Photo-Opt. Instr. Eng. (Instrumentation in Astronomy), 28, 173.

Heiles, C. E., 1970. Astrophys. J., 160, 51.

Herbig, G. H., 1975. Astrophys. J., 196, 129.

Hill, P. W., 1970. Mon. Not. R. Astr. Soc., 150, 23.

Hiltner, W. A., 1949. Science, 109, 165.

Hiltner, W. A., Garrison, R. R. & Schild, R. E., 1969. Astrophys. J., 157, 313.

Hiltner, W. A. & Johnson, H. L., 1956. Astrophys. J., 124, 367.

Honeycutt, R. K. & Chaldu, R. S., 1970. Astr. J., 75, 600.

Hoyle, F. & Wickramasinghe, N. C., 1962. Mon. Not. R. Astr. Soc., 124, 417.

Hoyle, F. & Wickramasinghe, N. C., 1968. Nature, 217, 415.

Hoyle, F. & Wickramasinghe, N. C., 1969. Nature, 223, 459.

Huang, Su-Shu & Struve, O., 1955. Astrophys. J., 122, 103.

Huffman, D. R., 1970. Nature, 225, 833.

Huffman, D. R. & Stapp, J. L., 1973. IAU Symposium No. 52, 297.

Hyland, A. R. & Mould, J. R., 1973. Astrophys. J., 186, 993.

Ishida, K., 1969. Mon. Not. R. Astr. Soc., 144, 55.

Jaschek, C., Conde, H. & de Sierra, A. C., 1964. Catalogue of MK Spectral Classifications (University of La Plata, Argentine).

Jaschek, M. & Brandi, E., 1973. Publ. Astr. Soc. Pacific, 85, 736.

Jaschek, M. & Jaschek, C., 1973. Publ. Astr. Soc. Pacific, 85, 12.

Johnson, F. M., Bailey, D. T. & Wegner, P. A., 1973. IAU Symposium No. 52, 317.

Johnson, H. L., 1963. Basic Astronomical Data, 204, ed. K. Aa. Strand (University of Chicago Press).

Johnson, H. L., 1967. Astrophys. J., 147, 912.

Johnson, H. L., 1968. Nebulae and Interstellar Matter, 167, eds. B. M. Middlehurst & L. H. Aller (University of Chicago Press).

Johnson, H. L. & Borgman, J., 1963. Bull. Astr. Insts. Neth., 17, 115.

Johnson, H. L. & Morgan, W. W., 1955. Astrophys. J., 122, 142.

Jones, C. & Liller, W., 1973. Astrophys. J. Lett., 184, L121.

Jones, R. V. & Spitzer, L., 1967. Astrophys. J., 147, 943.

Kamijo, F., 1963. Publs. Astr. Soc. Japan, 15, 440.

Knacke, R. F., Cudaback, D. D. & Gaustad, J. E., 1969a. Astrophys. J., 158, 151.

Knacke, R. F., Gaustad, J. E., Gillett, F. C. & Stein, W. A., 1969b. Astrophys. J. Lett., 155, L189.

Kraft, R. P. & Schmidt, M., 1963. Astrophys. J., 137, 249.

Krishna Swamy, K. S. & O'Dell, C. R., 1967. Astrophys. J., 147, 937.

Lee, T. A., 1970. Astrophys. J., 162, 217.

Lenham, A. P. & Treherne, D. M., 1966a. Observatory, 86, 36.

Lenham, A. P. & Treherne, D. M., 1966b. Optical Properties and Electronic Structure of Metals and Alloys, 196, ed. F. Abeles (North-Holland, Amsterdam).

Lillie, C. F. & Witt, A. N., 1969. Astrophys. Lett., 3, 201.

Lind, A. C. & Greenberg, J. M., 1966. J. Appl. Phys., 37, 3195.

Lindblad, B., 1935. Nature, 135, 133.

Lloyd Evans, T., 1969. Mon. Not. R. Astr. Soc., 146, 101.

Low, F. J. & Krishna Swamy, K. S., 1970. Nature, 227, 1333.

Lynds, B. T. & Wickramasinghe, N. C., 1968. Ann. Rev. Astr. Astrophys., 6, 215.

Manning, P. G., 1970a. Nature, 226, 829.

Manning, P. G., 1970b. Nature, 227, 1121.

Martin, P. G., 1971. Mon. Not. R. Astr. Soc., 153, 279.

Mathews, W. G., 1967. Astrophys. J., 147, 965.

Mathewson, D. S. & Ford, V. L., 1970. Mem. R. Astr. Soc., 74, 139.

Merrill, P. W., 1936. Astrophys. J., 83, 136.

Merrill, P. W. & Wilson, O. C., 1938. Astrophys. J., 87, 9.

Mie, G., 1908. Ann. Phys., 25, 377.

Moffat, A. F. J., 1974. Astr. Astrophys., 32, 103.

Morgan, D. H. & Nandy, K., 1974. Astrophys. Space Sci., 29, 285.

Morgan, W. W., Gonzales, G. & Gonzales, G., 1953. Astrophys. J., 118, 323.

Münch, G., 1968. Nebulae and Interstellar Matter, 365, eds. B. M. Middlehurst & L. H. Aller (University of Chicago Press).

Nandy, K., 1964. Publs. R. Obs. Edinb., 3, 142.

Nandy, K., 1965a. Publs. R. Obs. Edinb., 5, 13.

Nandy, K., 1965b. Nature, 208, 274.

Nandy, K., 1966. Publs. R. Obs. Edinb., 5, 233.

Nandy, K., 1967. Publs. R. Obs. Edinb., 6, 25.

Nandy, K., 1968. Publs. R. Obs. Edinb., 6, 169.

Nandy, K., Seddon, H., Wolstencroft, R. D., Ireland, J. G. & Wickramasinghe, N. C., 1968. Nature, 218, 1236.

Nandy, K. & Wickramasinghe, N. C., 1971. Mon. Not. R. Astr. Soc., 154, 255.

Nather, R. E., Churms, J. & Wild, P. A. T., 1974. Publ. Astr. Soc. Pacific, 86, 116.

Ney, E. P. & Allen, D. A., 1969. Astrophys. J. Lett., 155, L193.

Oort, J. H., 1946. Mon. Not. R. Astr. Soc., 106, 159.

Oort, J. H. & van de Hulst, H. C., 1946. Bull. Astr. Soc. Neth., 10, 187.

Pecker, J. C., 1972. Astr. Astrophys., 18, 253.

Penzias, A. A., Solomon, P. M., Jefferts, K. B. & Wilson, R. W., 1972. Astrophys. J. Lett., 174, L43.

Pollack, J. B., Toon, O. B. & Khare, B. N., 1973. Icarus, 19, 372

Purcell, E. M., 1969. Astrophys. J., 158, 433.

Purcell, E. M. & Spitzer, L., 1971. Astrophys. J., 167, 31.

Reddish, V. C., 1967. Mon. Not. R. Astr. Soc., 135, 251.

Reddish, V. C., 1973. Phys. Bull., 24, 661.

Rodgers, A. W., 1960. Mon. Not. R. Astr. Soc., 120, 163.

Schalen, C., 1939. Z. Astrophys., 17, 260.

Schild, R., Hiltner, W. A. & Sanduleak, N., 1969. Astrophys. J., 156, 609.

Schild, R., Neugebauer, G. & Westphal, J. A., 1971. Astr. J., 76, 237.

Schmidt, Th., 1958. Z. Astrophys., 46, 145.

Schmidt-Kaler, Th., 1967. IAU Symposium No. 31, 161.

Schoenberg, E. & Jung, B., 1932. Astr. Nachr., 247, 413.

Schulman, J. H. & Compton, W. D., 1963. Colour Centres in Solids (Pergamon).

Serkowski, K., Mathewson, D. S. & Ford, V. L., 1975. Astrophys. J., 196, 261.

Sharpless, S., 1952. Astrophys. J., 116, 251.

Sharpless, S., 1959. Astrophys. J. Suppl., 4, 257.

Sharpless, S., 1963. Basic Astronomical Data, 225, ed. K. Aa. Strand (University of Chicago Press).

Snow, T. P., 1973. Astr. J., 78, 913.

Snow, T. P. & Cohen, J. G., 1974. Astrophys. J., 194, 313.

Snow, T. P. & Wallerstein, G., 1972. Publ. Astr. Soc. Pacific, 84, 492.

Stebbins, J., Huffer, C. M. & Whitford, A. E., 1939. Astrophys. J., 90, 209.

Stebbins, J. & Whitford, A. E., 1943. Astrophys. J., 98, 20.

Stebbins, J. & Whitford, A. E., 1945. Astrophys. J., 102, 318.

Stecher, T. P., 1965. Astrophys. J., 142, 1683.

Stecher, T. P. & Donn, B., 1965. Astrophys. J., 142, 1681.

Stein, W. A. & Gillett, F. C., 1969. Astrophys. J. Lett., 155, L197.

Stein, W. A. & Gillett, F. C., 1971. Nature Phys. Sci., 223, 72.

Stibbs, D. W. N., 1964. Publ. R. Obs. Edinb., 4, 87.

Stoeckly, R. & Dressler, K., 1964. Astrophys. J., 139, 240.

Stratton, J. A., 1941. Electromagnetic Theory (McGraw-Hill).

Struve, O., McNamara, D. H. & Zebergs, V., 1955. Astrophys. J., 122, 122.

Struve, O. & Rudkjobing, M., 1949. Astrophys. J., 109, 92.

Taft, E. A. & Philipp, H. R., 1965. Phys. Rev., 138, A197.

Trumpler, R. J., 1930a. Lick Obs. Bull., 14, 154.

Trumpler, R. J., 1930b. Publ. Astr. Soc. Pacific, 42, 214.

Trumpler, R. J., 1930c. Publ. Astr. Soc. Pacific, 42, 267.

Turner, D. G., 1973. Astr. J., 78, 597.

van Breda, I. G., Glass, I. S. & Whittet, D. C. B., 1974. Mon. Not. R. Astr. Soc., 168, 551.

van de Hulst, H. C., 1949. Rech. Astr. Obs. Utrecht, 11, Part 2.

van de Hulst, H. C., 1957. Light Scattering by Small Particles (Wiley, New York).

Verschuur, G. L., 1969. Astrophys. J., 156, 861.

Vidal, N. V., Wickramasinghe, D. T. & Peterson, B. A., 1973. Astrophys. J. Lett., 182, L77.

Vrba, F. J., Strom, K. M., Strom, S. E. & Grasdalen, G. L., 1975. Astrophys. J., in press.

Wait, J. R., 1959. Electromagnetic Radiation from Cylindrical Structures (Pergamon).

Walborn, N. R., 1973. Astr. J., 78, 1067.

Walker, G. A. H., 1963. Mon. Not. R. Astr. Soc., 125, 141.

Walker, G. A. H., Hutchings, J. B. & Younger, P. F., 1968. Astr. J., 74, 1061.

Wampler, E. J., 1966. Astrophys. J., 144, 921.

Whiteoak, J. B., 1966. Astrophys. J., 144, 305.

Whitford, A. E., 1958. Astr. J., 63, 201.

Whittet, D. C. B., 1974. Mon. Not. R. Astr. Soc., 168, 371.

Whittet, D. C. B., van Breda, I. G. & Nandy, K., 1973. Nature Phys. Sci., 243, 21.

Wickramasinghe, N. C., 1967. Interstellar Grains (Chapman & Hall)

Wickramasinghe, N. C., 1969. Nature, 224, 656.

Wickramasinghe, N. C., 1973. Light Scattering Functions for Small Particles (Adam Hilger).

Wickramasinghe, N. C., 1974. Nature, 252, 468.

Wickramasinghe, N. C., 1975. Mon. Not. R. Astr. Soc., 170, 11P.

Wickramasinghe, N. C. & Guillaume, C., 1965. Nature, 207, 366.

Wickramasinghe, N. C., Ireland, J. G., Nandy, K., Seddon, H. & Wolstencroft, R. D., 1968. Nature, 217, 412.

Wickramasinghe, N. C. & Krishna Swamy, K. S., 1967. Nature, 213, 895.

Wickramasinghe, N. C., Lukes, T. & Dempsey, M. J., 1974. Astrophys. Space Sci., 30, 315.

Wickramasinghe, N. C. & Nandy, K., 1970. Nature, 227, 51.

Wickramasinghe, N. C. & Nandy, K., 1971. Mon. Not. R. Astr. Soc., 153, 205.

Wickramasinghe, N. C. & Nandy, K., 1972. Rep. Prog. Phys., 35, 157.

Wickramasinghe, N. C., Ray, W. D. & Wyld, C., 1966. Mon. Not. R. Astr. Soc., 132, 137.

Williams, E. G., 1936. Astrophys. J., 83, 279.

Wilson, R., 1958. Astrophys. J., 128, 57.

Wilson, R., 1960. Mon. Not. R. Astr. Soc., 120, 51.

Witt, A. N. & Lillie, C. F., 1973. Astr. Astrophys., 25, 397.

Wolstencroft, R. D., Ireland, J. G., Nandy, K. & Seddon, H., 1969. Mon. Not. R. Astr. Soc., 144, 245.

Woolf, N. J. & Ney, E. P., 1969. Astrophys. J. Lett., 155, L181.

Wright, A. E. & Barlow, M. J., 1975. Mon. Not. R. Astr. Soc., 170, 41.

Yolken, H. T. & Kruger, J., 1965. J. Opt. Soc. Amer., 55, 842.

York, D. G., 1971. Astrophys. J., 166, 65.